Title
Music from chaos: nonlinear dynamical systems as generators of musical materials

Author
Bidlack, Rick Aaron

Publication Date
1990

UNIVERSITY OF CALIFORNIA
SAN DIEGO

Music From Chaos:
Nonlinear Dynamical Systems as
Generators of Musical Materials

A dissertation submitted in partial satisfaction of the
requirements for the degree Doctor of Philosophy
in Music

by

Rick Bidlack

Committee in charge:

Professor Roger Reynolds, Chair
Professor Will Ogdon
Assistant Professor Rand Steiger
Professor Henry Abarbanel
Professor David Antin

1990

The dissertation of Rick Bidlack is approved, and it is acceptable in quality and form for publication on microfilm:

Henry D. I. Abarbanel

Will Ogdon

Chair

University of California, San Diego

1990

for

my Mother and my Father

and all my Friends

We find the order we want from the chaos we cause.

inscription in a college dormitory in Texas

Contents

List of Figures

List of Tables

Acknowledgements

A work such as this is inevitably the product of many individuals. I would like to extend special thanks to my chairman, Roger Reynolds, and to Henry Abarbanel, Director of the Institute for Nonlinear Science at UCSD, for their invaluable advice and careful readings of the early drafts; to Gary Cottrell, Dave Demers and the UCSD chaos group for their patience with my many questions; to Sylvie Gibet for her lucid explanations of the laws of physics; and to Alan Finke, John Stevens, Michael Tracey, Carol Vernallis and Bob Willey for their constant support and encouragement. While this work might have come into being without the input of these persons, it would not, undoubtedly, have been nearly as rewarding an undertaking.

Vita

November 14, 1958	Born, Tallahassee, Florida
1980	B.A. (German), Bowling Green State University, Ohio
1981	English language instructor in Hamburg, Germany
1982–1983	Teaching Assistant, Undergraduate Writing Program, UCSD
1983–1985	Research Assistant, Center for Music Experiment, UCSD
1985–1987	Research Assistant, Music Education Laboratory, UCSD
1986	M.A. (Music), UCSD
1988–1990	Software Consultant
1990	Ph.D. (Music), UCSD
1990–1991	Assistant Professor (visiting), Department of Music, State University of New York at Buffalo

Fields of Study

Composition	Professors Roger Reynolds, Joji Yuasa and Will Ogdon
Analysis	Professors Bernard Rands and Roger Reynolds
Theory	Professors Gerald Balzano and Will Ogdon
Computer Music	Professors F. Richard Moore and Joji Yuasa
History	Professor Will Ogdon

ABSTRACT OF THE DISSERTATION

Music From Chaos:
Nonlinear Dynamical Systems as
Generators of Musical Materials

by

Rick Bidlack
Doctor of Philosophy in Music
University of California, San Diego, 1990
Professor Roger Reynolds, Chair

A body of scientific/mathematical theory arising from a description of the behavior of complex dynamical systems is explored in terms of its pertinence to and utility in musical schemes for the generation of melodic lines and textures. Such systems are known to model significant behavioral features of real-world phenomena, including turbulent or chaotic behavior. Many of the features of nonlinear dynamical systems that are intriguing from a mathematical point of view, especially the properties and nature of chaos, are likewise suggestive of musical qualities. A variety of musical behaviors may be elicited from chaotic systems, some quite novel, while others are evocative of already well-known practices. Typical is a type of continuous variation form, in which motivic materials are spun out within a constantly evolving context.

Four archetypal chaotic systems, the Hénon and Lorenz systems, the standard map, and the Hénon-Heiles system, are explored in terms of their potential for the generation of melodic lines, textures and rhythms—raw materials suitable for further musical exploration and elaboration. Approximately one hour of recorded examples accompany the dissertation.

Chapter 1

Initial Conditions

1.1 Regimes of Chaos

In recent decades, a great deal of attention from the scientific and mathematical communities has been focused on the exploration of a class of mathematical objects known as nonlinear dynamical systems. Although the symbolic specification of many of these systems is simple to the point of apparent triviality, their behavior can often be extremely rich and complex, even unpredictable. This unpredictability, arising as it does from processes which are completely deterministic, has a certain flavor to it which is quite distinct from the uncorrelated randomness of white noise or from other probabilistic distributions. The generic term for this brand of deterministic unpredictability is *chaos*, and the body of theory which describes it is often called *chaos theory*. (The terms "nonlinear dynamical system," "chaotic dynamical system," or simply "chaotic system," are considered in the present context to be synonymous.) Nonlinear dynamical systems are interesting to scientists because they exhibit structural characteristics which are shared by forms found in nature. Chaotic systems are thought to underly or model important aspects of the motion (change in location) and/or evolution (change in form) over time of phenomena in the real world. The complexity of behavior exhibited by certain chaotic mathematical objects—specified as sets of equations—rivals that of real-world phenomena in many instances.

The aim of this work is to present a discussion of the application of nonlinear dynamical systems to the generation of raw musical materials, such that the reader may make his or her own evaluation of the utility and musical potential of this approach. The pursuit of this objective rests on two premises. The first of these is that the use of purely mathematical processes for the production of musical materials is valid from the point of view of both historical and contemporary musical practices. In fact, there are a great many precedents for the use of extra-musical concepts and procedures, especially mathematical ones, in the creation of musical works. This claim is largely taken as axiomatic; however, the relationship between the procedures explored in this work (and the nature of the musical material which is generated) to certain trends in the current musical practice of academia and the concert hall is discussed briefly later in this chapter and in the final chapter. The second premise is that chaotic systems are not only interesting objects in their own right, but that, furthermore, the behavioral traits which they exhibit bear a compelling resemblance to other types of behaviors which are generally agreed to be "musical," and that, therefore, the employment of chaotic systems in the semi-automatic generation of musical raw materials is worthy of exploration. The demonstration of this claim is lengthy and occupies the greater portion of the present study. Since the language of mathematics is unfamiliar to most musicians, the description of the basic concepts of nonlinear dynamics and of the particular chaotic systems discussed in this work remains on a fairly elementary level. The goal of the technical descriptions is simply to acquaint the reader with the broad outlines of the range of behavior one can expect from the manipulation of chaotic systems, so that the potentialities and limitations of the materials generated may be apprehended in a more efficient and informed manner. References to more sophisticated descriptions of the chaotic systems discussed herein are provided throughout the text.

The meshing of a number of events has raised the subject of chaos to its currently topical level within the scientific community. Improved methods for the analysis and theoretical description of dynamical systems were developed around the turn of the century by Poincaré and others. The advent of cheap and plentiful computers has made practical the computation and analysis of numerical solutions to nonlinear equations. Moreover, computers have made graphical representations of the behaviors of these systems possible, revealing extraordinary structures which would not immediately be apparent from the raw numerical data. Today, increasingly well-defined behavioral and structural parallels between chaotic systems and real-world phenomena are being found and described. The range of phenomena which are presently being studied in terms of underlying chaotic structure is diverse, and includes: fluid flow, aerodynamics and turbulence [43], orbital deviations and long-term instabilities of particles in electromagnetic storage rings [71], the physiological structures (organs) in living things [73], the dynamics of superconductivity [16], structural mechanics [74], celestial mechanics [51], ecology and population dynamics [45], and many others. The interest in chaotic systems has generated a certain sense of excitement among the general public as well, as manifested by the popularity of books such as James Glieck's non-fiction best-seller *Chaos: Making a New Science* [26], or Benoit Mandelbrot's treatise *The Fractal Geometry of Nature* [44]. Striking illustrations of intricate fractal objects, the "remnants" of nonlinear dynamical processes [27, p. 44], have been provided by Peitgen, Richter, Saupe and others [54,55].

The exploration of chaos is forcing a change in the definition of this word. Chaos is *not* formless anarchism; it is a highly structured phenomenon pervasive throughout the natural world. Its variations are rich and complex, and its properties are intriguing. Its study has invigorated large segments of the mathematical and scientific communities; perhaps it has the potential to inspire artistic activities as well.

1.2 Rudimentary Nonlinear Dynamics

Nonlinearity is a concept which is intuitively understood and applied in a wide range of everyday situations. The popular adage about the straw that breaks the camel's back is based on this understanding. In this quintessentially nonlinear situation, a small *quantitative* change to the "input" (the addition of one straw) is seen to cause a dramatic *qualitative* change in the "output" (the demise of the camel). Another example, used by Glieck [26, p. 23], is the traditional verse:

For want of a nail the shoe was lost
For want of a shoe the horse was lost
For want of a horse the rider was lost
For want of a rider the battle was lost
For want of a battle the kingdom was lost.

This is a perfect example of what is more formally known as *sensitive dependence on initial conditions*, the idea that a seemingly insignificant variance at the outset of a chain of events may nonetheless precipitate effects down the line that build up to irrevocably and drastically alter the final outcome. One might also think of the performance of the economy (seemingly immune to all theory and attempts at regulation), the occurrence of earthquakes (sudden jolts resulting from presumably constant tectonic pressures), or even the outbreak of war (an abrupt shift of international tension from the political to the military arena) as familiar examples of nonlinear dynamics at work.

Nonlinear dynamical systems are mathematical objects which behave in similarly structured but unpredictable ways. To understand how these expressions can be manipulated to produce musical results, certain basic concepts of dynamics and nonlinear equations must be understood. Among the terms to be introduced in this section and in the following chapters are: phase space, orbit, bifurcation, attraction, dissipative and conservative systems, transients, sensitive dependence on initial conditions, Poincaré section, iterated map and continuous flow. An operational definition of chaos, if not a rigorously mathematical one, will hopefully follow from a familiarity with these concepts.

Dynamical systems convey in their notation an implicit recognition of the passage of time. The length of time that passes is rather arbitrary; what is more important is the quality of the time, or how it is fundamentally conceived. If the mathematical expression of a dynamical system implies the passage of time in terms of discrete steps of a uniform size, then the system is a *difference* equation, of the form

$$x_{t+1} = f(x_t).$$

This is akin to a simple feedback system, in which the current output of the equation becomes the input for the next iteration. Systems expressed as difference equations are also called *iterated maps*, because the effect of the equation is to map one value, x_t, to another value, x_{t+1}, for each iteration of the equation. If, on the other hand, time is considered to be a continuous quantity, advancing smoothly, then the system is expressed as a *differential* equation in the form

$$\dot{x} = \frac{dx}{dt} = f(x),$$

where $\dot{x}$ is a measure of the rate of change of the dependent variable x with respect to time. These systems are called *continuous flows*, and what they produce are smooth, unbroken curves. In a digital computer, however, continuous time cannot exist—it is a theoretical concept that must be approximated in simulation. This is accomplished by reformulating the differential equations of the system into difference equations, a process called integration. Several methods have been developed for integrating differential equations [57], but only the simplest of these, Euler's method, is used in this study. Essentially, this procedure calculates a value $\dot{x}_n$ from the function $f(x_n)$, then computes a new x based on this value according to the formula

$$x_{n+1} = x_n + \dot{x}_n \Delta t,$$

where Δt is typically a very small value, 0.01 or less. The effect of this procedure is to move forward along the curve by very small, discrete steps (of unequal size). The programs listed in Appendix A.3 and A.5 illustrate situations in which this type of integration is employed.

In mathematical terms, nonlinear equations are simply those which are not linear. Linear *algebraic* equations are those in which the degree of the variables is unity, e.g., none of the variables of the equation are raised to any power other than one. An example is the linear equation $y = mx + b$, which defines a straight line of slope m and y-intercept b. On the other hand, the second-degree equation $y^2 = mx + b$, which defines a parabola, is not linear. This distinction applies in *differential* equations as well, although in this case the only variables for which the degree is significant are the *dependent* variables, the ones for which a derivative term occurs in the equation. For example, the equation

$$x^2\frac{dy}{dx} + y(x^3 - 2) = 2x^3$$

is linear in y, even though x is both squared and cubed, because the dependent variable y is always of degree one. The equation

$$A\frac{d^2y}{dx^2} + B\frac{dy}{dx} + Cy^3 = \cos(x)$$

is nonlinear in y because the dependent variable y is raised to the third power.

While the degree of an equation is critical in the distinction between linear and nonlinear dynamical systems, it is not the only factor in determining whether or not a given equation is nonlinear. The presence within an equation of a trigonometric function, or, in a differential equation, of the multiplication of two or more of the dependent variables by one another, are also sufficient to make the equation nonlinear.

One of the simplest nonlinear equations known to exhibit chaotic behavior is the *logistic* difference equation, also known as the quadratic or parabolic equation. This equation has been applied in studies of the population dynamics of a species from generation to generation [46]. It specifies the population P at successive time increments $0, 1, 2, \ldots, n$ as a function of its prior value:

$$P_{n+1} = KP_n(1 - P_n),$$

where K is a parameter whose value normally remains constant once an iteration sequence is initiated. The equation is nonlinear by virtue of the quantity P^2 (remember that $KP(1 - P) = KP - KP^2$). Despite its apparent simplicity, the dynamics of this equation are sufficiently complex to have warranted attention from many authors in the mathematical community; see for example Thompson and Stewart [69], Ruelle [62], Devaney [18] and Moon [50]. A program to generate orbits of the logistic equation may be found in Appendix A.1.

The equation may be iterated indefinitely, to produce an arbitrarily long sequence of numbers $P_0, P_1, \ldots, P_n$. This sequence is called the *orbit* or *trajectory*. The term orbit does not necessarily imply a smooth, continuous curve. While the orbit of the earth around the sun may be quite smooth, orbits of iterated maps such as the logistic function can be quite erratic. The equation becomes interesting when the orbits resulting from the adoption of different values for the constant K are compared. Table 1.1 lists the first thirty iterates of eight different orbits, each following from a different value for K. Although the initial value $P_0 = .5$ in all cases, each orbit is quite distinct from the others.

Three distinctly different modes of behavior are demonstrated by the orbits shown in Table 1.1. First, for K-values of 0.5, 1.0, 1.5, 2.0, 2.5 and 4.0, the orbit is drawn to a single point, or fixed point, where it remains. (For $K = 1.0$, the orbit is eventually drawn to 0.) This point is called an *attractor*. The rate at which the sequence of values converges on the single-point attractor varies from immediate ($K = 2.0$) to extremely gradual ($K = 1.0$). Second, for $K = 3.5$, the orbit is attracted to a *limit cycle*, where it oscillates indefinitely. In this case, the limit cycle is a periodic oscillation among four points. This is a periodic attractor. Third, for $K = 3.0$, the orbit describes a damped oscillation wherein the high and low values converge asymptotically. The two values will converge to a single point only when the limit of resolution of the program which is computing the orbit is reached—in other words, when the computer is no longer able to make a distinction between the two values. Depending on what this resolution is, this may not occur until after tens of thousands of iterations have been calculated.

Table 1.2 shows the first eighty iterations of eight more orbits of the logistic equation, each from an initial point $P_0 = .5$, for values of K starting at 3.55 and increasing in steps of 0.01125. These orbits illustrate modes of behavior which are again quite distinct from those shown in Table 1.1. Within the span of eighty iterations listed, only two of the orbits attain an unambiguously periodic state: the first, for $K = 3.55$, and the last, for $K = 3.62875$. In both of these cases, the P-values comprising each cycle do not repeat *exactly* until after the sixtieth iteration. The initial portion of the orbit, during which the eventual, settled behavior of the equation under the specified conditions (the

n	Value of Parameter K							
	0.5	1.0	1.5	2.0	2.5	3.0	3.5	4.0
0	0.500	0.500	0.500	0.500	0.500	0.500	0.500	0.500
1	0.125	0.250	0.375	0.500	0.625	0.750	0.875	1.000
2	0.055	0.188	0.352	0.500	0.586	0.563	0.383	0.000
3	0.026	0.152	0.342	0.500	0.607	0.738	0.827	0.000
4	0.013	0.129	0.338	0.500	0.597	0.580	0.501	0.000
5	0.006	0.112	0.335	0.500	0.602	0.731	0.875	0.000
6	0.003	0.100	0.334	0.500	0.599	0.590	0.383	0.000
7	0.002	0.090	0.334	0.500	0.600	0.726	0.827	0.000
8	0.001	0.082	0.334	0.500	0.600	0.597	0.501	0.000
9	0.000	0.075	0.333	0.500	0.600	0.722	0.875	0.000
10	0.000	0.069	0.333	0.500	0.600	0.603	0.383	0.000
11	0.000	0.065	0.333	0.500	0.600	0.718	0.827	0.000
12	0.000	0.060	0.333	0.500	0.600	0.607	0.501	0.000
13	0.000	0.057	0.333	0.500	0.600	0.716	0.875	0.000
14	0.000	0.054	0.333	0.500	0.600	0.610	0.383	0.000
15	0.000	0.051	0.333	0.500	0.600	0.713	0.827	0.000
16	0.000	0.048	0.333	0.500	0.600	0.613	0.501	0.000
17	0.000	0.046	0.333	0.500	0.600	0.711	0.875	0.000
18	0.000	0.044	0.333	0.500	0.600	0.616	0.383	0.000
19	0.000	0.042	0.333	0.500	0.600	0.710	0.827	0.000
20	0.000	0.040	0.333	0.500	0.600	0.618	0.501	0.000
21	0.000	0.038	0.333	0.500	0.600	0.708	0.875	0.000
22	0.000	0.037	0.333	0.500	0.600	0.620	0.383	0.000
23	0.000	0.036	0.333	0.500	0.600	0.707	0.827	0.000
24	0.000	0.034	0.333	0.500	0.600	0.622	0.501	0.000
25	0.000	0.033	0.333	0.500	0.600	0.706	0.875	0.000
26	0.000	0.032	0.333	0.500	0.600	0.623	0.383	0.000
27	0.000	0.031	0.333	0.500	0.600	0.704	0.827	0.000
28	0.000	0.030	0.333	0.500	0.600	0.625	0.501	0.000
29	0.000	0.029	0.333	0.500	0.600	0.703	0.875	0.000

Table 1.1 Eight orbits of the logistic equation, in numerical form, for different values of the parameter K. All orbits begin at the same point, $P_0 = 0.5$.

value of the parameter K and the initial value of P) is approached, is called the *transient* segment of the orbit. In the case of these two periodic orbits, the span of latent periodicity prior to the sixtieth iteration (approximately) comprises the transient portion. For the orbits shown in Table 1.1 which are attracted to a single point, the transient state consists of those points through which the orbit passes before it settles onto the fixed point. There is not necessarily a firm dividing line between the transient portion of an orbit and its settled state. Some orbits ease into their settled behaviors very gradually, while others show no transients at all.

Four other orbits in Table 1.2 appear to be headed toward a regime of periodicity, but none of them reaches this state within the span of eighty iterations shown here. For $K = 3.56125$, the orbit tends toward a period 8 oscillation. For $K = 3.57250$ the tendency is toward a period 24 oscillation, for $K = 3.58375$ it could be a period 12 (although it gets "noisier" rather than cleaner as it progresses), and for $K = 3.60625$ there is a clear period 10 oscillation. In practice, it is sometimes difficult to determine whether or not a given orbit is being attracted to a periodic state without following the orbit for a much longer span than has been illustrated in Table 1.2. These orbits may still be in a transient state, headed toward an ultimately periodic condition; on the other hand, it is possible that one or more of them has already settled into a long-term state of "noisy periodicity" within the span shown here. Adding to the ambiguity is the fact that a determination of a given orbit's periodicity is contingent on the numerical resolution used in the representation of that orbit. Long transient orbits appear to become shorter when fewer significant figures after the decimal point are used. On the other hand, the seemingly exact periodicities finally attained in the first and eighth orbits may simply be artifacts of there being only five significant figures after the decimal point.

The remaining two orbits in Table 1.2, for $K = 3.595$ and $K = 3.61750$, tend neither toward a fixed point, nor to a limit cycle. These are *chaotic* orbits, in which the sequence of values is quite erratic, and apparently random. The fact that these orbits are the result of a completely deterministic procedure (the equation itself) is one distinction between true randomness and chaos.

Taken together, Tables 1.1 and 1.2 demonstrate a remarkably rich (and potentially bewildering) range of behavior for an equation as apparently trivial as the logistic equation. Graphical methods of representation may be employed to clarify this behavior and relate it within a global context. One method is the construction of a *bifurcation diagram*, in which a large number of partial orbits are computed and plotted against a

	Value of Parameter K							
n	3.55000	3.56125	3.57250	3.58375	3.59500	3.60625	3.61750	3.62875
0	0.50000	0.50000	0.50000	0.50000	0.50000	0.50000	0.50000	0.50000
1	0.88750	0.89031	0.89312	0.89594	0.89875	0.90156	0.90438	0.90719
2	0.35445	0.34778	0.34100	0.33413	0.32714	0.32005	0.31284	0.30553
3	0.81229	0.80779	0.80281	0.79733	0.79133	0.78478	0.77766	0.76996
4	0.54129	0.55293	0.56554	0.57911	0.59363	0.60910	0.62548	0.64273
5	0.88145	0.88033	0.87778	0.87351	0.86723	0.85864	0.84742	0.83326
6	0.37096	0.37516	0.38327	0.39597	0.41393	0.43772	0.46774	0.50416
7	0.82839	0.83481	0.84444	0.85715	0.87212	0.88757	0.90061	0.90712
8	0.50466	0.49110	0.46928	0.43880	0.40094	0.35986	0.32381	0.30572
9	0.88742	0.89003	0.88975	0.88251	0.86347	0.83073	0.79208	0.77022
10	0.35466	0.34856	0.35044	0.37157	0.42381	0.50709	0.59577	0.64222
11	0.81251	0.80864	0.81321	0.83683	0.87788	0.90138	0.87119	0.83379
12	0.54080	0.55107	0.54266	0.48934	0.38541	0.32057	0.40594	0.50288
13	0.88159	0.88102	0.88662	0.89553	0.85155	0.78546	0.87237	0.90716
14	0.37058	0.37329	0.35912	0.33528	0.45446	0.60770	0.40278	0.30562
15	0.82804	0.83314	0.82222	0.79870	0.89130	0.85973	0.87018	0.77009
16	0.50548	0.49508	0.52221	0.57619	0.34831	0.43488	0.40865	0.64248
17	0.88739	0.89023	0.89136	0.87514	0.81603	0.88627	0.87419	0.83352
18	0.35474	0.34802	0.34595	0.39161	0.53970	0.36349	0.39787	0.50355
19	0.81259	0.80805	0.80834	0.85383	0.89308	0.83436	0.86664	0.90714
20	0.54062	0.55236	0.55348	0.44726	0.34327	0.49839	0.41809	0.30567
21	0.88164	0.88055	0.88291	0.88597	0.81044	0.90155	0.88010	0.77015
22	0.37044	0.37458	0.36933	0.36206	0.55229	0.32007	0.38173	0.64236
23	0.82791	0.83430	0.83212	0.82775	0.88892	0.78481	0.85377	0.83365
24	0.50580	0.49233	0.49905	0.51098	0.35498	0.60903	0.45163	0.50323
25	0.88738	0.89010	0.89312	0.89551	0.82314	0.85870	0.89591	0.90715
26	0.35477	0.34836	0.34101	0.33535	0.52336	0.43757	0.33735	0.30565
27	0.81263	0.80842	0.80282	0.79878	0.89679	0.88751	0.80867	0.77012
28	0.54054	0.55155	0.56552	0.57601	0.33275	0.36004	0.55971	0.64242
29	0.88167	0.88085	0.87779	0.87523	0.79819	0.83092	0.89148	0.83358
30	0.37037	0.37377	0.38324	0.39135	0.57909	0.50665	0.34998	0.50339
31	0.82785	0.83356	0.84442	0.85363	0.87626	0.90140	0.82296	0.90715
32	0.50593	0.49407	0.46934	0.44778	0.38980	0.32051	0.52706	0.30566
33	0.88738	0.89019	0.88977	0.88616	0.85509	0.78538	0.90173	0.77013
34	0.35479	0.34813	0.35040	0.36152	0.44546	0.60787	0.32057	0.64239
35	0.81264	0.80817	0.81317	0.82721	0.88806	0.85960	0.78791	0.83362
36	0.54050	0.55211	0.54275	0.51223	0.35738	0.43522	0.60451	0.50331
37	0.88168	0.88064	0.88660	0.89540	0.82563	0.88643	0.86486	0.90715
38	0.37035	0.37432	0.35919	0.33565	0.51756	0.36305	0.42280	0.30565
39	0.82782	0.83406	0.82229	0.79913	0.89764	0.83392	0.88282	0.77013

Table 1.2 Eight orbits of the logistic equation, in numerical form, for different values of K. Note that $P_0 = 0.5$ in all cases. Iterations 40-79 are continued on the next page.

n	*Value of Parameter K*							
	3.55000	3.56125	3.57250	3.58375	3.59500	3.60625	3.61750	3.62875
40	0.50598	0.49288	0.52205	0.57526	0.33031	0.49945	0.37424	0.64241
41	0.88737	0.89013	0.89139	0.87564	0.79524	0.90156	0.84716	0.83360
42	0.35480	0.34828	0.34587	0.39026	0.58539	0.32005	0.46839	0.50335
43	0.81265	0.80834	0.80826	0.85278	0.87253	0.78478	0.90076	0.90715
44	0.54049	0.55174	0.55365	0.44993	0.39983	0.60909	0.32337	0.30565
45	0.88168	0.88078	0.88284	0.88695	0.86268	0.85865	0.79152	0.77013
46	0.37034	0.37396	0.36951	0.35933	0.42588	0.43770	0.59695	0.64240
47	0.82781	0.83374	0.83230	0.82502	0.87900	0.88757	0.87037	0.83361
48	0.50601	0.49366	0.49865	0.51735	0.38235	0.35988	0.40815	0.50333
49	0.88737	0.89017	0.89312	0.89486	0.84899	0.83076	0.87386	0.90715
50	0.35480	0.34818	0.34102	0.33718	0.46089	0.50704	0.39877	0.30565
51	0.81265	0.80822	0.80284	0.80093	0.89325	0.90138	0.86730	0.77013
52	0.54048	0.55199	0.56549	0.57139	0.34280	0.32056	0.41634	0.64240
53	0.88168	0.88069	0.87780	0.87767	0.80991	0.78545	0.87905	0.83360
54	0.37033	0.37421	0.38321	0.38476	0.55348	0.60772	0.38461	0.50334
55	0.82781	0.83396	0.84440	0.84835	0.88847	0.85972	0.85620	0.90715
56	0.50602	0.49313	0.46939	0.46106	0.35624	0.43492	0.44538	0.30565
57	0.88737	0.89014	0.88978	0.89050	0.82445	0.88629	0.89358	0.77013
58	0.35480	0.34824	0.35036	0.34944	0.52031	0.36344	0.34400	0.64240
59	0.81265	0.80830	0.81313	0.81470	0.89727	0.83431	0.81634	0.83361
60	0.54048	0.55182	0.54283	0.54102	0.33138	0.49852	0.54238	0.50334
61	0.88168	0.88075	0.88657	0.88991	0.79654	0.90155	0.89788	0.90715
62	0.37033	0.37404	0.35926	0.35111	0.58262	0.32007	0.33170	0.30565
63	0.82781	0.83381	0.82236	0.81649	0.87421	0.78481	0.80191	0.77013
64	0.50603	0.49348	0.52188	0.53697	0.39534	0.60904	0.57465	0.64240
65	0.88737	0.89016	0.89141	0.89104	0.85937	0.85869	0.88422	0.83360
66	0.35480	0.34820	0.34580	0.34794	0.43447	0.43759	0.37035	0.50334
67	0.81266	0.80825	0.80818	0.81307	0.88331	0.88752	0.84357	0.90715
68	0.54048	0.55193	0.55383	0.54467	0.37054	0.36001	0.47736	0.30565
69	0.88168	0.88071	0.88277	0.88878	0.83850	0.83089	0.90252	0.77013
70	0.37033	0.37415	0.36970	0.35424	0.48683	0.50671	0.31825	0.64240
71	0.82781	0.83391	0.83247	0.81980	0.89813	0.90140	0.78488	0.83360
72	0.50603	0.49325	0.49822	0.52943	0.32893	0.32052	0.61078	0.50334
73	0.88737	0.89015	0.89311	0.89283	0.79354	0.78539	0.85998	0.90715
74	0.35480	0.34823	0.34104	0.34290	0.58899	0.60784	0.43560	0.30565
75	0.81266	0.80828	0.80285	0.80749	0.87028	0.85962	0.88937	0.77013
76	0.54048	0.55186	0.56546	0.55710	0.40585	0.43518	0.35592	0.64240
77	0.88168	0.88073	0.87782	0.88425	0.86688	0.88641	0.82928	0.83360
78	0.37033	0.37408	0.38317	0.36680	0.41486	0.36311	0.51215	0.50334
79	0.82781	0.83384	0.84436	0.83235	0.87269	0.83398	0.90384	0.90715

Table 1.2 (cont.) Eight orbits of the logistic equation, in numerical form. Iterations 40-79.

range of values of the constant parameter. Figure 1.1 shows two versions of a bifurcation diagram for the logistic equation over the range $0 \leq K \leq 4$. In the first version, the first 150 points of each orbit are plotted, while in the second version iterations 150 through 300 are plotted. Thus, the first version illustrates the transient behavior of the system, while the second version shows the settled behavior (this assumes that most transients have died down by the 150th iteration). Figure 1.2 shows two successive magnifications of the diagram, the first in the range $3 \leq K \leq 4$, the second in the range $3.55 \leq K \leq 3.62875$. Several important features of the behavior of the logistic equation emerge from an examination of these diagrams. When the value of K is less than 3.0, the orbit is attracted to a single point (for $K < 1$, this point is 0). At $K = 3.0$, a *bifurcation* of the attractor is evident. At $K \approx 3.46$, a further bifurcation is seen, forming a period 4 oscillation (compare Table 1.1, for the orbit at $K = 3.5$). Yet another bifurcation occurs just before $K = 3.55$, and again between 3.56125 and 3.5725. The period of the oscillation is thus doubled at each bifurcation node, in a sequence called the *period-doubling cascade*. Eventually, the nature of the attractor undergoes a change from a condition of periodicity to one of chaos. For the logistic equation, the *chaotic regime* begins at around $K = 3.567$ and extends to the maximum value of $K = 4.0$ (orbits at higher values of K are unstable). Nonetheless, periodic windows are found interspersed throughout the chaotic regime; note, for example, the large period 3 window around $K = 3.84$. Figure 1.2(b) provides a new perspective on the eight orbits listed in Table 1.2. The period 24 window at $K = 3.5725$ is barely discernible, while the period 12 orbit at $K = 3.58375$ is seen to lie right on the edge of a periodic window. Chaotic orbits for $K = 3.595$ and $K = 3.6175$ lie squarely within chaotic regimes.

Thus far, all of the numerical orbits listed, as well as the four bifurcation diagrams plotted, have been initiated from $P_0 = 0.5$. In fact, any initial value of P_0 between 0 and 1 could have been used to produce basically the same results. For those values of K which lead to periodic orbits, only the initial transient portions of the orbits would be different. For those values of K which lead to chaotic orbits, the exact sequence of points along the orbit would be quite different for different values of P_0, but the range of values over which the orbit wanders would remain the same. Thus, the two bifurcation diagrams in Figure 1.2, which do not plot the transient portion of the orbits, would look essentially the same no matter what the initial value of P_0. This is the significance of the term *attractor*—orbits are drawn to the same attractor regardless of their respective starting positions as long as the parameter values (just K in this case) are equivalent.

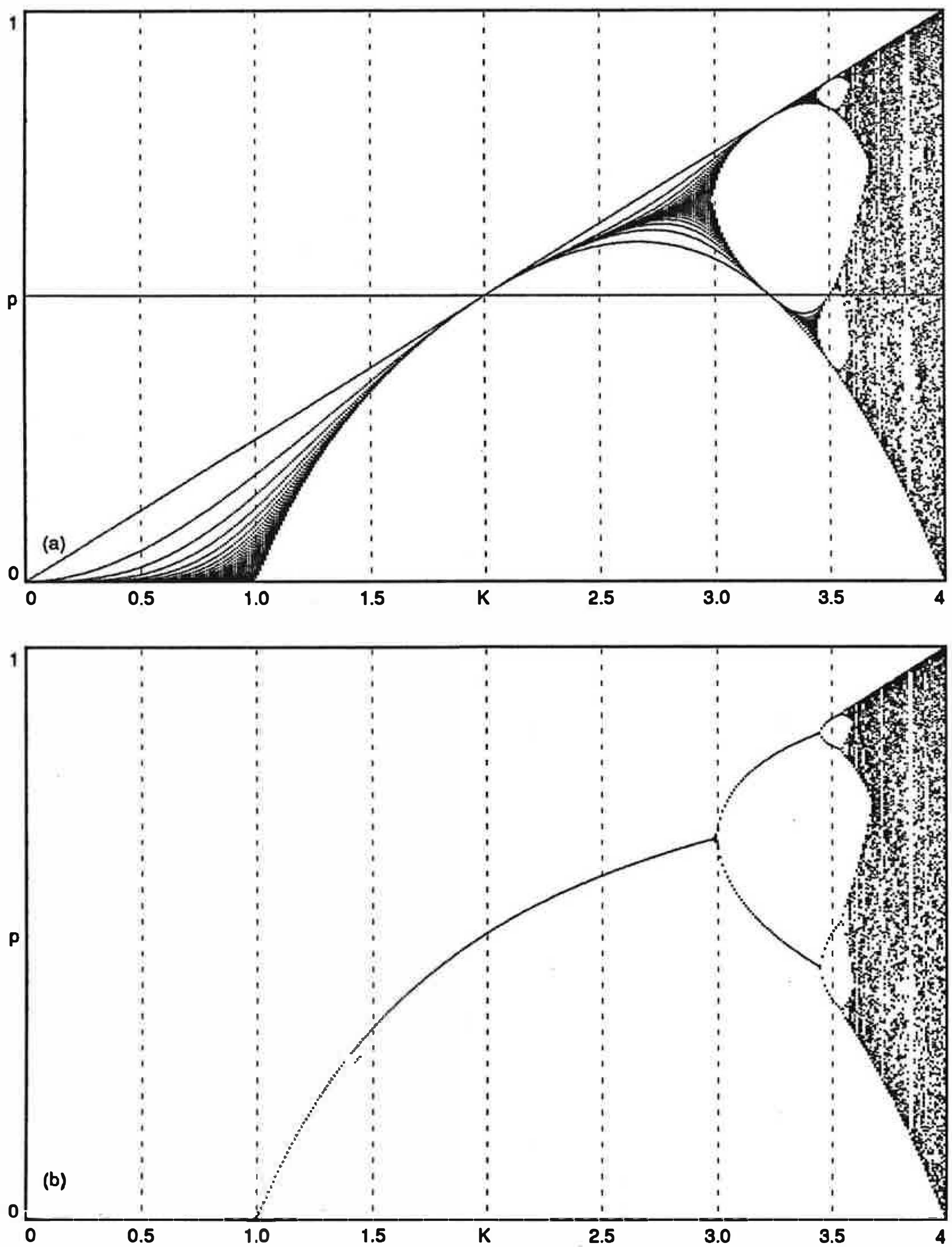

Figure 1.1 Bifurcation diagrams of the logistic equation, over the range $0 \le K \le 4$, with $P_0 = .5$; (a) showing transient behavior (first 150 iterations), (b) showing settled behavior (next 150 iterations).

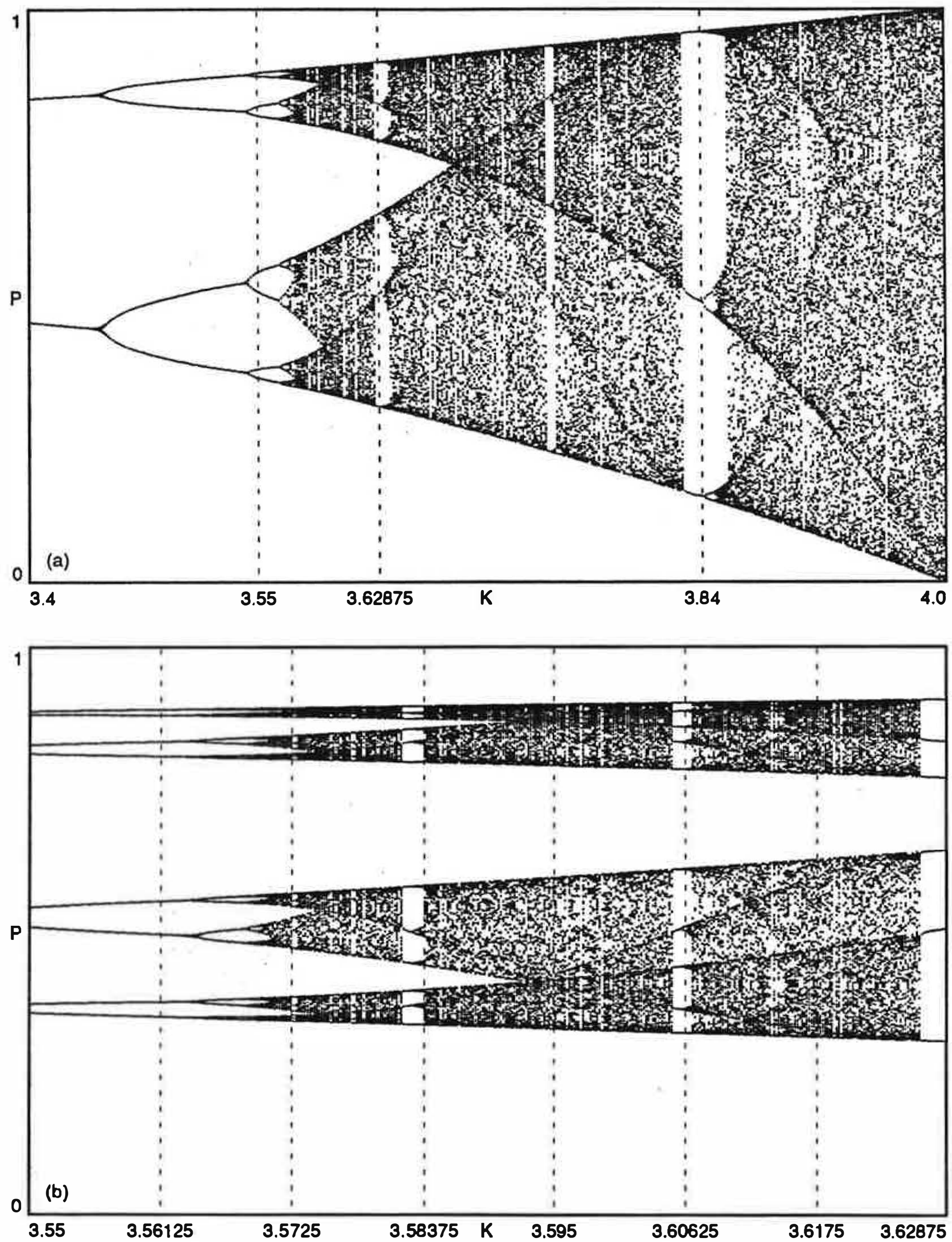

Figure 1.2 Magnification sequence of bifurcation diagrams of the logistic equation; (a) in the range $3 \leq K \leq 4$, (b) in the range $3.55 \leq K \leq 3.62875$. Iterations 150 through 300 are plotted.

n	Orbit 1	Orbit 2	n	Orbit 1	Orbit 2
0	0.40000	0.40001	12	0.54707	0.50531
1	0.96000	0.96001	13	0.99114	0.99989
2	0.15360	0.15357	14	0.03514	0.00045
3	0.52003	0.51995	15	0.13561	0.00180
4	0.99840	0.99841	16	0.46887	0.00720
5	0.00641	0.00636	17	0.99612	0.02859
6	0.02547	0.02526	18	0.01545	0.11111
7	0.09928	0.09850	19	0.06083	0.39504
8	0.35768	0.35518	20	0.22853	0.95594
9	0.91898	0.91610	21	0.70522	0.16849
10	0.29782	0.30743	22	0.83154	0.56040
11	0.83650	0.85167	23	0.56034	0.98541

Table 1.3 Two orbits of the logistic equation, demonstrating sensitive dependence on initial conditions. $K = 4.0$ for both orbits, while P_0 differs only by 1/100000. The orbits remain fairly similar through fourteen iterations.

(There are exceptions to this rule. In certain situations, different initial conditions may lead to different attractors under the same parameter values. An example of this follows, and another is included in the discussion of the Hénon map in the next chapter.)

Another intriguing aspect of chaotic orbits is their *sensitive dependence on initial conditions.* Two orbits which begin at *almost* the same point will eventually diverge from one another. An example of this is shown in Table 1.3. Here two orbits are followed through twenty-four iterations. For both orbits, $K = 4.0$, while the initial value P_0 differs by only 1/100000. Nonetheless, this difference causes a complete divergence of the two orbits within the span of fourteen iterations. This effect can be demonstrated with any chaotic dynamical system, no matter how small the initial difference. Incidentally, a comparison of these two orbits with the last orbit listed in Table 1.1 (for $K = 4.0$) demonstrates the effect mentioned in the paragraph above, that co-existing attractors may emerge for different initial conditions.

The phenomenon of sensitive dependence on initial conditions has wide-ranging ramifications for anyone working with chaotic systems. Since real numbers can only be represented with finite precision in a computer, rounding errors in the calculation of any orbit are inevitable. These errors eventually accumulate, causing the calculated orbit to diverge exponentially from the theoretical orbit. Slight differences in the implementation of an algorithm to compute an orbit (for example, the order in which mathematical operations are carried out), the precision employed, or the use of a different computer, are sufficient to cause a divergence of trajectories. One may rely on the *global* behavior of a chaotic system to remain roughly the same from machine to machine, but not the precise sequence of a given orbit. In the preparation of this document, the computer used to produce the graphic illustrations (an Apple LaserWriter running PostScript) often computed orbits which were quite different than those produced on the machine used to create the audio examples (an IBM AT compatible, running software written in 'C'), even with identical parameter values and starting conditions. Special care had to be taken to find good matches between the graphic plots and the musical examples meant to correspond to those illustrations. In some cases, the printer had to be manually coerced to reproduce the behavior generated in numerical form on the IBM. Intrepid souls wishing to *precisely* replicate the results presented in this document should expect to encounter similar difficulties.

This study approaches the issue of the generation of musical materials by means of nonlinear dynamical systems through an examination of four distinct systems: the Hénon map, the Lorenz system, the standard map, and the Hénon-Heiles system. These systems, only slightly more complex than the logistic equation just discussed, were chosen not only because they are well-known and widely studied, but because they are exemplary of certain fundamental classifications of nonlinear dynamical systems in general.

The Hénon map and the standard map are iterated maps, objects in which the passage of time is represented in discrete steps of equal size, as would be appropriate in the periodic measurements of things such as populations, water levels, or stock prices. The *phase space*, or the area in which the dynamics of the system take place, is two-dimensional for both of these maps. In the case of the Hénon map, the significant portion of the phase space may be represented on the Cartesian plane, between approximately -1.5 and 1.5 on the x-axis, and between approximately -0.4 and 0.4 on the y-axis. The phase space of the standard map is the two-dimensional surface of the unit torus (a torus whose circumference and girth are both 2π). Its phase space is therefore periodic in 2π, along both dimensions.

The Lorenz and Hénon-Heiles systems are continuous flows, phenomena in which the passage of time is—theoretically—represented in an unbroken manner, as would be appropriate to the calculation of celestial orbits or to the representation of wind speeds over a continuous span of time. The stable phase space of the Lorenz attractor is three-dimensional, roughly symmetrical around the origin along both x and y axes, and lying entirely in the positive region along the z-axis. The stable phase space of the Hénon-Heiles system is four-dimensional, and remains bounded within a volume which intersects the (x, y) plane as a triangular region whose center lies at the origin. The remaining two dimensions are measured in terms of the rate of change of the variables x and y with respect to time.

The Hénon and Lorenz systems are *dissipative*, that is, they are representatives of a class of phenomena in which the total energy of the system is dissipated over time. (The logistic equation is also a member of this class.) In analytic terms, this means that the phase space of the system shrinks over time. The dissipation of energy occurs during the initial transient portion of the orbit. Orbits of dissipative systems are drawn to an attractor, which may be either a point (a single-point attractor), a set of points (a limit cycle or periodic attractor), or a complexly folded region of space (a chaotic attractor or strange attractor). The great majority of earth-bound dynamical systems are dissipative, due to energy loss through friction.

The standard map and the Hénon-Heiles system are *conservative*. They are representative of phenomena in which friction does not play a role, those in which energy is conserved. These systems are also called Hamiltonian systems or area-preserving systems, because their phase spaces do not shrink with time. Thus, they cannot properly be said to have an attractor, although they do exhibit periodic and chaotic behaviors in a manner parallel to that of the dissipative systems. Such systems occur within the realm of celestial mechanics, and on earth, within the electromagnetic storage rings of particle accelerators.

The study of dynamical systems began historically as the attempt to understand the complex motions of heavenly bodies. Many conservative systems, the Hénon-Heiles system included, were initially introduced as theoretical models of aspects of celestial dynamics. Thus the claim could be made that the use of these systems in musical contexts will finally lead to the true music of the spheres!

1.3 Musical Rationale: Historical and Contemporary

There is a great deal of precedence, both historical and contemporary, for the application of mathematical constructs to the theory and composition of music. This is due in no small part to the highly ephemeral nature of music, especially in comparison to the other arts which are, as a rule, externally grounded in either visual or linguistic references. The intangible, transitory nature of sound and music would present overwhelming difficulties to composers, theorists and performers in their efforts to communicate musical issues were it not for the highly formalized prescriptive and descriptive theoretical systems underlying musical practice that have been developed over the past two and a half millennia. Throughout the history of Western music, fundamental relationships in the areas of pitch (scale structure and harmony), meter (the patterning of pulse), and form (the structure of content) have been defined in mathematical terms. In this century, composers have explored mathematically based methods to inform or determine virtually every aspect of a musical composition. The rigor of mathematical logic has provided a secure base for the exploration of expanded notions of musical structure.

The establishment of basic concepts of pitch and pitch relationships—what Xenakis has called the structure *outside-time* [75]—was accomplished as early as the sixth century B.C. in Greece, and in the fourth century B.C. in China. Historical changes in musical style have often been accompanied by redefinitions of consonance and dissonance, scale formations and tuning systems. New theories of pitch structure have invariably been expressed in mathematical terms: ratios, sets, combinatorialities, and permutations. Barbour [6] and Lloyd [39] present retrospective accounts of these changes as they have occurred throughout musical history.

The foundations of the current Western conception of meter as an iterative and recursive hierarchical structure were laid before the fourteenth century. At that time, procedures involving the permutation of basic rhythmic elements, the rhythmic modes, had been in use for several centuries [70]. At the beginning of the fourteenth century, the composer and theorist Phillippe de Vitry, in preparing his landmark treatise *Ars Nova* [56], felt compelled to enlist the aid of the mathematician Gersonides in order to ensure a solid foundation for his arguments in favor of extensions to the metrical/rhythmical structure of the Ars Antiqua [72,1]. Time, meter and tempo continue to be notated in terms of arithmetic ratios.

Form, the structure of music *in time*, relies on notions of pattern, iteration, hierarchy, diminution and augmentation as applied to phrases and sections. Rule-based schemes for composition are seen in the development of canonic forms, exemplified by the riddle canons of the 15th and 16th centuries, or Bach's *Goldberg Variations* [36]. The isorhythmic motet of the 14th and 15th centuries exploited pitch and rhythm cycles of differing lengths to create musical structures designed around the metrical Least Common Multiple between the *color* (melodic pattern) and the *talea* (rhythmic pattern). Machaut's motets stand at the pinnacle of this particular device.

In our own time, the variety and extent of the application of mathematical formalisms to musical thought has been extraordinary. A partial list includes: Debussy, for the exploration of the harmony of symmetrical subsets of the twelve-tone scale (whole-tone scales, diminished and augmented chords), and the alleged use of Fibonacci numbers and the golden mean [34]; Schoenberg, whose use of the twelve-tone row may be considered an early application of algorithmic technique to the generation of melodic lines and harmonies; Webern, for the exploitation of intervalic, rhythmic and formal symmetries and permutations [20]; Carter, for his sophisticated rhythmic techniques and the development of metric modulation [7]; Nancarrow, for the use of irrational numerical ratios in the temporal relationships between canonic voices [68]; Cage, whose personal definition of music developed at least partially from a numerical conception of formal durational relationships and a physical description of sound [12,52]; Babbitt, for his extreme approach in the application of strictly serial principles to virtually all of the musical parameters in a composition [3,2]; Xenakis, for his in-depth focus on statistical analysis and probability theory as the basis for his structures [75]; Boulez, for his occupation with multiplications of complex matrices of pitch and durational materials [66]; Stockhausen, for his detailed analysis of the relationship between time and frequency [67]; Reynolds, for his use of geometric proportions and iterative algorithms [60]; and Wuorinen [59] and Dodge [19] for their explicit use of fractal methods in the generation of musical textures.

In the theoretical domain, Balzano [4] has shown how group-theoretical techniques can be used not only in the analysis of tonal music, but in the exploration of microtonal systems of functional tonality; Forte [24] has employed set theory in the harmonic analysis of atonal music; Partch [53] explored alternative scale structures and tuning systems; and both Werner-Eppler [48] and Meyer [47] have made forays into information theory as an analytic tool for understanding the perception of music. Rule-based systems of harmonic and melodic generation have been reported by many composers and theorists [61], including the use of cellular automata [8,11] and parallel distributed processing techniques [42]. Waschka and Alexandria [35] have experimented with the use of chaotic iterated maps as waveform generators by means of granular synthesis, and Degazio [17] has explored the relationship between fractal geometry and music.

The procedures explored in the present study are thus aligned with a general tendency of current compositional practice to utilize formalized methods and mathematical constructs in the preparation of materials for compositional purposes. In particular, the quality of the materials produced by means of chaotic systems would seem to address concerns of composers interested in the generation of variant patternings of quasi-motivic materials which are related by virtue of a common underlying method: in this case, the equations of the system employed. One might speak of a morphology of meta-patterning in this instance. This will become especially clear in the demonstrations presented in the following chapters. Although the audio examples included are synthetically produced, one should not automatically conclude that the most comfortable domain of music from chaos is the electronic medium. Transcriptions for acoustic instruments would seem to be a natural application, although the rhythmic structure of materials generated by these means does not comfortably lie within the confines of traditional metrical structures. Note that the materials—pitches, rhythms, textures—which are generated in this study inhabit a middle level of musical hierarchy. Issues concerning the lowest level—waveform synthesis—are not discussed, nor are issues at the highest level—the structure of phrases, sections, or overall form.

1.4 The Experimental Apparatus

It is desirable, in an initial exploration of a potential compositional technique, that highly subjective issues be removed from the picture, or at least minimized as much as possible. The question at hand is not: "How can I make music with this dynamical system?" Rather, it is: "How much music inherently resides in this system?" Once that question is answered, the details of the extraction of the music become the idiosyncratic, personal domain of the composer, and lie outside the domain of the present study. This question can only be answered by neutralizing as far as possible the "sonic vehicle" by means of which the potential musical properties of the dynamical system are assessed. To this end, the musical space into which the orbits of these systems are projected is configured in a uniform manner which remains unaltered from example to example and from chapter to chapter. This space is defined by the use of a single timbre for all pitched examples, reminiscent of a hammered dulcimer with infinitely and instantly tunable strings. This timbre is replaced by an unpitched snare drum sound in those examples which relate rhythmic and dynamic information only. The pitch space encompasses a four-octave range centered around middle C, with a pitch resolution of less than two cents (see below), which effectively creates a continuum of infinite frequency resolution. This allows harmonic relationships other than those obtainable with the dodecaphonic equal-tempered tuning system to be auditioned.

The musical examples are synthesized with a TX802 FM Tone Generator manufactured by the Yamaha Corporation. This instrument provides a pitch resolution of 1024 equal divisions per octave, or $1200/1024 \approx 1.1719$ cents, well below the human threshold of pitch discrimination. The programs used to generate the examples were written by the author, and run on an IBM-PC/AT compatible computer. The program listed in Appendix B, used to generate musical examples from the Hénon map, is typical of the software used in the generation of examples from the other systems as well. Communication between the computer and the synthesizer is via Musical Instrument Digital Interface (MIDI), a standard communications protocol widely used in the music industry and by the academic computer music community [49]. Itself a highly parametricized language, MIDI lends itself well to the parametrical description of musical space that underlies the generation of the musical materials in this work.

In MIDI, pitch is expressed as a key number from 0 to 127, where 60 is represents middle C. An additional "pitch bend" message is sent to indicate pitch resolution finer than the semitone. Amplitude is expressed in terms of a parameter called "velocity" (the term alludes to the speed or force with which a key is struck), measured on a scale from 1 (softest) to 127 (loudest). Velocity is not purely a measure of loudness, however. As with acoustic instruments, in which increased amplitude is invariably associated with a brightening of the timbre (i.e., an increase in the energy of the high-frequency spectral components), MIDI velocity is also typically mapped to timbral components of the synthesis algorithm. The more interesting and lifelike sound which results from this strategy hopefully outweighs the potential confusion caused by the linkage of timbre and amplitude in the examples. MIDI does not strictly impose a temporal resolution on the placement of events in time. In the examples, the inter-note onset time (INOT), the time separating the onset of one note from the start of the next, is resolved to 120 pulses per second, or 8.333 milliseconds. The inter-note onset time is either held constant, for those examples which focus only on pitch and velocity relationships, or allowed to vary within a given range in those examples in which one of the orbital coordinates is mapped to rhythm.

A graphical scoring system has been devised to provide a visual reference for the musical examples. The coordinate system of the scores is similar to that of traditional musical notation, in that pitch is read on the vertical axis and time is read horizontally. The biggest difference is that the pitch axis of the graphical scores is continuous, rather than discrete, and the distance of a semitone is everywhere the same, rather than variable

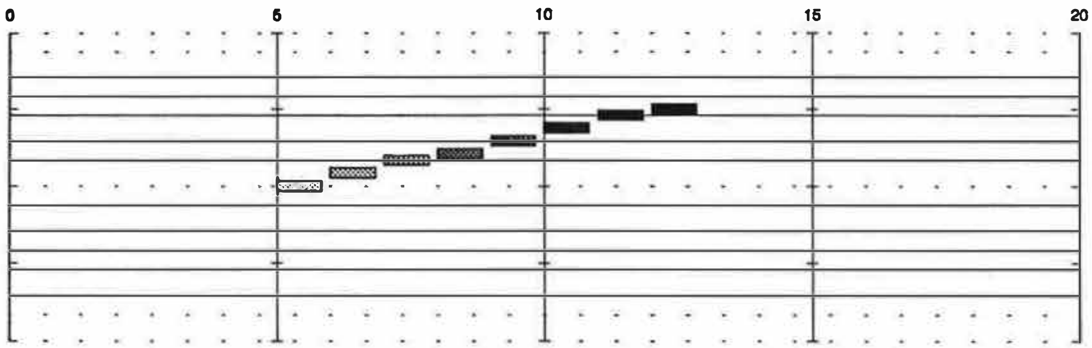

Figure 1.3 Example of the graphical scoring system. A one-octave C major scale is notated. The scale starts softly and increases in volume. Note that the tick marks on each "bar line" indicate the positions of C's, and that the horizontal dashed lines indicate positions where ledger lines would normally be written. Time is measured in five-second intervals.

in size as is the case with traditional notation. This allows an accurate notation of pitch without the use of accidentals, and is as readily adaptable to the notation of infinitely variable pitch as to the equal-tempered scale. For the sake of reference, each score is inscribed with the lines of the traditional grand staff. Time is indicated by vertical bars placed at five second intervals. Each line of score corresponds to twenty seconds in time. Figure 1.3 illustrates the notation of a one-octave C major scale, beginning on middle C. The velocity of each note is conveyed by its shading—the darker a note, the louder it is.

The discussion in the following chapters rests on the foundation of knowledge which has now been established. Relatively few new terms or concepts will be introduced; instead, the discussion will shift to a format in which technical aspects of the new system are explained, followed by a presentation of musical examples which are drawn from the technical illustrations. Comments pertaining to the aesthetic ramifications of these procedures are reserved for the final chapter.

Chapter 2

The Hénon Map

2.1 Technical Description

The Hénon system is a dissipative, two-dimensional iterated map which was first introduced in 1976 by Michel Hénon of the Observatory in Nice [32]. Unlike the other systems discussed in this study, whose derivations all stem from explicit attempts to model various aspects of natural phenomena, the Hénon map has no explicit counterpart in the real world, but is an abstract system formulated for the express purpose of studying chaotic systems in general. At the time the map was introduced, most of the known chaotic dynamical systems were defined as continuous flows in three or more dimensions. The computation of numerical solutions to these flows involves the integration of differential equations, a time-consuming and computationally expensive process. The Hénon map, on the other hand, exhibits all of the interesting features of a higher-dimensional chaotic flow (sensitive dependence on initial conditions, interspersed regimes of chaos and periodicity, complex topological structure, a strange attractor, etc.), but is much easier and faster to compute since it is specified in terms of difference equations. In addition, the inaccuracies which arise inevitably in the process of integration may be avoided altogether, rendering the Hénon system more susceptible to mathematical analysis than a higher-dimensional flow.

The Hénon map is expressed by the equations

$$\begin{aligned} x_{n+1} &= y_n + 1 - Ax_n^2 \\ y_{n+1} &= Bx_n, \end{aligned}$$

where the succession of points (x_0, y_0), (x_1, y_1),...,(x_n, y_n) specifies the orbit on the

n	x_n	y_n	n	x_n	y_n
0	0.000000	0.000000	10	-1.046109	0.354942
1	1.000000	0.000000	11	-0.177139	-0.313833
2	-0.400000	0.300000	12	0.642238	-0.053142
3	1.076000	-0.120000	13	0.369401	0.192671
4	-0.740887	0.322800	14	1.001631	0.110820
5	0.554322	-0.222266	15	-0.293751	0.300489
6	0.347552	0.166297	16	1.179684	-0.088125
7	0.997187	0.104266	17	-1.036442	0.353905
8	-0.287869	0.299156	18	-0.149992	-0.310933
9	1.183140	-0.086361	19	0.657571	-0.044998

Table 2.1 Orbit of the Hénon map in numerical form through the first twenty iterates. $A = 1.4$, $B = 0.3$, the initial point is $(0, 0)$.

plane, and A and B are constant parameters. The equations are nonlinear by virtue of the squared variable x. In his initial discussion of the system, Hénon assigned the values 1.4 and 0.3 to A and B, respectively; these have since become the "classical" values used to produce the familiar form of the attractor; see Figure 2.1. A program to generate orbits of the Hénon map in numerical form may be found in Appendix A.2. Hénon's paper, as well as information presented by Thompson and Stewart [69], and Ruelle [63], provides the substance of the summary of the behavior of the equations which follows.

Table 2.1 presents in numerical form the first twenty iterates of the orbit for the parameter values $A = 1.4$ and $B = 0.3$, from an initial point $(0,0)$. Like the logistic map, the orbit of the Hénon system wanders from point to point along the attractor in an erratic manner. Technically speaking, the attractor itself can never be represented. The points plotted in the three phase portraits of Figure 2.1 lie on the attractor, but they do not comprise it. (A phase portrait or phase plot is simply a plot of the points along an orbit in the phase space of the system.) Iterates 0 through 3 can still be individually distinguished in Figure 2.1(c) (the zeroth iterate lies exactly in the center of the plot), and clearly lie far from the attractor; these points, along with the next two or three, constitute the initial transient portion of the orbit before it settles onto the attractor. There is no specific number of iterates after which one can say the transient portion has ended and the attractor has been reached. For example, although the fourth iterate cannot be individually distinguished in Figure 2.1(c), at a higher resolution it could be, and it would also be seen not to lie on the attractor.

The attractor itself consists of an apparently infinite number of finely spaced

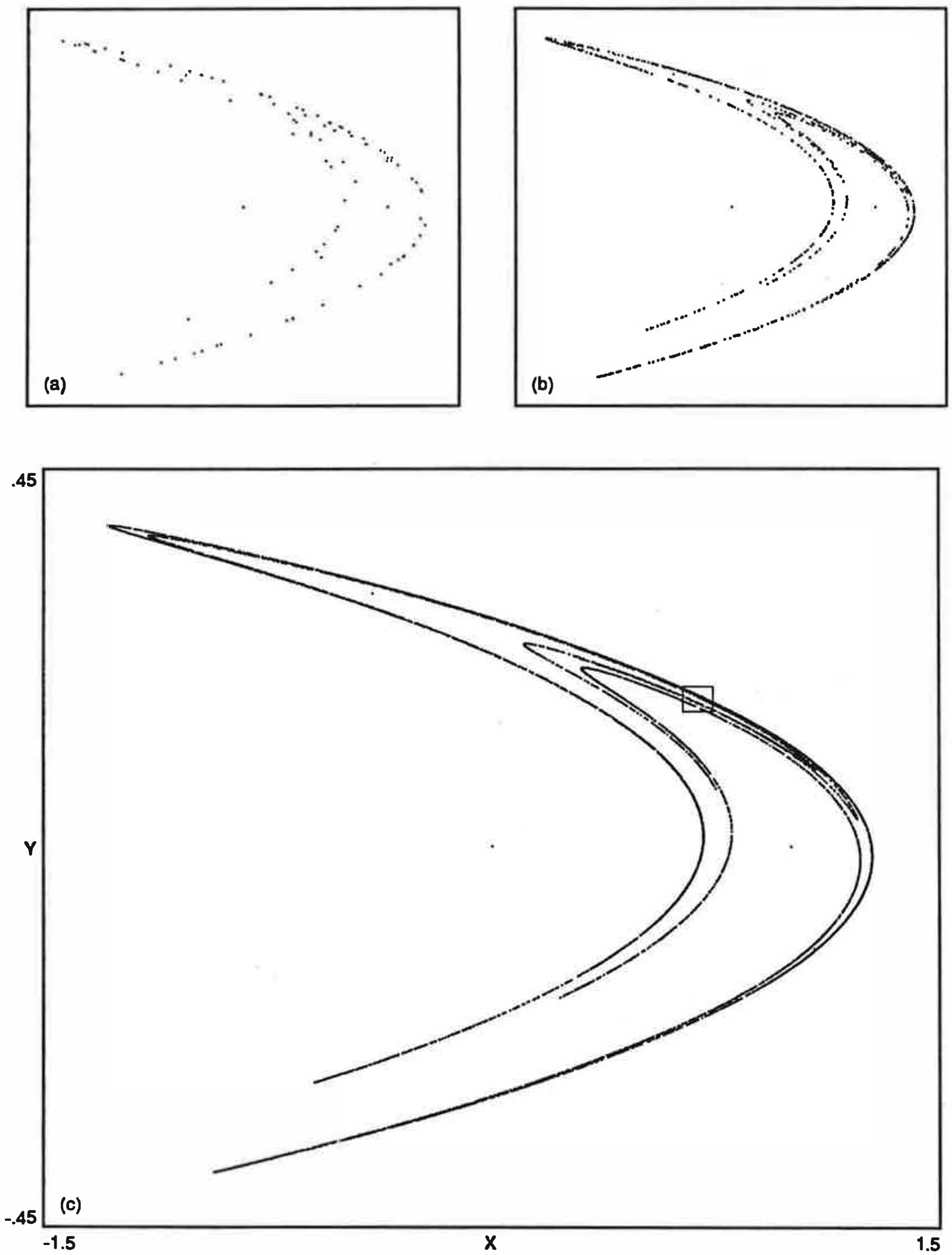

Figure 2.1 The Hénon map, (a) after 100 iterations, (b) after 1000 iterations, (c) after 10000 iterations. The initial point is (0,0), the parameters are $A = 1.4$, $B = 0.3$. The area of the inset square in (c) is magnified in Figure 2.2.

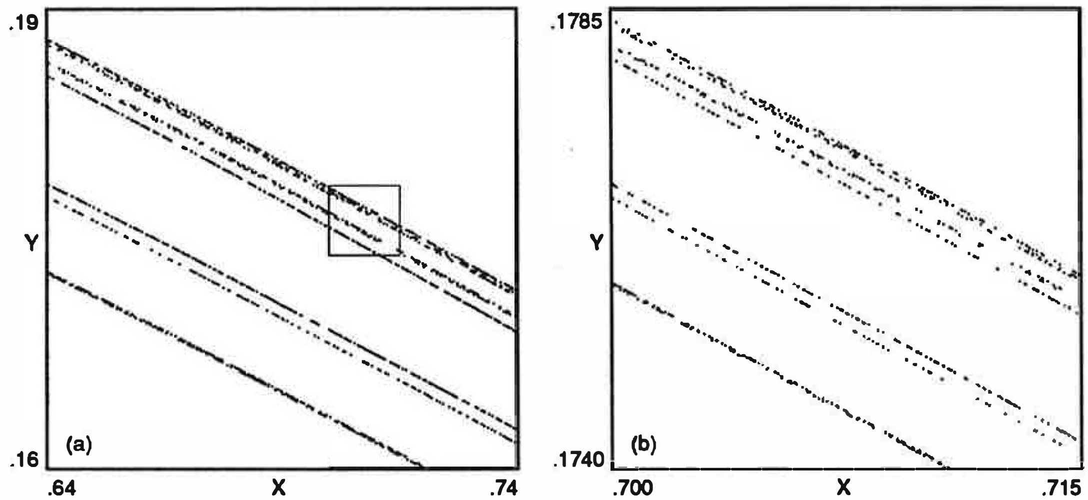

Figure 2.2 Magnification sequence of the Hénon map. Initial conditions are as for Figure 2.1. Note that many more iterations of the map must be computed in order to produce a sufficient number of points to fall within the graphed areas; (a) after 100000 iterations, (b) after 500000 iterations.

filaments, along which the points of a given trajectory are scattered. Figure 2.2 shows a magnified view of the area within the small inset rectangle in Figure 2.1(c). The structure of the spacing of the filaments at different levels of magnification is indicative of the fractal Cantor set structure underlying the Hénon attractor. Note that, due to the increasingly small area graphed in the magnification sequence of Figure 2.2, many more points of the orbit must be computed in order to adequately fill the graphed area.

The *basin of attraction* is that set of points, any one of which taken as an initial point (x_0, y_0) of an orbit, produces an orbit which is stable and is drawn to the attractor. Figure 2.3 shows the basin of attraction as the unshaded area, with the attractor itself superimposed. Points which lie outside the basin of attraction produce orbits which are repelled from this area and escape to infinity.

Like the logistic equation, the form of the Hénon attractor varies as the parameter values A and B change. The bifurcation diagrams shown in Figures 2.4 through 2.6 exhibit a period-doubling cascade quite similar in form to that of the logistic equation, followed by a regime of chaos interspersed with periodic windows of varying widths. These diagrams were made by holding the parameter B constant at 0.3 and sweeping A across the range of values indicated for each diagram. Phase plots corresponding to some of the values indicated in the diagrams with vertical dotted lines are shown in Figure 2.7. Note the correspondence, for example, between the four and six-band chaotic regimes

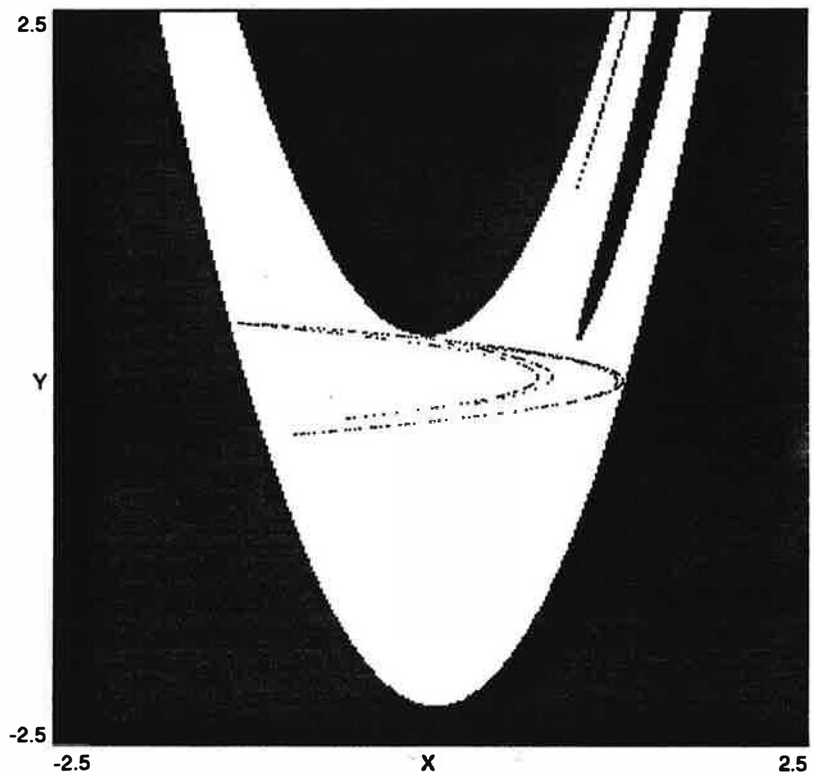

Figure 2.3 Basin of attraction of the Hénon map, with the attractor superimposed, for parameters $A = 1.4$, $B = 0.3$. Any orbit starting from a point in the shaded area is repelled from the basin of attraction and tends to infinity.

located at $A = 1.076$ and $A = 1.078$ in both the bifurcation diagrams and in the two plots of Figures 2.7(b) and (c). Figures 2.7(c) and (d) illustrate co-existing attractors for the *same* value of A emerging from different initial points of the orbit. Other marked positions in the bifurcation diagrams correspond to orbits chosen for the musical examples following in the next section. The orbit marked at $A = 1.3$, even though appearing to be be located squarely within a regime of chaos, is actually positioned in a very narrow period 7 window which does not show up at the resolution of Figure 2.5.

For the sake of comparison, a bifurcation diagram sweeping the parameter B and holding A constant is shown in Figure 2.8. Bifurcation diagrams plotting changes in y may be produced as well, and are similar in appearance to those plotted against x, except for the change in scale. The behavior of both variables is globally similar: if x is periodic, y is also periodic, if x varies chaotically, so does y.

Further discussion on the Hénon map may be found in Shaw [64], Eckmann and Ruelle [21], Ruelle [62], and Froehling, et al. [25].

2.2 Musical Examples

Musical mappings of the Hénon system exploring a range of characteristic behaviors were made over nine different values of the parameter A. These values—0.2, 0.5, 1.0, 1.046, 1.054, 1.076, 1.078, 1.3, and 1.4—may all be located among the phase plots and bifurcation diagrams in the preceding section. The initial point (0,0) is used for all examples (Example 10 excepted), and the parameter B is held constant at 0.3 throughout.

There are a large number—infinite, actually—of possible mappings of the phase space to the musical domain. Each of the variables x and y could be mapped to any one of the musical parameters; in addition, a variety of orientations are possible. For example, values along each axis could be mapped *inversely* to a given parameter, such that an increase in the value along the axis would cause a decrease in the value of the musical parameter. The phase space could be quantized, interpreted logarithmically, or multiplied by itself. Clearly a comprehensive exploration of possible mapping configurations would take several lifetimes. A more calculated approach is required.

Four different configurations mapping variables of the equations to specific musical parameters have been employed, summarized in Table 2.2. Configurations (a) and (b) provide mappings only to pitch and velocity, and hold the rate of note succession

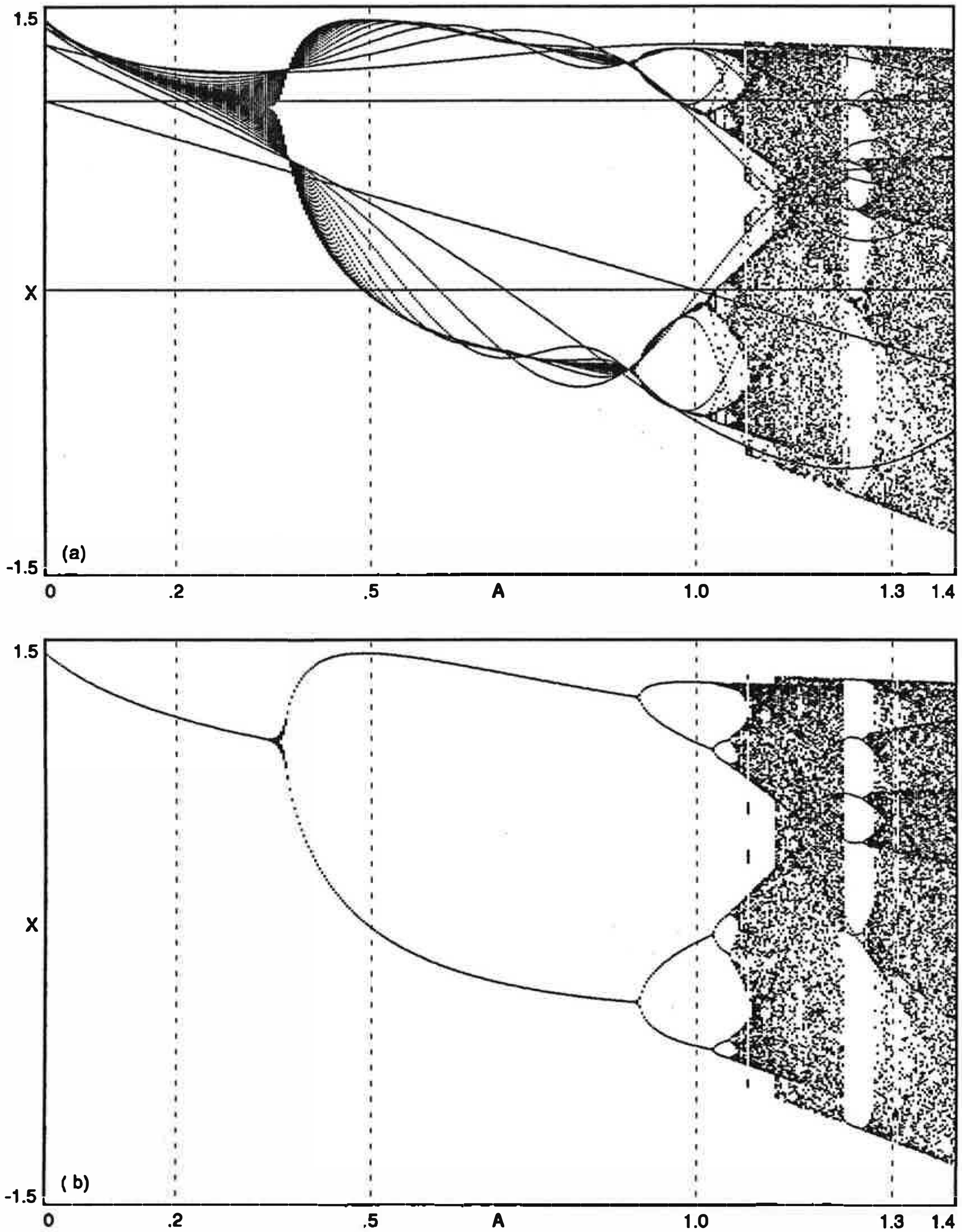

Figure 2.4 Bifurcation diagrams of the Hénon map comparing (a) initial transient behavior (the first 150 iterations) to (b) settled, stable behavior (the next 150 iterations). Each plot sweeps parameter A from 0 to 1.4, holding B constant at 0.3. The initial point of all orbits is the origin, (0,0).

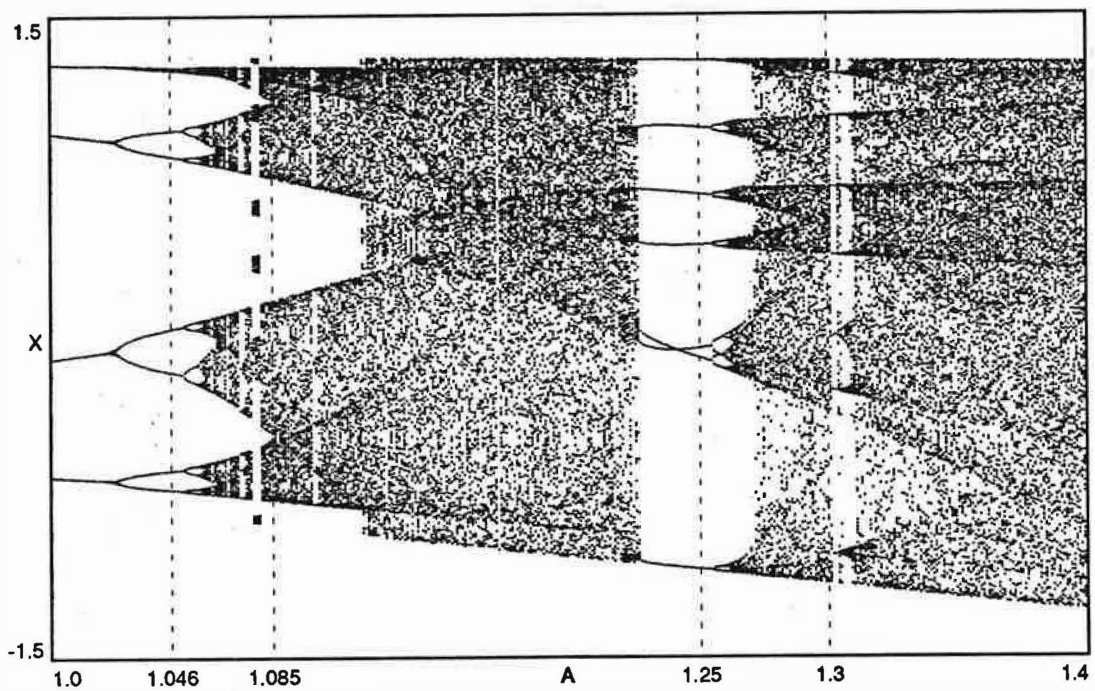

Figure 2.5 Magnification of a section of the bifurcation diagram from $A = 1$ to $A = 1.4$. A period 16 bifurcation is discernible just before the onset of the chaotic regime at approximately $A = 1.055$. Note the large period 7 window around $A = 1.25$, as well as other, less extensive regimes of periodicity interspersed through the chaotic regime. This diagram shows the settled behavior of the system.

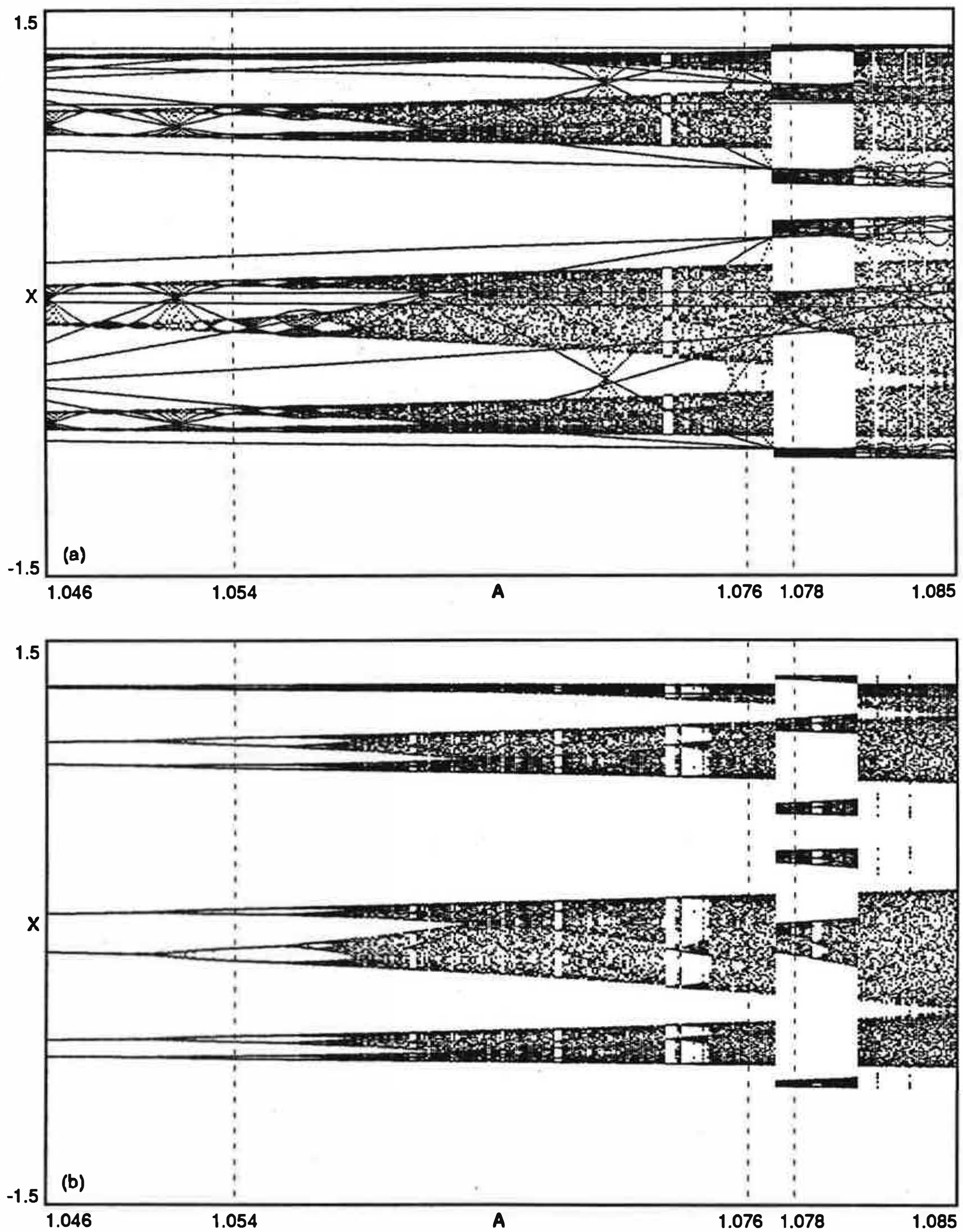

Figure 2.6 Further magnification of the Hénon bifurcation diagram, focusing on the transition to turbulence. The two illustrations plot (a) transient behavior (the first 150 iterations), and (b) settled behavior (the next 150 iterations). At this level of resolution, an additional period 32 bifurcation can be barely discerned just above $A = 1.054$. Note as well the abrupt shift in the structure of the attractor, from four bands of chaos to six, which occurs between $A = 1.076$ and $A = 1.078$.

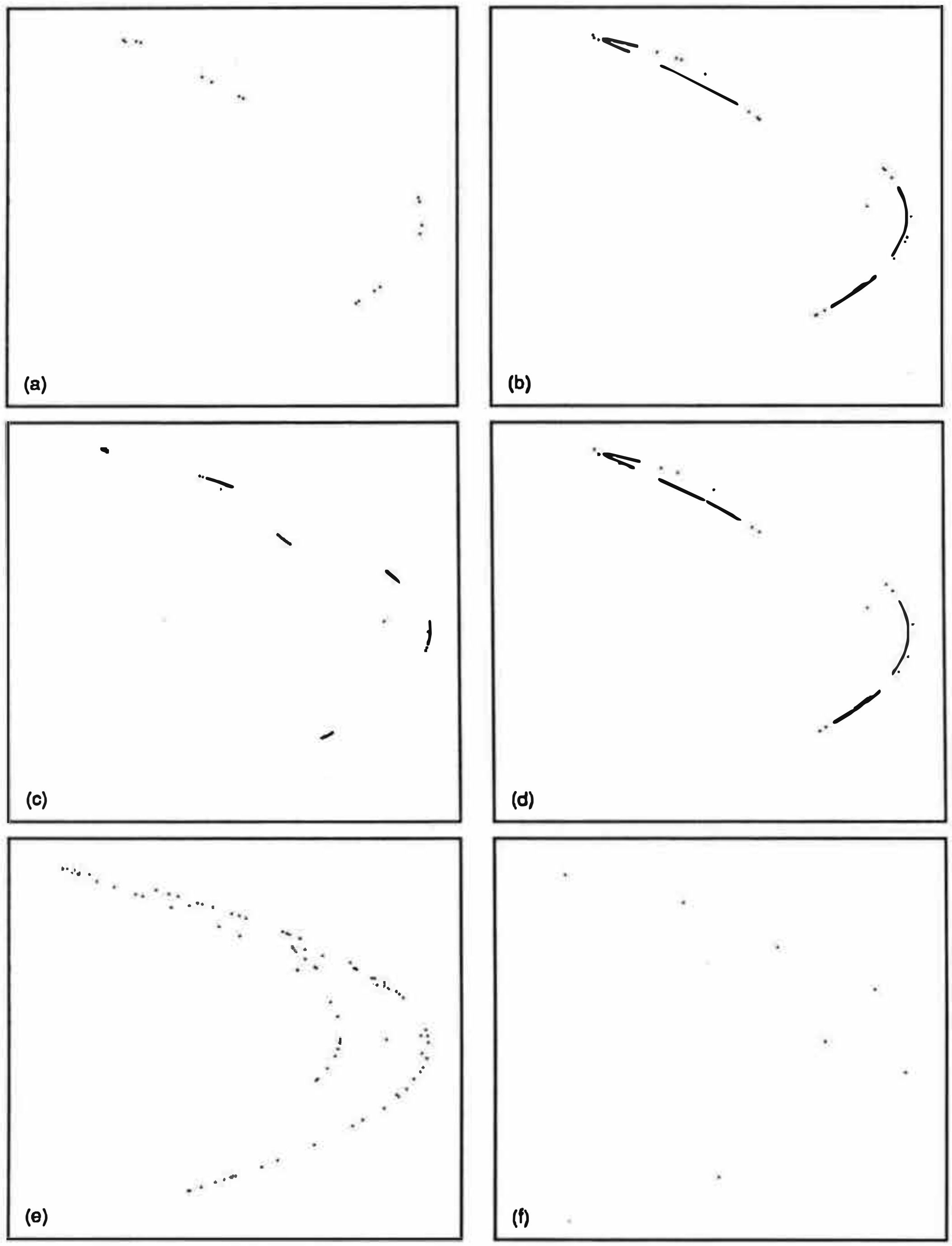

Figure 2.7 Phase portraits of the Hénon map. Parameter $B = 0.3$ for all orbits. Initial point is the origin $(0, 0)$ for all orbits except (d); (a) period 16 orbit at $A = 1.054$, (b) chaotic attractor at $A = 1.076$, (c) chaotic attractor at $A = 1.078$, (d) co-existing chaotic attractor at $A = 1.078$, from initial point (.1, 0), (e) first 150 iterations of apparently chaotic orbit at $A = 1.3$, however, (f) period 7 orbit emerges from chaos after approximately 120 iterations at $A = 1.3$.

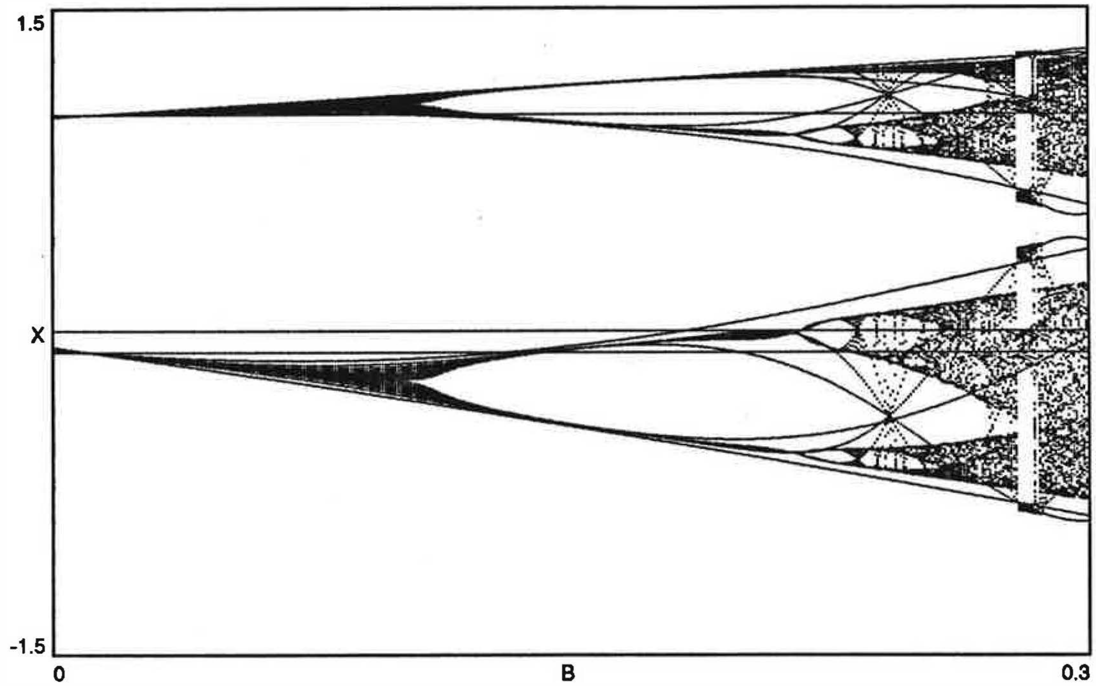

Figure 2.8 Bifurcation diagram of the Hénon attractor, plotting B against x. Parameter A is constant at 1.1 for all trials. The first 150 points of each orbit are plotted.

(INOT) constant. Configuration (c) maps velocity and INOT only, and holds pitch constant. Configuration (d) is like (c), but maps pitch according to the sum of the squares of the two variables. (This idea of creating additional handles onto a dynamical system by performing simple arithmetic operations on the variables was suggested by Edward Lorenz in conversation [40].) For all configurations, the extent of the Cartesian phase space was taken to be -1.43 to 1.43 on the x-axis, and -0.43 to 0.43 on the y-axis. These values were discovered empirically to encompass the totality of the phase space of the Hénon map under the conditions employed in the musical examples.

Each mapping configuration results in a characteristic musical texture. The rate at which notes succeed one another in the examples may be either a constant or a variable quantity. This rate is specified in terms of a number of clock pulses. Since a clock rate of 120 pulses per second is used consistently in the generation of the examples, a note succession rate of 30 indicates four notes per second, while a variable rate of 0–60 indicates that the inter-note onset time varies between zero and a half of a second. The number of notes in each example is equal to the number of iterations n through which the orbits are computed. Graphic scores for all examples except those of configuration (c) are included in the following figures. Note that some of the scores are truncated before the end of the recorded example to which they correspond.

The first several examples are straightforward and require little explanation or comment. Example 1(a) begins with an oscillation between two values which, during a brief transient phase, is quickly damped to a single point, a sequence of repeated notes. In Example 2(a), the transient phase consists of a widening oscillation which stabilizes on a period 2 attractor. Examples 3(a) and 3(b) illustrate the sometimes subtle effect that switching the mapping configuration can have on the musical texture. The transient portion of the sequence appears shorter at first glance than it does in Examples 1(a) and 2(a), but in fact it is just about as long, requiring 16 iterations before it stabilizes. Example 3(c) demonstrates the effect of a period 4 orbit from a purely rhythmic perspective. In Example 4(a), the transient portion is both longer and more irregular than in the previous examples. The period 8 orbit is finally stabilized after twelve seconds. Examples 5(a), 5(b) and 5(c) are presented at a quicker rate for variety. The period 16 oscillation follows a short transient phase. Again, the effect of the switch in the mapping configuration between (a) and (b) is subtle. Example 5(c) employs the snare drum timbre.

Examples 6(a), 6(b) and 6(d) are taken from a regime in which the phase space is divided into four distinct bands of chaos. In the score to Examples 6(a) and 6(b), two broad layers are easily perceived. Each of these layers is in turn subdivided into two bands. In the lowest band of the lowest layer, extending from approximately B–D♯ in the octave below middle C, a downward-tending three-note pattern is apparent as the primary constituent, in which a longer pattern of either four or five notes is interspersed. The second band, extending from approximately the F♯ below middle C to the D above, is similar to the first band, but with a contrary sense of motion. In the upper layer, the third band, from the C an octave above middle C to the F♯ above that, is similar to the lowest band, but with a slightly wider ambitus. The fourth and highest band is also like the first and third, but compressed in ambitus and offset in phase slightly. Example 6(b) illustrates the subtle effect of switching the mapping configuration. However, the configuration used in 6(d) presents a new disposition of material, in which the ranges of the two middle bands overlap around the F below middle C. Note that in this example, pitch varies according to the sum of the squares of x and y.

Six distinct chaotic bands determine the texture of Examples 7(a) and 7(d). The effect is of greater regularity or periodicity than in Example 6, because of the reduced

Configuration	*Pitch*	*Velocity*	*INOT*
(a)	y	x	—
(b)	x	y	—
(c)	—	x	y
(d)	$x^2 + y^2$	x	y

Table 2.2 Mapping configurations of the musical examples.

range in which the values of each band may vary. The configuration of 7(d) superimposes two of the bands along the pitch axis, in the bottom of the range. Examples 8(a) and 8(d) illustrate an interesting sequence in which a long transient phase eventually settles into a period 7 orbit.

Examples 9(a), 9(b) and 9(d) are generated from the full-blown chaotic attractor plotted in Figure 2.1. The effect of the switch in the mapping configuration between (a) and (b) is both audibly and visually more distinct than in prior examples of such a switch. Note that in (a), louder notes are clustered in the middle of the range, whereas in (b) the disposition of the attractor in space, allied with the mapping configuration, has the effect of placing medium-velocity notes at the top of the range, while simultaneously increasing and decreasing note velocities toward the bottom of the pitch range in superimposed layers. The loud layer extends the lowest into the pitch range and produces the auditory illusion of a separate bass line. In Example 9(d) this orientation is more or less reversed, with the medium-velocity notes in the lowest part of the pitch range. A hocketing effect is heard in all three of these examples as the ear forms independent melodic lines from notes of similar velocity levels arrayed within consistent registral dispositions.

Example 10(a) is an example of sensitive dependence on initial conditions as applied to the generation of harmony. Three voices are generated synchronously, which proceed from initial points which are very close together: (0.000000, 0), (0.000001, 0), and (0.000002, 0). The three voices/orbits remain virtually identical through at least twenty iterations before the effect of their different initial positions precipitates a rapid divergence of the orbits from one another. Note that the first voice in this example (the one which begins exactly at the origin) is identical with the sequence in Example 9(a), with the reduced tempo taken into account.

Example	*Attractor*	*A*	*Rate*	*n*	*Graphic Score*
1(a)	single-point	0.2	30	50	Figure 2.9
2(a)	period 2	0.5	30	50	Figure 2.9
3(a)(b) 3(c)	period 4	1.0	30 0-60	50	Figure 2.10 —
4(a)	period 8	1.046	30	80	Figure 2.10
5(a)(b) 5(c)	period 16	1.054	15 0-30	100	Figure 2.11 —
6(a)(b) 6(d)	chaos (4 bands)	1.076	15 0-30	200	Figure 2.12
7(a) 7(d)	chaos (6 bands)	1.078	30 0-30	200	Figure 2.13
8(a) 8(d)	period 7	1.3	30 0-60	150	Figure 2.14
9(a) 9(b) 9(d)	chaos	1.4	15 15 0-30	350	Figure 2.15 Figure 2.16 Figure 2.18
10(a)	(three voices)	1.4	90	80	Figure 2.19

Table 2.3 Format of the musical examples.

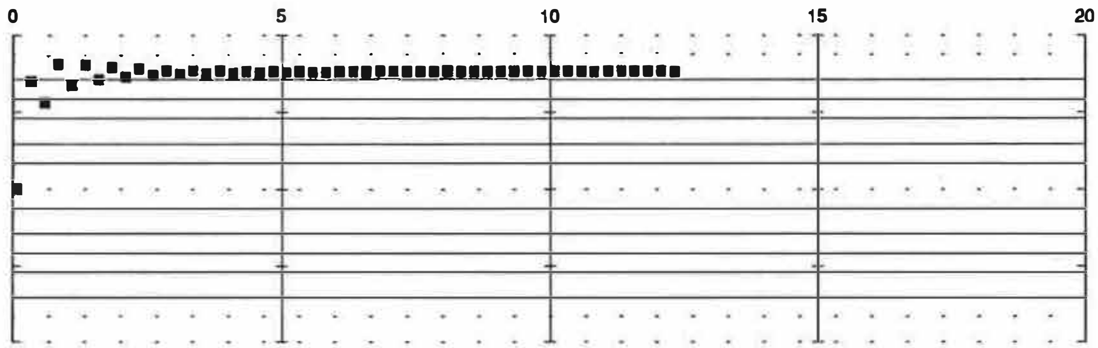

Example 1(a)

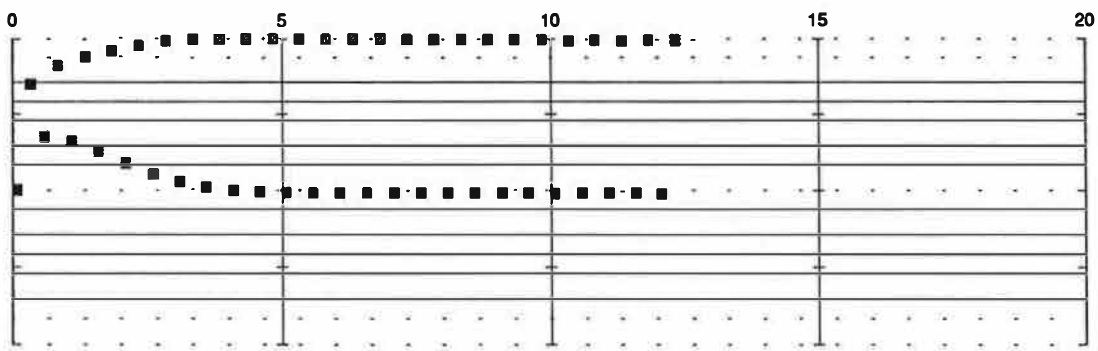

Example 2(a)

Figure 2.9 Scores to Example 1(a), single-point attractor; and to Example 2(a), period 2 oscillation.

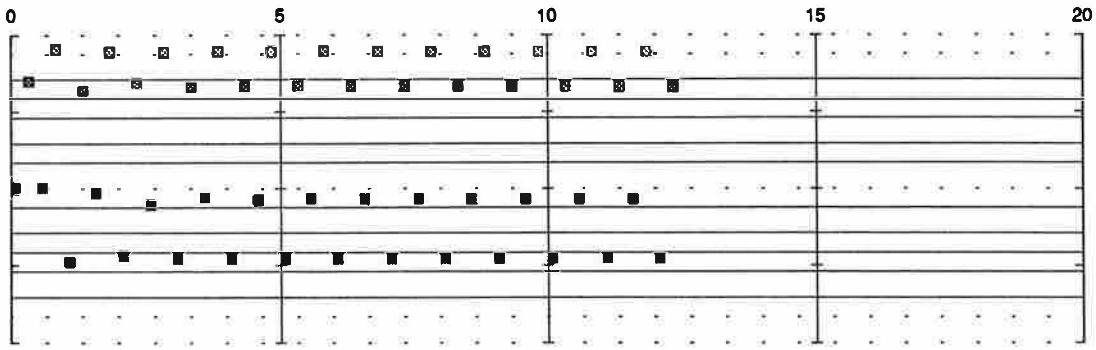

Example 3(a)

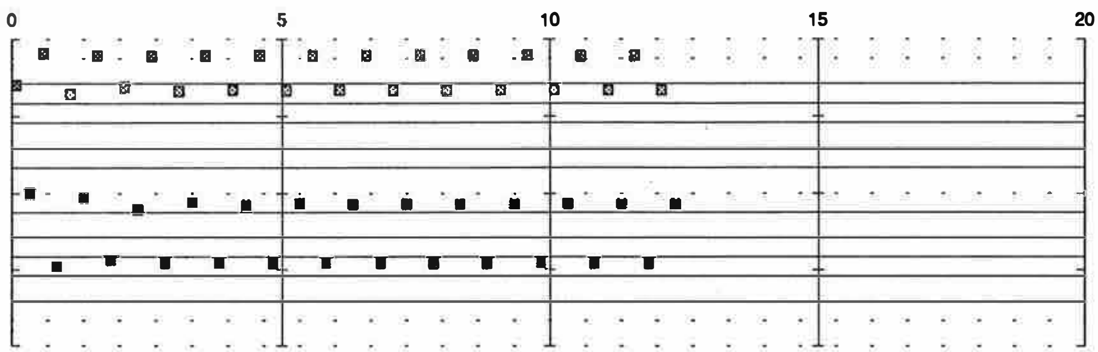

Example 3(b)

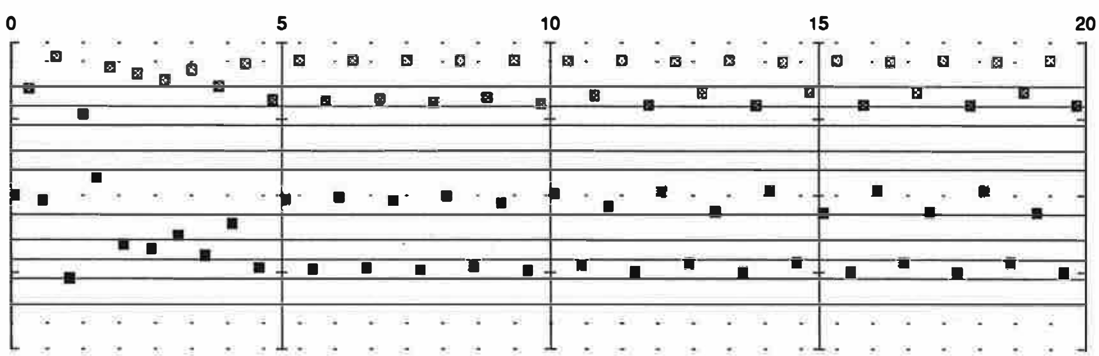

Example 4(a)

Figure 2.10 Scores to Examples 3(a) and 3(b), period 4 oscillation; and to Example 4(a), period 8 oscillation.

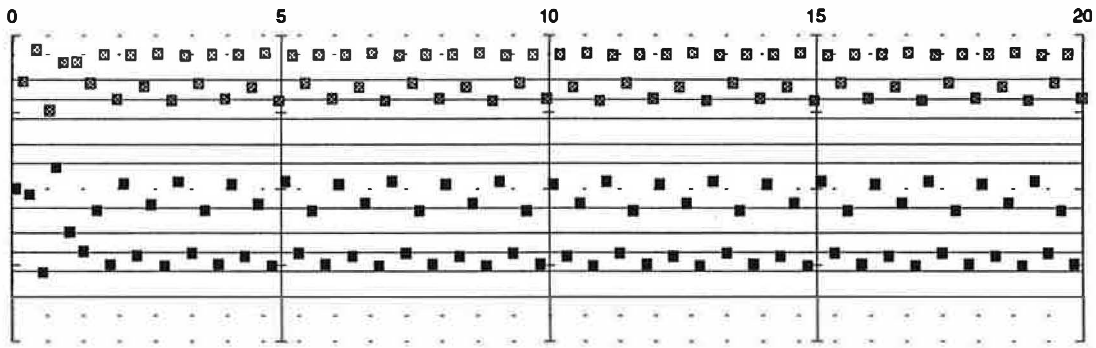

Example 5(a)

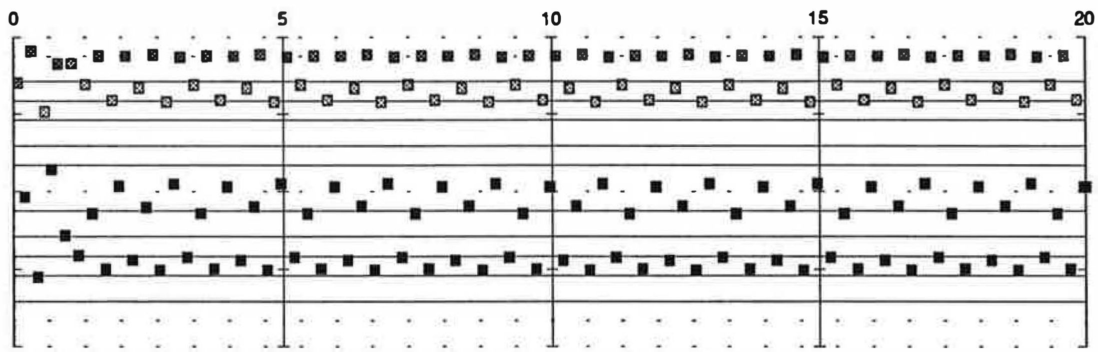

Example 5(b)

Figure 2.11 Scores to Examples 5(a) and 5(b), period 16 oscillation.

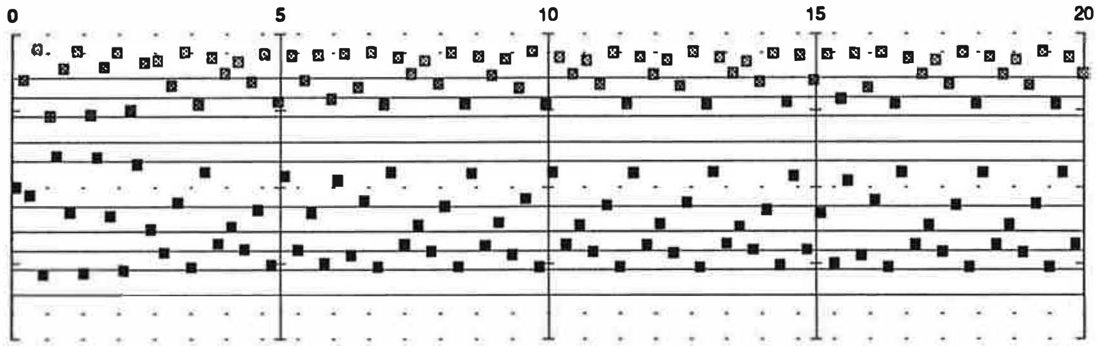

Example 6(a)

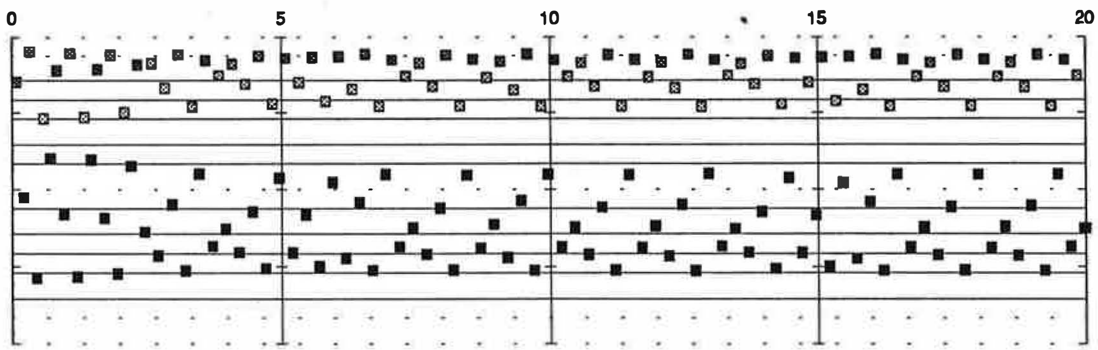

Example 6(b)

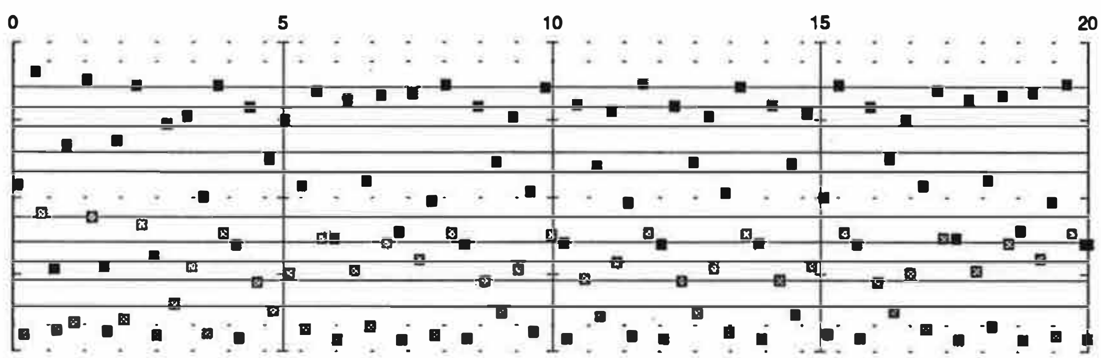

Example 6(d)

Figure 2.12 Scores to Examples 6(a), 6(b) and 6(d), chaos in four bands.

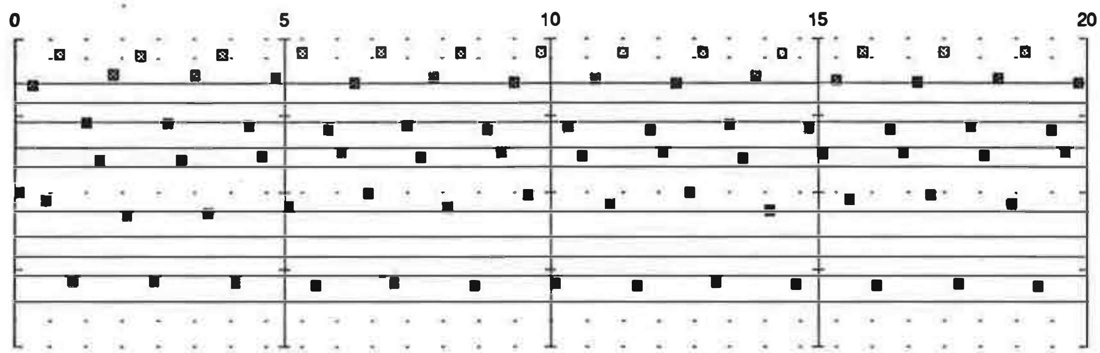

Example 7(a)

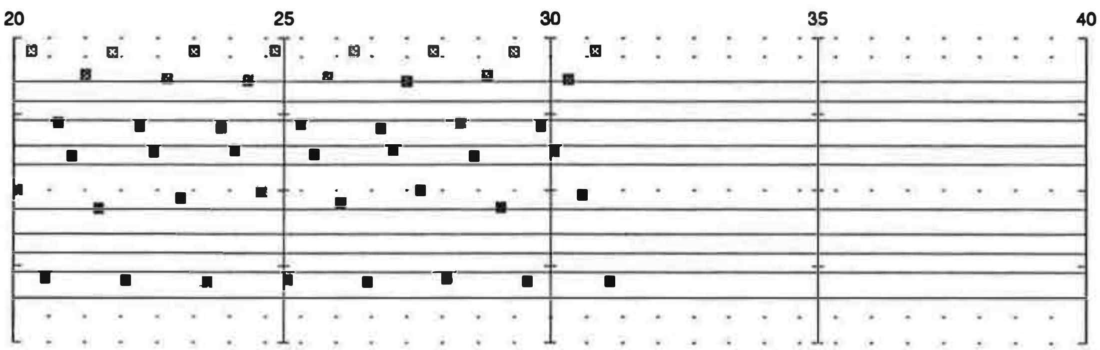

Example 7(a)

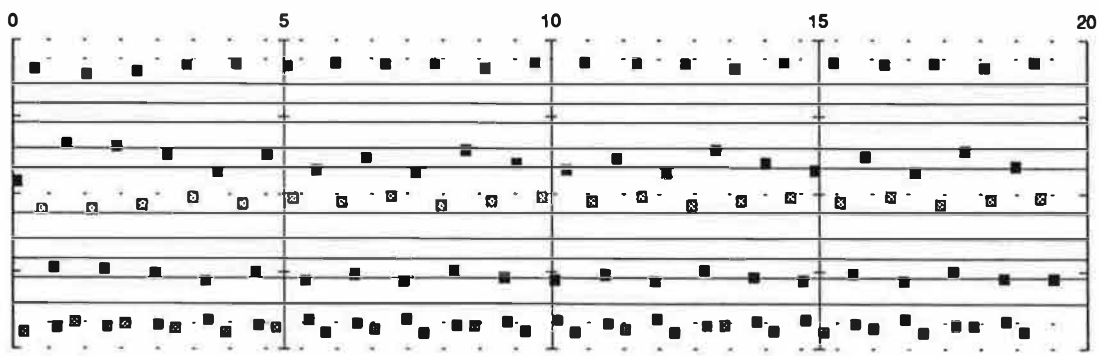

Example 7(d)

Figure 2.13 Scores to Examples 7(a) and 7(d), chaos in six bands (noisy periodicity).

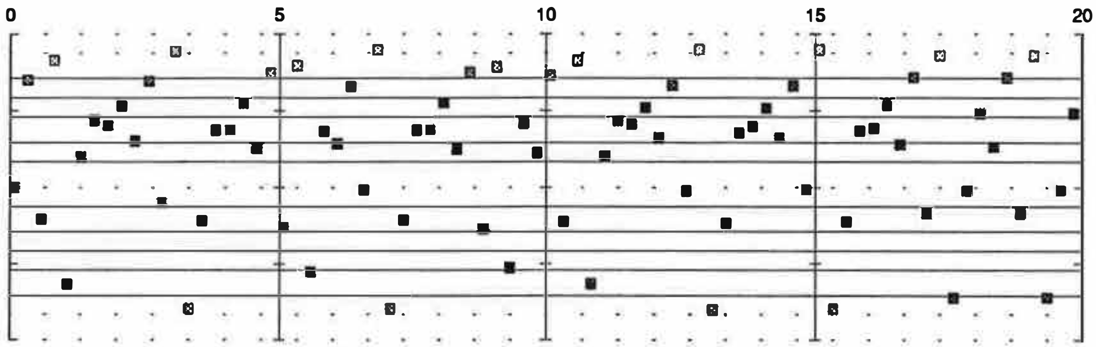

Example 8(a)

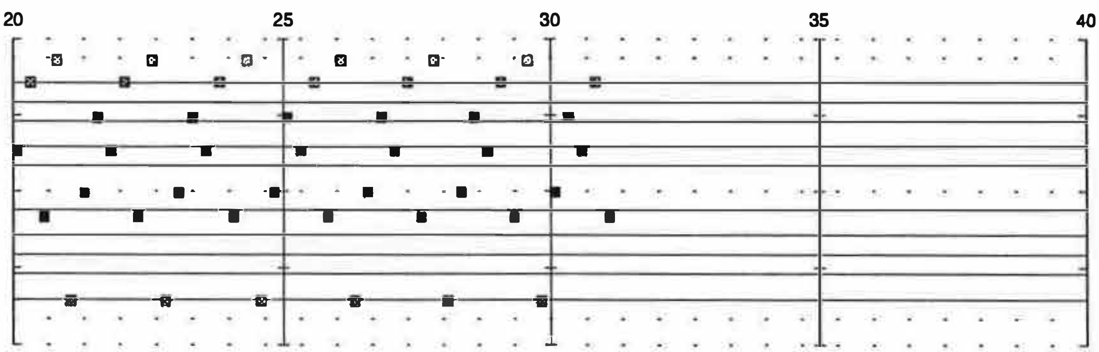

Example 8(a)

Figure 2.14 Score to Example 8(a), period 7 oscillation.

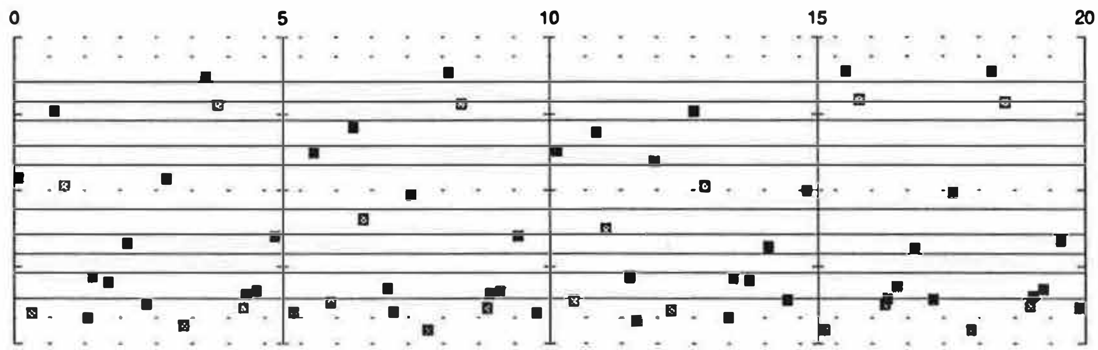

Example 8(d)

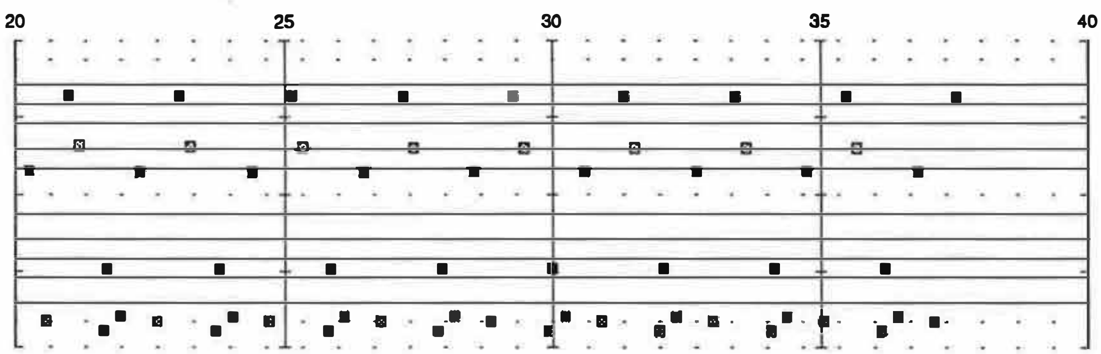

Example 8(d)

Figure 2.15 Score to Example 8(d), period 7 oscillation.

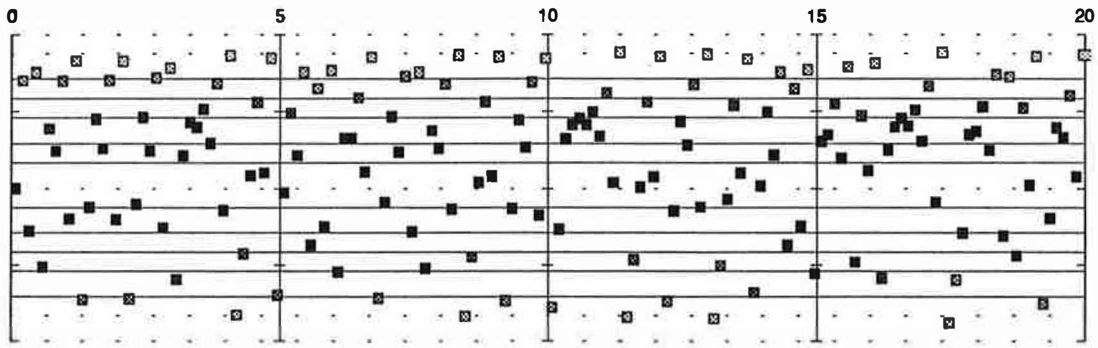

Example 9(a)

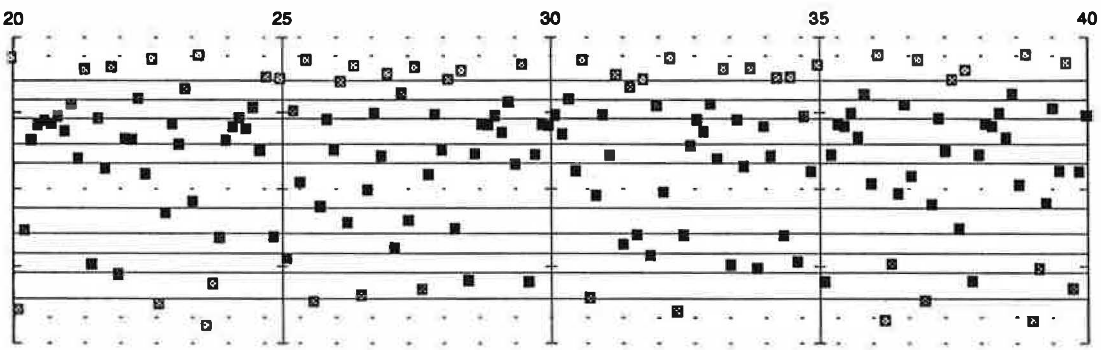

Example 9(a)

Figure 2.16 Score to Example 9(a), chaotic sequence.

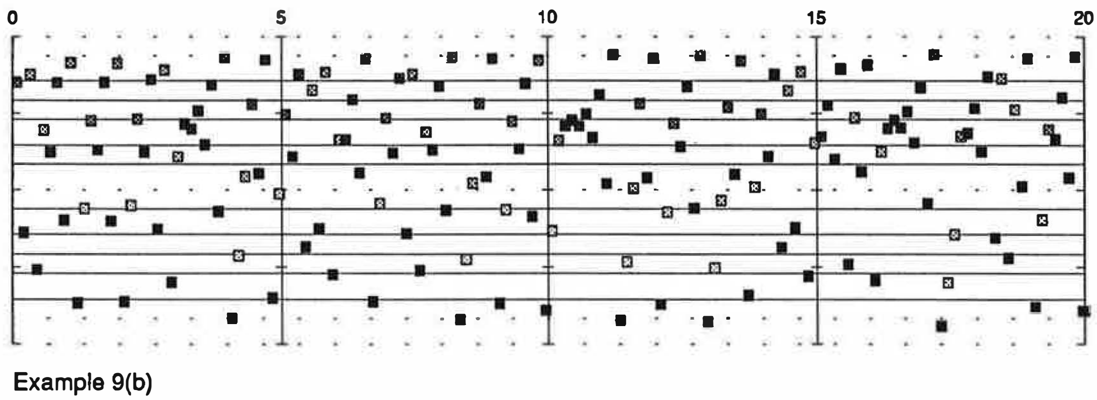

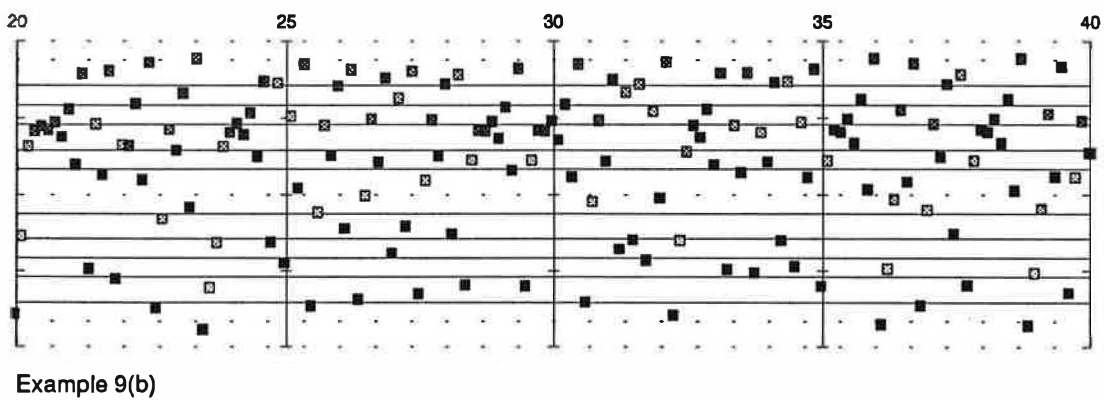

Figure 2.17 Score to Example 9(b), chaotic sequence.

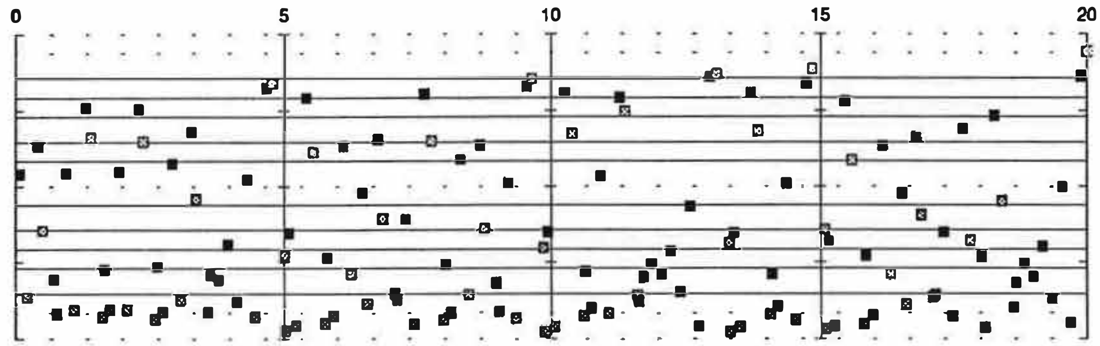

Example 9(d)

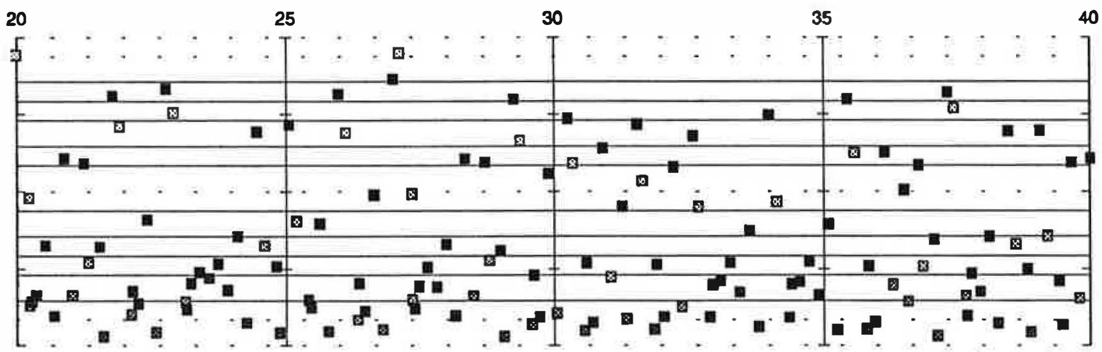

Example 9(d)

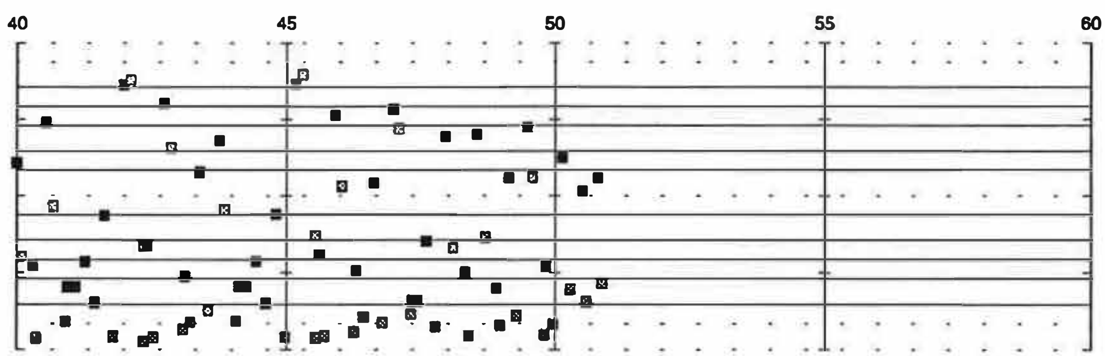

Example 9(d)

Figure 2.18 Score to Example 9(d), chaotic sequence.

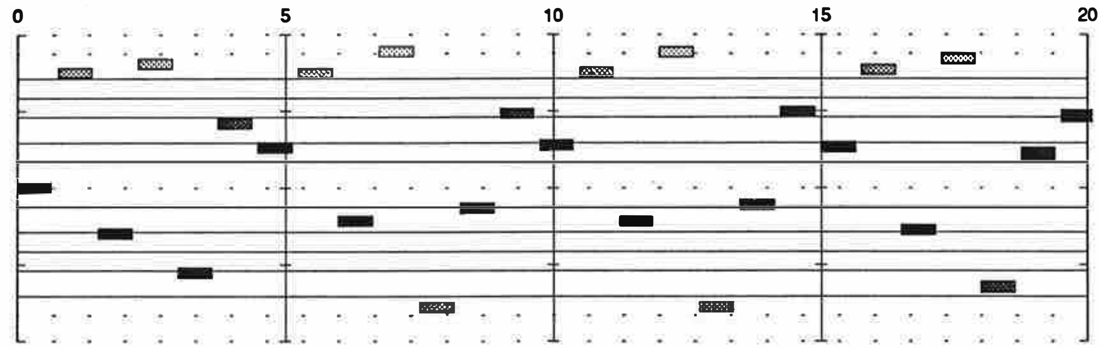

Example 10(a)

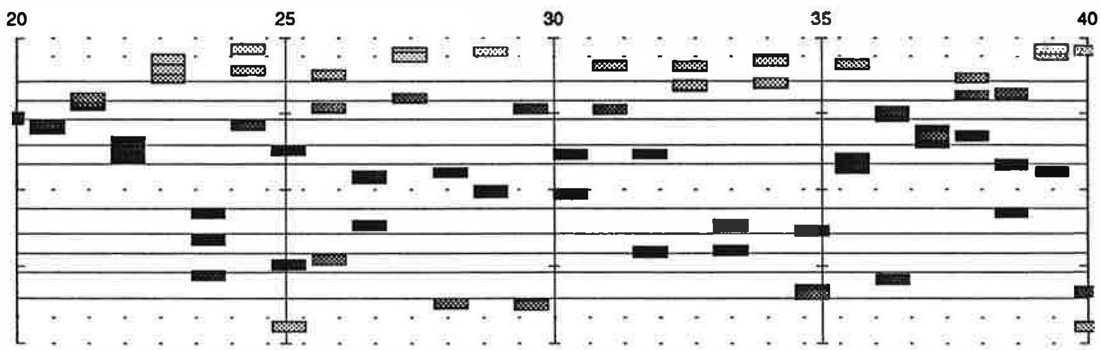

Example 10(a)

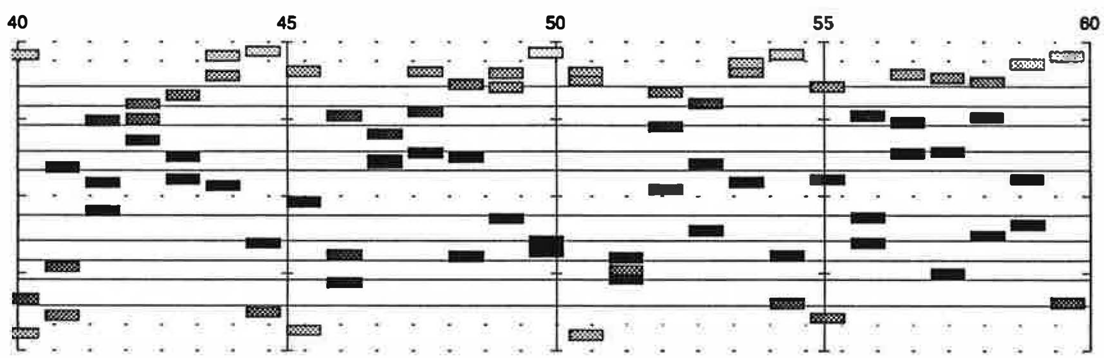

Example 10(a)

Figure 2.19 Score to Example 10(a), three voices proceeding from almost the same initial point, demonstrating sensitive dependence on initial conditions.

Chapter 3

The Lorenz System

3.1 Technical Description

The earliest explicit recognition that stable regimes of chaotic behavior could arise spontaneously from the dynamics of a system of nonlinear equations is generally attributed to mathematician and meteorologist Edward Lorenz, whose landmark 1963 paper entitled "Deterministic nonperiodic flow" [41] describes the system named after him. From a conventional model of the dynamics of fluid convection, Lorenz evolved a simplified version expressed as a system of three partial differential equations:

$$\begin{aligned}\dot{x} &= \sigma(y - x)\\ \dot{y} &= Rx - y - xz\\ \dot{z} &= xy - Bz,\end{aligned}$$

where σ, R and B are positive constant parameters. The system becomes unstable if any of these parameters is negative. The equations are nonlinear by virtue of the multiplication of the variable x with each of the other two variables of the system. Solutions to the equations may be described as a continuous trajectory or a flow embedded in a three-dimensional Euclidian space. The equations specify a dissipative system whose basin of attraction encompasses all of real space. A program to generate orbits of the Lorenz system may be found in Appendix A.3.

The clear exhibition of extreme sensitivity to initial conditions that Lorenz was able to demonstrate in the behavior of this system had profoundly negative implications for the feasibility of long-term weather prediction. Since, by definition, an accurate measurement of the instantaneous state of the atmosphere is impossible (because of the finite resolution of measuring devices), then the long-term predictions of any computer simulation used to model atmospheric conditions forward from the present state will eventually diverge exponentially from the actual conditions. This situation has come to be known as the "butterfly effect," because of the implication that a phenomenon as seemingly insignificant as the flutter of a butterfly's wings in Japan may exert an enormous influence on the weather in California a week later.

Lorenz adopted the parameter values $\sigma = 10, R = 28$ and $B = 8/3$ in his numerical study of the equations. These values reveal a chaotic attractor bounded within a region of space whose extent is a function of the three constant parameters. The orbit along the attractor describes an alternating sequence of spiral revolutions around two *stationary points*, P1 and P2, located at $(\sqrt{B(R-1)}, \sqrt{B(R-1)}, (R-1))$ and $(-\sqrt{B(R-1)}, -\sqrt{B(R-1)}, (R-1))$; see Figures 3.1 and 3.2. A typical orbit spirals out from one of the stationary points a variable number of times (as few as one, or as many as 50 or more revolutions) until it is attracted towards the neighborhood of the other stationary point, and begins the cycle again.

Like the logistic equation and the Hénon map, the Lorenz system exhibits regimes of single-point attraction, periodicity, and chaos. The creation of bifurcation diagrams for the Lorenz system, however, is extraordinarily more expensive and time-consuming to compute due to the fact that the equations must be integrated over extended spans of time in order for the underlying order to become apparent. In his extensive survey of the system, Sparrow [65] provides several hand-drawn sketches of the locations of some of the bifurcation nodes in the total phase space. It is from Sparrow's study that the following summary of the global behavior of the system is condensed.

A third stationary point (in addition to P1 and P2) exists at the origin (0, 0, 0), and is stable for all parameter values—meaning that any orbit which begins there, stays there. The origin is also globally attracting for $0 < R < 1$, meaning that all orbits tend toward the origin and remain there if $R < 1$, no matter where they are initiated.

The z-axis is invariant for all parameter values. Any orbit which starts on the z-axis (the line in the phase space along which both x and y are 0) will remain on that axis and tend toward the origin.

The critical value $R \approx 24.74$ marks a reversal in the character of the two stationary points P1 and P2. At the supercritical value adopted by Lorenz, $R = 28$, these two points are non-stable or repelling, whereas at subcritical values of R, they are stable or attracting. In other words, for subcritical values of R, all orbits are attracted to one

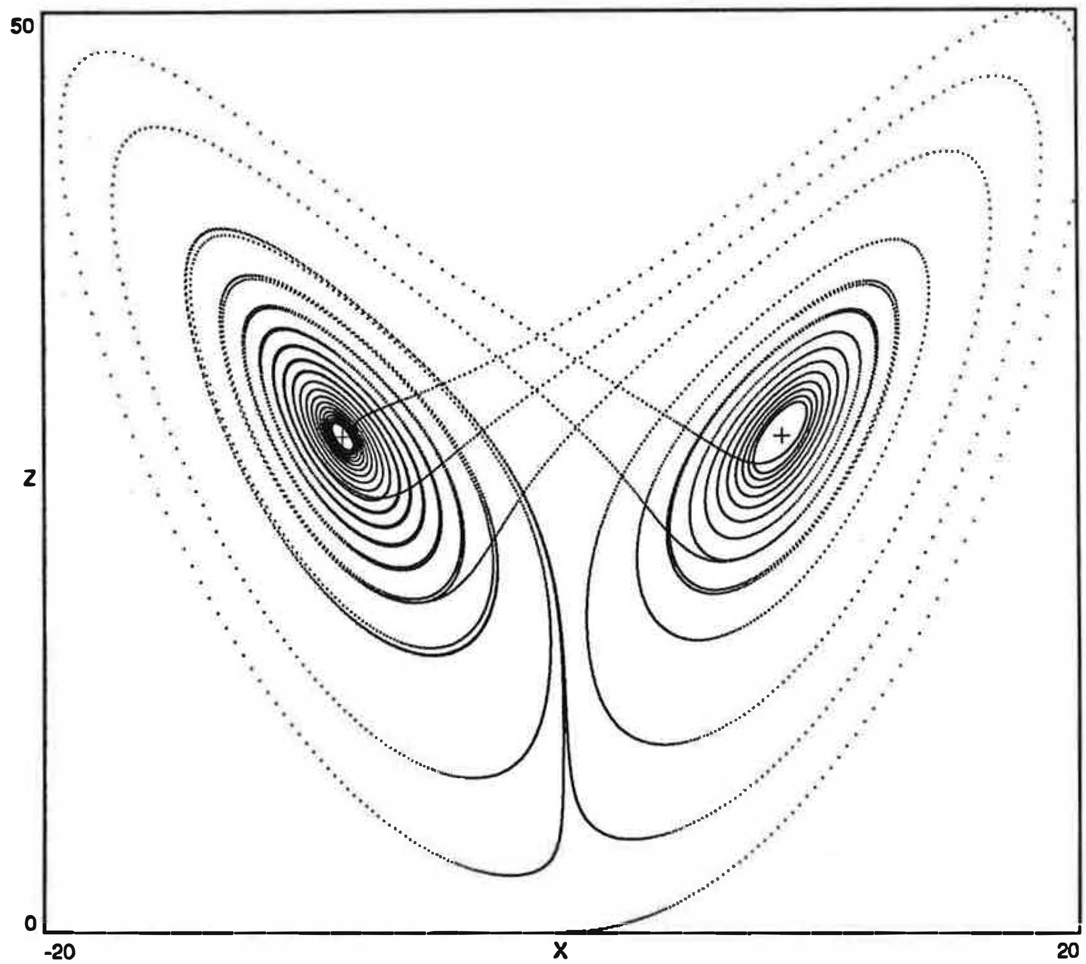

Figure 3.1 Phase portrait of the Lorenz system projected onto the (x, z) plane along the y-axis. The attractor lies within a region of real space measured in the positive direction along the z-axis. The crosshairs at the centers of the two lobes mark the locations of the two stationary points P1 and P2. Constant parameters are $\sigma = 10$, $R = 28$, $B = 8/3$. The initial point is (0.1, 0.1, 0.1), located at the bottom of the graph right above the "X".

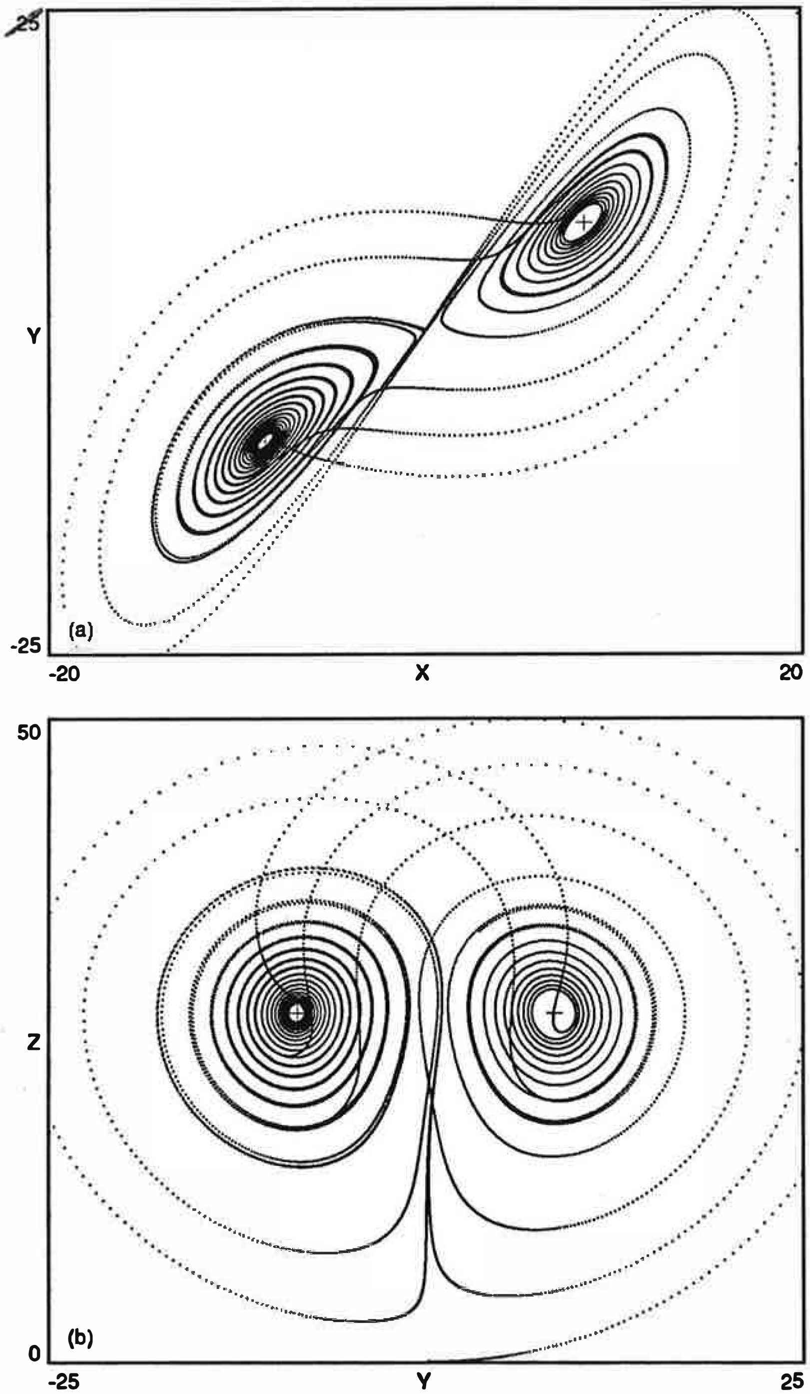

Figure 3.2 Phase portraits of the Lorenz system projected onto (a) the (x, y) plane, and (b) the (y, z) plane. Crosshairs mark the locations of the stationary points. Parameters values and initial point are the same as for Figure 3.1. Both graphs plot the same orbit.

of the stationary points P1 or P2, or to the origin. Orbits are not necessarily chaotic for all super-critical values of R, however. Regimes of periodicity are interspersed within regimes of chaos across a wide range of values. Figure 3.3(a) illustrates a periodic orbit at $R = 150$. A change in the value of parameter B to 0.25, however, while leaving R at 150, produces another chaotic orbit; see Figure 3.3(b).

An alternate perspective on the structure of continuous dynamical systems is afforded by the *surface of section* obtained by plotting the intersection of the trajectory with a plane which slices through that trajectory. The resulting two-dimensional map plots the position of the trajectory as it "punctures" the plane of the section. A method of analysis of dynamical systems based on this procedure was developed by Poincaré toward the end of the nineteenth century. Also called Poincaré sections or return maps, these two-dimensional reductions of the dynamics of a higher-dimensional flow bear a strong resemblance to iterated maps such as the Hénon system. For example, a Poincaré section of a periodic orbit would show simply as a few points on the plane, similar to phase plots of periodic regimes of the Hénon map. For a chaotic orbit, a scattering of points across the plane is produced. Figures 3.4 and 3.5 illustrate surfaces of section taken across planes which pass through one or both of the stationary points P1 and P2. These sections correspond to the parameter values and initial conditions plotted in Figures 3.1 and 3.3(b). Figure 3.5, especially, illustrates the reduction of phase-space as the orbit passes through its transient phase and into the region of the attractor in the center of the plot.

Despite the data reduction represented in a Poincaré section, its computation requires as much time as the computation of the entire trajectory does, because it is still necessary to calculate all of the points along the orbit between punctures of the sectional plane in order to know where the next puncture will be. The derivation of a set of difference equations (an iterated map) from a given set of differential equations (a continuous flow), in a manner which would allow a direct computation of the Poincaré section of the flow, is unfortunately neither trivial nor obvious. There is some speculation that a higher-dimensional flow exists for every true iterated map (of which the map might be considered a surface of section of the hypothetical flow), but the existence of such has not been proved to date. Nonetheless, Shaw [64] demonstrates morphological similarities between the Hénon attractor and the hypothetical section of a certain generic flow.

Further discussion on the Lorenz equations may be found in Thompson and Stewart [69], Lichtenberg and Lieberman [38], Helleman [31], and Ruelle [63].

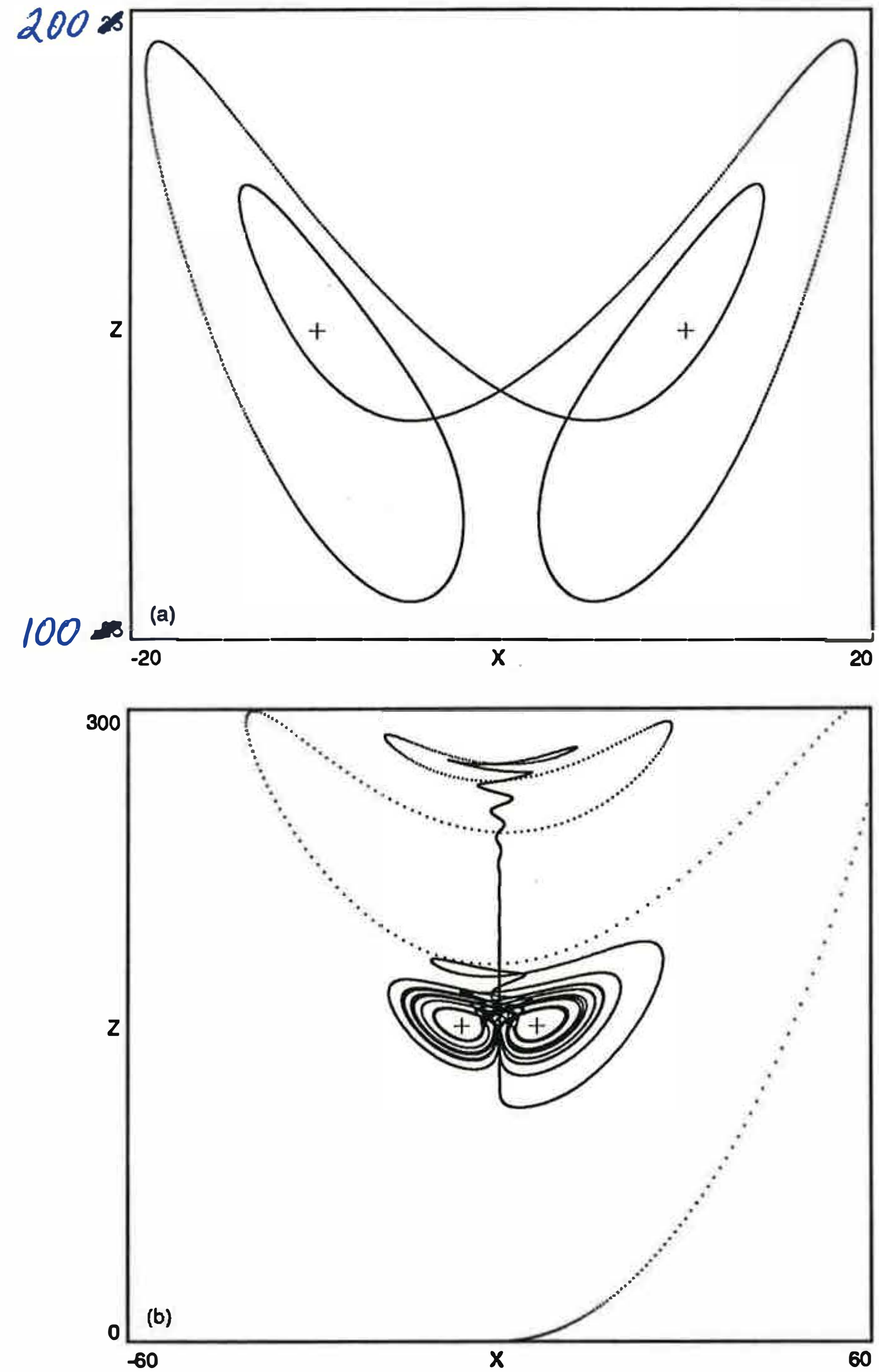

Figure 3.3 Two orbits of the Lorenz attractor at $R = 150$, $\sigma = 10$; (a) periodic orbit for $B = 8/3$, shown without the initial transient; (b) chaotic orbit for $B = 1/4$, including the transient portion. Both portraits are projections onto the (x, z) plane along the y-axis, and the initial point is also (0.1, 0.1, 0.1) for both. Crosshairs mark the locations of the stationary points P1 and P2.

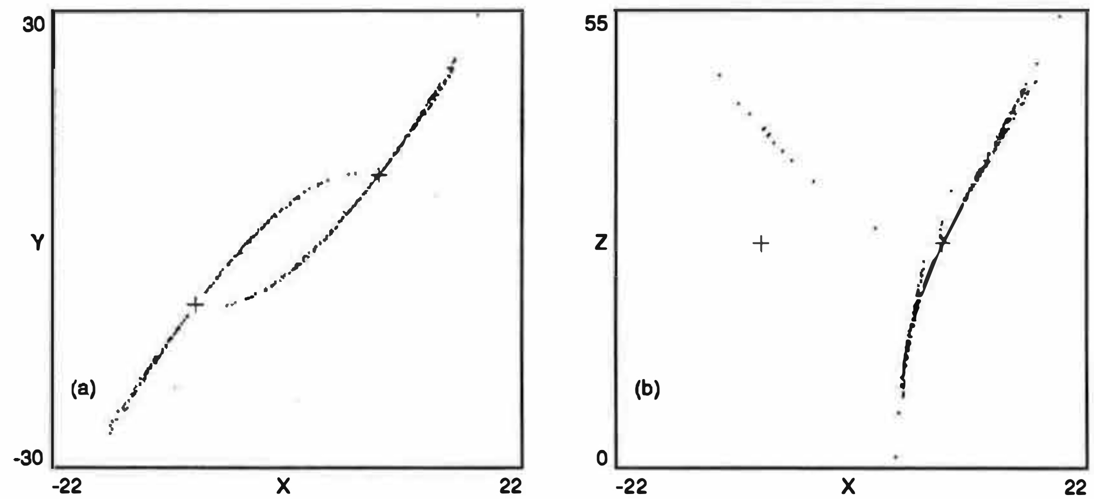

Figure 3.4 Surfaces of section through the Lorenz attractor, for the parameter values $\sigma = 10$, $R = 28$, and $B = 8/3$; (a) on the (x, y) plane at $z = (R - 1) = 27$, (b) on the (x, z) plane at $y = 8.485281$. Crosshairs mark the locations of the stationary points.

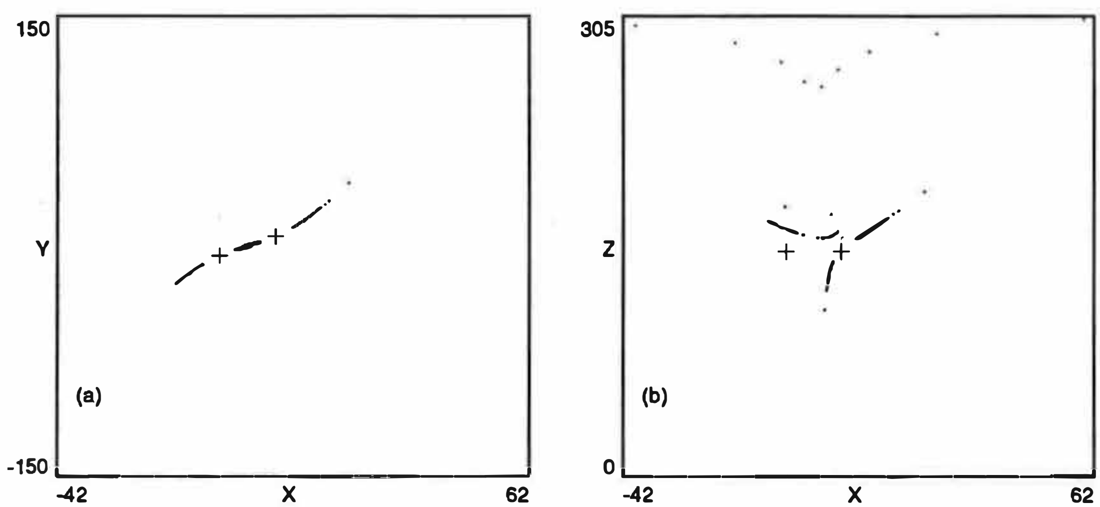

Figure 3.5 Surfaces of section through the Lorenz attractor, parameter values $\sigma = 10$, $R = 150$, and $B = 1/4$; (a) on the (x, y) plane at $z = (R - 1) = 149$, (b) on the (x, z) plane at $y = 6.103278$. Crosshairs mark the locations of the stationary points.

3.2 Musical Examples

Musical mappings of orbits of the Lorenz equations were made with the two sets of parameters explored in the preceding technical section, namely $\sigma = 10$, $R = 28$, $B = 8/3$ (Set A), and $\sigma = 10$, $R = 150$, $B = 1/4$ (Set B). Because of the different region of phase space occupied by the orbit under each of these two sets of parameter values, the ranges along each of the three axes of the coordinate space which map to minimum and maximum values of the musical domain space must be different as well. These relationships are summarized in Table 3.1. The first two examples explore the musical potential of the Lorenz equations as a continuous flow, while Examples 3 through 6 map surfaces of section into the musical domain. In Examples 1 and 2, inter-note onset time varies between zero and a quarter of a second. For the cross-sectional examples (3 through 6) of configuration (a), inter-note onset time is constant at 20 pulses, or 1/6 of a second, while in those of configuration (b), this rate varies according to the sum of the squares of the two variables mapped, i.e., between zero and 1/3 of a second. Except for the first example, the initial point of each sequence is (0.1, 0.1, 0.1). Table 3.2 summarizes the format of the musical examples.

Example 1 charts the courses of two orbits which begin at almost the same location, specifically (0.1, 0.1, 0.1) and (0.1001, 0.1001, 0.1001). The two orbits remain virtually identical for at least 100 seconds before the difference in their initial positions causes them to diverge. This example lasts just over five minutes, a span barely long enough for the initial transients to subside and for behavior more typical of the settled orbit to manifest itself. Pitch varies according to z, velocity according to x, and the inter-note onset time according to y. A given mapping configuration has the effect of aligning parameters into consistent relationships: for example, around middle C notes are all at a medium velocity and speed, while the lowest notes are also the loudest and fastest, etc. The low, fast dips correspond to single revolutions of the orbit around the stationary point located in the $(-x, -y, z)$ quadrant. On the grand staff, this point is located at approximately the F below middle C. The "humps" in the upper register correspond to revolutions around the other stationary point, in the (x, y, z) quadrant. This point is located at approximately G above middle C. Although the orbit makes only single and double revolutions around the stationary points at the beginning, this behavior is only transitory. A sequence of five revolutions around the lower stationary point begins after 150 seconds (note the dips located approximately at 152, 157, 162, 168 and 176 seconds), and a similar sequence around the upper stationary point begins after 180 seconds. The outward spiral of the orbit as it is repelled from a stationary point is reflected in the increasing ambitus of the oscillations in each of these sequences. The last revolution before a transition to the opposite stationary point is always the greatest in extent.

Example 2 illustrates the first two minutes of a much different orbit. This span of time represents the first third of a long transient phase of a chaotic orbit which would eventually settle down onto an attractor contained within a region extending about a major third from either side of middle C. The rate of note succession has been mapped *inversely* according to z (as the orbit moves in the positive direction along the z-axis, the rate decreases, therefore that the tempo increases). Velocity varies according to x, and pitch varies according to y. Interestingly, these first two examples are strikingly reminiscent of Percy Grainger's *Free Music* experiments from the late 40's and 50's [28]. It is noteworthy that the essence of the contours drawn freely and intuitively by Grainger can be generated algorithmically from the Lorenz equations.

Examples 3(a) and 3(b) are made from Poincaré sections made on the plane at $z = R - 1 = 27$ (see Figure 3.4(a)), which includes both of the stationary points P1 and P2. In the graphical scores, these two points are located at the vertices of the sideways V-shaped figures visible and audible throughout the examples. These figures, opening to the right as time moves forward, are evidence of the outward spiral of the orbit around each point. The presence of these motive-like figures of restricted pitch range distinguishes these sections from the much more even distribution of notes in the pitch space attained by means of the Hénon map. The orbital information which is represented over a span of five minutes in Example 1 occupies only the first ten seconds of Example 3. These examples thus present in a condensed format a picture of the behavior of the Lorenz system over a much longer span of time. As with the continuous flow in Example 1, the mapping aligns musical parameters in a consistent manner: all of the notes in the lower part of the range (around the lower stationary point) are softer than those in the upper part of the range.

Examples 4(a) and 4(b) are sections taken at $y = \sqrt{B(R-1)} = 8.485282$. Although these examples are made from precisely the same orbit as that of Example 3, the pattern recorded is entirely different due to the change in the geometry of the sectional plane with respect to the course of the flow. A careful comparison of the disposition of points in Figure 3.4(b) with the mapping configurations as described in Table 3.2 explains the reduced dynamic range of Example 4(a) as opposed to 4(b). The latter example is

Set	*Parameters*	$x(min, max)$	$y(min, max)$	$z(min, max)$
A	$\sigma = 10$, $R = 28$, $B = 8/3$	$-22, 22$	$-30, 30$	$0, 55$
B	$\sigma = 10$, $R = 150$, $B = .25$	$-42, 62$	$-150, 150$	$0, 305$

Table 3.1 Parameters and coordinate space mappings.

Ex.	*Description*	*Params*	*Pitch*	*Vel.*	*INOT*	*Rate*	*Score*
1	continuous flow	Set A	z	x	y	0-30	Figure 3.6
2	continuous flow	Set B	y	x	$1/z$	0-30	Figure 3.7
3(a)	section @ $z = 27$	Set A	y	x	—	20	Figure 3.8
3(b)			$x^2 + y^2$	y	x	0-40	Figure 3.9
4(a)	section @ $y = 8.485282$	Set A	z	x	—	20	Figure 3.10
4(b)			$x^2 + z^2$	z	x	0-40	Figure 3.11
5(a)	section @ $z = 149$	Set B	y	x	—	20	Figure 3.12
5(b)			$x^2 + y^2$	y	x	0-40	Figure 3.13
6(a)	section @ $y = 6.103278$	Set B	z	x	—	20	Figure 3.14
6(b)			$x^2 + z^2$	z	x	0-40	Figure 3.15

Table 3.2 Format of the musical examples.

interesting for the hocketing effect caused by the almost total split of the single voice into two widely separated registers of the pitch space.

Examples 5(a) and 5(b) are made from sections at $z = 149$ ($= R - 1$ using the parameters of Set B; see Figure 3.5(a)). The span of time represented in the two minutes of Example 2 is compressed to within the first two seconds of these examples. The drastic reduction in the range of the musical texture as the initial transient dies out in the first several seconds is a demonstration of the loss of energy common to all dissipative systems. The nature of the attractor visible in the center of the pitch range is also clearly quite different than that of Examples 3 and 4, even considering the change of scale.

Examples 6(a) and 6(b) are made from sections at $y = \sqrt{B(R-1)} = 6.103278$ (see Figure 3.5(b)). The distinction between the transient portion of the orbit (the first two seconds of each example) and the settled orbit is especially clear in these examples. Interestingly, irregularities in the texture occur here at locations where the corresponding texture in Example 5 is fairly smooth. Like Examples 3 and 4, these sections demonstrate the variation in textural contour which can be attained by judicious placement of the sectioning plane.

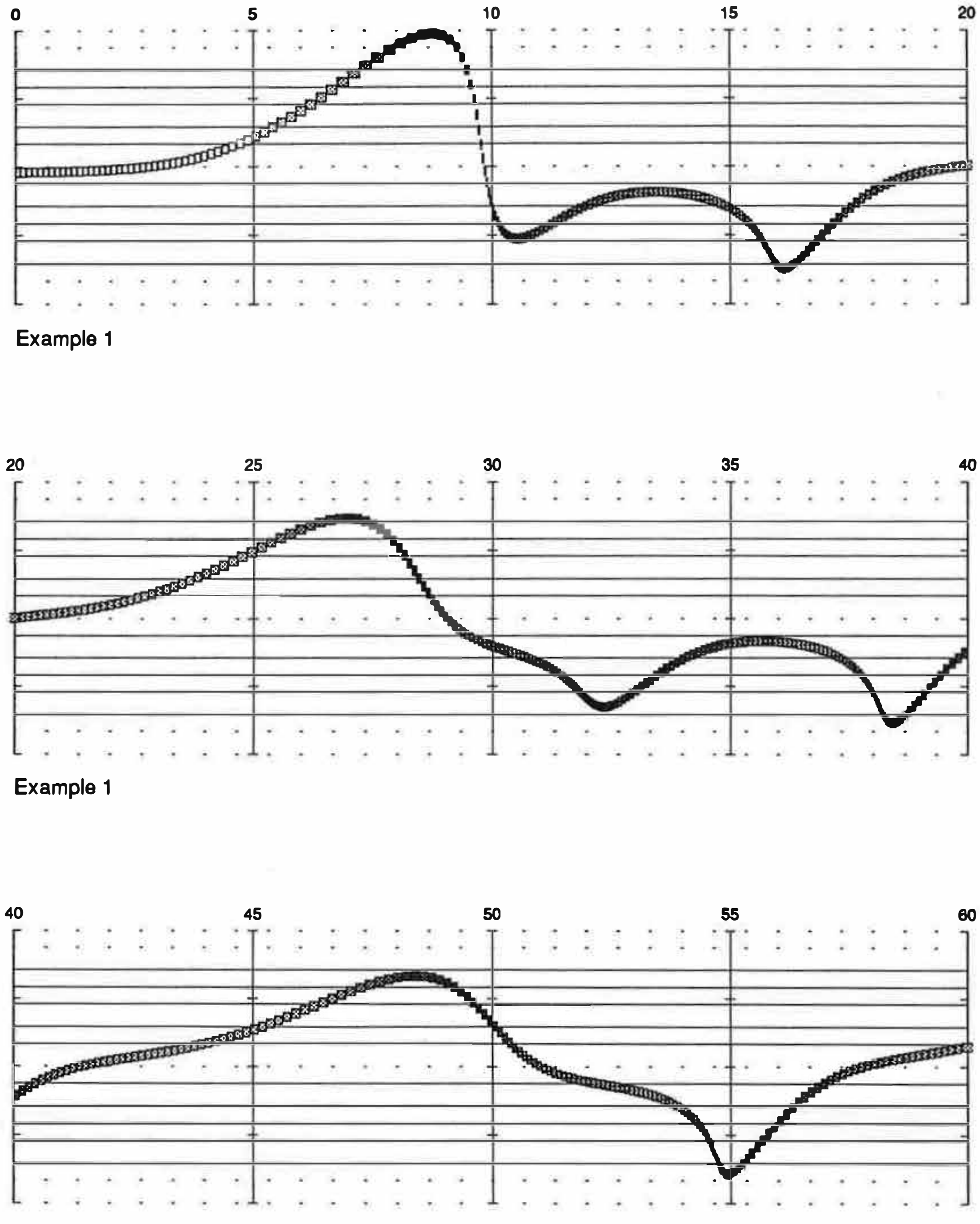

Figure 3.6 Score to Example 1, two voices diverging due to sensitive dependence on initial conditions. Continues on next page.

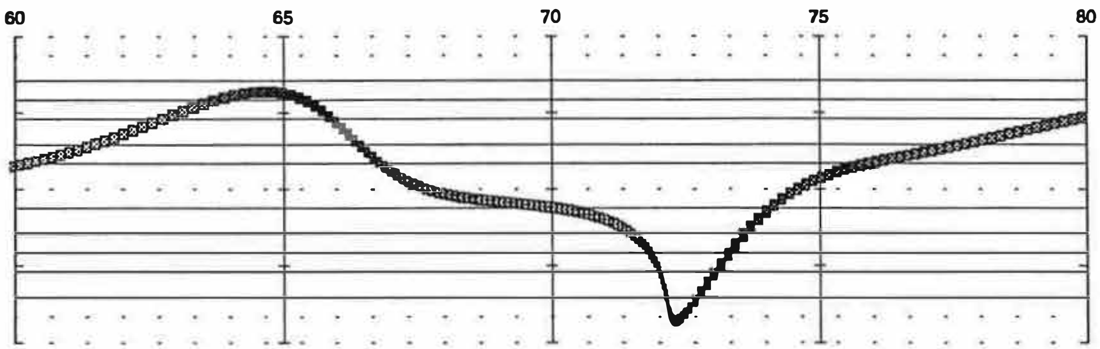

Example 1

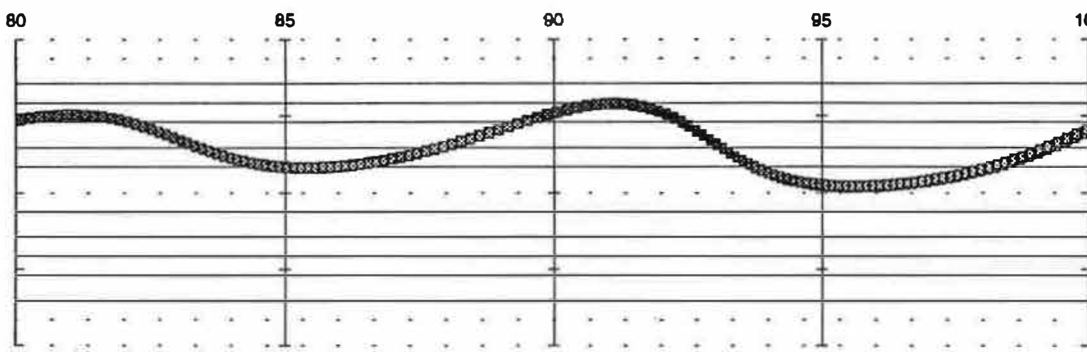

Example 1

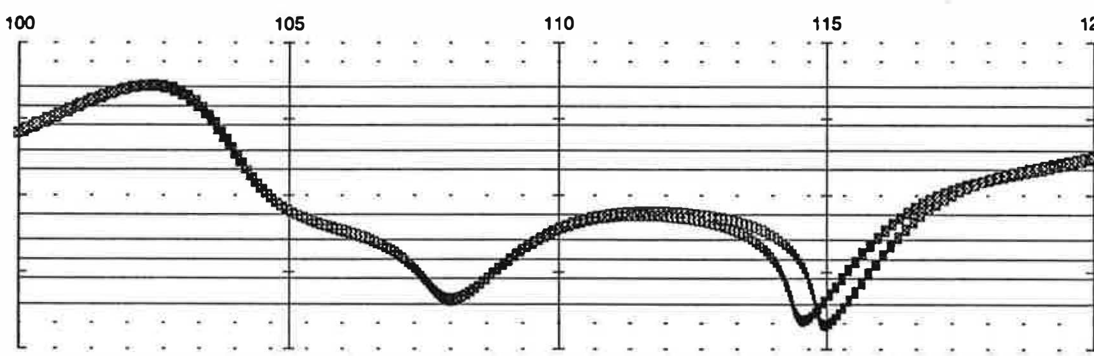

Example 1

Figure 3.6 Score to Example 1, continued.

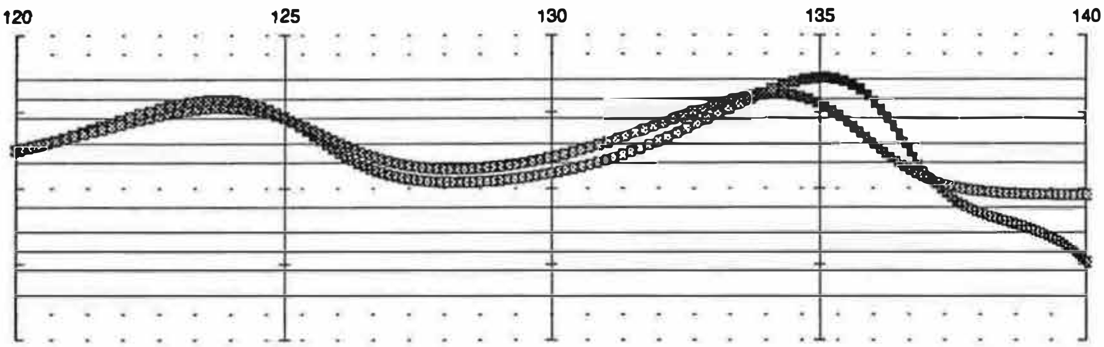

Example 1

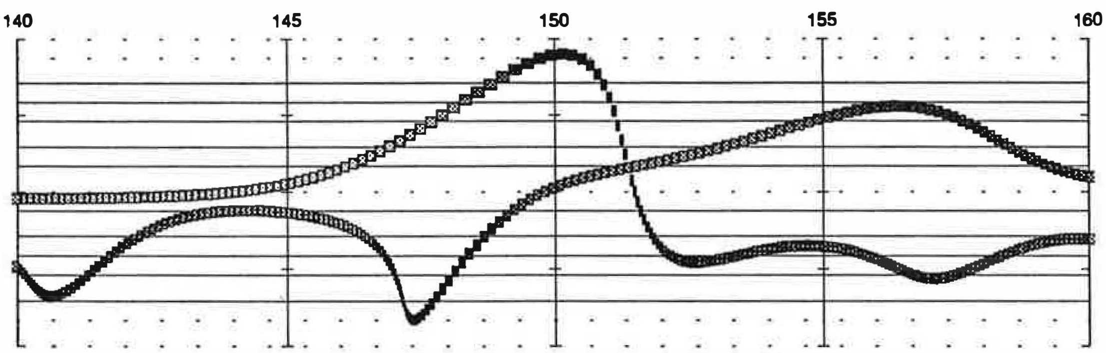

Example 1

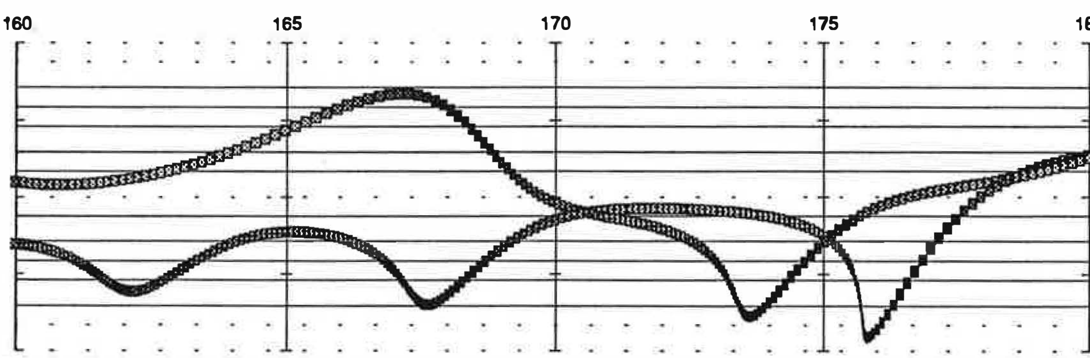

Example 1

Figure 3.6 Score to Example 1, continued.

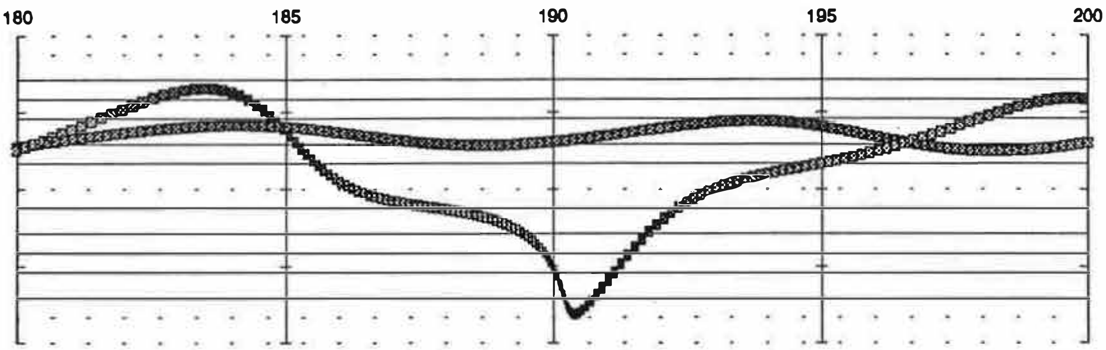

Example 1

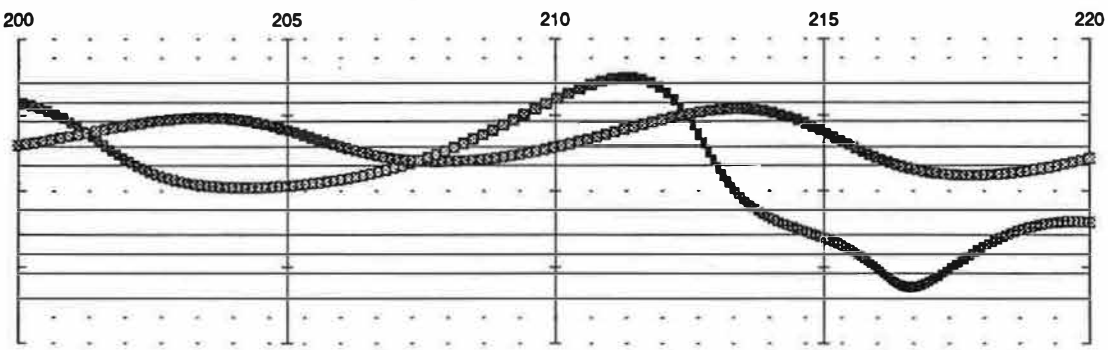

Example 1

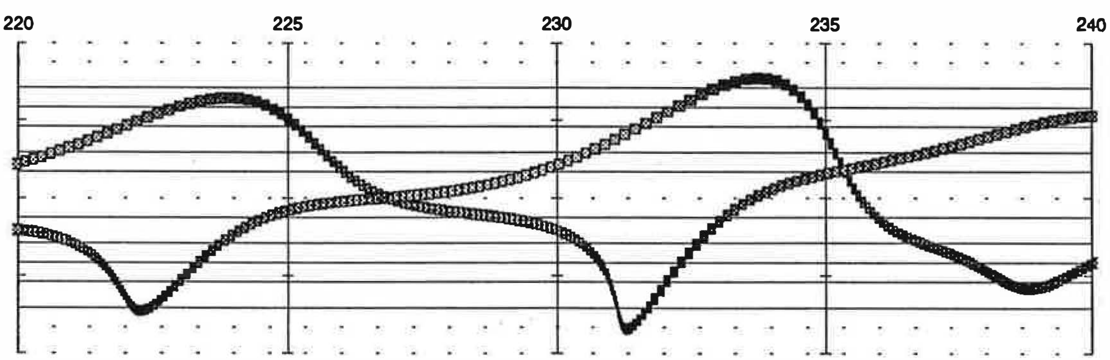

Example 1

Figure 3.6 Score to Example 1, continued.

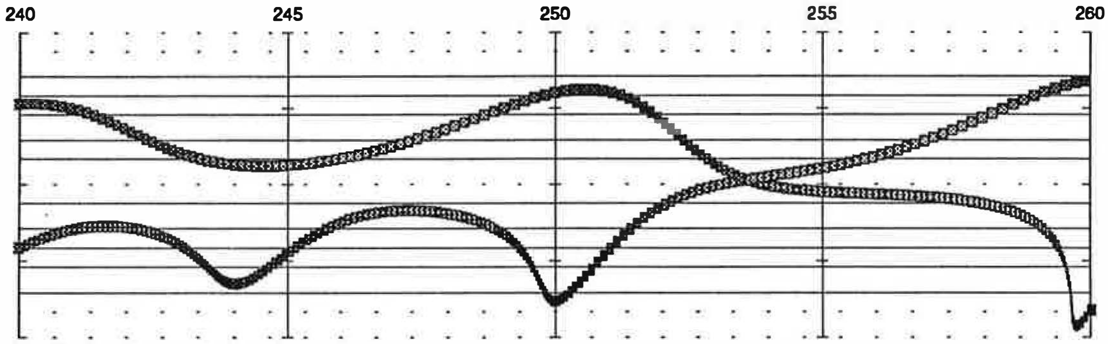

Example 1

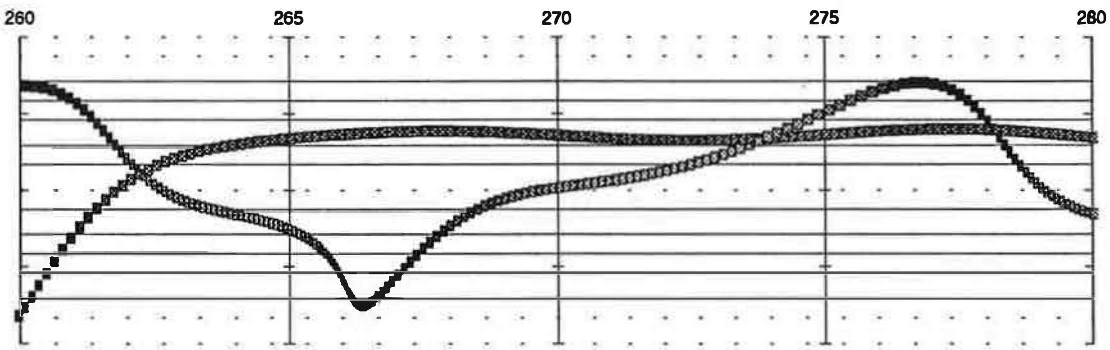

Example 1

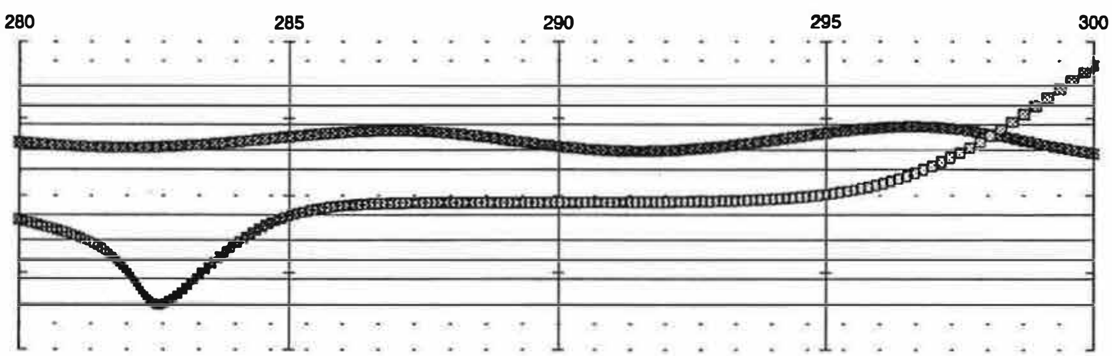

Example 1

Figure 3.6 Score to Example 1, continued.

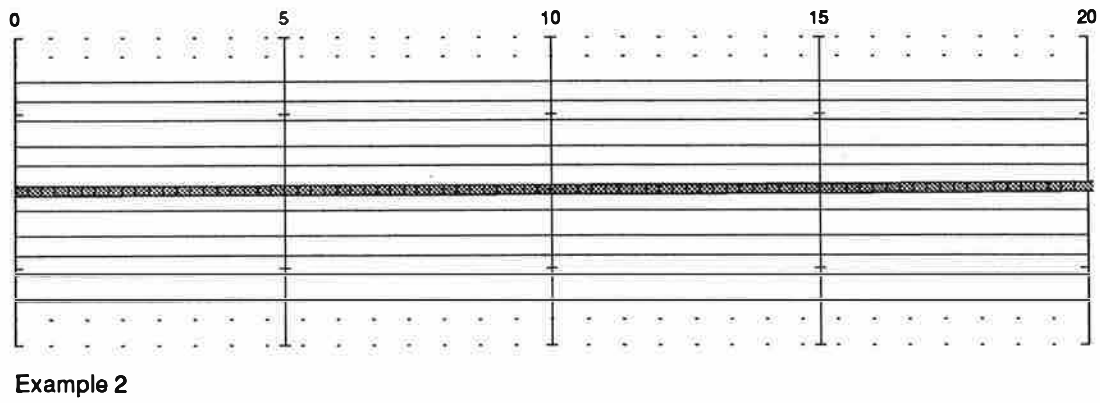

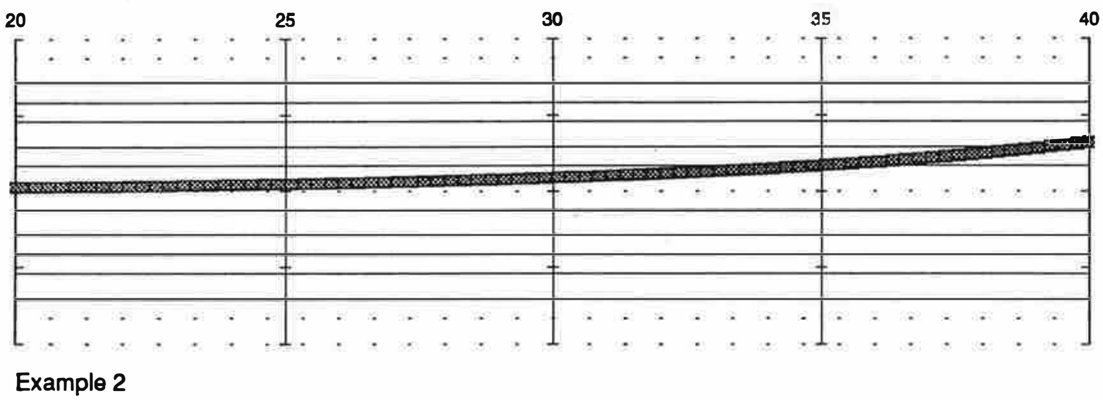

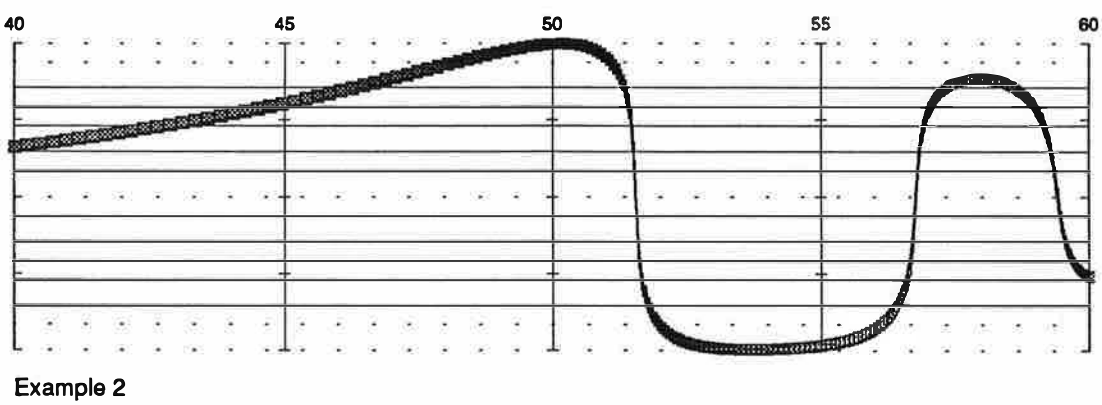

Figure 3.7 Score to Example 2, portion of a transient orbit. Continued on next page.

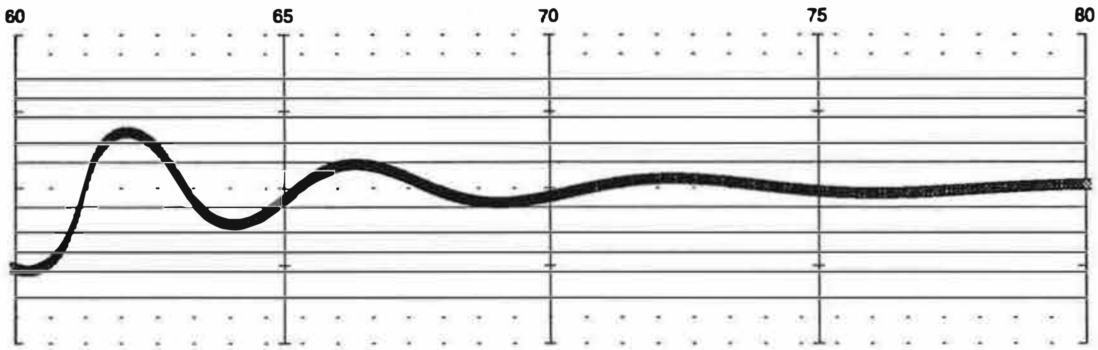

Example 2

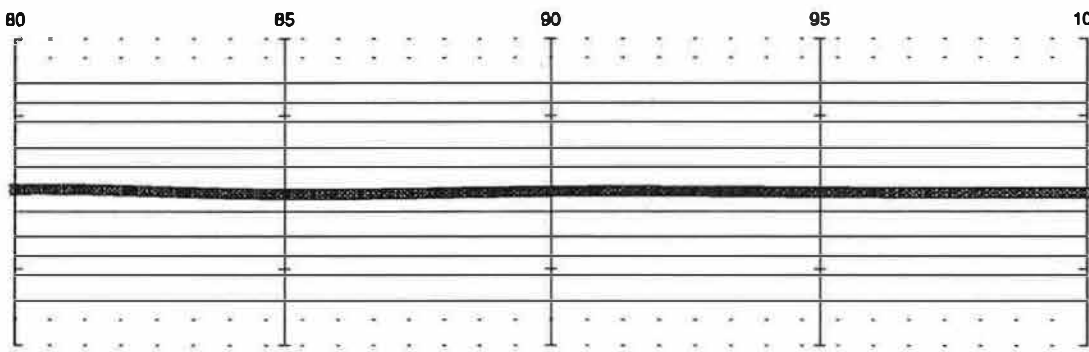

Example 2

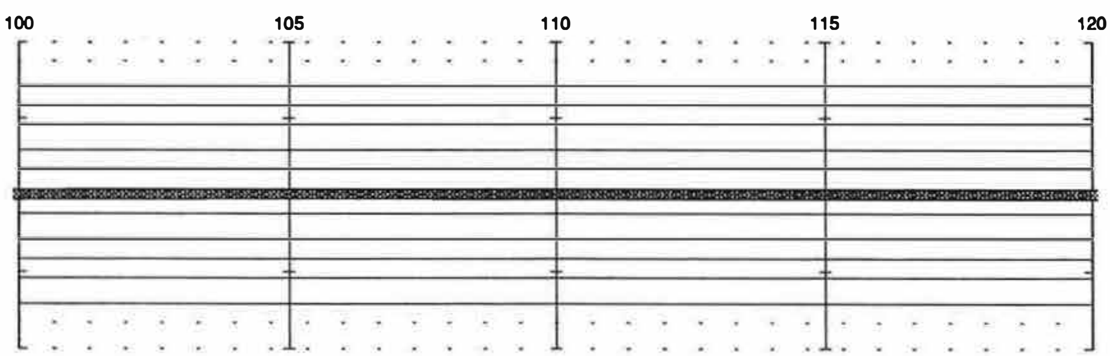

Example 2

Figure 3.7 Score to Example 2, continued.

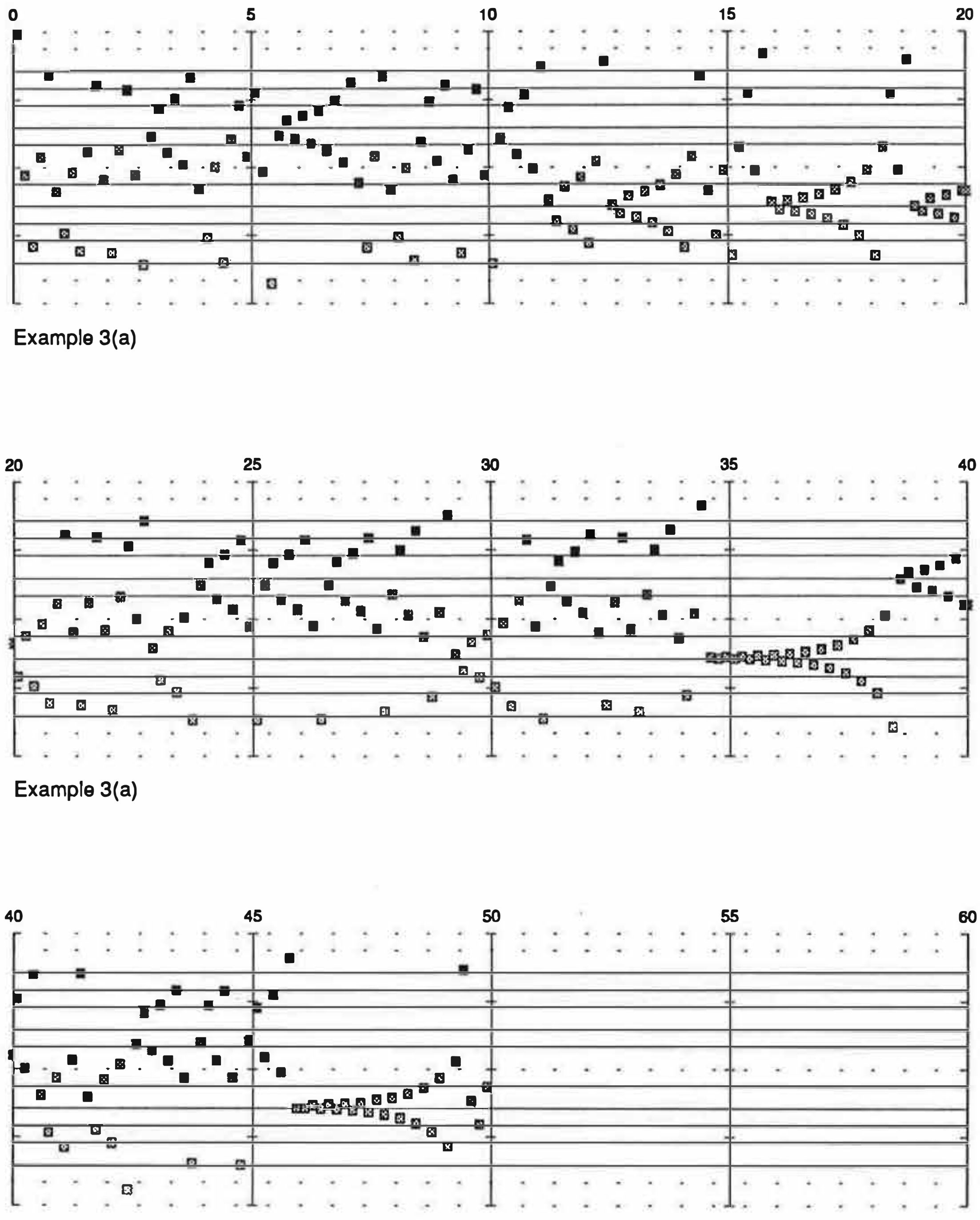

Figure 3.8 Score to Example 3(a), section at $z = 27$.

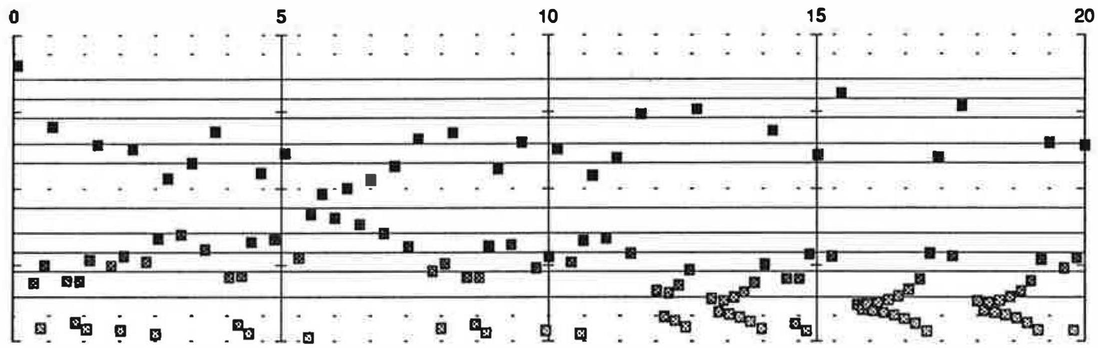

Example 3(b)

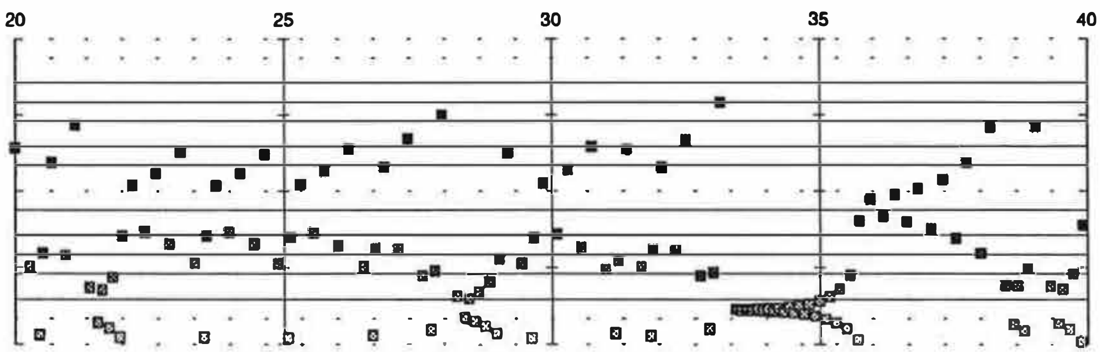

Example 3(b)

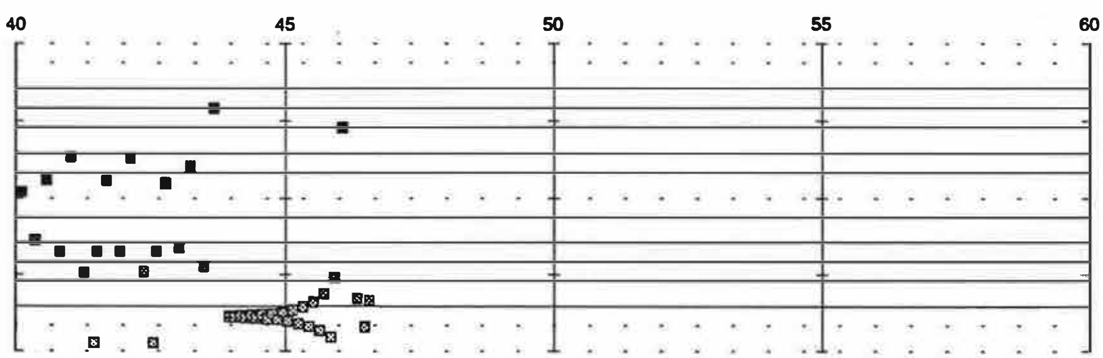

Example 3(b)

Figure 3.9 Score to Example 3(b), section at $z = 27$.

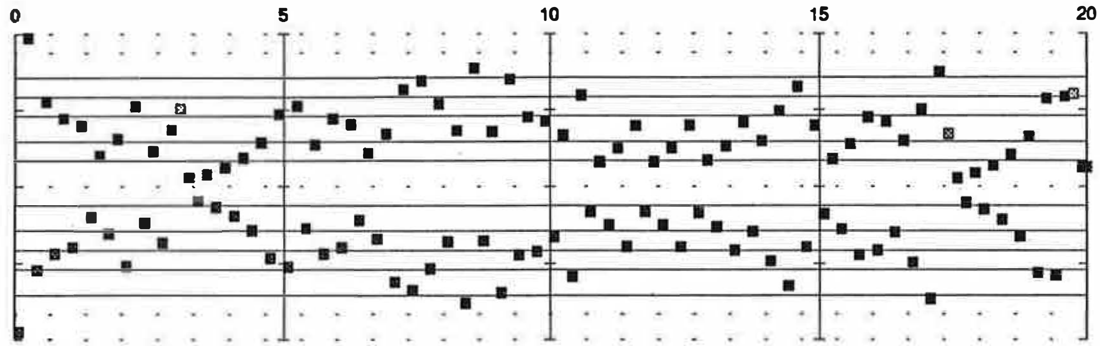

Example 4(a)

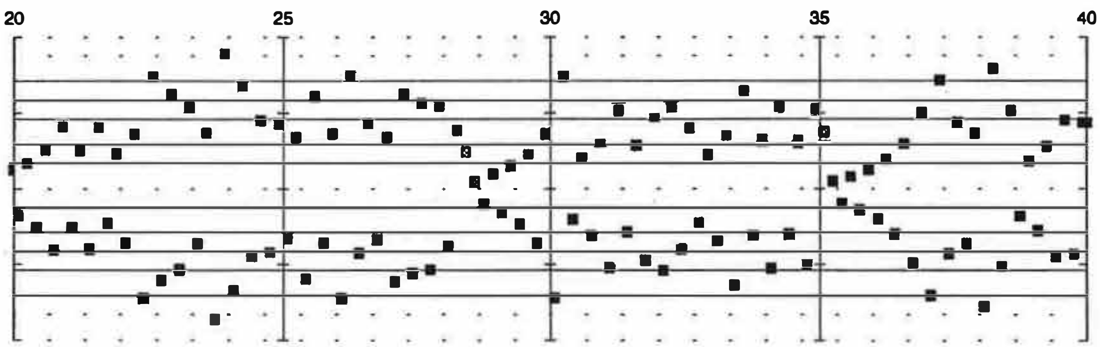

Example 4(a)

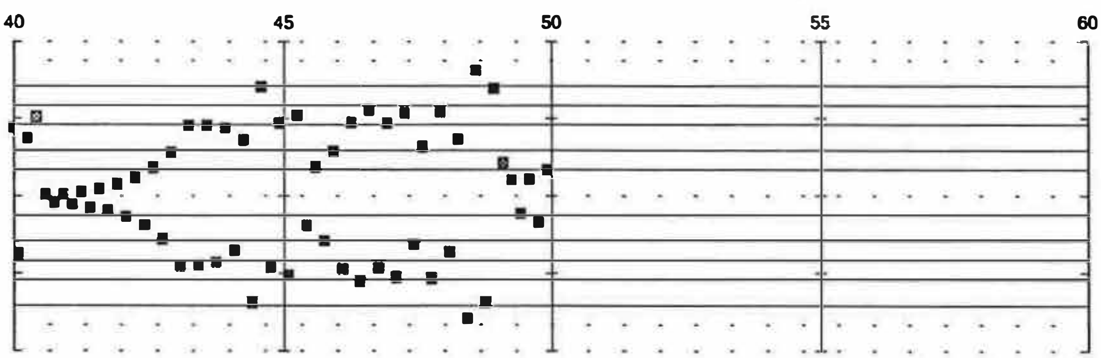

Example 4(a)

Figure 3.10 Score to Example 4(a), section at $y = 8.485282$.

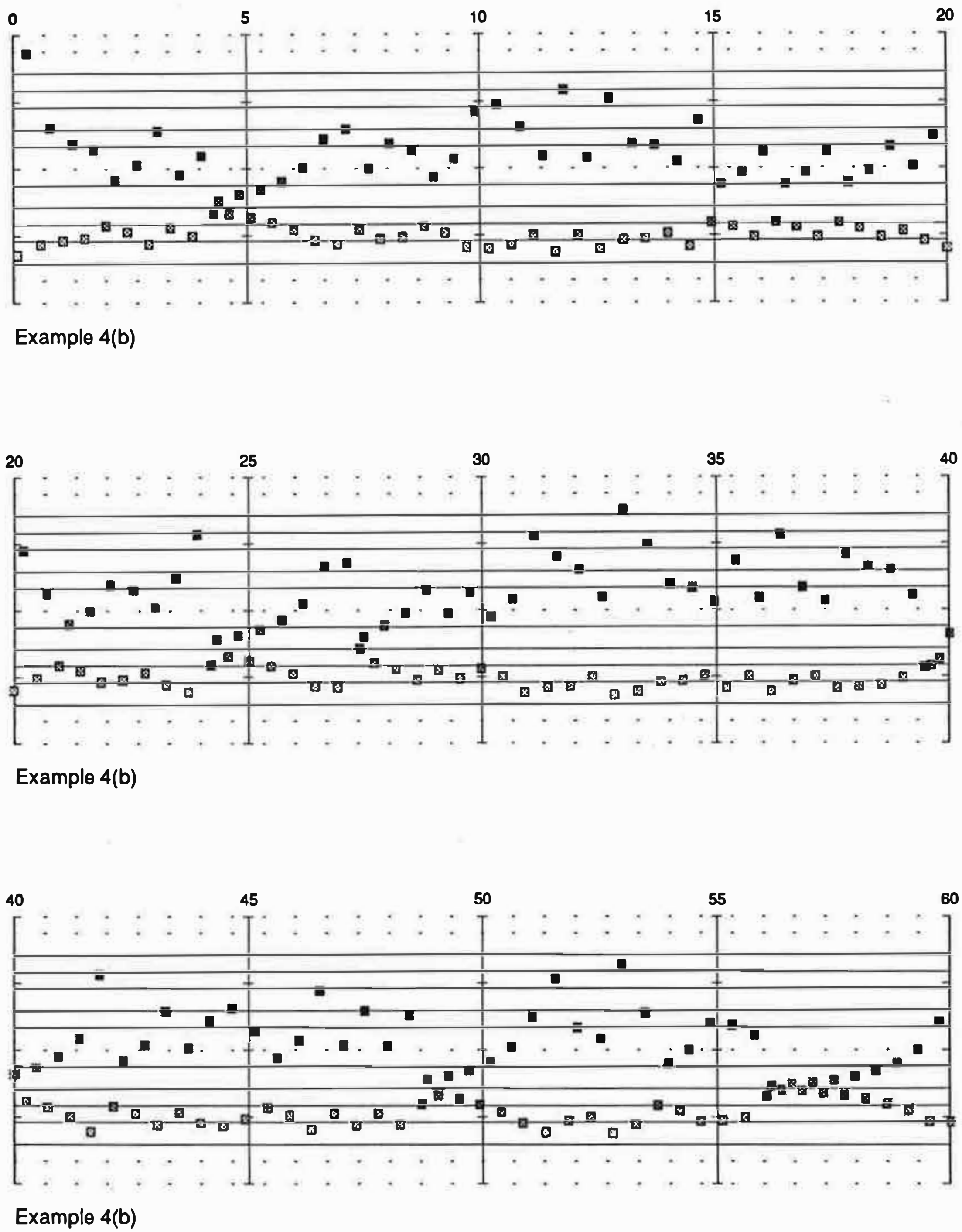

Figure 3.11 Score to Example 4(b), section at $y = 8.485282$.

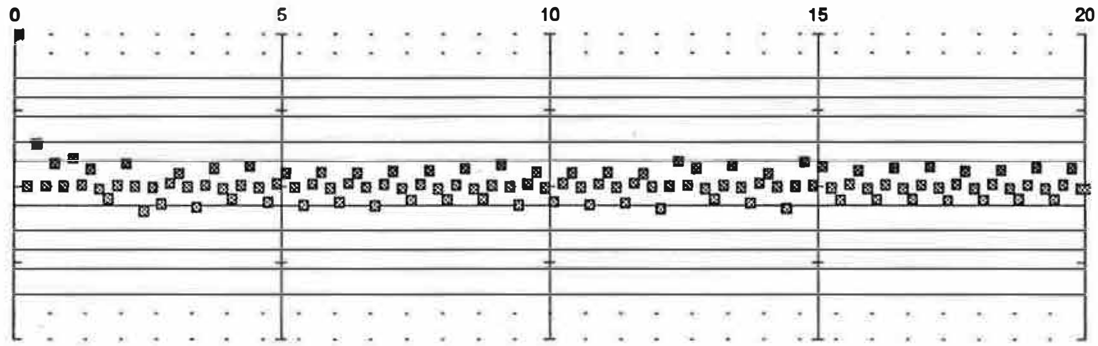

Example 5(a)

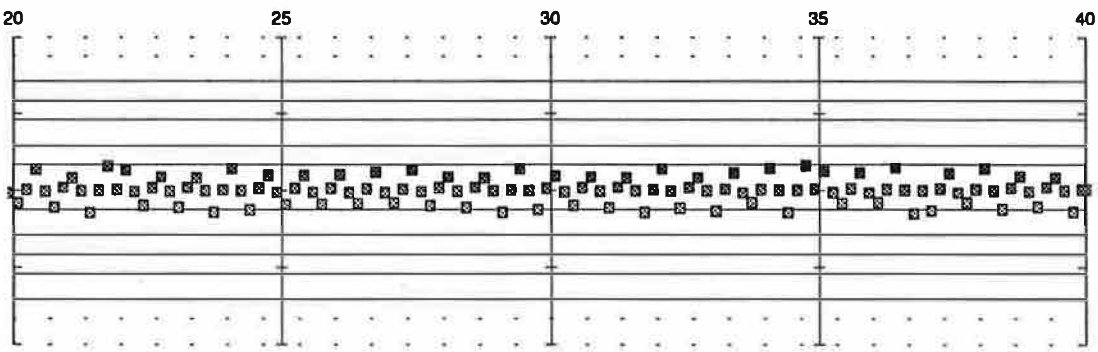

Example 5(a)

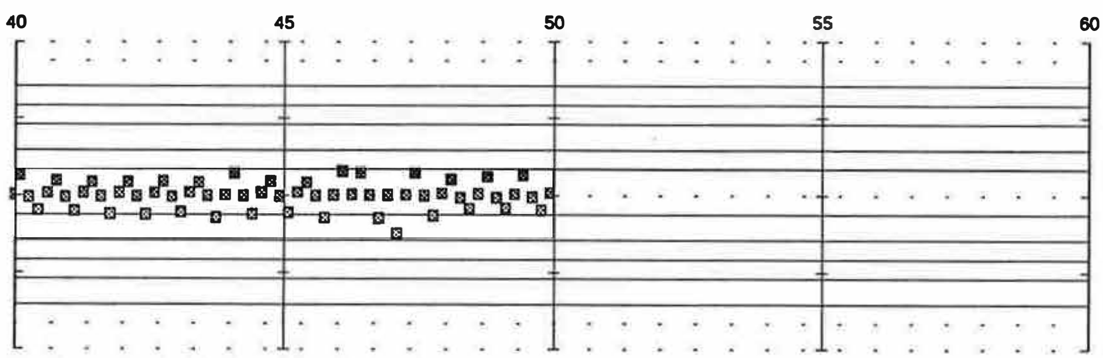

Example 5(a)

Figure 3.12 Score to Example 5(a), section at $z = 149$.

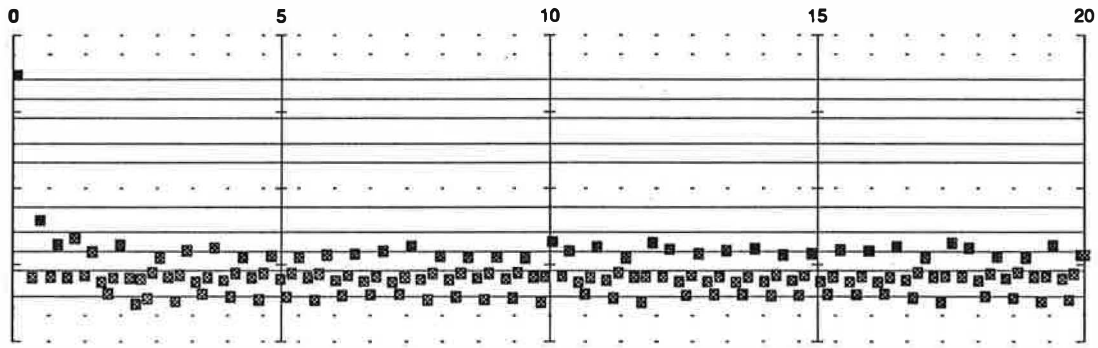

Example 5(b)

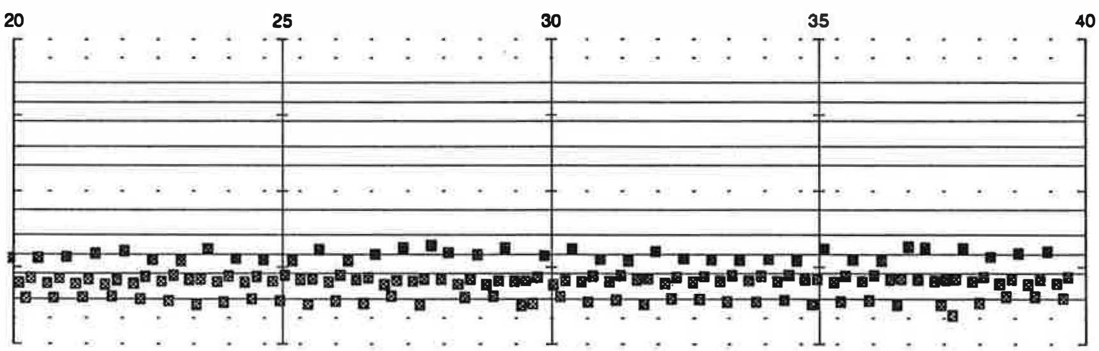

Example 5(b)

Figure 3.13 Score to Example 5(b), section at $z = 149$.

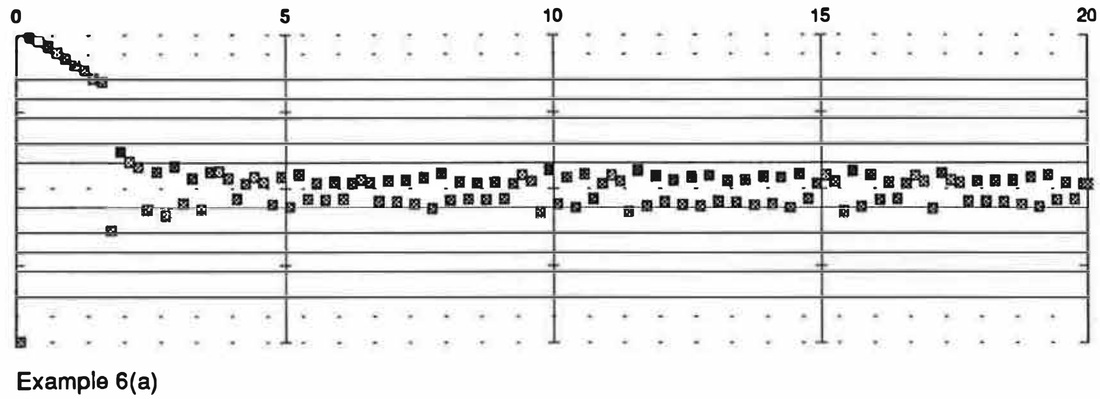

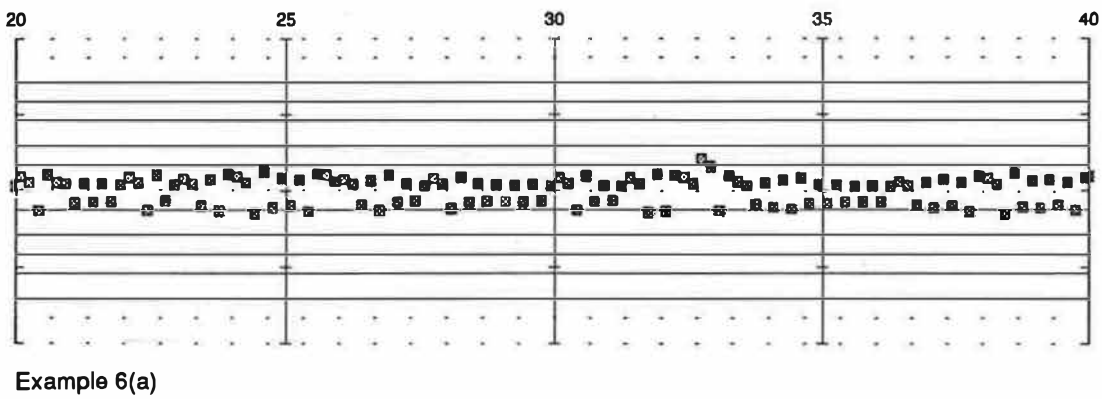

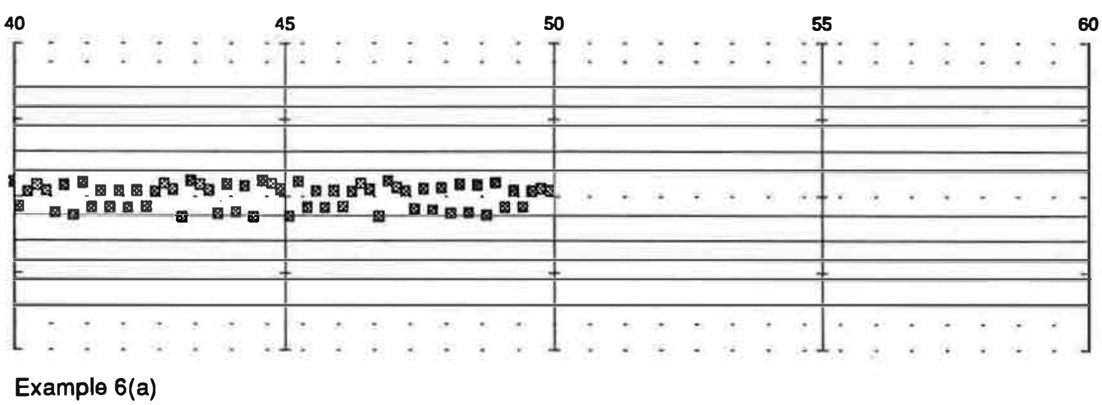

Figure 3.14 Score to Example 6(a), section at $y = 6.103278$.

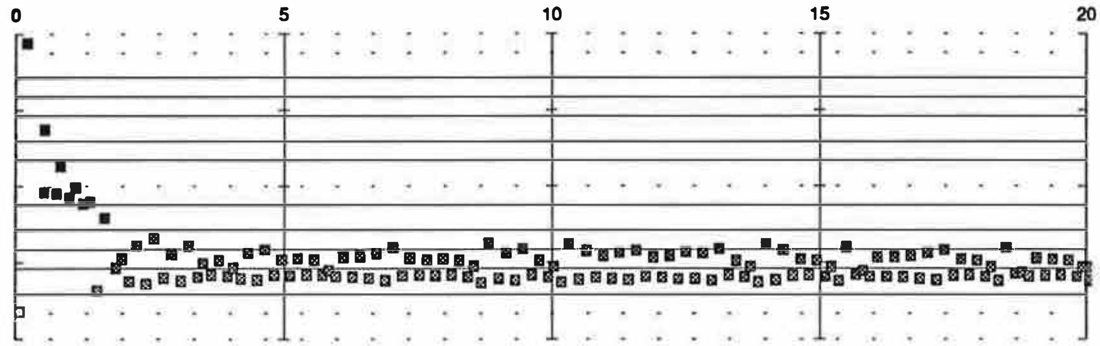

Example 6(b)

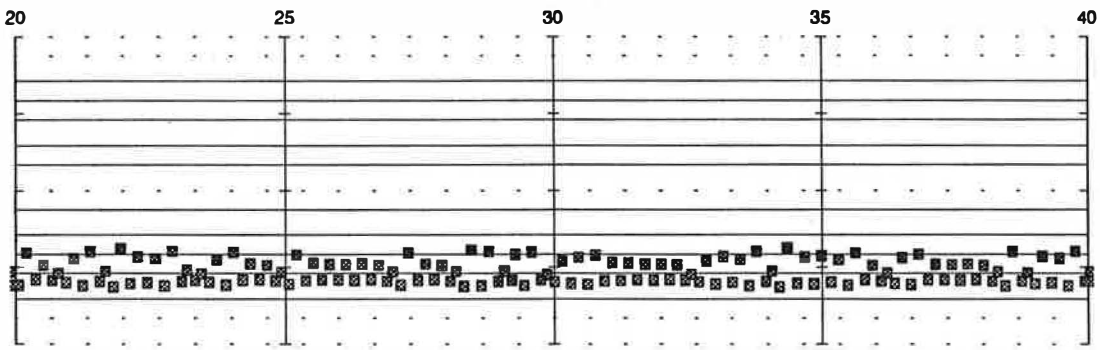

Example 6(b)

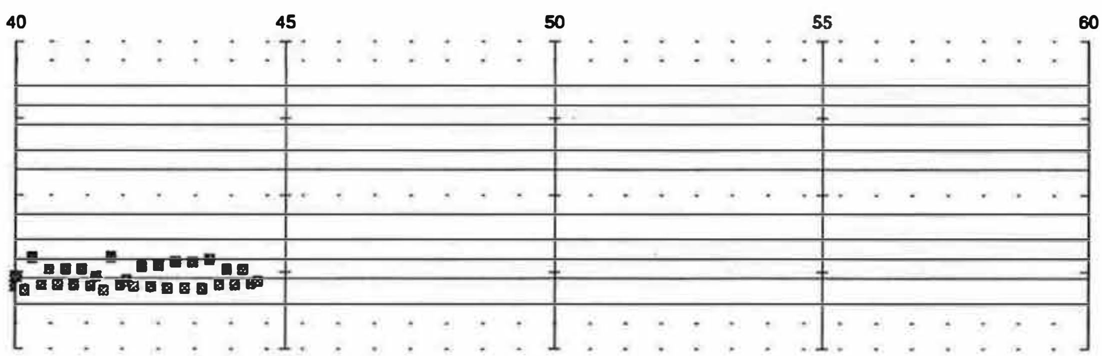

Example 6(b)

Figure 3.15 Score to Example 6(b), section at $y = 6.103278$.

Chapter 4

The Standard Map

4.1 Technical Description

The standard map, sometimes known as the Chirikov map after the Soviet physicist who studied it extensively, is an area-preserving iterated map in two dimensions. Chirikov demonstrates that the standard map is derived from a model of a pendulum acted upon by an external periodic perturbation, and that it is important as a description of "the motion near the separatrix of a fairly general nonlinear resonance." [13, p. 310] The following summary of the behavior of the map is distilled primarily from his study. The system is commonly expressed as:

$$\begin{aligned} I_{n+1} &= I_n + K \sin \theta_n \\ \theta_{n+1} &= \theta_n + I_{n+1}, \end{aligned}$$

where I and θ are taken modulo 2π in the interval from 0 to 2π. The external periodic perturbation is supplied by the sine function, and the equations are nonlinear by virtue of its presence. The ***perturbation parameter***, K, determines the amplitude, or degree, of the perturbation. Since the phase space of the standard map is periodic in both I and θ (of period 2π), it is topologically equivalent to a torus. For simplicity, the orbit may be mapped onto a planar surface of length 2π in both dimensions; see Figure 4.1. Bear in mind that the left and right edges of the phase plane are identical, as are the top and bottom edges. Since the values of I and θ are always mapped in the interval 0 to 2π, the orbit can never escape to infinity. Thus all initial conditions produce stable orbits. There are two stationary points, at (0,0) and $(\pi, 0)$ (or $(0, 2\pi)$ and $(\pi, 2\pi)$); an orbit initiated at either of these points remains stationary at that location. A program to generate orbits of the standard map in numerical form may be found in Appendix A.4.

Orbits may be classified into two main categories. Those orbits which appear to form smooth loops around the "pole" at $(\pi, 0)$ (see Figure 4.4), will be called *cyclic* in the present context (mathematicians prefer to speak of "KAM surfaces," after Kolmogorov, Arnold and Moser, when referring to this classification of orbits). These orbits are of greater interest than they appear. If the domain along I in the phase space is shifted by π in the positive direction, so that I varies between π and 3π, then such an orbit can be plotted as a single closed curve in the middle of the phase space. These orbits are formed from an apparently infinite sequence of points which cycle around the circumference of the curve at an interval which is, for all intents and purposes, irrational relative to the circumference, such that the sequence of points does not appear to repeat itself; see Figure 4.2. In fact, there is some question as to whether these orbits constitute truly infinite sequences, or whether they are actually periodic sequences of very great length. Some cyclical orbits also break up into two or more smaller loops, called "chains of islands" by Hénon and Heiles [33]. Several of these are also evident in Figure 4.2.

The second classification of orbits are those which are chaotic. Chaotic orbits will eventually visit the entire range of values along I, from 0 to 2π, although it may take a very long time to do so. The greater the *ergodicity* of a chaotic orbit, the greater the range of I-values visited within a given number of iterations.

The effect of the perturbation parameter K is to drive cyclical orbits into chaos as K increases. For most initial conditions, the threshold above which an orbit is likely to be chaotic lies around $K = 1$. Orbits become flatter along I as K decreases to zero, and increasingly chaotic as K rises above 1. As with the dissipative Hénon and Lorenz systems, narrow cyclical (read "periodic") regimes are interspersed throughout the surrounding regimes of chaos. The effect of an increasing value of K is shown in Figure 4.3, which plots six orbits of the standard map from the same initial point for different values of K.

Figure 4.4 shows phase plots of the standard map across a range of eight different initial conditions, over three different values of the parameter K. These values have been chosen to lie around the threshold at which most orbits are driven to chaos. Note, however, that $K = 1$ is only an approximate threshold. Some orbits are already chaotic at $K = 0.97$, while others are still cyclic at $K = 1$. Still others remain cyclic even at $K = 1.3$. The closer to the pole $(\pi, 0)$ that an orbit begins, the more it seems to resist the transition to chaos as K increases. Virtually all orbits are chaotic at a value of $K = 4$.

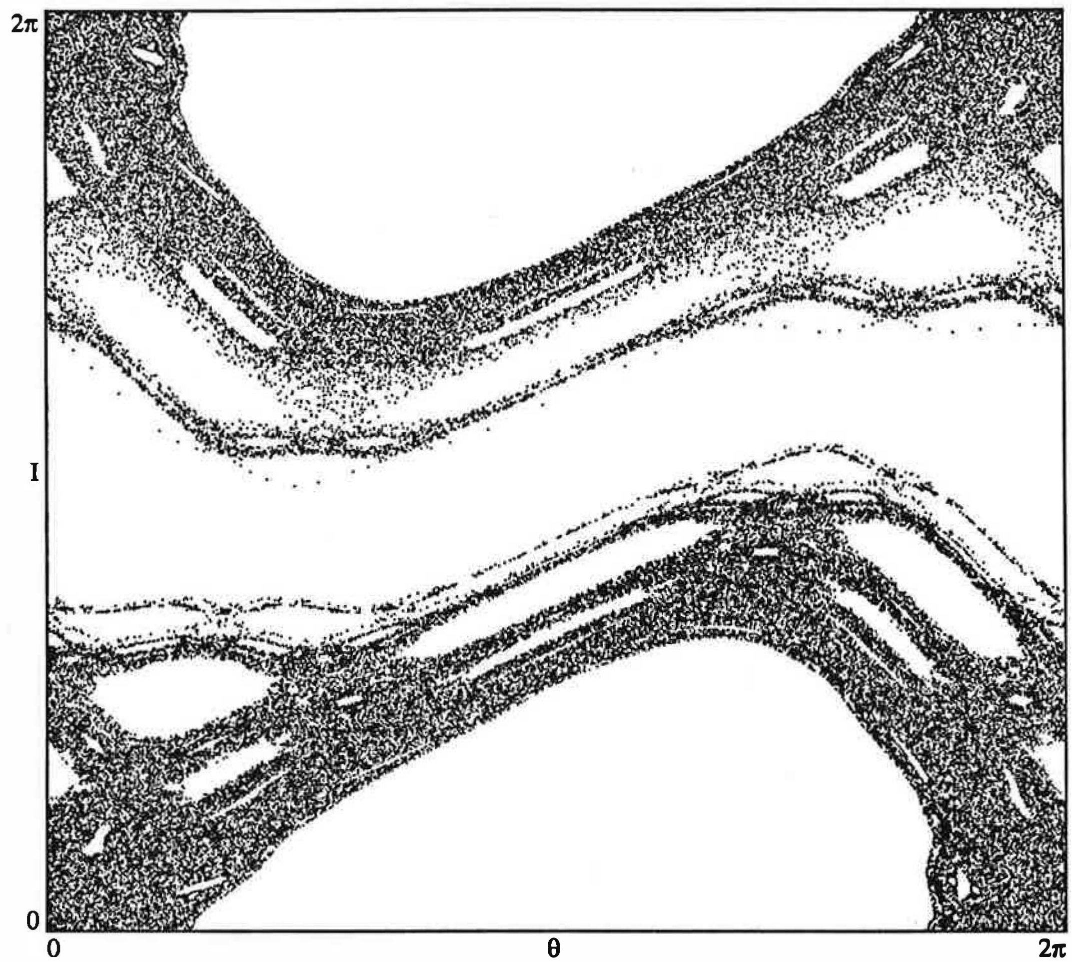

Figure 4.1 Phase portrait of the standard map after 80000 iterations. $K = 1.05$, and the initial point is $(\theta_0 = \pi/2,\ I_0 = \pi/4)$.

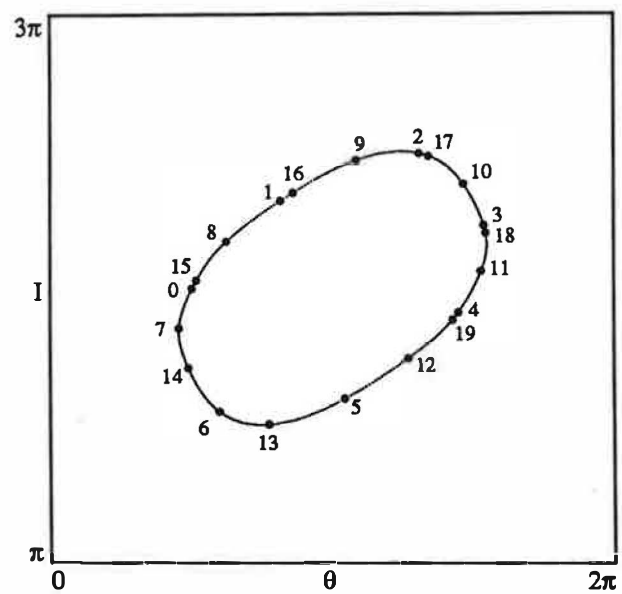

Figure 4.2 Sequence of points forming a cyclical orbit of the standard map around the invariant point at $(\pi, 2\pi)$. 1500 iterations are plotted, with the first twenty iterates marked. $K = 1.0$, $I_0 = 0$, $\theta_0 = \pi/2$. This is the same orbit as that shown in the second plot, top row of Figure 4.4.

As mentioned above, a chaotic orbit will eventually wander over the entire range along the I-axis, although the number of iterations required to accomplish this can be enormous, depending on the initial conditions and value of K. For $K \approx 1$, chaotic orbits tend to remain confined to narrow bands of resonance for extended periods of time before beginning a transition to an adjacent band. The *transition time* between resonance overlaps—that is, the number of iterations required to complete a transition from one band to the next—is inversely proportional to the value of K. As K increases past 2.0, the transition time becomes effectively zero, and the orbit occupies the entire range of values in I. As K decreases below 1.0, the transition time becomes effectively infinite, and the orbit remains confined to the band in which it begins.

The same method used to produce bifurcation diagrams of the Hénon map may be applied to the standard map as well, although the result appears quite differently. Two bifurcation diagrams are shown in Figure 4.5, for both I and θ. The radical change in the character of the orbits on either side of $K = 1$, from orderly to chaotic, is clearly visible in these diagrams. Note that the range of values visited by a given orbit along θ always encompasses the full range from 0 to 2π, while the same holds true along I only for some orbits, and even then only for values of K above 1.0. The funneling of values into a small

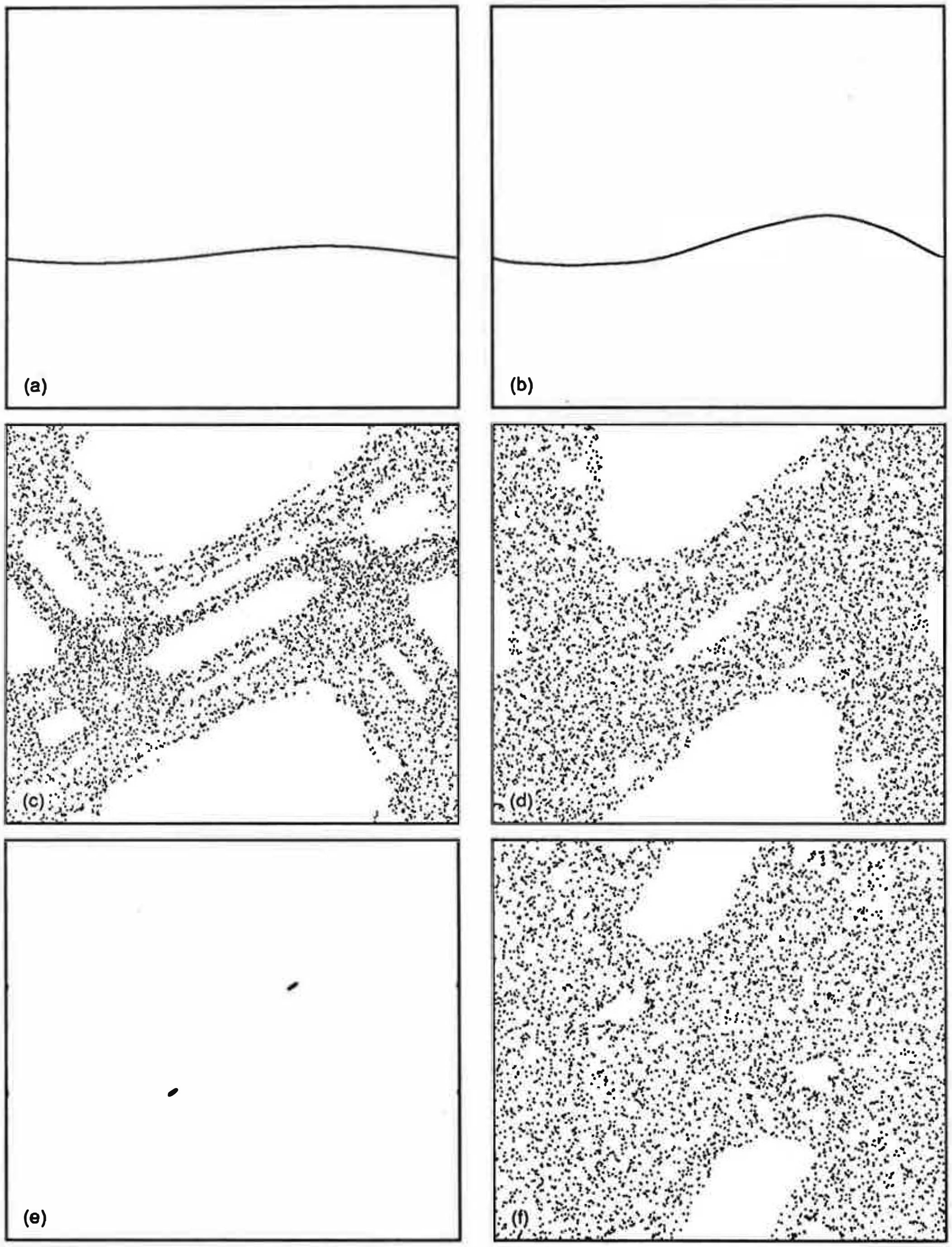

Figure 4.3 Six orbits of the standard map, from an initial point $(3\pi/4, 3\pi/4)$. Each orbit is plotted to 5000 iterations. The value of K is (a) 0.25, (b) 0.75, (c) 1.25, (d) 1.75, (e) 2.25, (f) 2.75. Note that (e), a cyclical orbit, is located within an otherwise chaotic regime.

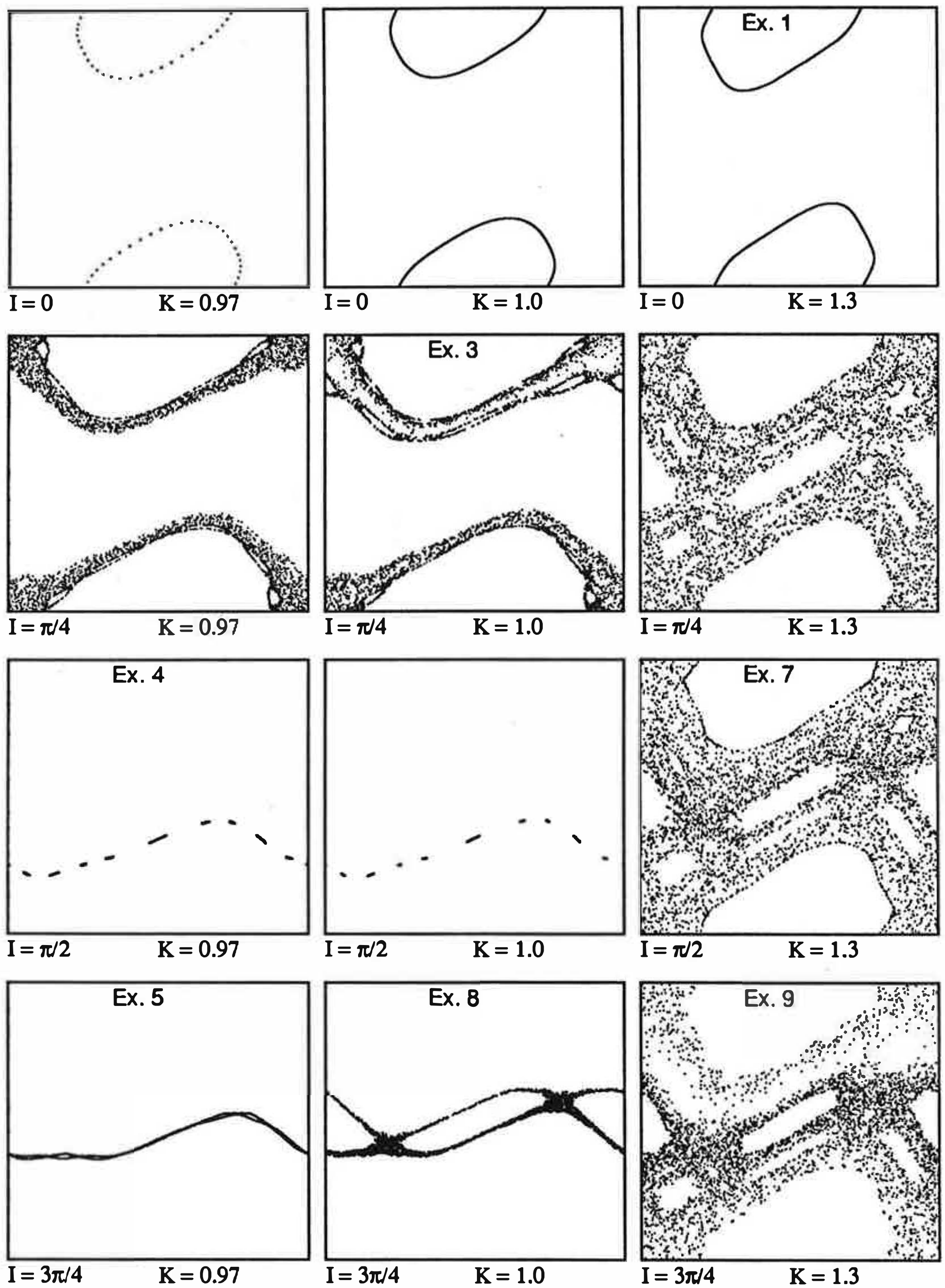

Figure 4.4 Phase plots of the standard map, for K of 0.97, 1.0, and 1.3. The initial value $\theta_0 = \pi/2$ is the same for all of the plots. The initial value I_0 changes with each row, as indicated. Each orbit is plotted to 4000 iterations. Orbits used in the musical examples are marked.

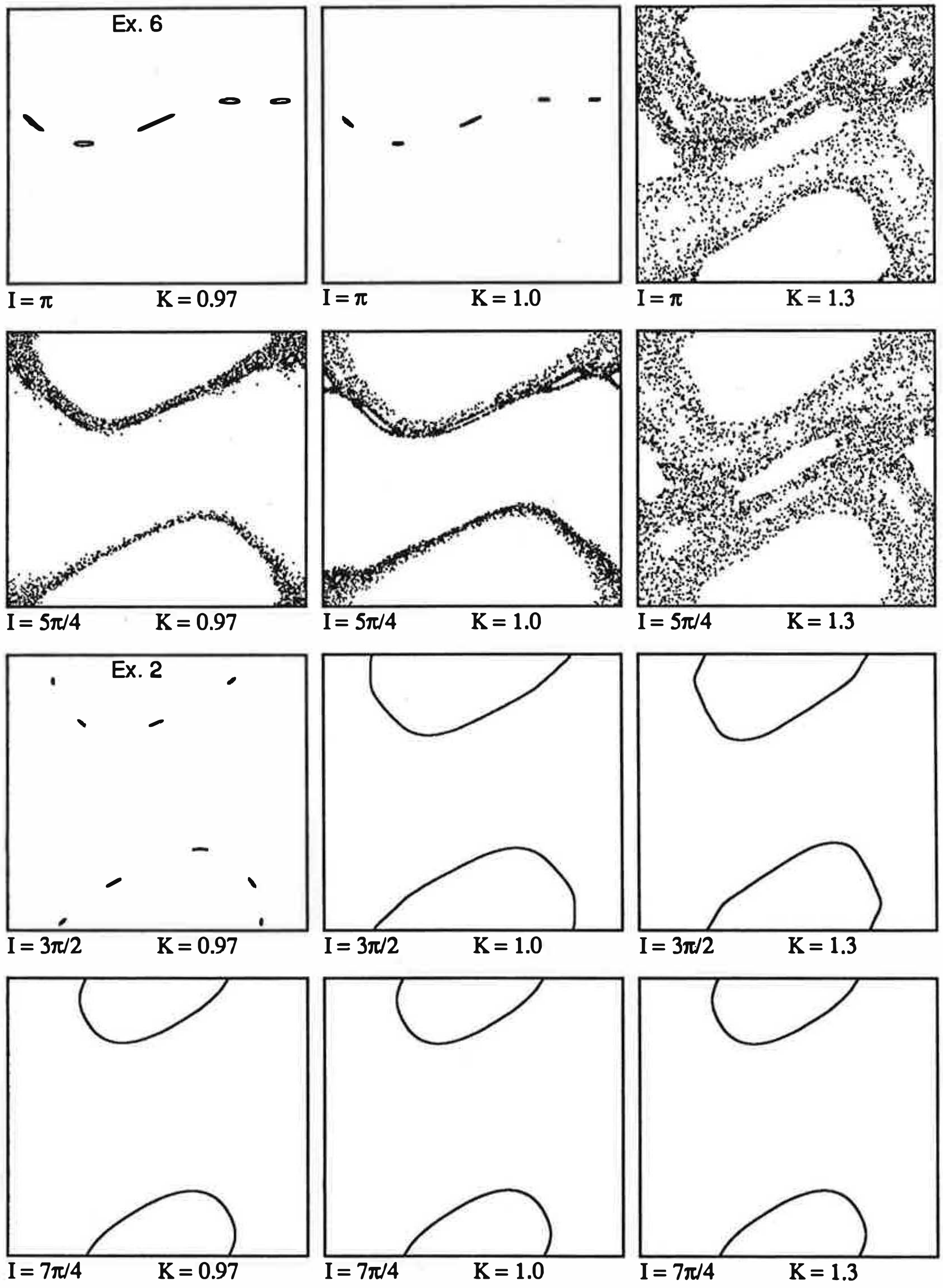

Figure 4.4 (cont.) Phase plots of the standard map, for K of 0.97, 1.0, and 1.3. The initial value $\theta_0 = \pi/2$ is the same for all of the plots. The initial value I_0 changes with each row, as indicated. Each orbit is plotted to 4000 iterations. Orbits used in the musical examples are marked.

number of strands around $K = 1.0$ in both diagrams (ten in the θ diagram, five for I) is evidence of the island chains formed for these particular initial conditions ($\theta_0 = \pi/2$, $I_0 = \pi/2$) at this value of K (compare the corresponding phase plot in Figure 4.4).

Further discussion of the standard map may be found in Moon [50], Thompson and Stewart [69], Greene [29], and Lichtenberg and Lieberman [38].

4.2 Musical Examples

The musical examples are drawn from phase plots shown in Figure 4.4, and illustrate a range of typical behaviors elicited from the standard map. As with the plots in Figure 4.4, the initial value $\theta_0 = \pi/2$ is used for all of the musical examples. Only K and I_0 are varied. Six mapping configurations are employed, which are summarized in Table 4.1. Inter-note onset time varies from example to example, within the general range established in the previous chapters. The format of the examples is summarized in Table 4.2.

In Example 1(a), made from a cyclical orbit, the disposition of the split loop in the phase space causes pitch in the musical space to wrap around the register from top to bottom. In Example 1(b), because of the switch in the mapping configuration, velocity is wrapped around the range from soft to loud while pitch oscillates smoothly. The effect of the irrational ratio of the distance between points along the loop to the length of the loop itself is directly observable as the somewhat disorderly scattering of pitch in Example 1(a). The disorder is only apparent, however, since a longer sinusoidal pattern may be discerned in the pitch distribution when the score is viewed edge on. Such a hidden sinusoidal pattern in the sequence of values is typical of cyclical orbits, and may even be discerned in chaotic orbits to some extent. Examples 2(a) and (b) demonstrate textures similar to those in Example 1, but are formed from a cyclical orbit which has split into a "chain of islands."

Example 3(b) is from a chaotic orbit. The sinusoidal oscillation heard in the cyclical orbits is also present here, but in a more irregular form. Softer sections of the example (between 30 and 35 seconds, and from 38 to 56 seconds) are the result of the confinement of the orbit to the lower portion of the phase space (along I), while the louder interjection after the 35th second is the result of a jump in the orbit to the upper region of the phase space. Examples 3(c) and 3(d) employ the same initial conditions as 3(b), but map the orbit into configurations in which pitch is held constant, demonstrating the

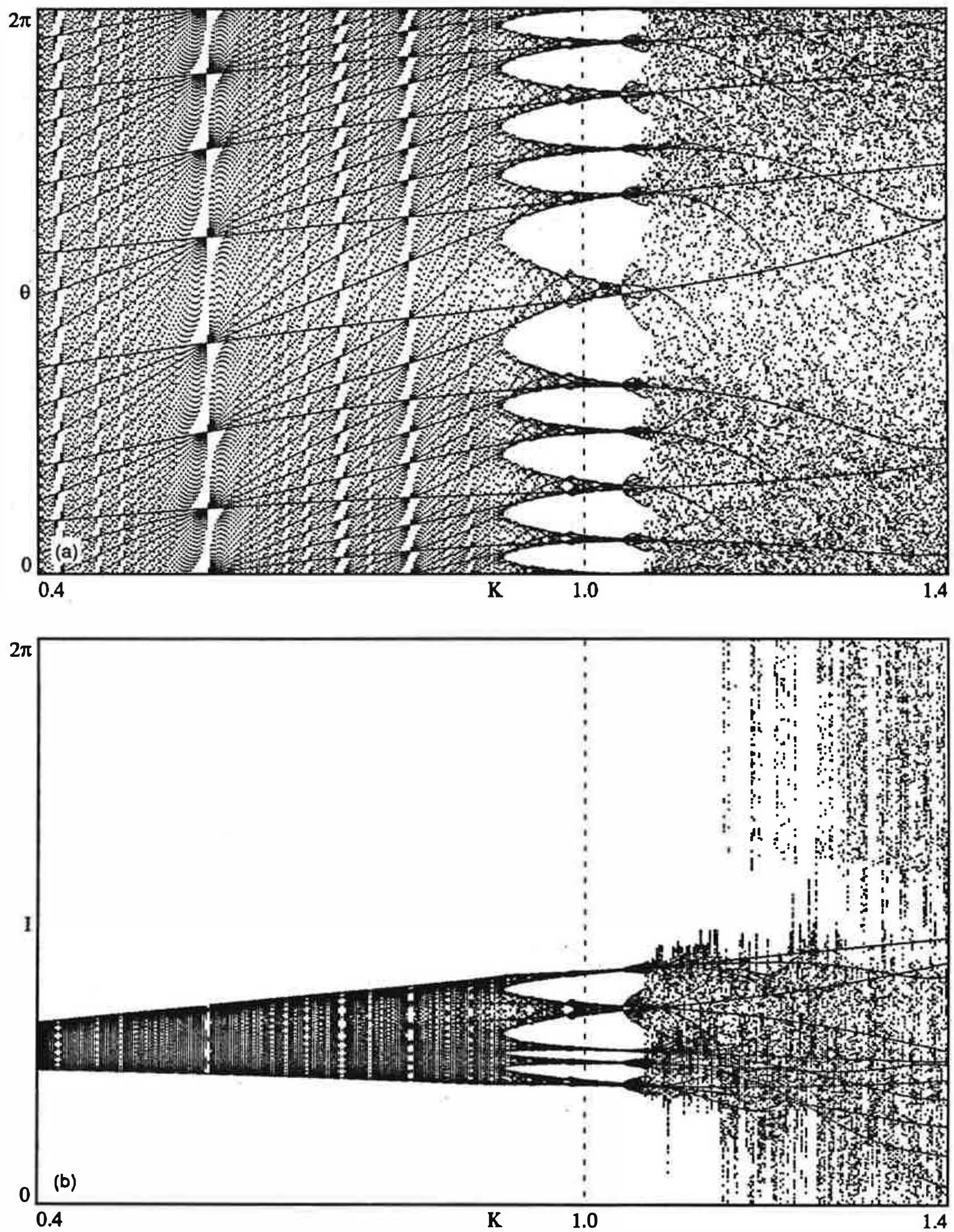

Figure 4.5 Bifurcation diagrams of the standard map, over the range $0.4 \leq K \leq 1.4$, for (a) θ, and (b) I. For all orbits $\theta_0 = \pi/2$, $I_0 = \pi/2$. Orbits are plotted to 120 iterations.

Configuration	*Pitch*	*Velocity*	*INOT*
(a)	I	θ	—
(b)	θ	I	—
(c)	—	θ	I
(d)	—	I	θ
(e)	I	$I^2 + \theta^2$	θ
(f)	θ	I	$I + \theta$

Table 4.1 Mapping configurations of the musical examples.

effectiveness of the same orbit in a purely rhythmic context.

Examples 4(a), 5(a) and 6(a) demonstrate differences and similarities in the musical textures formed from orbits which share similar graphical contours, but differ in detail. Example 4(a) is a cyclical version of the same contour used for Example 5(a). Example 6(a) is also cyclical, but is not composed of as many separate "islands" as 4(a). Example 7(c) illustrates the purely rhythmic potential of a chaotic orbit.

Example 8(e) is quite long, and demonstrates an extended transition time from the lower portion to the upper portion of the braid-like contour of the orbit. Slower, less dramatic oscillations within the initial narrow band are audible. The graphic score shows excerpts from the beginning and the end of the sequence.

Example 9(f) is another long example, from a highly chaotic orbit. Significant variations in local behavior result from the momentary visitation of the orbit to confined regions of the phase space in which it resonates for several iterations before commencing a transition to a another region. The length of each resonance, as well as the size of the region in which it occurs, is variable. At times the sequence becomes almost, but never quite, periodic. At the end (from 150 seconds on), the sequence slips into a resonant band mapped into a softer dynamic range from which it does not escape during the course of this example. Note that certain patterns of melodic contours are repeated, sometimes on an almost note for note basis, at widely separated points in time: for example, the three-tiered pattern in the 6th and 7th seconds recurs at the 144th second, and in inverted form at 61 seconds; and the loud-soft oscillation typical of Examples 1 through 3 is heard briefly at 72 seconds, 83 seconds, 110 seconds, and at 125 seconds.

Example	*Orbit*	*K*	I_0	*Rate*	*n*	*Graphic Score*
1(a)(b)	cyclical	1.3	0	30	75	Figure 4.6
2(a)(b)	cyclical	.97	$3\pi/2$	30	75	Figure 4.7
3(b)	chaotic	1.0	$\pi/4$	15	500	Figure 4.8
3(c)(d)				0-60	75	—
4(a)	cyclical	.97	$\pi/2$	15	150	Figure 4.9
5(a)	chaotic		$3\pi/4$			
6(a)	cyclical		π			
7(c)	chaotic	1.3	$\pi/2$	0-20	500	—
8(e)	chaotic	1.0	$3\pi/4$	0-15	3000	Figure 4.10
9(f)	chaotic	1.3	$3\pi/4$	5-20	2000	Figure 4.11

Table 4.2 Format of the musical examples.

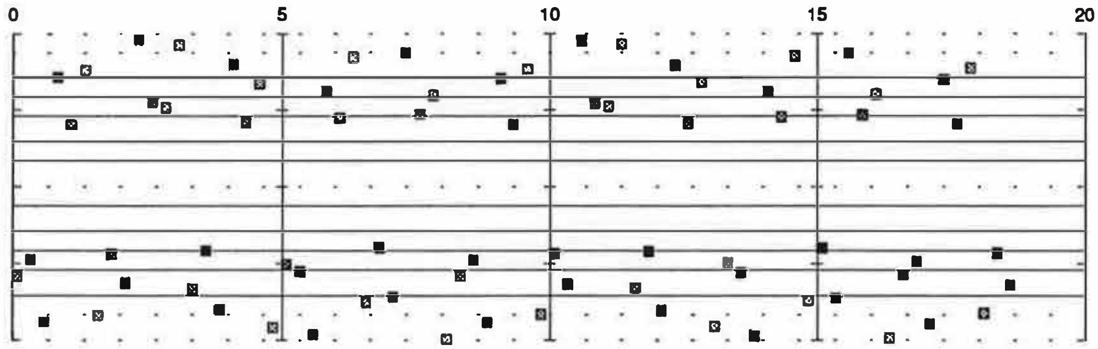

Example 1(a)

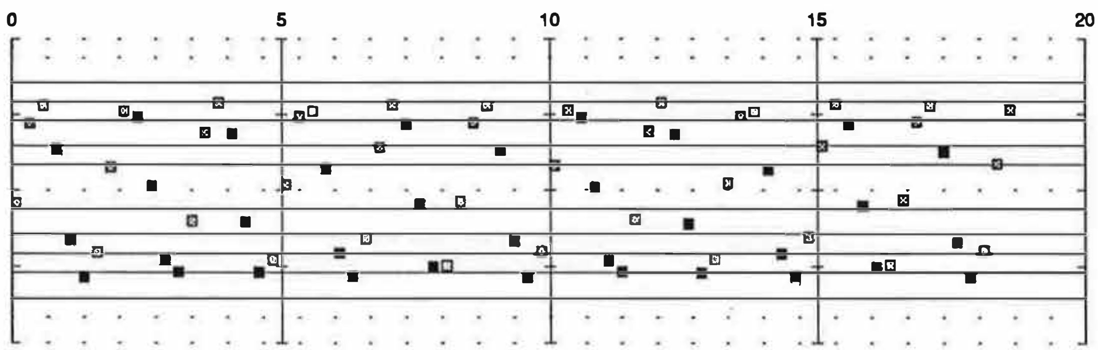

Example 1(b)

Figure 4.6 Scores to Examples 1(a) and 1(b).

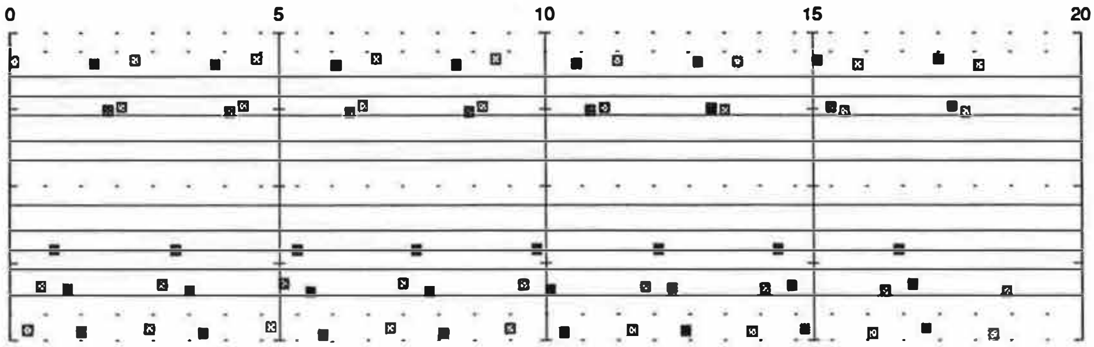

Example 2(a)

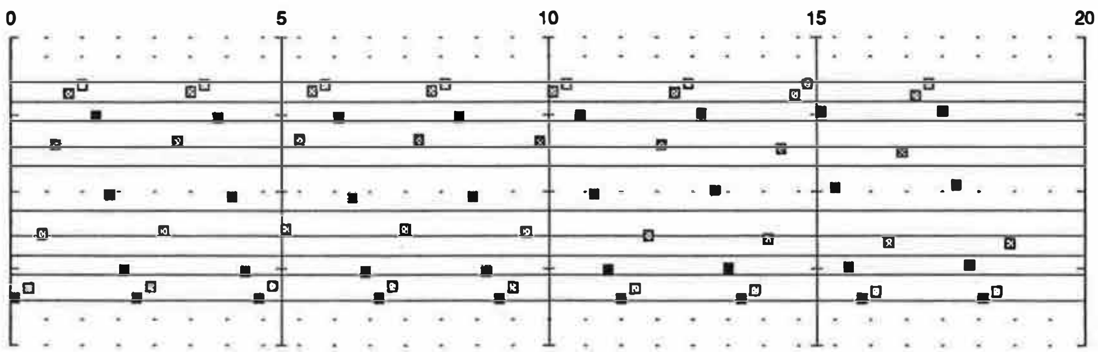

Example 2(b)

Figure 4.7 Scores to Examples 2(a) and 2(b).

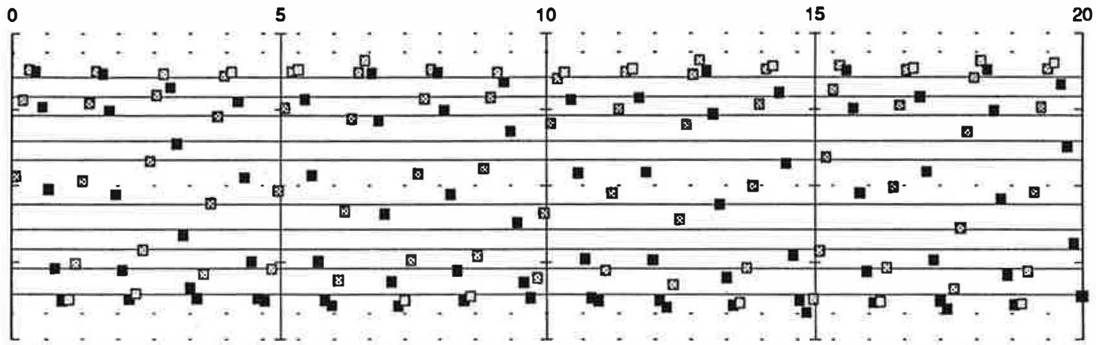

Example 3(b)

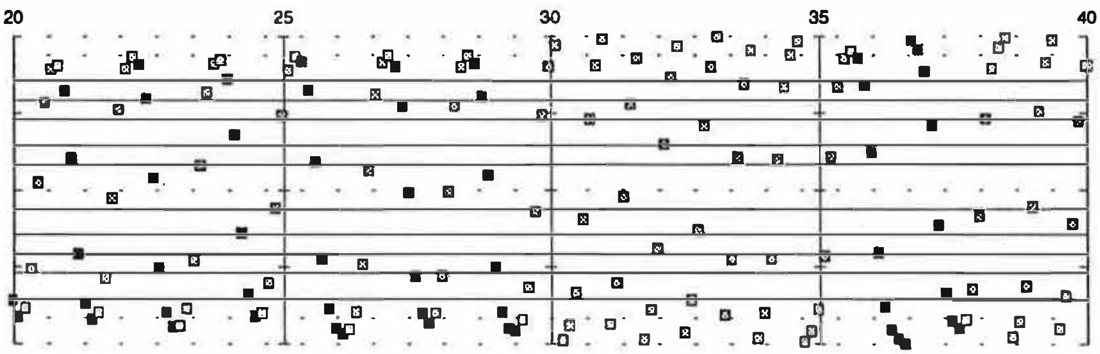

Example 3(b)

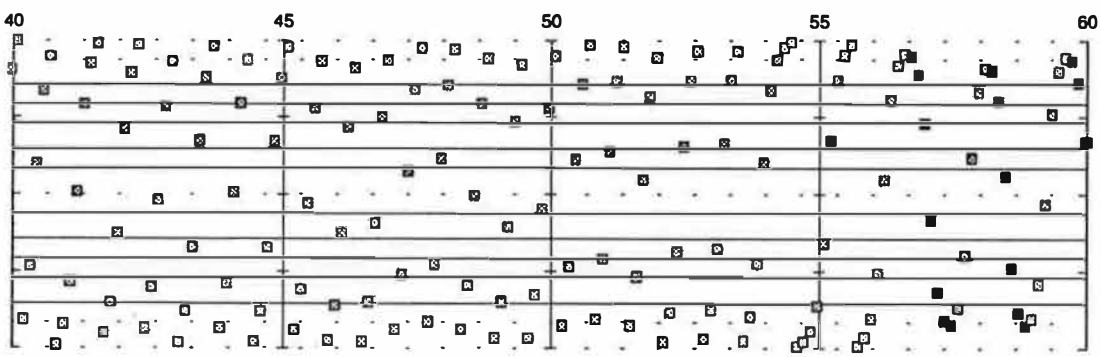

Example 3(b)

Figure 4.8 Score to Example 3(b).

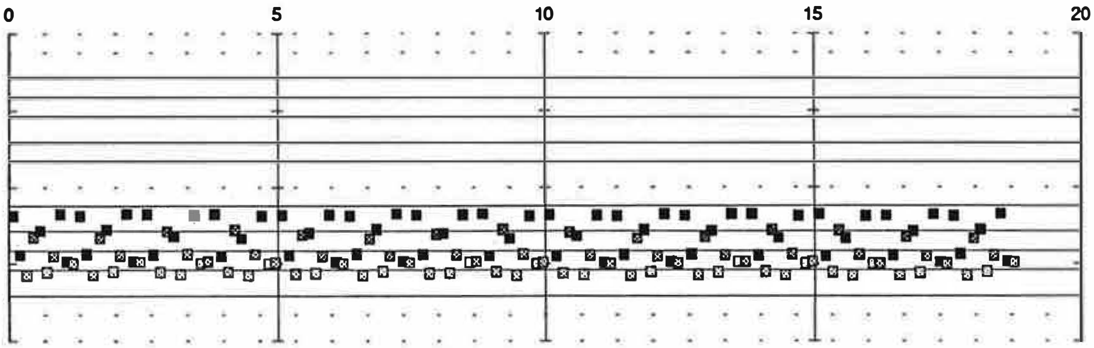

Example 4(a)

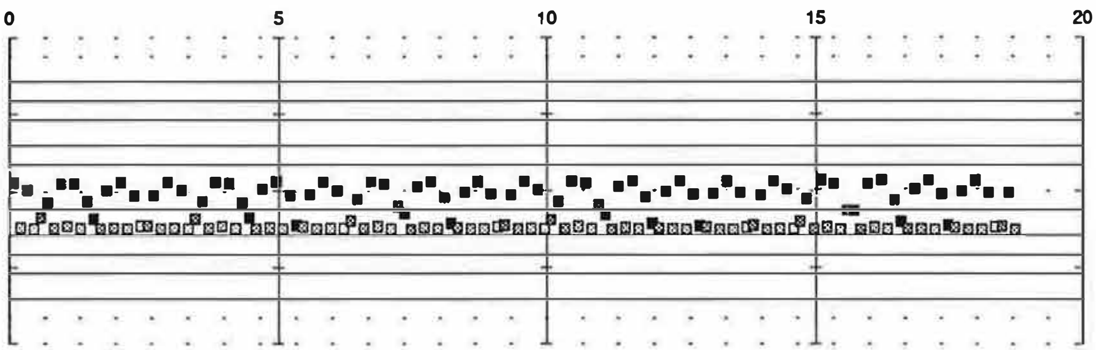

Example 5(a)

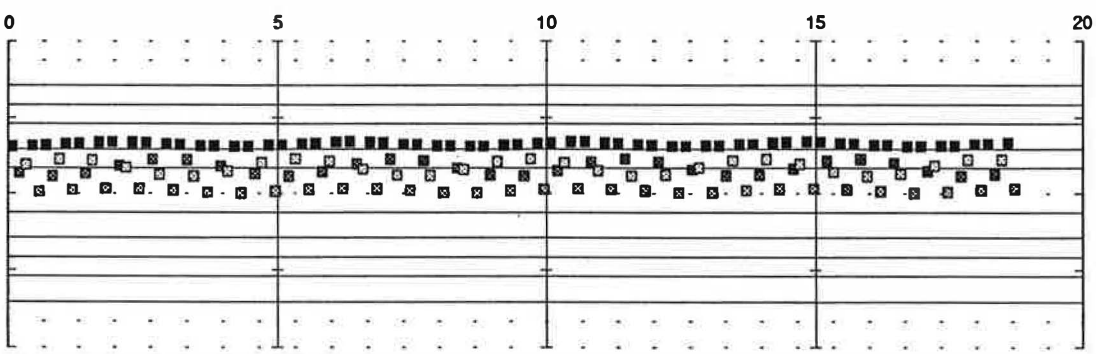

Example 6(a)

Figure 4.9 Scores to Examples 4(a), 5(a) and 6(a).

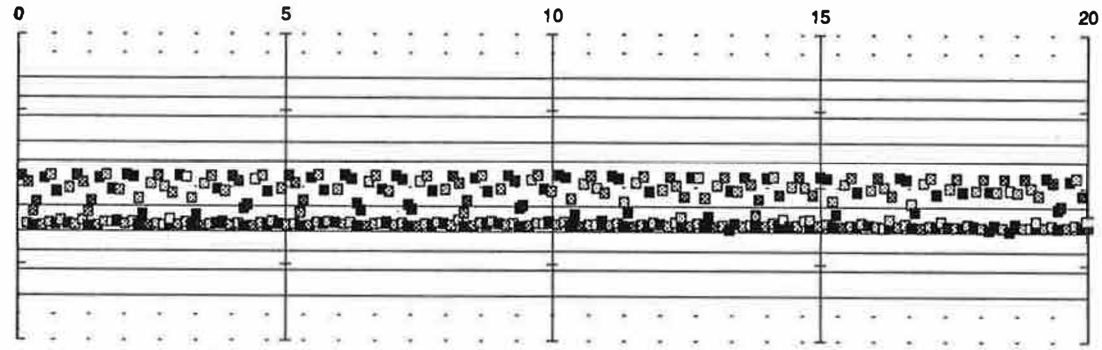

Example 8(e)

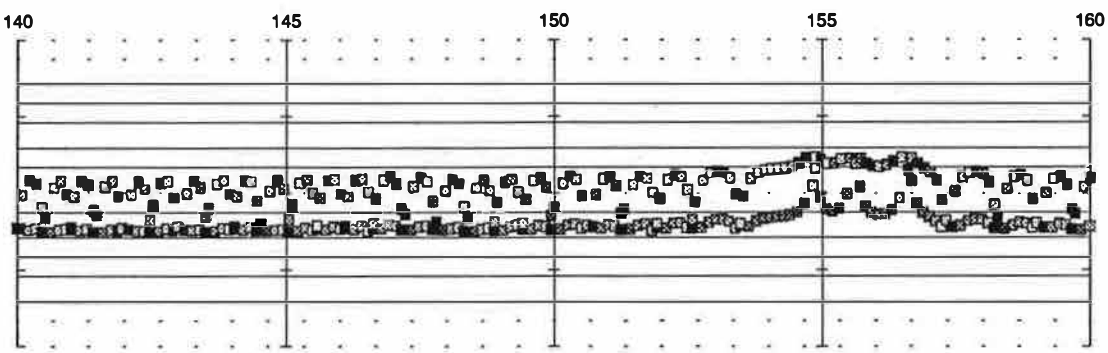

Example 8(e)

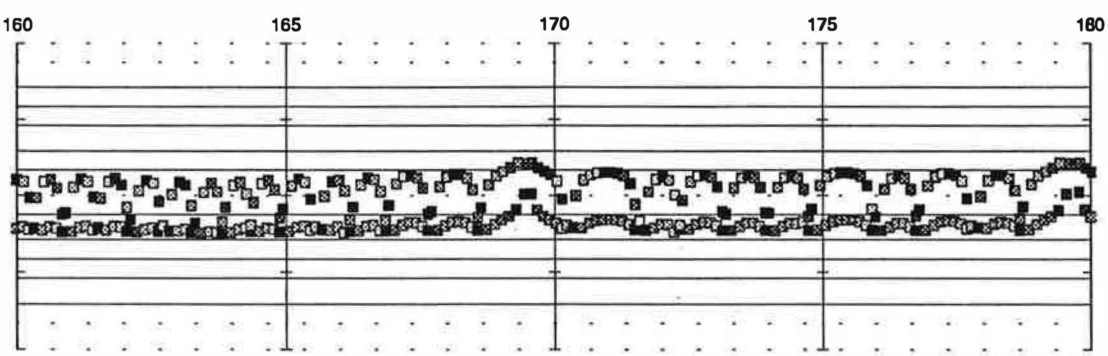

Example 8(e)

Figure 4.10 Score to Example 8(e), excerpts from the beginning and the end.

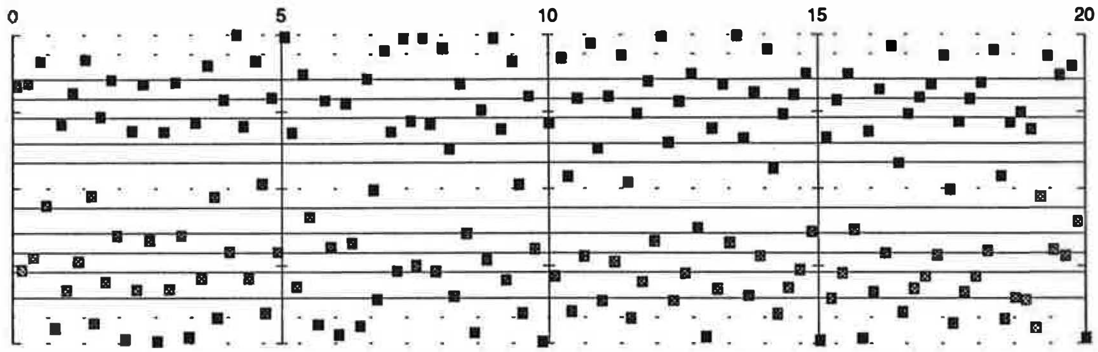

Example 9(f)

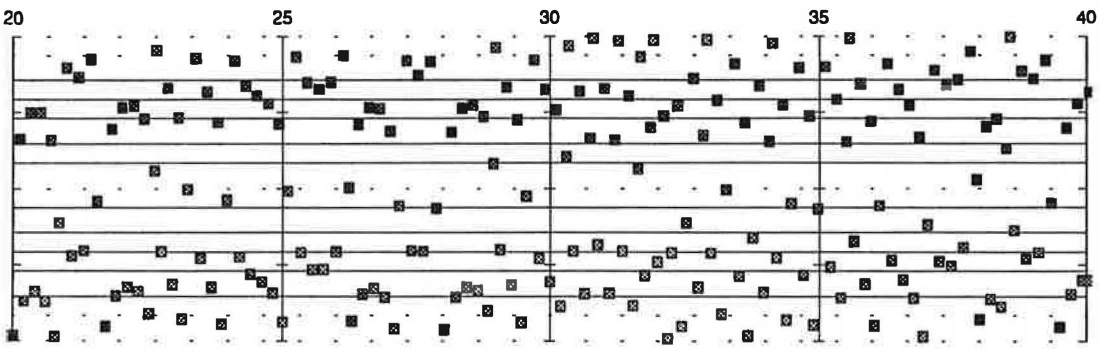

Example 9(f)

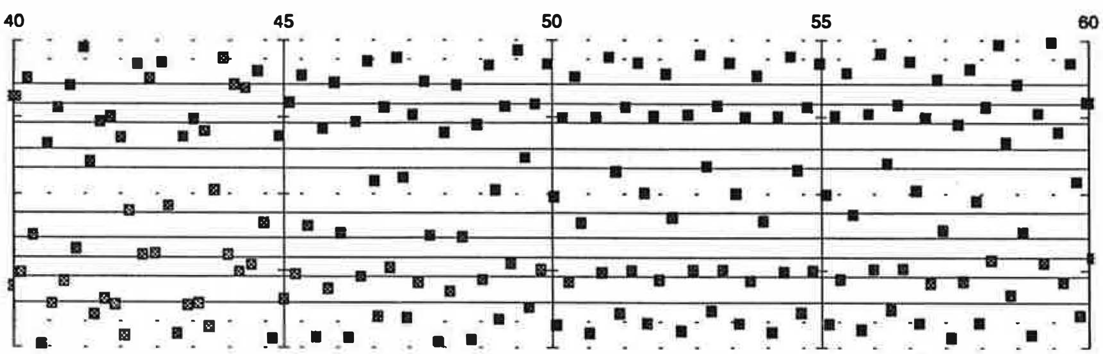

Example 9(f)

Figure 4.11 Score to Example 9(f). Continued on next page.

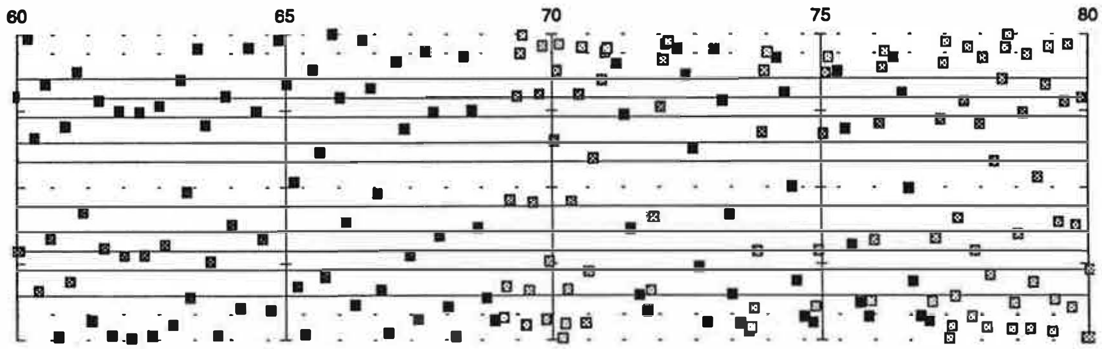

Example 9(f)

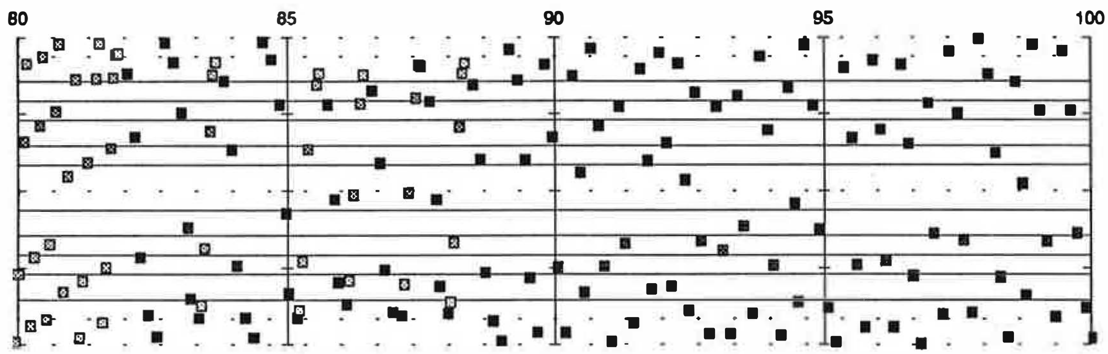

Example 9(f)

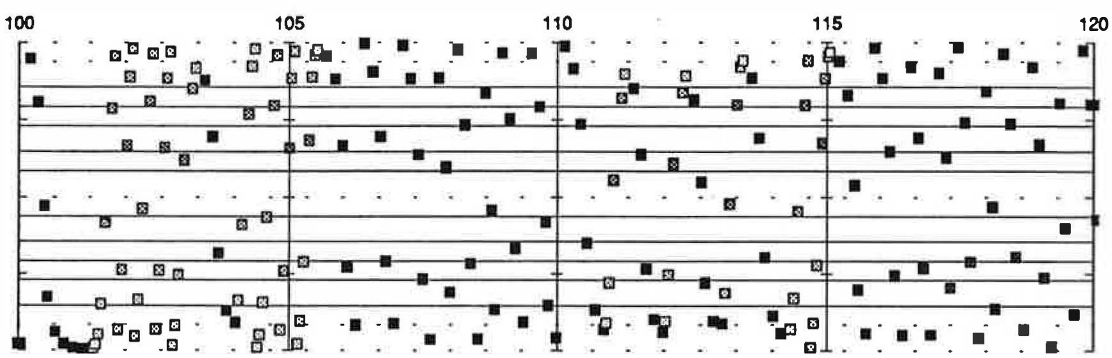

Example 9(f)

Figure 4.11 (cont.) Score to Example 9(f). Continued on next page.

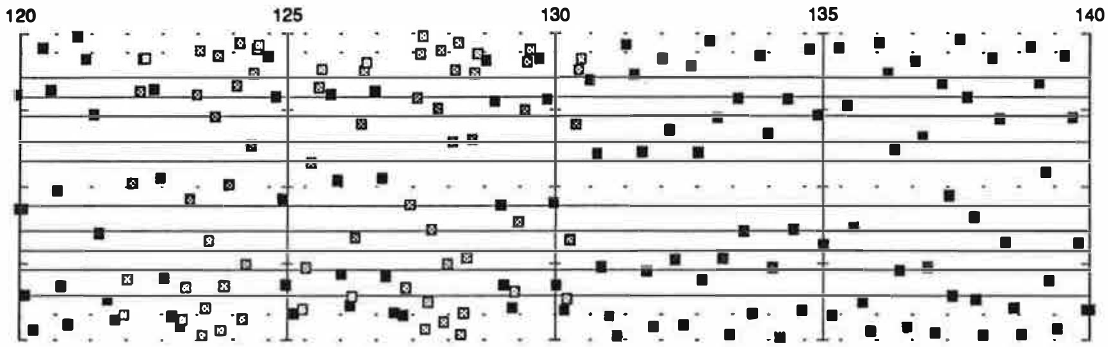

Example 9(f)

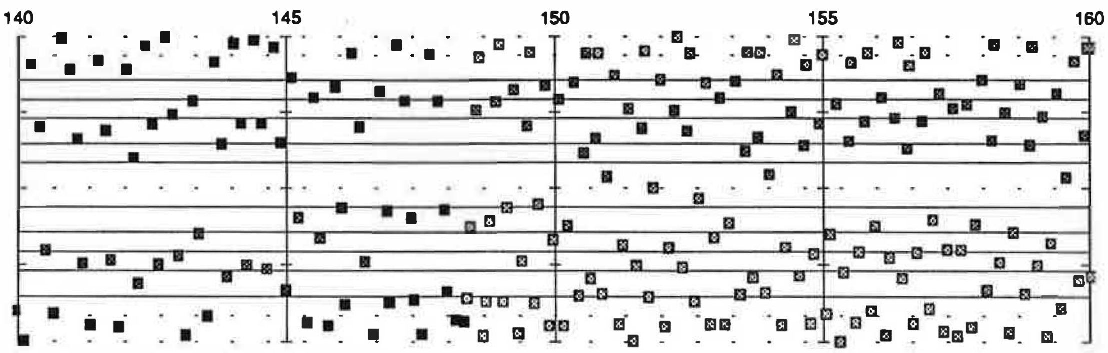

Example 9(f)

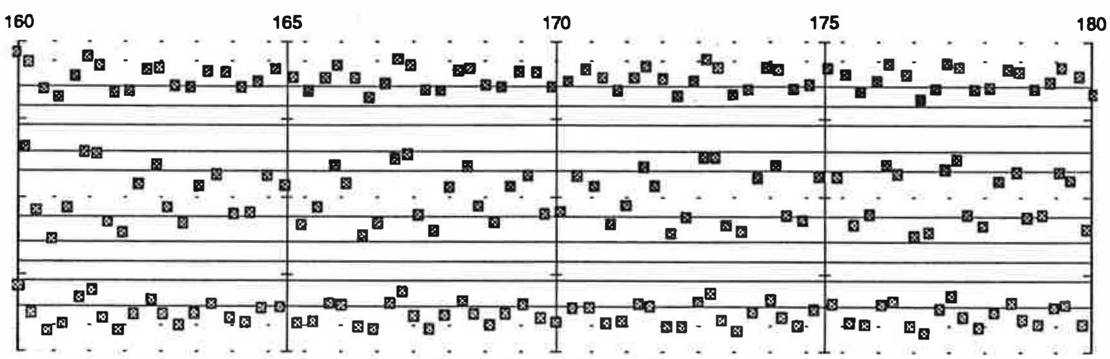

Example 9(f)

Figure 4.11 (cont.) Score to Example 9(f).

Chapter 5

The Hénon-Heiles System

5.1 Technical Description

This system was first introduced by Michel Hénon and Carl Heiles in a 1964 paper discussing certain aspects of galactic motion [33]. According to Helleman, the system "describes the motion of a test-star in the effective potential due to the other stars in the galaxy and a number of other phenomena in physics and chemistry" [31, p. 175]. It is a conservative, area-preserving flow in four dimensions $(x, y, \dot{x}, \dot{y})$:

$$\begin{aligned} \ddot{x} &= -x - 2xy \\ \ddot{y} &= -y - x^2 + y^2, \end{aligned}$$

where $\ddot{x}$ and $\ddot{y}$ are second derivatives of x and y with respect to time. The equations are nonlinear by virtue of the squared quantities. A program to generate orbits of the system in numerical form may be found in Appendix A.5. The following summary of technical aspects of the system is summarized primarily from Hénon and Heiles [33], Gustavson [30], and Ford [23].

One parameter of interest is the total energy E in the system, expressed as

$$E = \frac{1}{2}(x^2 + y^2 + 2x^2y - \frac{2}{3}y^3) + \frac{1}{2}(\dot{x}^2 + \dot{y}^2). \tag{5.1}$$

The behavior of the system varies in a known way as the total energy changes. A degree of control over the output of the system may be facilitated by specifying the initial conditions relative to a desired value for this total energy. A typical means for accomplishing this is to define an orbit in terms of E and a $(y, \dot{y})$ intercept, setting x to zero. Equation (5.1) may then be solved for $\dot{x}^2$. The necessity that $\dot{x}^2$ be positive (so that $\dot{x}$ is not a complex

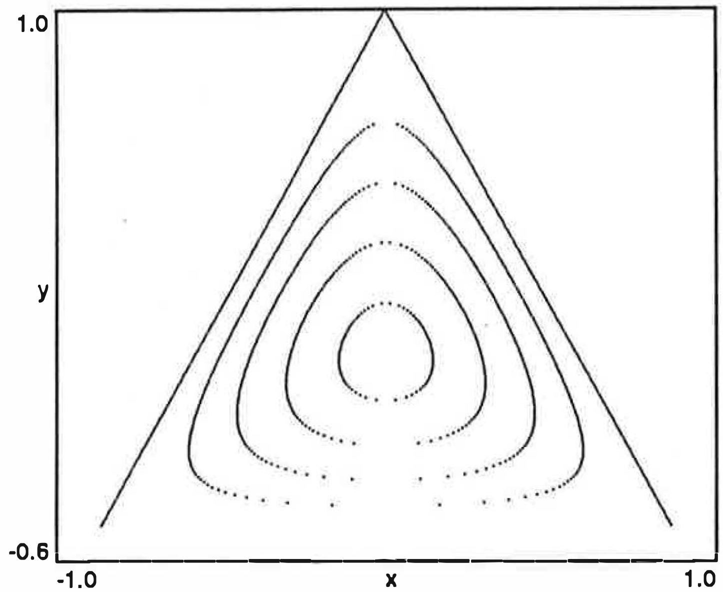

Figure 5.1 Phase space of the Hénon-Heiles system, for five values of E: 1/6, 1/8, 1/12, 1/24, and 1/100. The triangular region corresponds to the maximum energy of 1/6. The space assumes a spherical form and shrinks as the energy decreases.

number) screens out potentially "illegal" initial conditions. If $\dot{x}^2$ is positive, then there are two solutions for $\dot{x}$, one positive, the other negative. This gives two points, $(0, y, \dot{x}, \dot{y})$ and $(0, y, -\dot{x}, \dot{y})$, either of which may be used as the initial point in an orbit of the energy desired. In the illustrations and musical examples which follow, this procedure is used consistently to specify the given orbits. The positive solution of $\dot{x}$ is used in all cases.

Stable orbits of the system are confined to a volume of space defined by Equation (5.1). The shape of this space changes according to the energy of the system. At the maximum energy level of 1/6, the volume intersects the (x, y) plane as a triangular region centered around the origin (0,0,0,0). As the energy decreases, the volume of the phase space shrinks and becomes increasingly spherical. Figure 5.1 graphs the maximum extent of the space as it intersects the (x, y) plane for five different energy levels. Figures 5.2 and 5.3 illustrate two orbits of the system at energy levels of 1/6 and 1/12, respectively. Adopting the terminology established in the preceding chapter, the orbit at $E = 1/12$ will be called cyclic, while that at 1/6 is chaotic. The distinction will become even more palpable in the forthcoming discussion of Poincaré sections taken from these orbits.

The threshold to chaos for most orbits of the Hénon-Heiles system occurs at approximately $E = 1/8$. For energy levels less than this value, all orbits move in closed, cyclical trajectories. At $E = 1/8$, a significant number of initial points produce chaotic

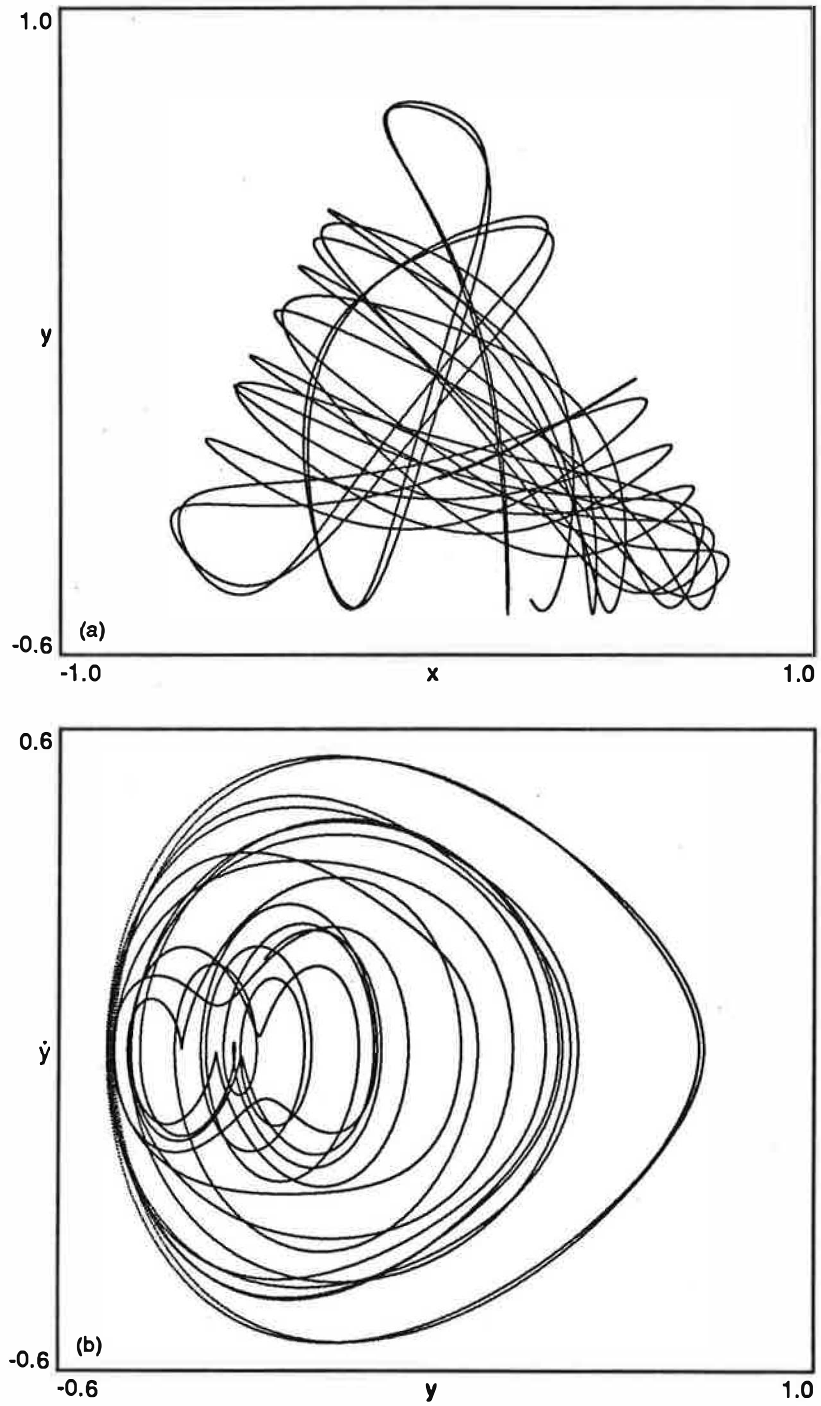

Figure 5.2 Phase portraits of the Hénon-Heiles system, for a chaotic orbit at $E = 1/6$, $y_0 = -.166667 = -E$, $\dot{y}_0 = .166667 = E$; (a) projection onto the (x, y) plane, (b) projection onto the $(y, \dot{y})$ plane.

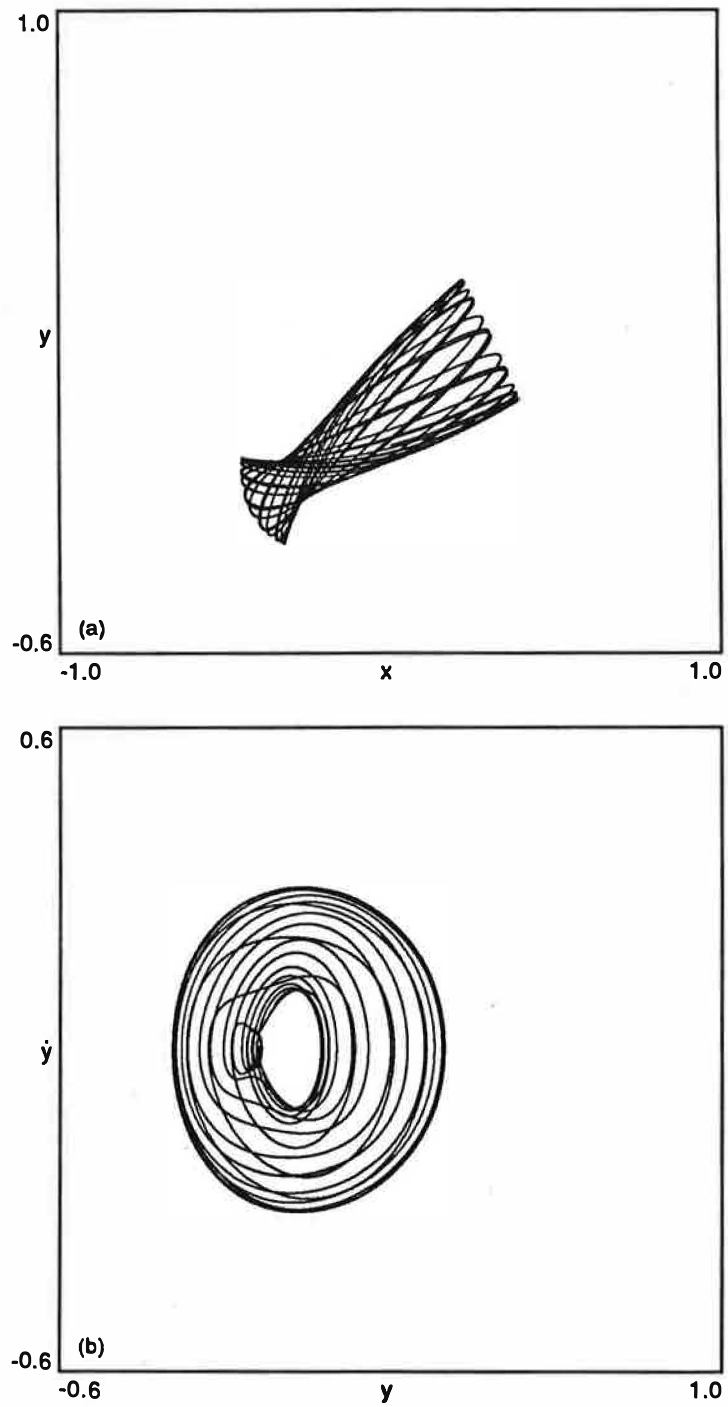

Figure 5.3 Phase portraits of the Hénon-Heiles system, for a cyclical orbit at $E = 1/12$, $y_0 = -.083333 = -E$, $\dot{y}_0 = .083333 = E$; (a) projection onto the (x, y) plane, (b) projection onto the $(y, \dot{y})$ plane.

orbits. This marks the transition to the chaotic regime, which, like the other systems discussed, also contains interspersed regimes of periodicity. As E continues to increase towards 1/6, the ergodicity of a given trajectory increases as well. Nonetheless, there remain a small number of initial points which still produce cyclic orbits. Above the critical value $E = 1/6$, all orbits become unstable.

The Poincaré section affords a superior means by which an overview of the global behavior of the system may be attained. The usual method is to place the sectional plane at $x = 0$ and to plot the values of y and $\dot{y}$ whenever the orbit punctures the plane in the positive direction (which means that $\dot{x}$ will be positive). This produces a three-dimensional section $(y, \dot{x}, \dot{y})$, of which only the y and $\dot{y}$ coordinates are plotted. For the sections illustrated in Figures 5.4 through 5.6, the initial $(y_0, \dot{y}_0)$ points are specified in terms of the energy E. Eight such points have been chosen, which are employed consistently throughout the sectional graphs; these are $(-2E, 2E)$, $(-E, E)$, $(0,0)$, $(0, 2E)$, (E, E), $(2E, E)$, $(3E, 0)$, and $(3E, -E)$. Note that, like the standard map, cyclical orbits are confined to non-overlapping resonance loops, while chaotic orbits tend to overlap completely, filling the entire volume of the phase space. Another feature of the standard map shared by this system are the "chains of islands" formed by some cyclical orbits.

Further discussion of the Hénon-Heiles system may be found in Contopoulos [15], Lebowitz and Penrose [37], Rauh, Andrade and Kougias [58], and Barbanis [5] in a more generalized form.

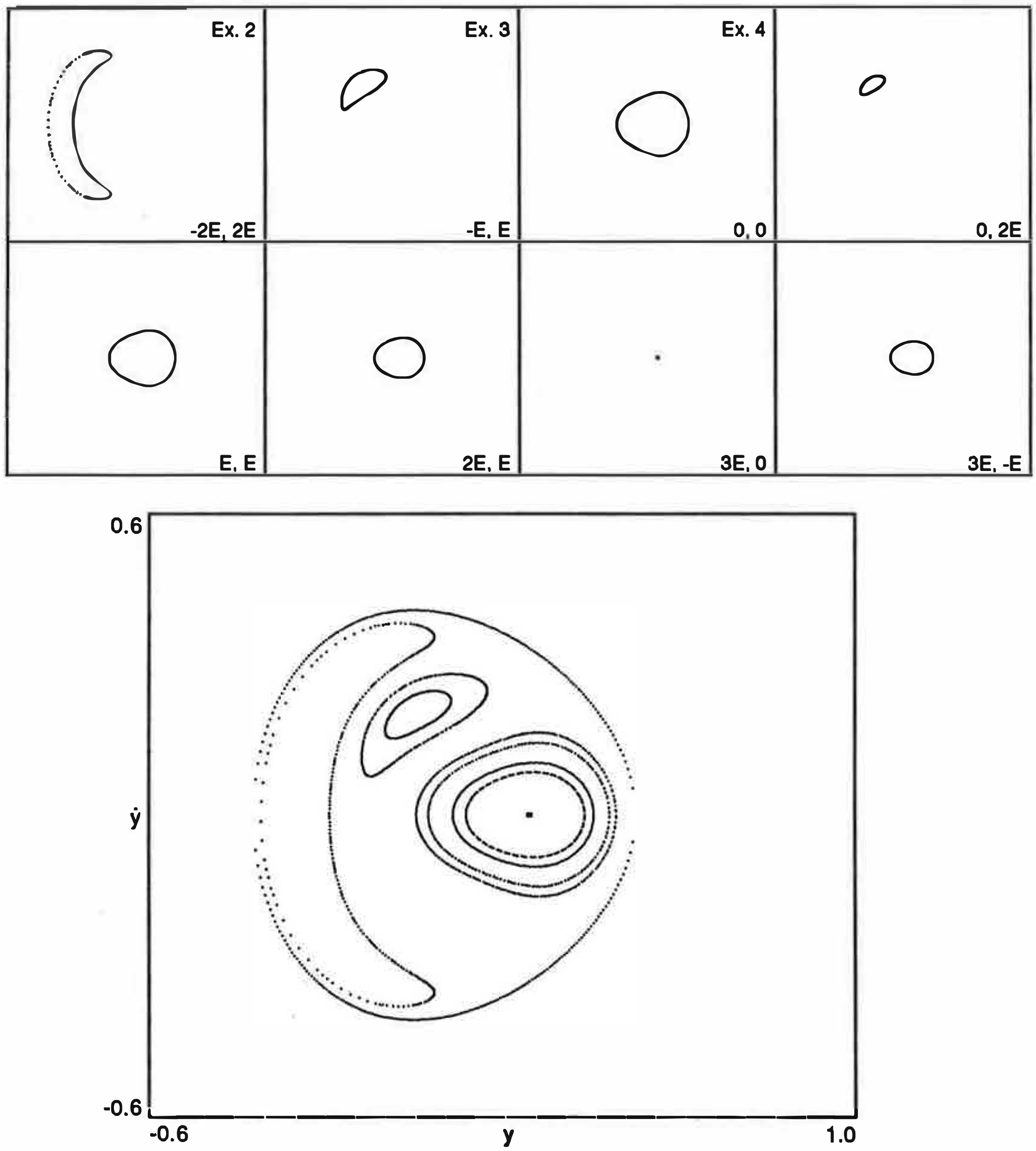

Figure 5.4 Poincaré sections of the Hénon-Heiles system, at $E = 1/12$. Eight orbits are shown individually, and in superimposition in the large graph. The initial $(y_0, \dot{y}_0)$ point of each orbit is given in the lower right-hand corner of each of the eight smaller plots. The outer-most curve circumscribing the orbits in the large graph marks the boundary of the region in which all stable orbits remain confined. At this energy level, all orbits are cyclical and non-overlapping. Orbits which are used in the musical examples are marked.

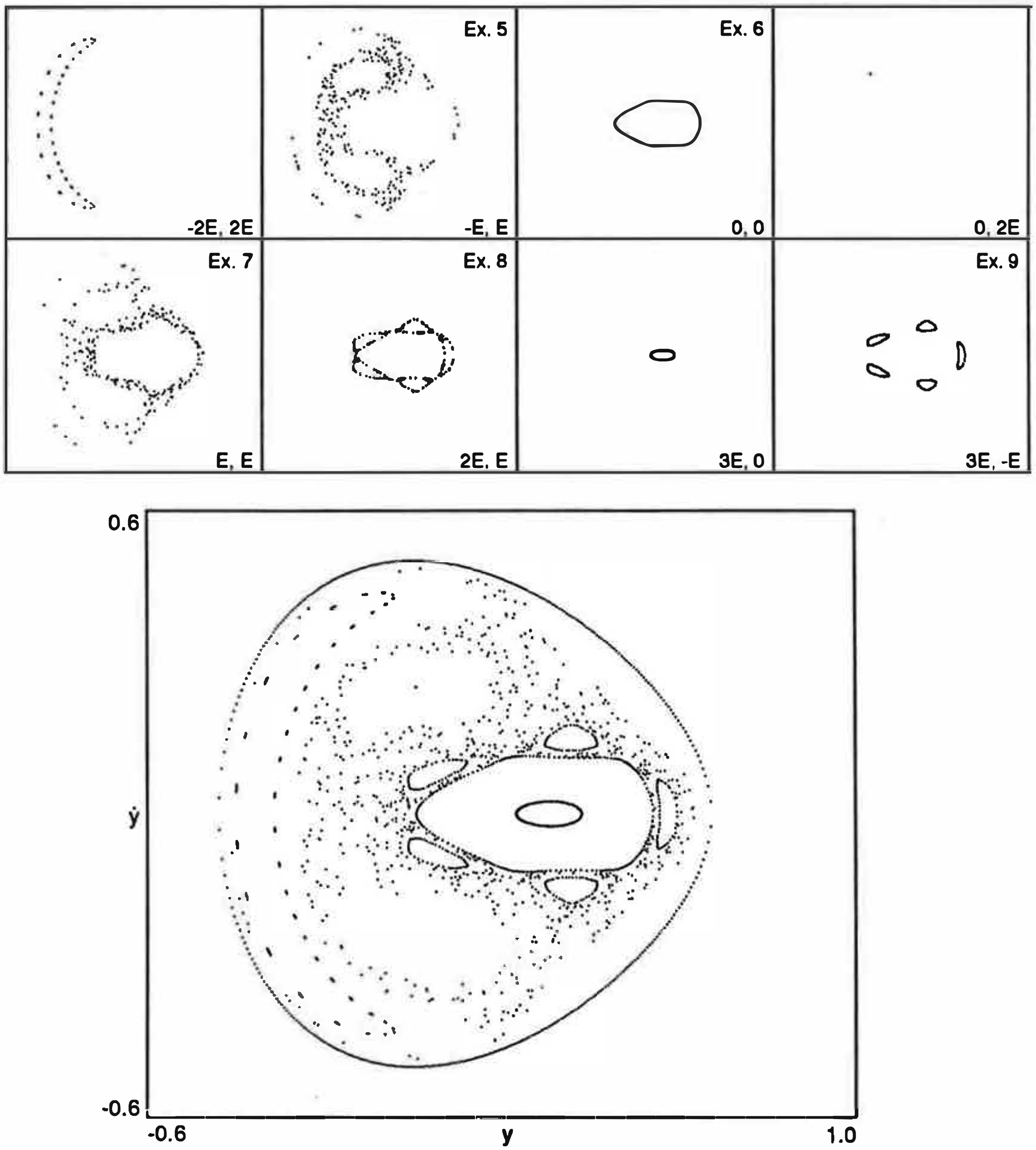

Figure 5.5 Poincaré sections of the Hénon-Heiles system, at $E = 1/8$. Eight orbits are shown individually, and in superimposition in the large graph. At this energy level, a number of orbits are still cyclical, while others are chaotic. Note that the three orbits beginning at (0,0), $(2E, E)$ and $(3E, -E)$ do not overlap, whereas the space filled by the two chaotic orbits beginning at $(-E, E)$ and (E, E) does. The cyclical orbits starting from $(-2E, 2E)$ and $(3E, -E)$ have split to form chains of islands. Orbits which are used in the musical examples are marked.

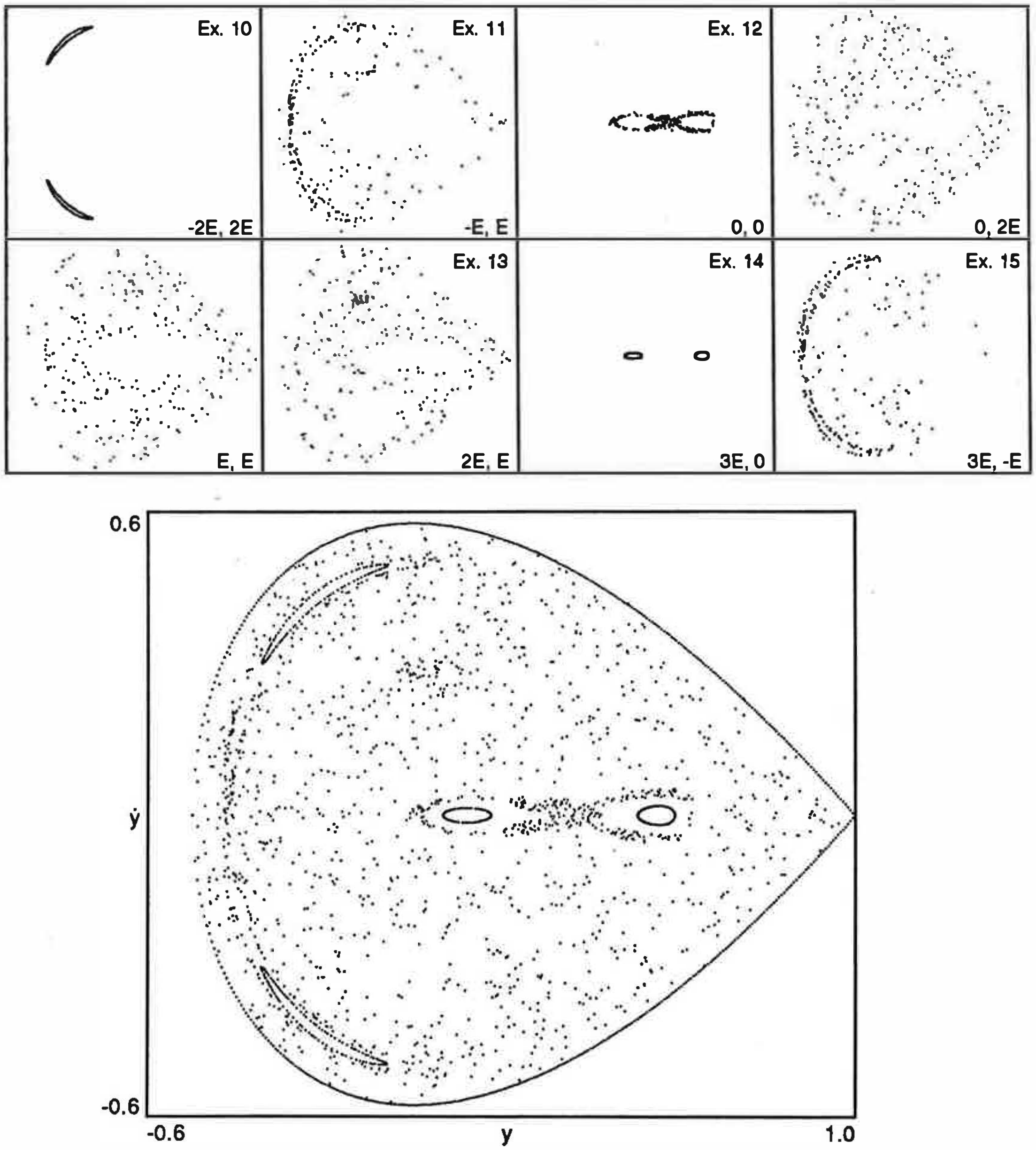

Figure 5.6 Poincaré sections of the Hénon-Heiles system, at $E = 1/6$. Eight orbits are shown individually, and in superimposition in the large graph. At this energy level, most orbits are chaotic, though a few cyclical trajectories remain. The chaotic orbit starting at (0,0) will eventually break out of its confinement and fill the entire region in the manner of the other chaotic orbits. Note the small areas of relatively higher concentration of points in the orbits starting at $(-E, E)$, $(2E, E)$ and $(3E, -E)$. Orbits which are used in the musical examples are marked.

5.2 Musical Examples

The musical examples consist on one long sequence with two voices, generated from continuous orbits of the Hénon-Heiles system, followed by a number of short sequences generated from Poincaré sections of the system. The cross-sectional examples employ two mapping configurations, which are summarized in Table 5.1. Although the Poincaré maps illustrated in the previous section plot the positions of only two coordinate values (y and $\dot{y}$), the musical examples take advantage of all three coordinates values (x, y and $\dot{y}$) obtained in the process of computing the sections. The format of the musical examples is summarized in Table 5.2. In all of the Examples 2 through 15, the inter-note onset time (INOT) varies between 5 and 20 pulses, that is, between 1/24 and 1/6 of a second.

Example 1 demonstrates the effect of a small difference in the starting positions of two continuous chaotic orbits as sensitive dependence on initial conditions causes a divergence between the two trajectories. The initial point of the first voice is ($y_0 = -0.166667$, $\dot{y}_0 = 0.166667$), while the initial point of the second voice is ($y_0 = -0.1666$, $\dot{y}_0 = 0.1666$). The energy E is 1/6 (= 0.166667) for both voices. The first voice therefore corresponds to the orbit plotted in Figure 5.2. The mapping configuration for both voices is as follows: pitch varies according to $\dot{y}$, velocity according to x, and inter-note onset time according to y. The last variable, $\dot{x}$ allows a mapping of one additional parameter in the musical domain. In this example, $\dot{x}$ has been mapped to the volume of a second synthesizer which is synchronized with the primary voices. The effect of this is to add additional tone color as the value of $\dot{x}$ increases. Inter-note onset time varies between 0 and 30 pulses, that is, between 0 and a quarter of a second. In general, the divergence of the voices is more gradual than is the case with the first example from the Lorenz system, and the behavior of the voices remains more consistently the same throughout the span of the example.

Examples 2, 3 and 4 demonstrate the effect of cyclical, low-energy orbits of various dispositions in the phase space (see Figure 5.4). The sound of these examples is comparable to that of the similarly cyclical orbits generated produced from the standard map, although the presence of three variables, rather than only two, adds some richness.

At an energy level of 1/8, the system generates a mix of chaotic and cyclical orbits (see Figure 5.5). Examples 5(a) and 5(b) illustrate two mappings of the same chaotic orbit, and demonstrate the very different melodic contours to be obtained through the employment of alternate mapping configurations from the same data. Nonetheless, a careful examination of the two scores reveals correlations (with slight differences in timing): behavior A, from 0 to 7 (8) seconds; behavior B, from 7 (8) to 20 (21) seconds; return to A from 20 (21) to 26 seconds; behavior C from 26 to 34 seconds; return to A at the end. Unlike the mappings of chaotic orbits of the standard map, which retain a consistency of register, these sequences are far more erratic in their excursions through the pitch space.

Example 6(a) is generated from a large loop in the middle of the phase space. The variability of the texture is perhaps greater than one might expect from the visual appearance of the orbit. Example 7(a) presents another chaotic orbit, similar to Example 5. The more concentrated distribution of points in the middle of the phase space relative to Example 5 is reflected in the more even texture and the less extensive variation in ambitus of the melodic contour. Examples 8 and 9 compare two orbits with similar visual shapes, the chains of five chaotic islands and five cyclical islands of Figure 5.5. Although the eye makes a ready distinction between the two orbits, their aural effects are more subtle. Evidently the alternating sequence of points among the five islands is already sufficiently complex that the slight additional turbulence in the chaotic version is inadequate to radically alter the sound.

At the highest energy level, $E = 1/6$, most orbits are highly ergodic and fill the entire volume, although a few cyclical holdouts remain (see Figure 5.6). Examples 10(a) and 10(b) illustrate a cyclical orbit that is split into two islands, one at each tip of the "crescent moon" area in the left side of the phase plot. The configuration of 10(b) makes the registral distinction between the two islands obvious, while for 10(a) this distinction is mapped into rhythm and is not as apparent. Examples 11(a) and 11(b) are generated from a chaotic orbit which also devotes a considerable number of iterations to filling in the same crescent-shaped area. This concentration of activity takes place during the latter half of the example, after 15 seconds have elapsed. Note that the crescent-shaped area filled in is larger and more loosely defined than that of Example 10, one artifact of which is the generally even distribution of pitch across the space in the latter half of 11(b). The two or three second sequence of points confined to a tight range starting at the 10th second is also the result of a similar filling of a small region of the phase space. The concentration of points which correspond to this sequence is not easily visible in Figure 5.6, although a comparable and more easily visible activity takes place in Example 13, forthcoming.

Example 12(a) illustrates a confined chaotic orbit in which the concentration

Configuration	*Pitch*	*Velocity*	*INOT*
(a)	y	$\dot{x}$	$\dot{y}$
(b)	$\dot{y}$	y	$\dot{x}$

Table 5.1 Mapping configurations of the musical examples.

of points in the space provides little audible variety. Example 13(a) is from another highly chaotic sequence. The small area centered around ($y = 0$, $\dot{y} = 0.3$) in Figure 5.5, containing a higher than average density of points, is filled in twice during the course of the example, once between 5 and 10 seconds, and again between 31 and 36 seconds. Example 14(b) illustrates a cyclical orbit between two islands, in the same general region of the phase space as the orbit for Example 12(a). The mapping configuration distinguishes notes generated from each of the islands by velocity rather than pitch. Example 15(b) is another chaotic orbit in the style of Example 11—its latter half is confined within the boundaries of the crescent moon area (it would eventually break out of this confinement if allowed to run long enough). Interestingly, this orbit becomes nearly periodic from between approximately 26 and 33 seconds.

In terms of ease of use, the sections of the Hénon-Heiles system suffers from the same inconvenience in handling as do the sections of the Lorenz system, namely that they must be pre-computed and stored for later use. The versatility of the melodic/textural contours possibly justifies this overhead, however.

Example	E	*Orbit*	y	$\dot{y}$	n	*Graphic Score*
1	1/6	chaotic	$-E$	E	(5 min.)	Figure 5.7
2(a)(b)	1/12	cyclical	$-2E$	$2E$	100	Figure 5.8
3(a)	1/12	cyclical	$-E$	E	100	Figure 5.8
4(a)	1/12	cyclical	0	0	100	Figure 5.9
5(a) 5(b)	1/8	chaotic	$-E$	E	250	Figure 5.9 Figure 5.10
6(a)	1/8	cyclical	0	0	100	Figure 5.10
7(a)	1/8	chaotic	E	E	250	Figure 5.11
8(a) 8(b)	1/8	chaotic	$2E$	E	100	Figure 5.11 Figure 5.12
9(a)(b)	1/8	cyclical	$3E$	$-E$	100	Figure 5.12
10(a)(b)	1/6	cyclical	$-2E$	$2E$	100	Figure 5.13
11(a) 11(b)	1/6	chaotic	$-E$	E	250	Figure 5.14 Figure 5.15
12(a)	1/6	chaotic	0	0	100	Figure 5.15
13(a)	1/6	chaotic	$2E$	E	250	Figure 5.16
14(b)	1/6	cyclical	$3E$	0	100	Figure 5.16
15(b)	1/6	chaotic	$3E$	$-E$	250	Figure 5.17

Table 5.2 Format of the musical examples.

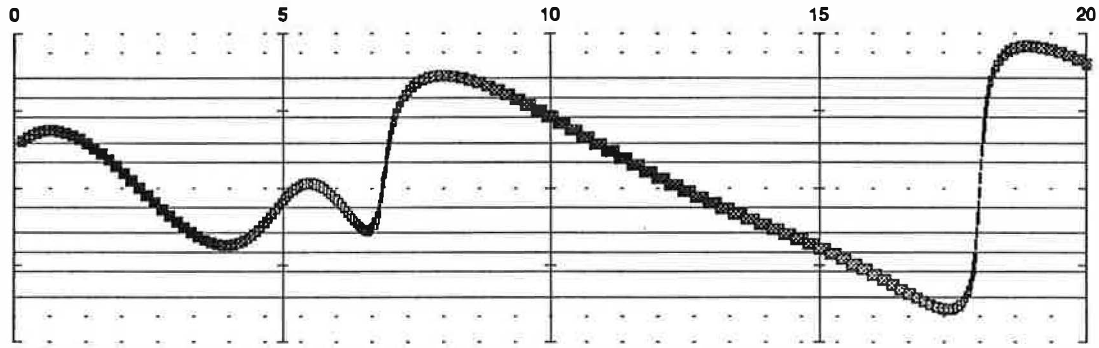

Example 1

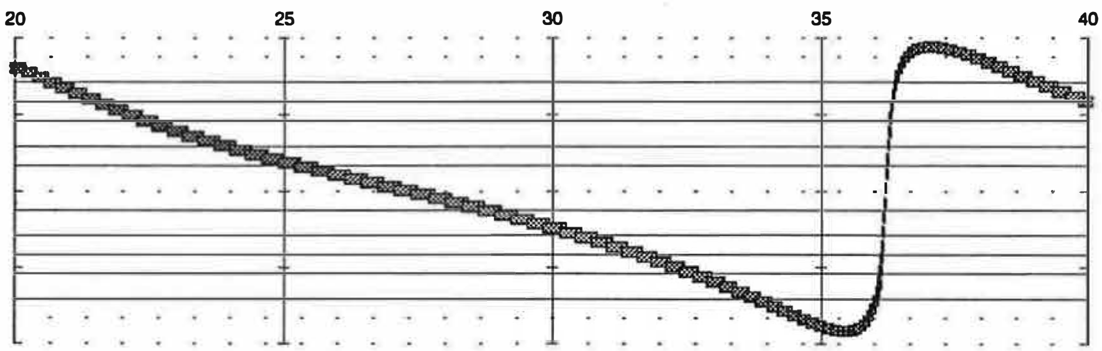

Example 1

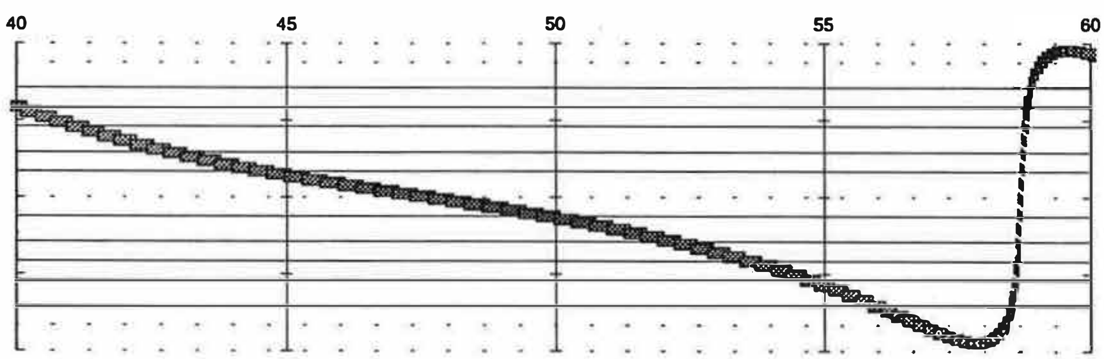

Example 1

Figure 5.7 Score to Example 1. Continued on next page.

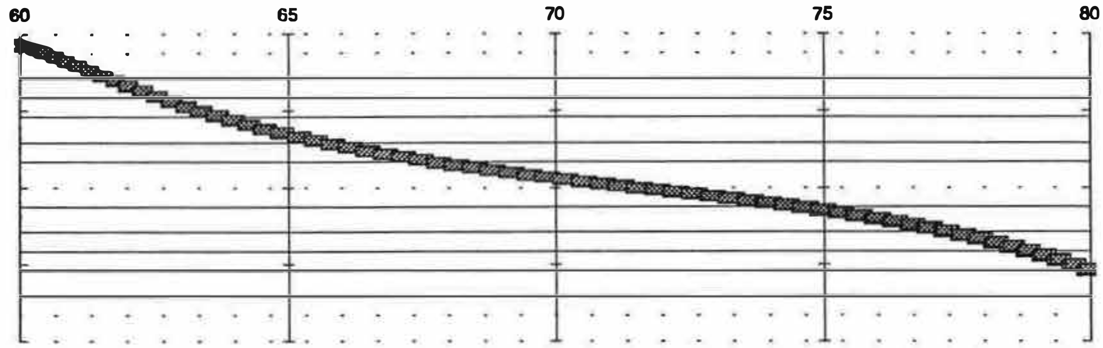

Example 1

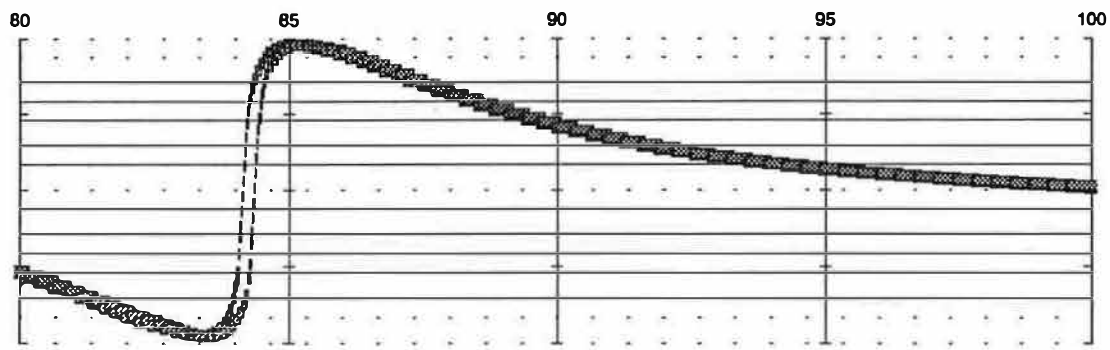

Example 1

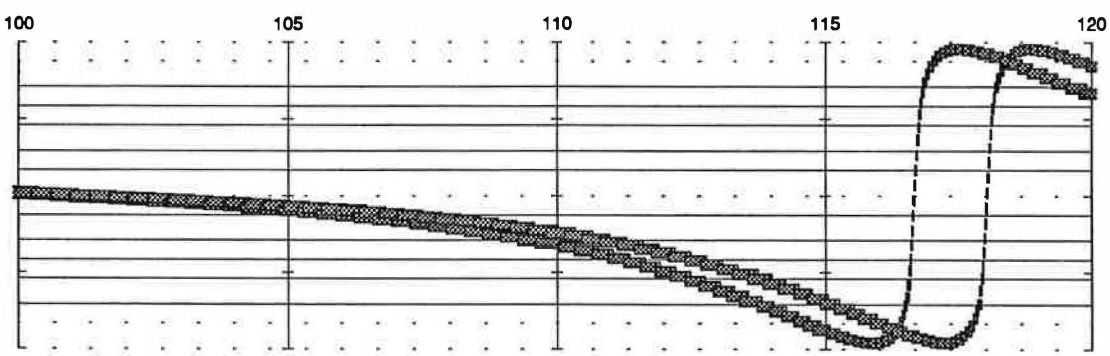

Example 1

Figure 5.7 (cont.) Score to Example 1. Continued on next page.

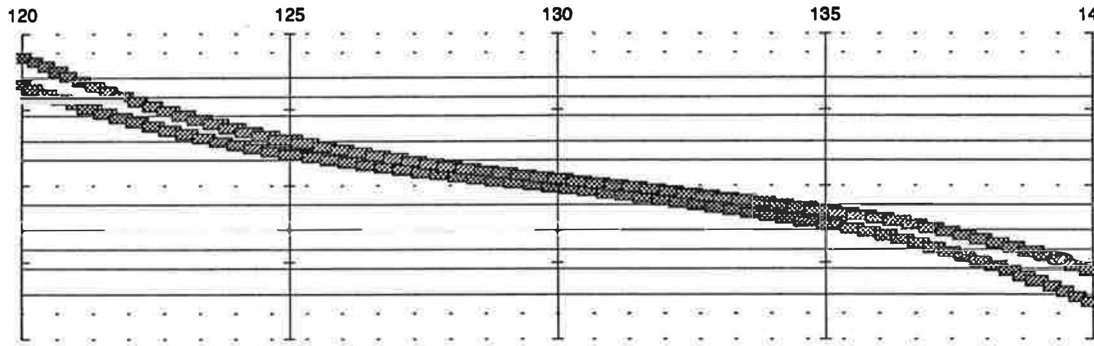

Example 1

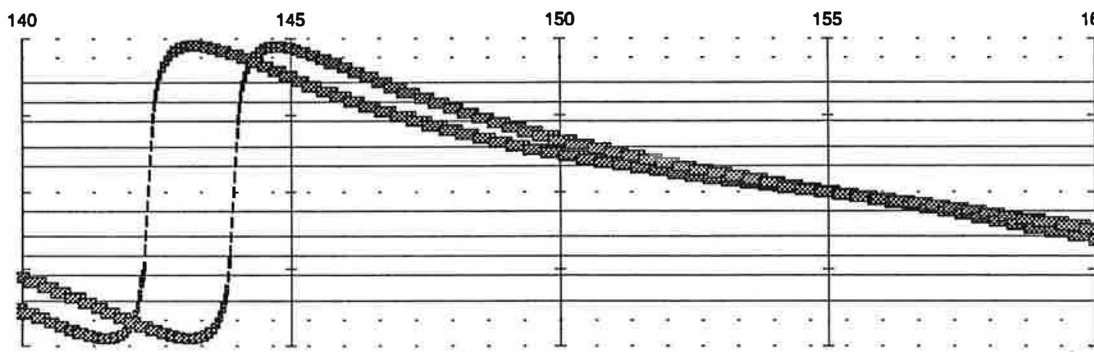

Example 1

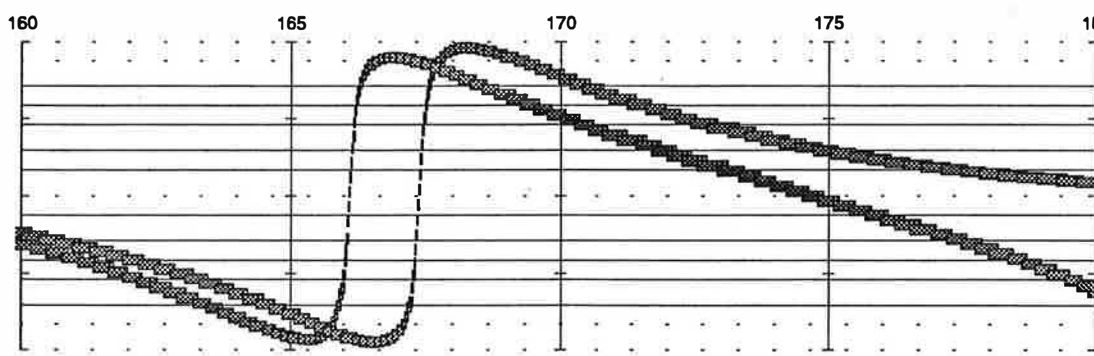

Example 1

Figure 5.7 (cont.) Score to Example 1. Continued on next page.

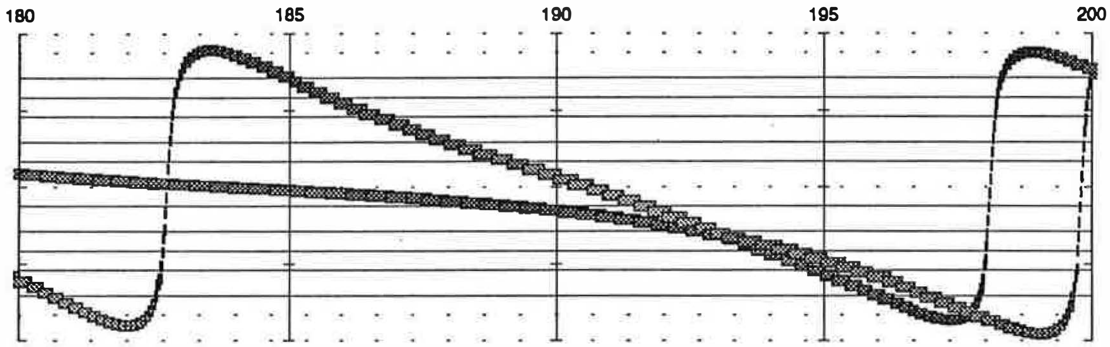

Example 1

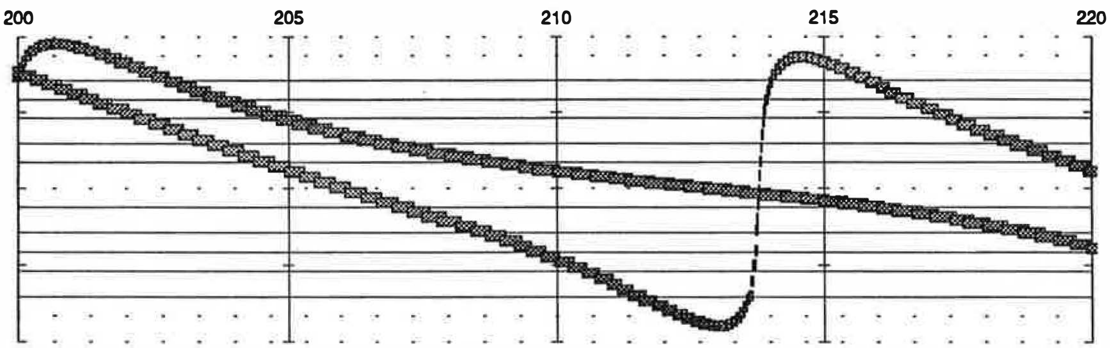

Example 1

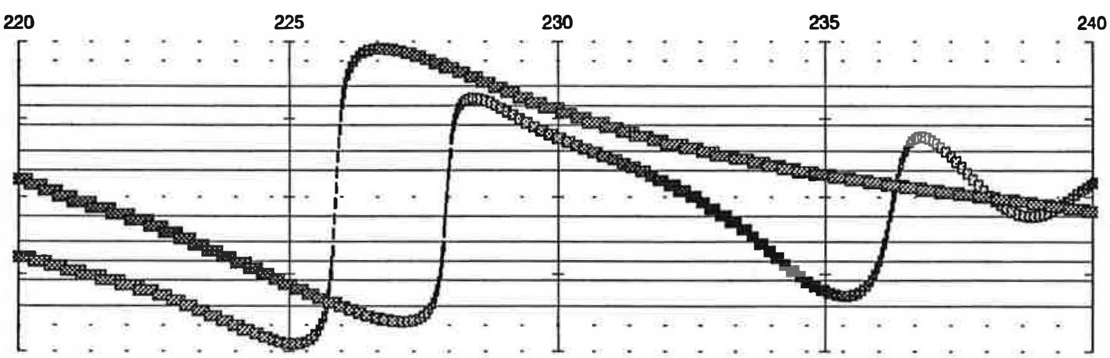

Example 1

Figure 5.7 (cont.) Score to Example 1. Continued on next page.

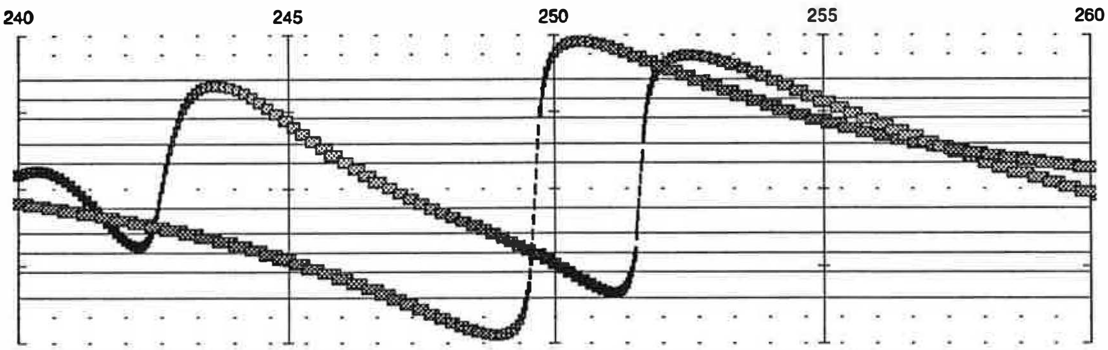

Example 1

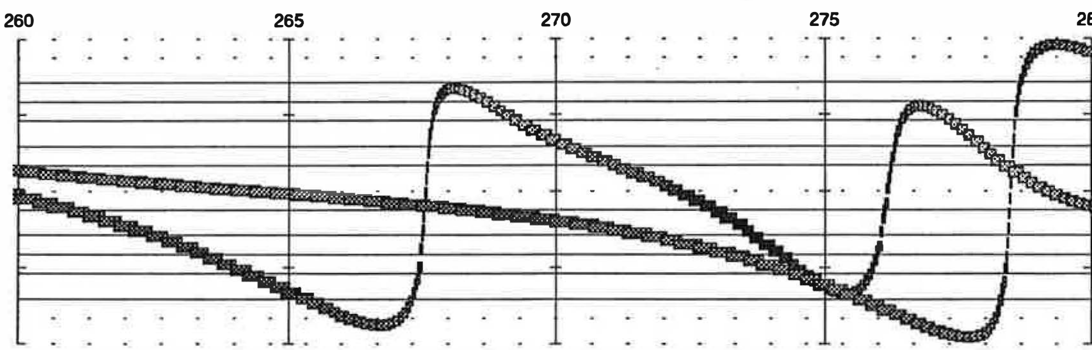

Example 1

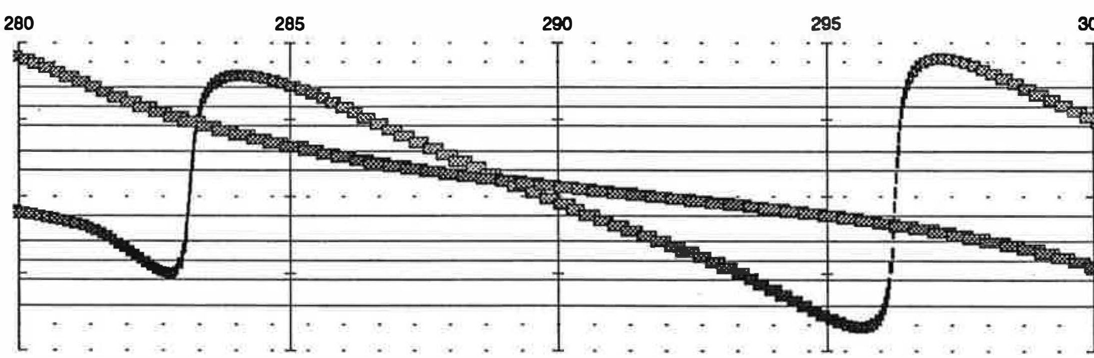

Example 1

Figure 5.7 (cont.) Score to Example 1.

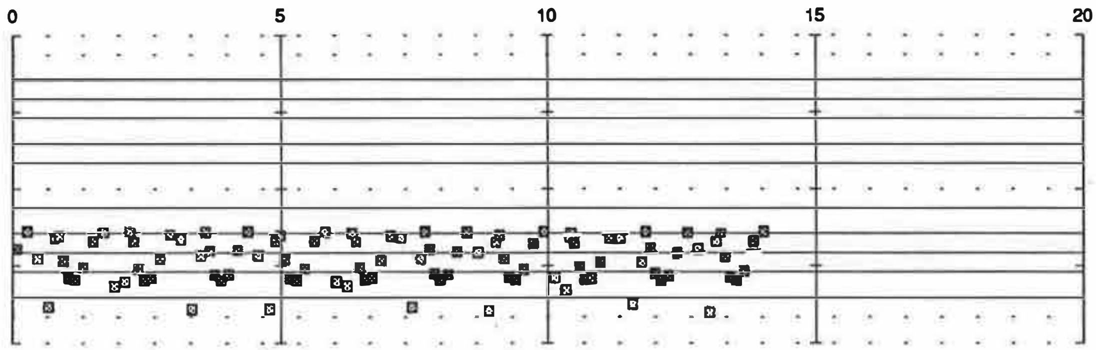

Example 2(a)

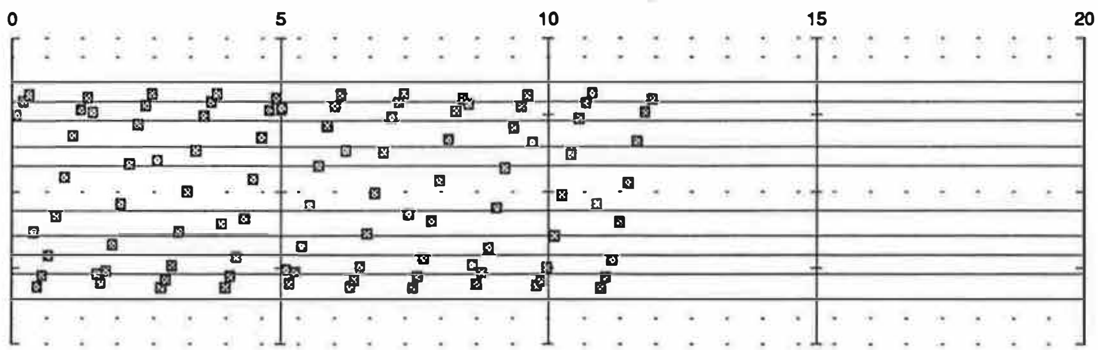

Example 2(b)

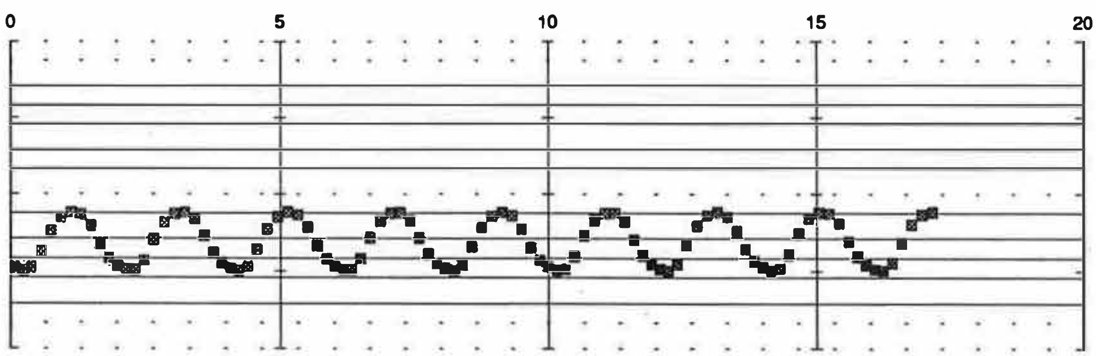

Example 3(a)

Figure 5.8 Scores to Examples 2(a), 2(b) and 3(a).

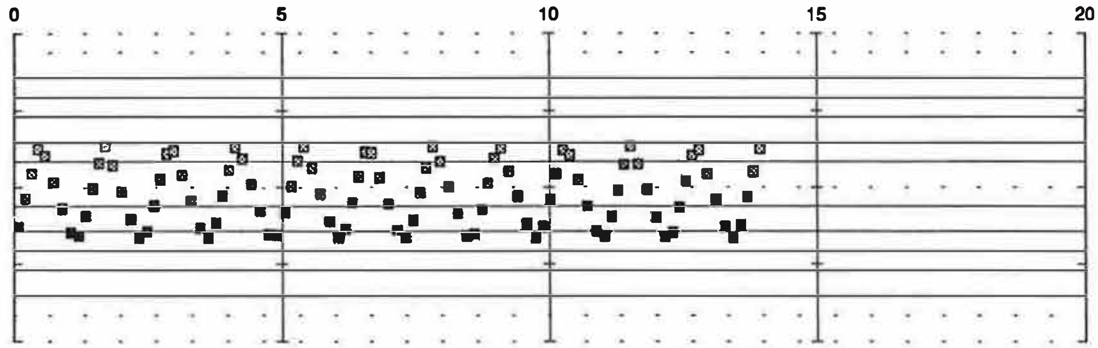

Example 4(a)

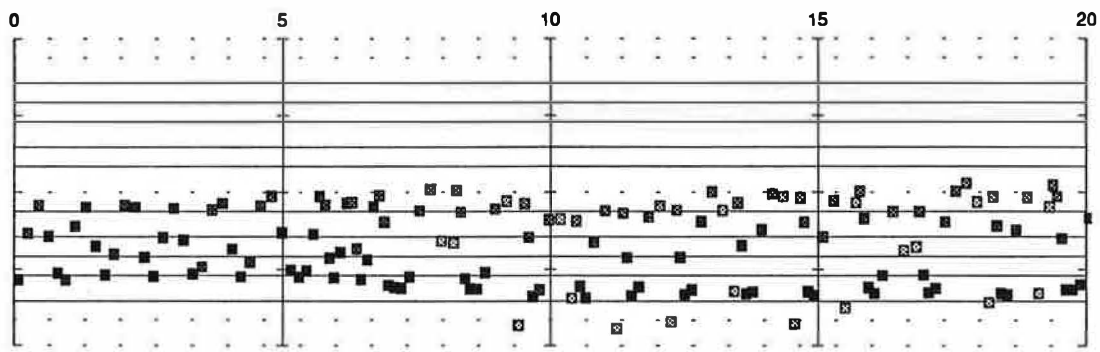

Example 5(a)

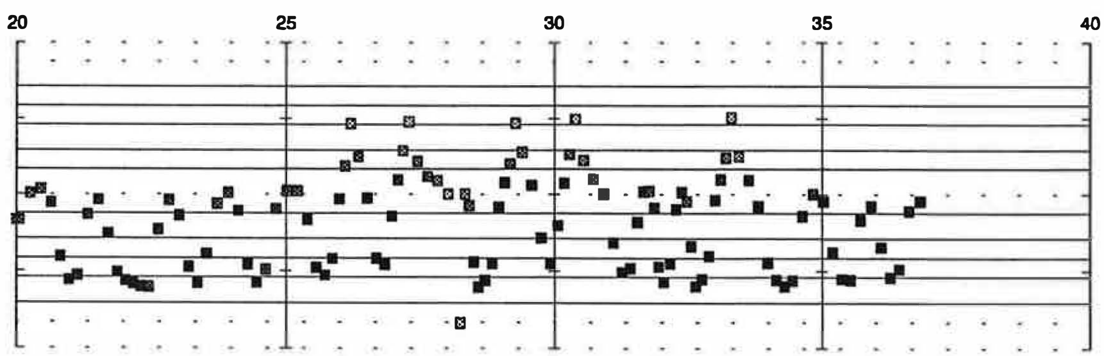

Example 5(a)

Figure 5.9 Scores to Examples 4(a) and 5(a).

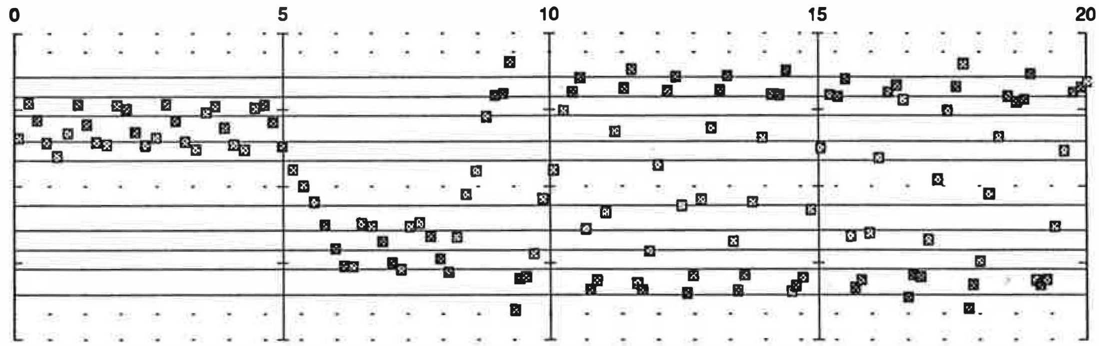

Example 5(b)

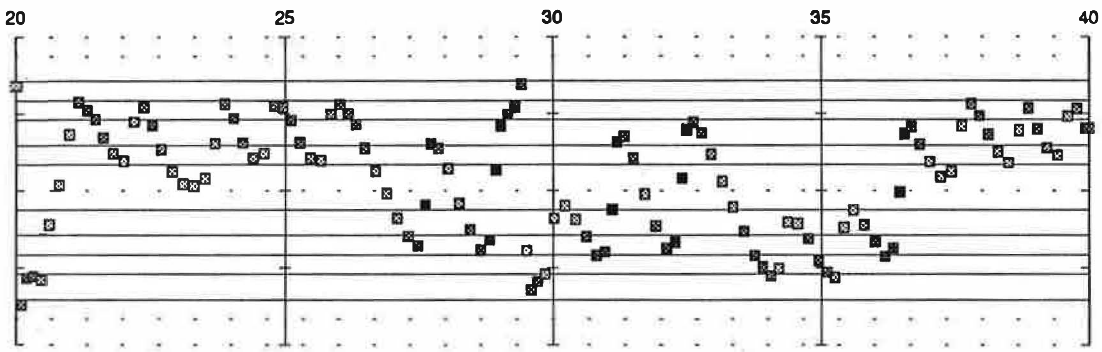

Example 5(b)

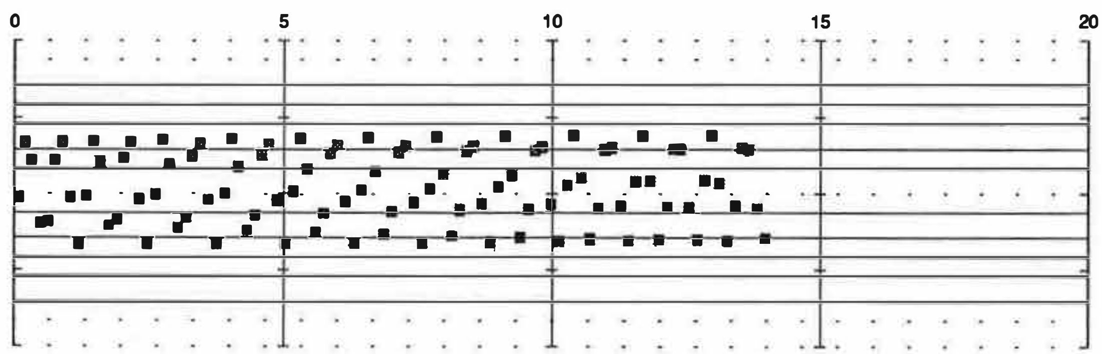

Example 6(a)

Figure 5.10 Scores to Examples 5(b) and 6(a).

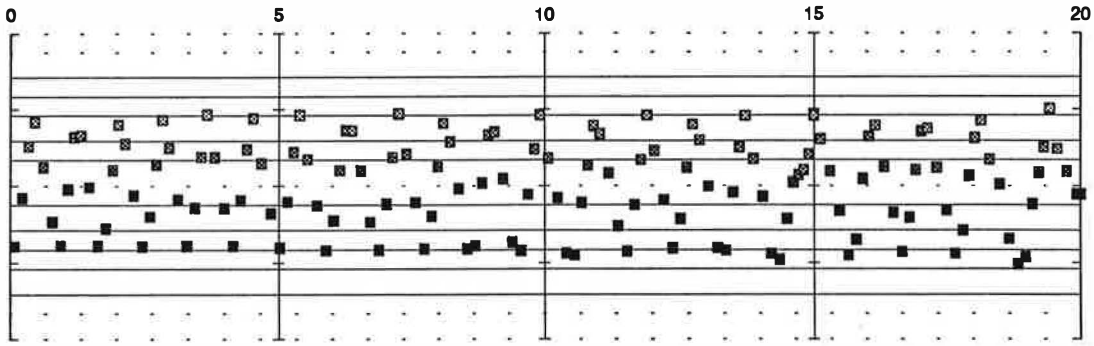

Example 7(a)

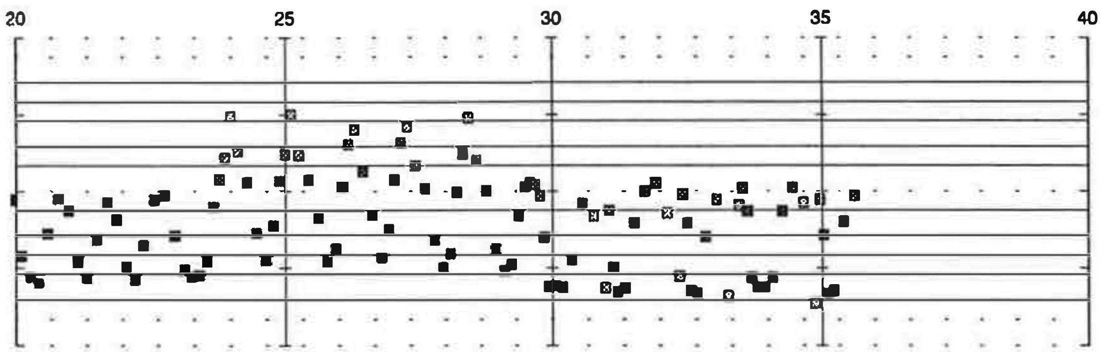

Example 7(a)

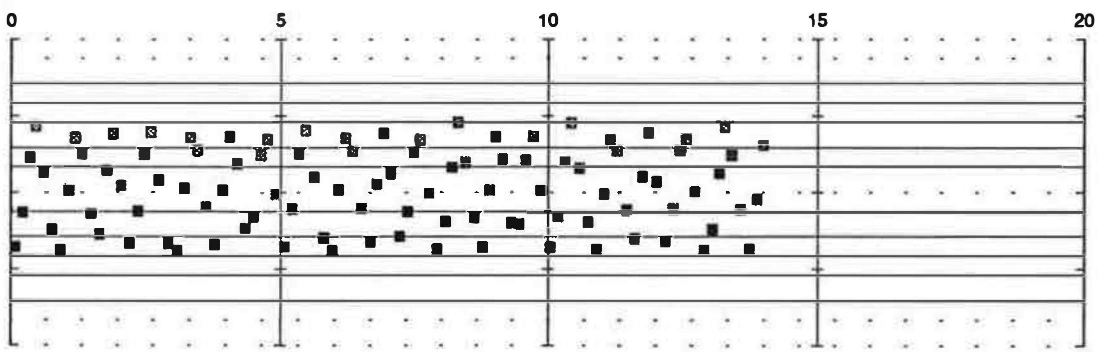

Example 8(a)

Figure 5.11 Scores to Examples 7(a) and 8(a).

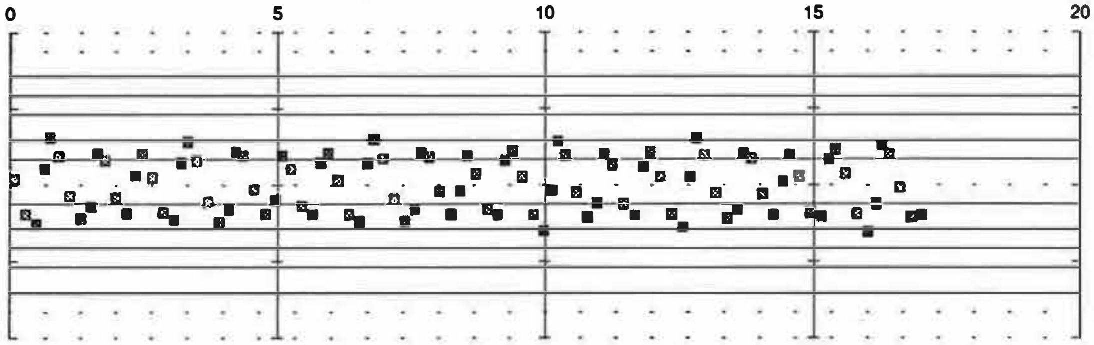

Example 8(b)

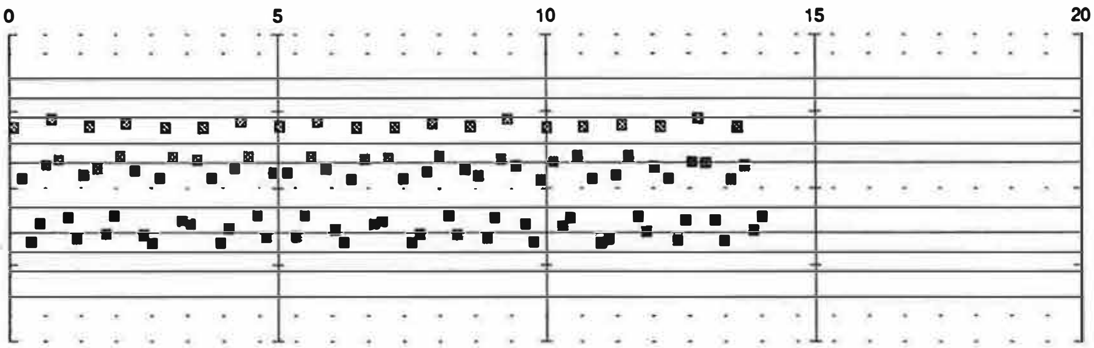

Example 9(a)

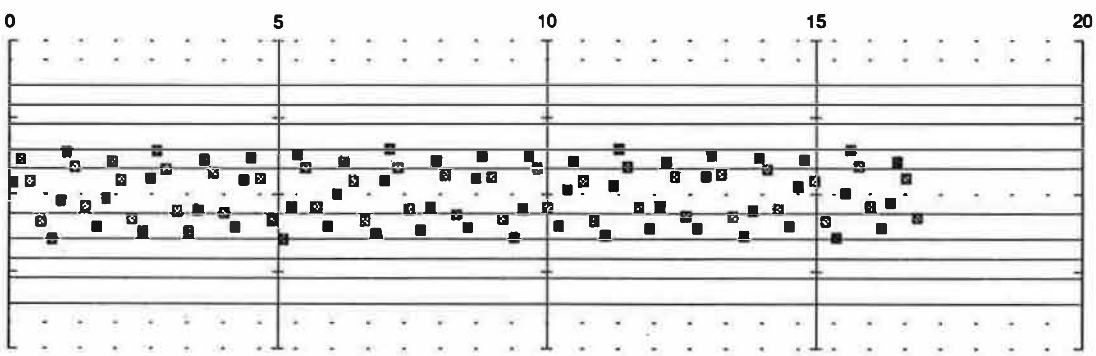

Example 9(b)

Figure 5.12 Scores to Examples 8(b), 9(a) and 9(b).

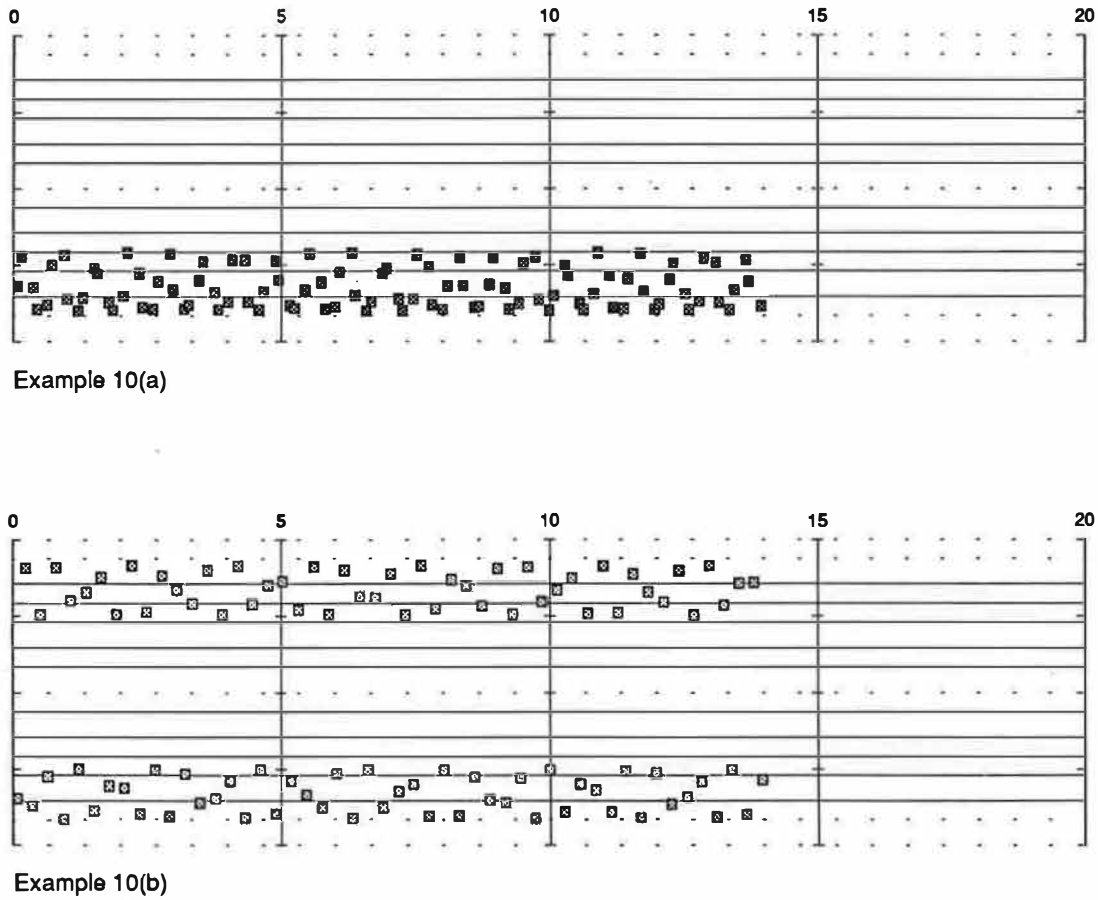

Figure 5.13 Scores to Examples 10(a) and 10(b).

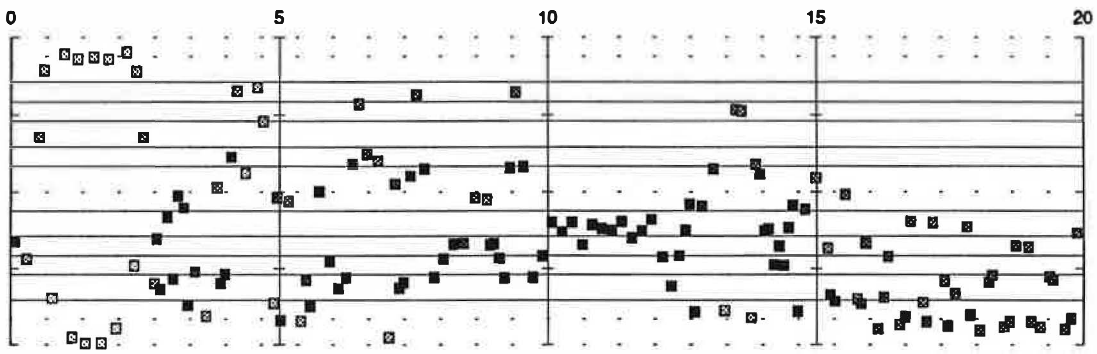

Example 11(a)

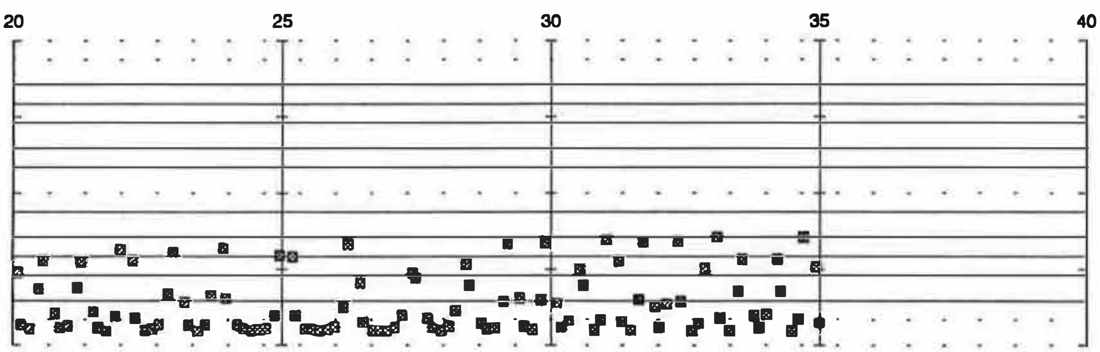

Example 11(a)

Figure 5.14 Score to Example 11(a).

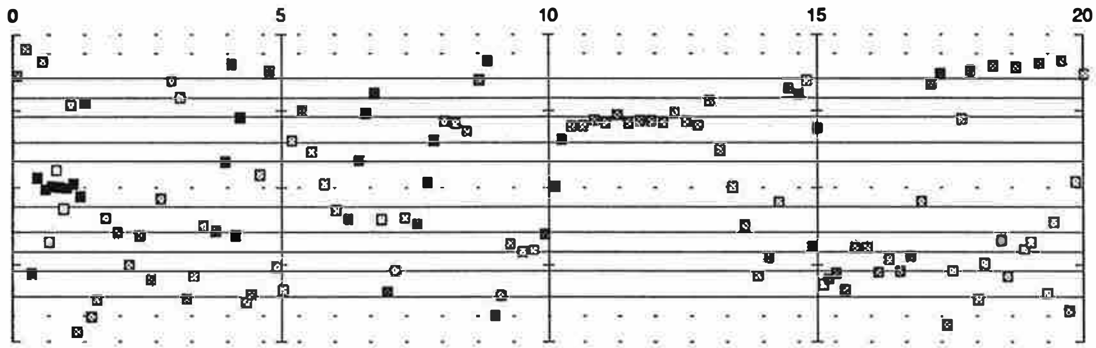

Example 11(b)

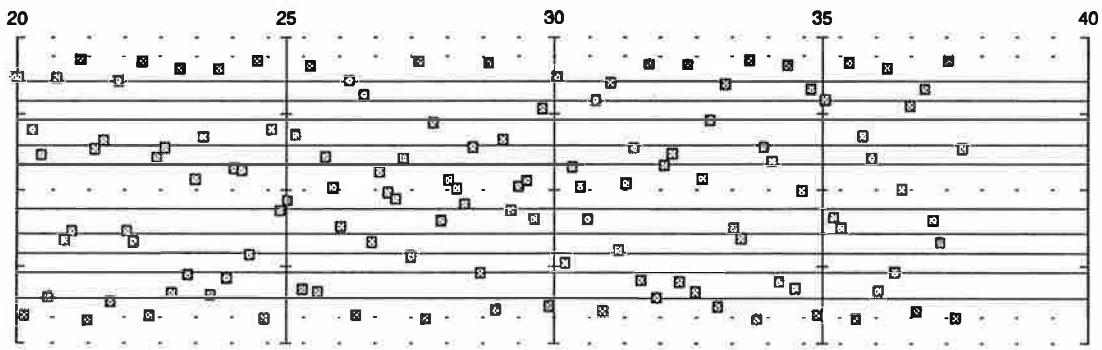

Example 11(b)

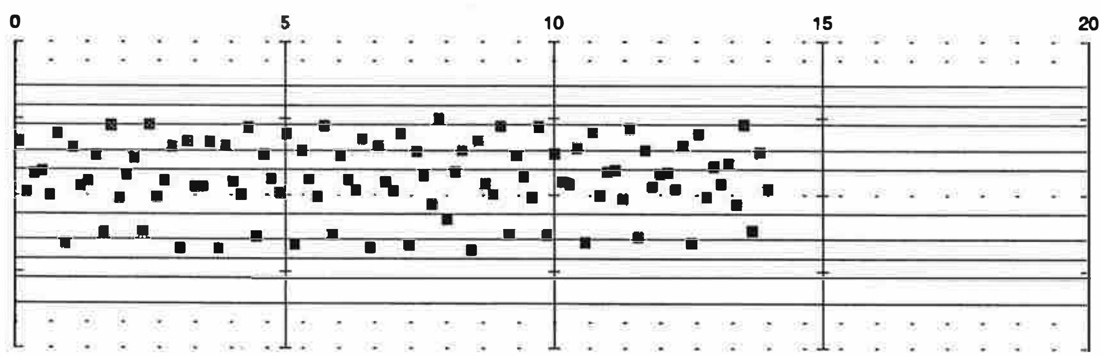

Example 12(a)

Figure 5.15 Scores to Examples 11(b) and 12(a).

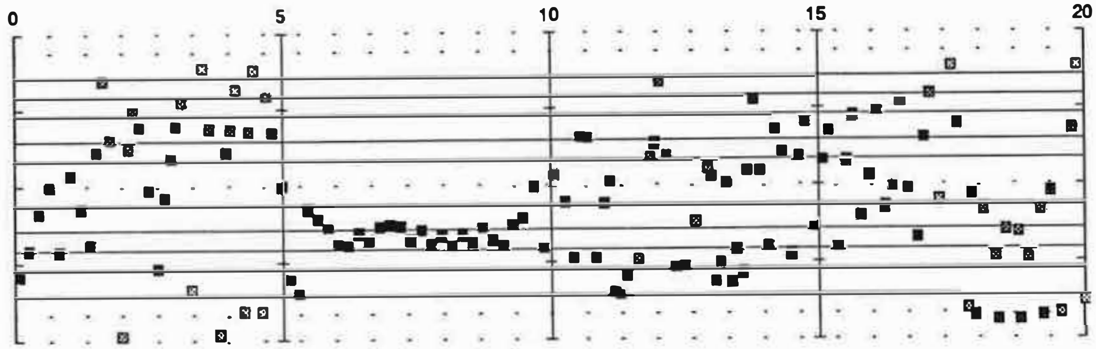

Example 13(a)

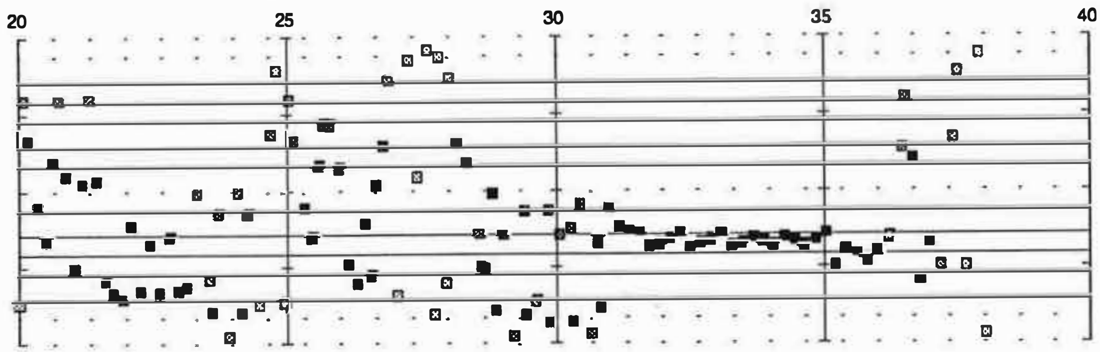

Example 13(a)

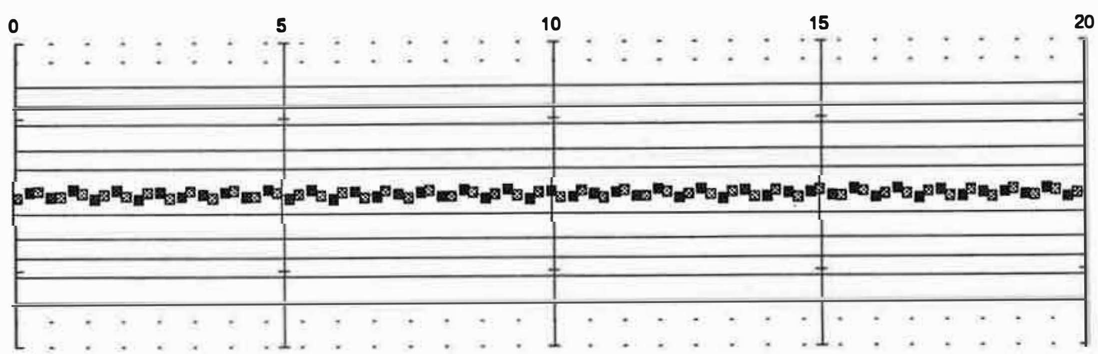

Example 14(b)

Figure 5.16 Scores to Examples 13(a) and 14(b).

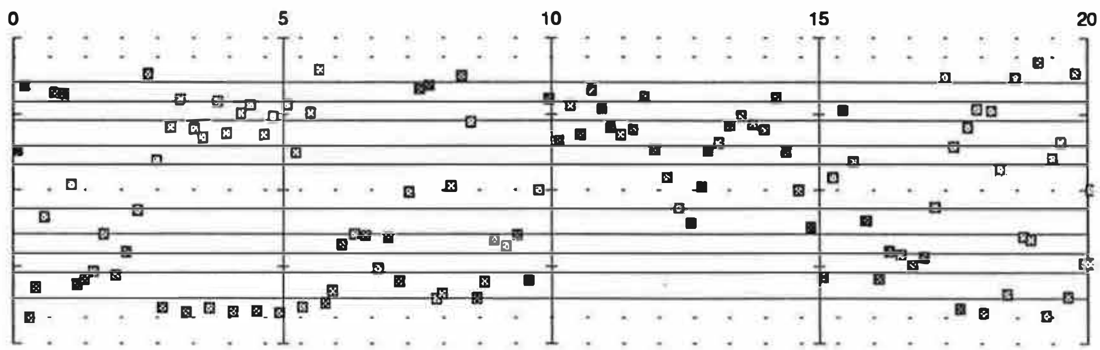

Example 15(b)

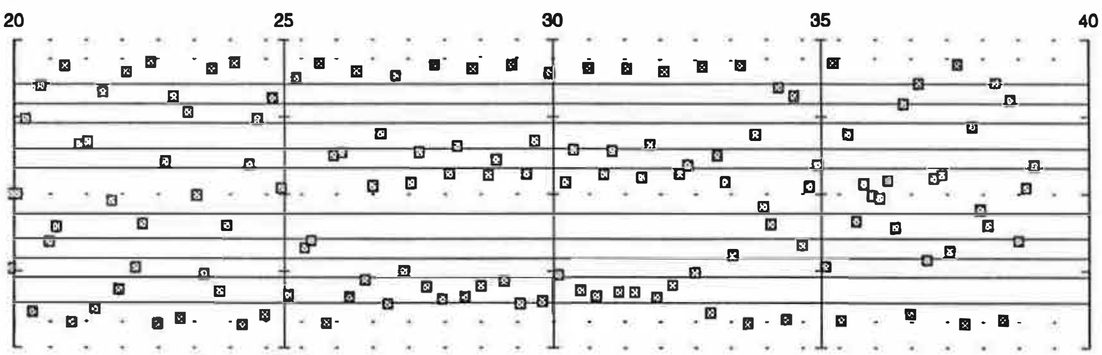

Example 15(b)

Figure 5.17 Score to Example 15(b).

Chapter 6

Musical Implications

In a discussion concerning historical changes in the structure of musical forms which have been brought about by changes in the nature of local structures, Boulez begins with a quotation from Claude Lévi-Strauss:

> Form and content are of the same nature and amenable to the same analysis. Content derives its reality from its structure, and what is called *form* is the "structuring" of local structures, which are called content [10, p. 90].

Boulez goes on to say:

> We have seen that the generation of networks of possibilities, which are the raw material for *l'opérateur*—to use a significant term of Mallarmé's—has from the outset tended increasingly to produce a material that is constantly evolving. ... [W]e can only work towards connections that are constantly evolving, and in the same way this morphology will be matched by a correspondingly non-fixed syntax [10, p. 90].

Although that was written well before the subject of chaos burst onto the scene, Boulez' thoughts dovetail very nicely with the quality of material that one can expect to generate as a matter of course by means of nonlinear dynamical systems such as those discussed in this work. The subject matter of chaotic systems is, indeed, the structuring of local structures, in connections that are constantly evolving.

Nonetheless, there is a quality to the music of chaos which is distinct and not to be confused with products of the human mind—although there is also an undeniably natural feel to much of the material produced by the methods explored in this work. Still, the quality of these materials is closer to that of figuration than to *bel canto* aria. If music may be thought of as the art of projecting, in an interesting way, a moving line or a group of moving lines through a multi-dimensional grid measured in terms of frequency, volume, time and timbre (which is itself multi-dimensional), then nonlinear dynamical systems furnish a powerful and novel means for the specification and control of these lines through this grid space. The process of understanding these systems is the process of learning how they behave under a variety of conditions. Their global behaviors are learnable and therefore predictable from the point of view of being useful in the generation of musical raw materials. Orbits which are known to produce desirable effects may be calculated on demand. One may treat these systems as musical commodities, natural resources to be exploited at will. In fact, the term "natural resource" is doubly fortuitous because of its dual associations: textures generated from these systems are "natural" in that they undeniably share qualities of real-world phenomena to which we are able to respond. Textures generated from these systems are also "resources" in that they may be exploited (or not) like any other musical resource.

A number of interesting qualities are exhibited in these textures. The paradoxical condition of a "consistent variety" of motivic material generated is foremost among them. The materials carry with them an inherent suggestion that they be employed in sequences of (at least) intermediate duration, because the character of the material is made manifest only after a number of iterations. In several of the examples a greater sense of order is admitted by the ear in listening to the music than by the eye in looking at the score. Several of the graphical scores which appear either erratic or boringly amorphous actually *sound* quite rich—the ear hears relationships that the eye tends to miss. In some of the simpler cases, this may have to do with the visual similarities that certain scores share with common patterns used in graphical designs—the even loops in the score to Example 2(a) from Chapter 4, for example, might look quite nice as a sofa covering or a wallpaper design, but there has been little precedence for this type of melodic motion in musical contexts. The musical effect of these designs, therefore, is quite novel.

The qualities of the textures generated from conservative systems differ from those of the dissipative systems. Whereas dissipative systems produce orbits (after the initial transient) which wander consistently and evenly through the phase space over all but the shortest spans of time, conservative systems may restrict an orbit to a confined area of the total phase space for extended periods of time before embarking on a transition to a new resonance space (chaotic, rather than cyclical or periodic orbits, are the intended target of these comments). Thus, while iterations 1000 through 2000 of the Hénon map are guaranteed to be much the same qualitatively as iterations 10000 through 11000, this is not the case for the standard map or for Poincaré sections of the Hénon-Heiles system. The effect of the conservative systems is to create textures with a more local focus, in which a small range of the total ambitus is examined for a while before the spotlight moves on to another area. Alternation of textural qualities is the hallmark of the conservative systems.

The respective qualities of periodic/cyclic orbits of dissipative and conservative systems are also different. Whereas cyclic orbits of the conservative maps can sound fairly irregular, periodic orbits of dissipative systems sound quite regular and periodic. This is due to the exact repetition of points in periodic orbits of the dissipative systems as opposed to the effectively irrational relationship of points in a cyclic orbit of a conservative system with regard to the length of the cycle. Nonetheless, quasi-periodic orbits of dissipative systems (in which points are distributed among a small number of discrete layers) might be used to similar effect.

In dissipative systems there is a diminishing of activity after the initial transient. With conservative systems the activity remains at a constant level, perhaps even sporadically increasing (perceptually speaking) due to the resonance overlaps which result in changes in the overall texture. However, the transient portions of the orbits of dissipative systems may be exploited for unique sequences of events which do not recur in the systems' settled state. This is not to imply that these transient states are more interesting than the settled orbits, but only that one can expect to generate a different quality of material with the transient portions than with the settled orbits. Unlike the settled behavior, however, transient trajectories are difficult or impossible to predict and therefore must be tested until the courses of particular transients arising from particular initial conditions become known on an empirical basis.

Critical to the musical effect of a particular dynamical system are not only the values of the system's constant parameters and the initial point of the orbit, but also the mapping of the phase space to the musical domain. It would be difficult to claim a universal preference for a particular mapping configuration over another. While the effect of a given configuration relative to another may differ wildly, the utility of a particular configuration depends entirely on what is desired. Mappings that sound subjectively good under one set of initial conditions may be less effective under a different set of initial conditions. In the case of Poincaré sections generated from flows, a simple reorientation of the sectional plane relative to the phase space of the flow has been shown in the examples from the Lorenz equations to exert an overwhelming influence on the quality of the texture produced.

There remains much room for the experimentation with more complex mapping schemes not explored in this study. For example, the succession of (x, y) coordinate pairs in orbits of the Hénon system need not be consistently mapped to an invariant set of musical parameters throughout the course of a sequence, but may alternate between two complementary mappings; e.g., (x_0, y_0) to (key, velocity), (x_1, y_1) to (velocity, key), (x_2, y_2) back to (key, velocity), and so on. This produces a new musical texture quite different from those presented in the earlier examples generated from the Hénon map, but which still contains essential qualities of that system. Another cue can be taken from the traditional quantization of the musical domain into twelve (or less) pitch classes and the hierarchical division of rhythm and note duration. Orbital mappings may be quantized on the computer to any desired resolution, in any dimension: pitch, time, volume, timbre. Additionally, the structure of the quantization itself need not be regular, but can be organized so as to produce chords, specific rhythmic groupings, etc. Chaotic sequences may also be used to drive production grammers in place of white or colored noises which are often used. Nor need the utility of these systems be confined to the generation of note textures. The Lorenz attractor, for example, might be quite interesting as a three-dimensional spatialization path, or in a waveform synthesis algorithm (informal experiments have indicated that chaotic transient orbits which become periodic over time produce interesting attack characteristics, much like delay-line and plucked-string algorithms).

While the overall behavior of a given chaotic orbit is, in a strict sense, not predictable, in an operational sense, it is. It is clear, for example, that the settled orbit of the Hénon map will not suddenly visit a point far from the attractor, an orbit of the Hénon-Heiles system will not suddenly depart from its bounding volume, and the phase space of the standard map will always be the unit torus. Nonetheless, these systems (especially the conservative ones) are productive of sequences of events in which sudden, unexpected changes may occur—albeit within the limits of their global repertoire of behavioral possibilities. This is a type of behavior not seen in purely random sequences, which maintain an even consistency throughout, incapable of evoking surprise. Spectra of chaotic systems do, however, resemble $1/f$-noise in that longer-term correlations are present and obvious (see Farmer, et al. [22]). Nonetheless, the character is noticeably different. Chaos is generated by ***deterministic*** procedures (indicating therefore the presence of some measure of "volition," even if it is exercised only by mindless equations), whereas white noise and $1/f$-noise are ***probabilistic*** outcomes.

These qualities notwithstanding, the *long-term* behavior of all of these systems is static. The volition exercised by the equations is of local rather than global extent; they contain no inherent specification of sustained drive or impetuousness. There is no overarching teleological force guiding the sequence of notes to some grand conclusion. There is no phrase structure. What is missing in these materials is *directionality*, the sense that the structure evolves according to the dictates of a human will. All of these qualities must be added by the musician "by hand." Moments of localized directionality, in which a serendipitous turns of events catches the attention, must be isolated and elaborated.

Nonlinear dynamical systems have the potential for creating the theoretical foundation of a new and idiosyncratic idiom of computer music, of an intrinsic fluency wholy independent of external derivations from tape and instrumental music. Chaotic systems are a means by which computer music may move beyond the limited possibilities of sequencing (a technique appropriated from analogue electronic music) or the often simplistic processing roles to which it is often consigned. Chaos opens a door to synthesis of formal melodic material in addition to waveforms synthesis at the sample level. Dynamical systems are versatile generators of "meta-sequences"—sequences of motivic material made more flexible by virtue of their specification as *rules* of natural behavior rather than as fixed sets of notes. Chaos affords composers working with computers the opportunity to address musical issues at a level of organization which has remained largely uninvestigated in the medium to date: the generation of melodic and harmonic materials at the note level.

This work closes with the inclusion in Appendix C of a study composed from fragments of a single orbit of the Lorenz system. Its inclusion is meant to serve as a tangible example within an extended setting of music from chaos.

Appendix A

Chaotic Systems in 'C'

A.1 The Logistic Equation

```
/* logistic.c */

#include <stdio.h>
#include <math.h>

main(argc, argv)
int argc; char **argv;
{
    float K, p;
    int count, num;

    if (argc != 4) {
        printf("USAGE: logistic <K> <p0> <num>\n");
        exit(1);
    }
    /* Get commandline arguments */
    K = atof(argv[1]);
    p = atof(argv[2]);
    num = atoi(argv[3]);

    /* Print <num> iterations */
    for(count=0; count<num; count++) {
        printf("%d: %f\n", count, p);
        p = K * p * (1.0 - p);
    }
}
```

A.2 The Hénon Map

```
/* henon.c */

#include <stdio.h>
#include <math.h>

main(argc, argv)
int argc; char **argv;
{
    float A, B, x, y, newx;
    int count, num;

    if (argc != 6) {
        printf("USAGE: henon <A> <B> <x0> <y0> <num>\n");
        exit(1);
    }
    /* Get commandline arguments */
    A = atof(argv[1]);
    B = atof(argv[2]);
    x = atof(argv[3]);
    y = atof(argv[4]);
    num = atoi(argv[5]);

    /* Print <num> iterations */
    for(count=0; count<num; count++) {
        printf("%d: %f %f\n", count, x, y);
        newx = y + 1.0 - (A * x * x);
        y = B * x;
        x = newx;
    }
}
```

A.3 The Lorenz System

```
/* lorenz.c */

#include <stdio.h>
#include <math.h>

main(argc, argv)
int argc; char **argv;
{
```

```
    float S, R, B, x, y, z, delta;
    float xdot, ydot, zdot;
    int count, num;

    if (argc != 9) {
        printf("USAGE: lorenz <S> <R> <B> <x0> <y0> <z0> <dt> <num>\n");
        exit(1);
    }
    /* Get commandline arguments */
    S = atof(argv[1]);
    R = atof(argv[2]);
    B = atof(argv[3]);
    x = atof(argv[4]);
    y = atof(argv[5]);
    z = atof(argv[6]);
    delta = atof(argv[7]);
    num = atoi(argv[8]);

    /* Print <num> iterations */
    for(count=0; count<num; count++) {
        printf("%d: %f %f %f\n", count, x, y, z);
        xdot = S * (y - x);
        ydot = (R * x) - y - (x * z);
        zdot = (x * y) - (B * z);
        x += (xdot * delta);
        y += (ydot * delta);
        z += (zdot * delta);
    }
}
```

A.4 The Standard Map

```
/* standard.c */

#include <stdio.h>
#include <math.h>

main(argc, argv)
int argc; char **argv;
{
    float I, theta, K, twopi;
    int count, num;

    if (argc != 5) {
```

```
        printf("USAGE: standard <K> <th0> <I0> <num>\n");
        exit(1);
    }
    /* Get commandline arguments */
    K = atof(argv[1]);
    I = atof(argv[2]);
    num = atoi(argv[3]);
    theta = atof(argv[4]);

    twopi = (8.0 * atan(1.0));

    /* Print <num> iterations */
    for(count=0; count<num; count++) {
        printf("%d: %f %f\n", count, theta, I);
        I += K * sin(theta);
        theta += I;
        while (I >= twopi) I -= twopi;
        while (I < 0.0) I += twopi;
        while (theta >= twopi) theta -= twopi;
        while (theta < 0.0) theta += twopi;
    }
}
```

A.5 The Hénon-Heiles System

```
/* henheil.c */

#include <stdio.h>
#include <math.h>

main(argc, argv)
int argc; char **argv;
{
    float E, x, y, delta;
    float xdot, ydot, xdotdot, ydotdot;
    float xdotsqrd;
    int count, num;

    if (argc != 6) {
        printf("USAGE: henheil <E> <y0> <ydot0> <delta> <num>\n");
        exit(1);
    }
    /* Get commandline arguments */
    E = atof(argv[1]);
```

```
    y = atof(argv[2]);
    ydot = atof(argv[3]);
    delta = atof(argv[4]);
    num = atoi(argv[5]);

    /* Solve volume equation for xdot */
    x = 0.0;
    xdotsqrd = (2.0*E) - (y*y) + ((4.0/3.0)*y*y*y) - (ydot*ydot);
    if (xdotsqrd < 0.0) {
        printf("KaBoom!\n");
        exit(1);
    }
    xdot = sqrt(xdotsqrd);

    /* Print <num> iterations */
    for(count=0; count<num; count++) {
        printf("%d: %f %f %f %f\n", count, x, y, xdot, ydot);
        xdotdot = -x - (2.0 * x * y);
        ydotdot = -y - (x * x) + (y * y);
        xdot += (xdotdot * delta);
        ydot += (ydotdot * delta);
        x += (xdot * delta);
        y += (ydot * delta);
    }
}
```

Appendix B

Generation of Music from Chaos

An abridged and somewhat simplified version of the program used to generate the musical examples from the Hénon map is listed below. The routine `midihenon()` executes the equations of the system and generates MIDI note statements based on the (x, y) values of the current iterate. The mapping of the phase space to MIDI-space is specified by command-line arguments. Note that `midihenon()` schedules itself anew for each iteration of the equations. The program would normally be linked to an external library providing a driver for the MIDI interface (a Roland MPU-401), MIDI write routines, and a *moxie*-like scheduler [14]. Dummy definitions of pertinent routines from this library are included at the bottom of the listing, with indications as to their functions.

```
/ *midihen.c */

#include <stdio.h>
#include <malloc.h>
#include <math.h>
#include <sched.h>
#include <mpu401.h>

#define KEY     0
#define VEL     1
#define NEXT    2
#define DUR     20                          / *duration of each note */

float   x, y;                               / *initial conditions */
float   alfa, beta;                         / *constant parameters */
int     xparam, yparam, sparam;             / *parameter assignments */
float   kpmin, kpmax, vpmin, vpmax;         / *parameter value ranges */
float   npmin, npmax;                       / *parameter value ranges */
int     running = 1;                        / *know when to hold 'em */
long    limit;                              / *know when to fold 'em */

int midihenon();
```

```
main(int argc, char **argv)
{
    if (argc != 15) {
        printf("midihen: x0 y0 a b xp yp sp km kM vm vM nm nM limit\n");
        exit (1);
    }
    /* Get commandline arguments */
    x = atof(argv[1]);
    y = atof(argv[2]);
    alfa = atof(argv[3]);
    beta = atof(argv[4]);
    xparam = atoi(argv[5]);
    yparam = atoi(argv[6]);
    sparam = atoi(argv[7]);
    kpmin = atof(argv[8]);
    kpmax = atof(argv[9]);
    vpmin = atof(argv[10]);
    vpmax = atof(argv[11]);
    npmin = atof(argv[12]);
    npmax = atof(argv[13]);
    limit = atol(argv[14]);

    /* MPU and scheduler initialization */
    initmpu();
    if (!initsched(&mpuclock)) {
        fprintf(stderr, "Can't initialize scheduler!\n");
        exit();
    }

    /* Go! */
    cause(10, midihenon);
    while (running) {
        sched();
        if (kbhit()) if (getche()) running = 0;
    }

    /* Clean up and quit */
    all_notes_off();
    mpu_deinit();
}

midihenon()
{
    static long count = 0;
    static float fnext = 0.0;
    float newx, newy, sqrsum;
```

```
float fxval, fyval, fsval;
float xval, yval, sval;
int key, vel, next;
int chan = 0;
float fkey;

if (count++ == limit) return;

/* Get next iterate */
newx = y + 1.0 - (alfa * (x * x));
newy = beta * x;
x = newx;
y = newy;

/* Get sum of squares */
sqrsum = (x * x) + (y * y);

/ *Normalize values from 0 to 1 */
fxval = (newx + 1.43) / 2.86;
fyval = (newy + 0.43) / 0.86;
fsval = sqrsum / 1.85;

/ *Assign to parameters */
switch (xparam) {
    case KEY: fkey = ((fxval * (kpmax - kpmin)) + kpmin); break;
    case VEL: vel = (int)((fxval * (vpmax - vpmin)) + vpmin); break;
    case NEXT: fnext += ((fxval * (npmax - npmin)) + npmin); break;
}
switch (yparam) {
    case KEY: fkey = ((fyval * (kpmax - kpmin)) + kpmin); break;
    case VEL: vel = (int)((fyval * (vpmax - vpmin)) + vpmin); break;
    case NEXT: fnext += ((fyval * (npmax - npmin)) + npmin); break;
}
switch (sparam) {
    case KEY: fkey = ((fsval * (kpmax - kpmin)) + kpmin); break;
    case VEL: vel = (int)((fsval * (vpmax - vpmin)) + vpmin); break;
    case NEXT: fnext += ((fsval * (npmax - npmin)) + npmin); break;
}
key = (int)fkey;
next = (int)fnext;
fnext -= (float)next;

/ *Make sure values are legal */
if (key > 127) key = 127;
if (key < 0) key = 0;
if (vel > 127) vel = 127;
```

```
    if (vel < 1) vel = 1;

    /* Send pitch bend data for fine tuning */
    midi_pfbend(chan, fkey - (float)key);
    /* Send MIDI key on message */
    midi_kon(chan, key, vel);
    /* Schedule key off message */
    cause(DUR, midi_koff, chan, key);

    /* Schedule next note */
    cause(next, midihenon);
}

initmpu()
{
    /* Install interrupt handler */
    /* Set MPU tempo and timebase */
    /* Start MPU clock-to-host messages */
}

initsched(long *clock)
{
    /* Initialize scheduler event queue */
    /* inform scheduler of clock address */
}

cause(int next, void(*routine)(), arg1, arg2, arg3, arg4, arg5)
{
    /* Insert <routine> with optional arguments into event queue */
    /* Events are inserted in time order */
}

sched()
{
    /* Check event queue for ripe events */
}

all_notes_off()
{
    /* Turn off all notes on all channels, reset pitch bend */
}

mpu_deinit()
{
    /* Turn off MPU functions and deinstall interrupt handler */
}
```

Appendix C

Sensitive Dependence: A Study of the Lorenz System

Dodecanon I (Sensitive Dependence) is a sequence of twelve canons of twelve voices each made from fragments of a single orbit of the Lorenz system. The basic structural principles of the piece are derived directly from an analysis of Conlon Nancarrow's *Study No. 37 for Player Piano* [9]. This work, also a twelve-voice, twelve-part canon, is revolutionary in the sense that his employment of canonic technique is used as a device to create what are essentially monophonic (or monolithic) structures, rather than polyphonic textures as has been the primary application of canonic technique since its inception in the thirteenth century. This is accomplished by assigning to each voice an independent tempo as well as pitch transposition, and then carefully arranging the voices in such a way that a cohesive structure is created from their combination. A fixed set of twelve tempo ratios, allied with other structural principles which are applied with varying degrees of rigor and consistency, are used throughout each of the twelve canons (in Nancarrow's work as well as in *Dodecanon I*). Significant among the structural principles employed are the methods for synchronizing the canonic voices. A point of synchronization is determined for each canon, which may be at the beginning, the end, or in the middle of the canon. According to where this point is located, either the entrances or the exits of canonic voices are staggered, or both if the point of synchronization is located in the middle.

Dodecanon I was conceived for either computer-controlled piano or an ensemble of synthesizers. It was selected for performance at the 1989 International Computer Music Conference at the Ohio State University in Columbus, Ohio, held in November of 1989.

Dodecanon I (Sensitive Dependence)

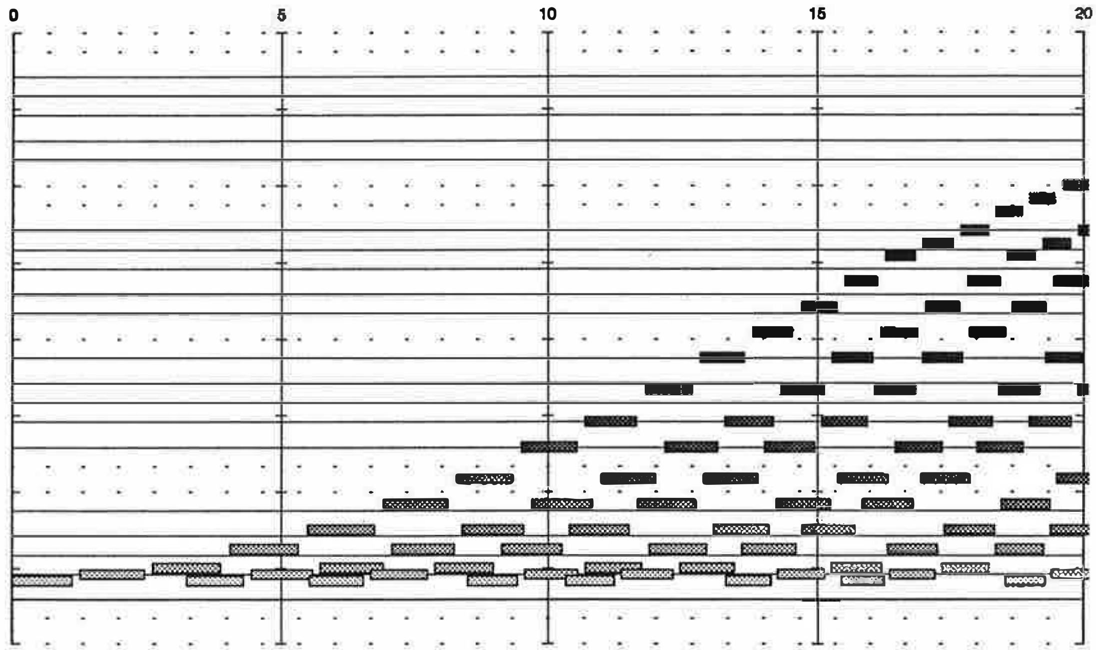

Canon I

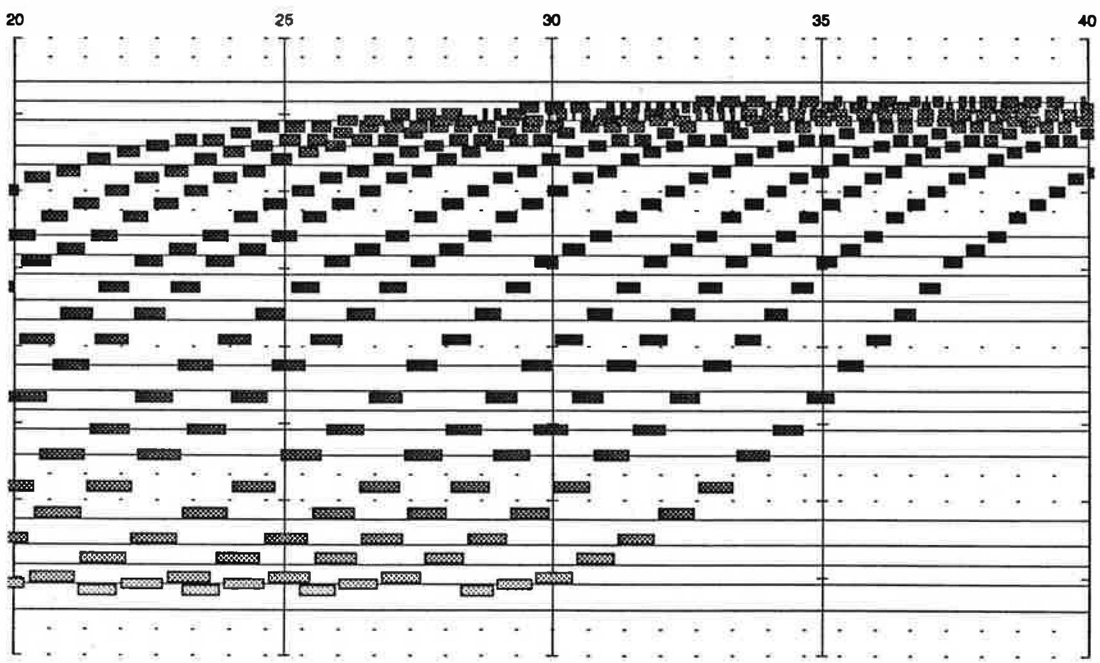

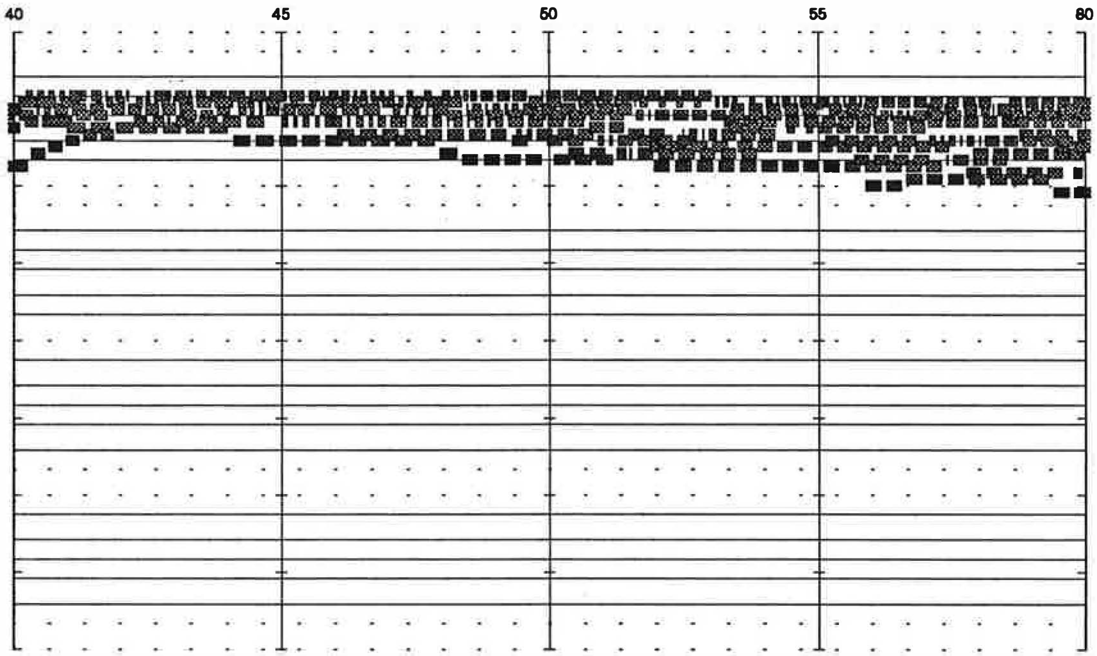
40
45
50
55
60

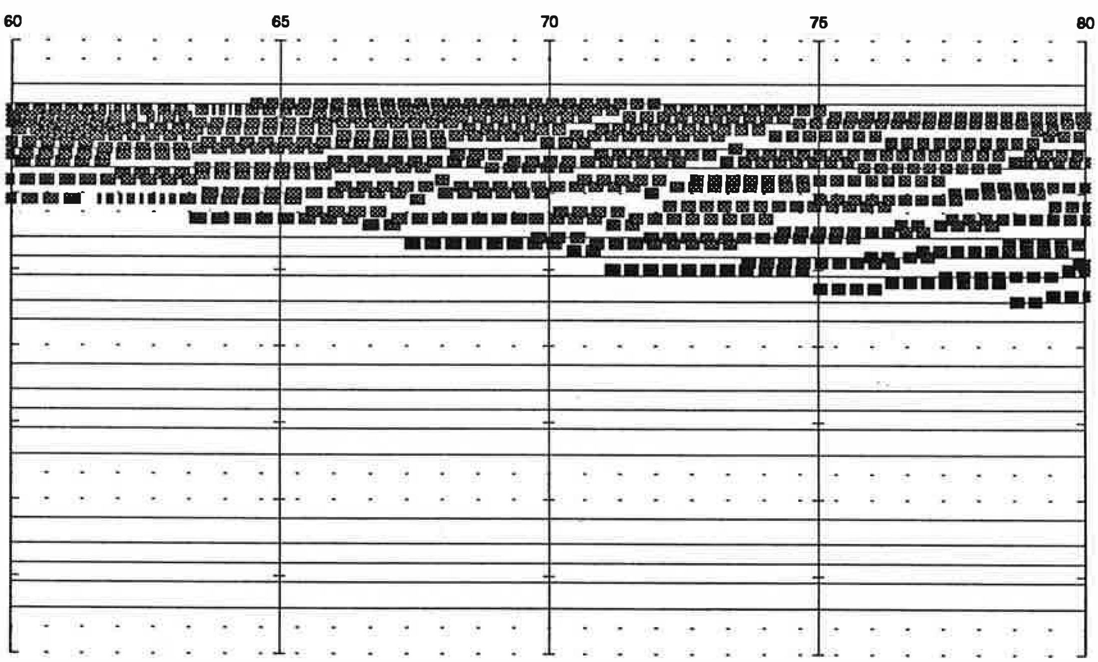
60
65
70
75
80

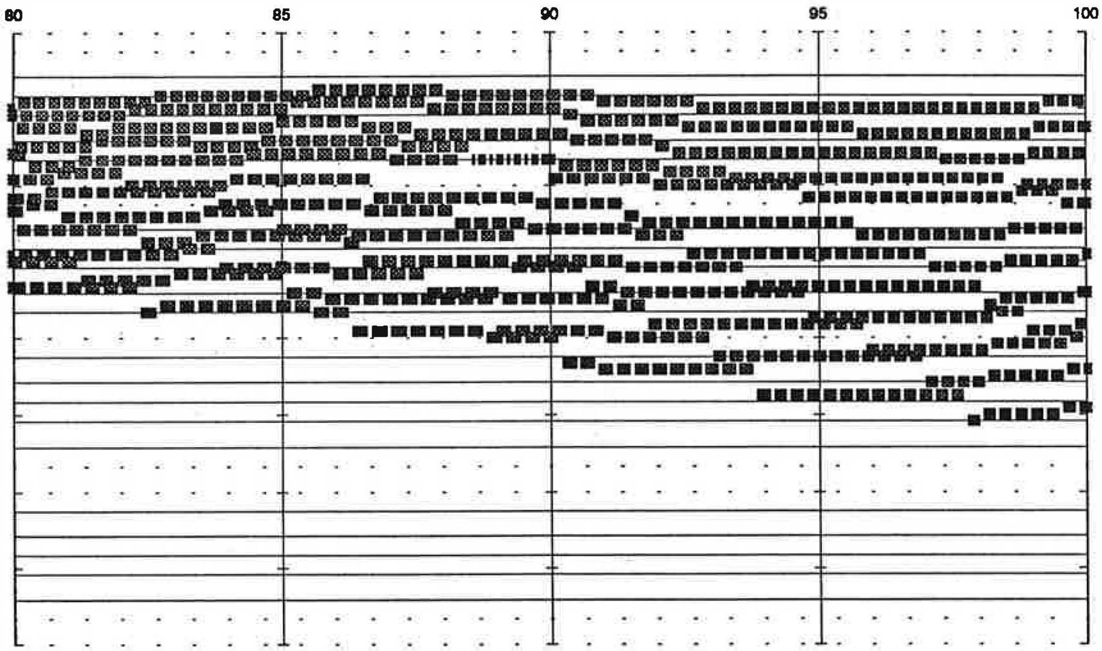
80
85
90
95
100

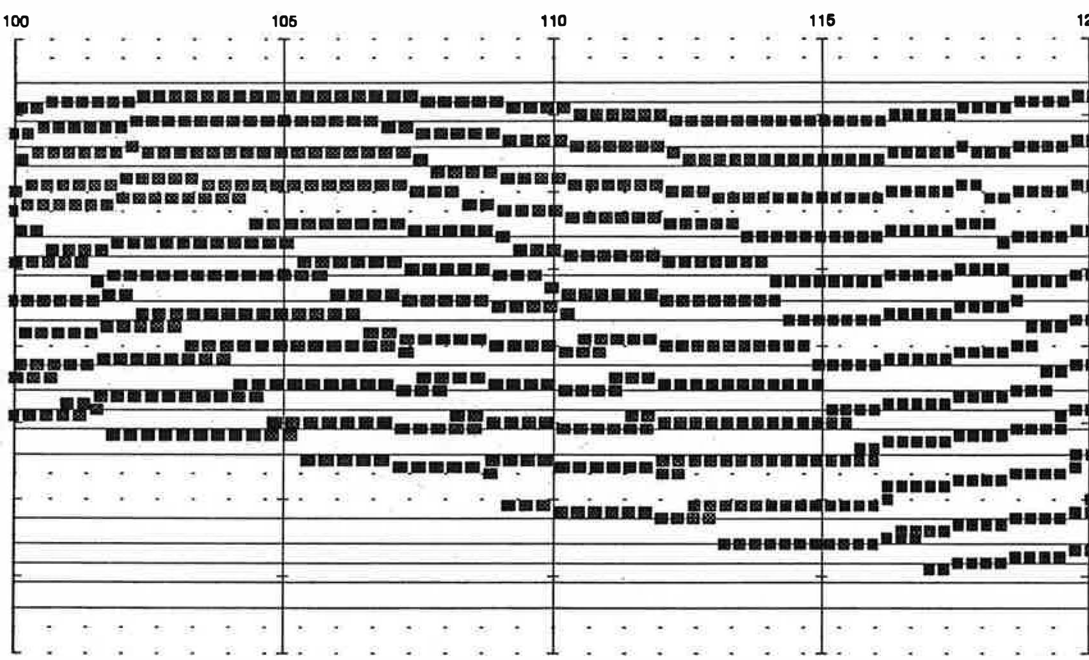
100
105
110
115
120

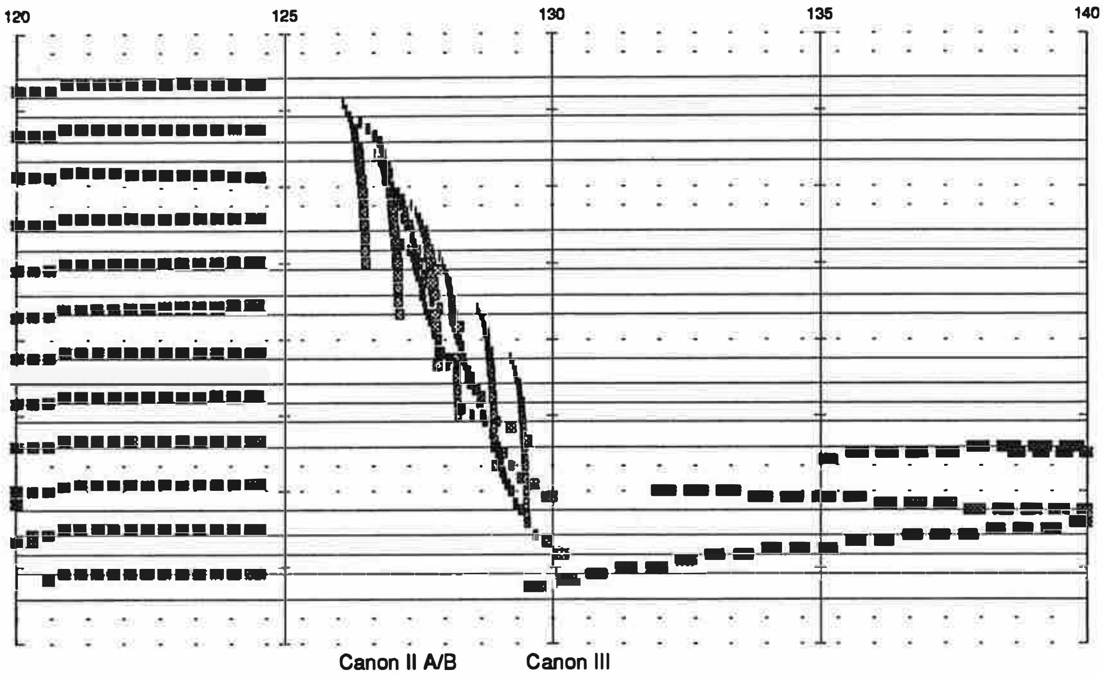
120
125
130
135
140
Canon II A/B
Canon III

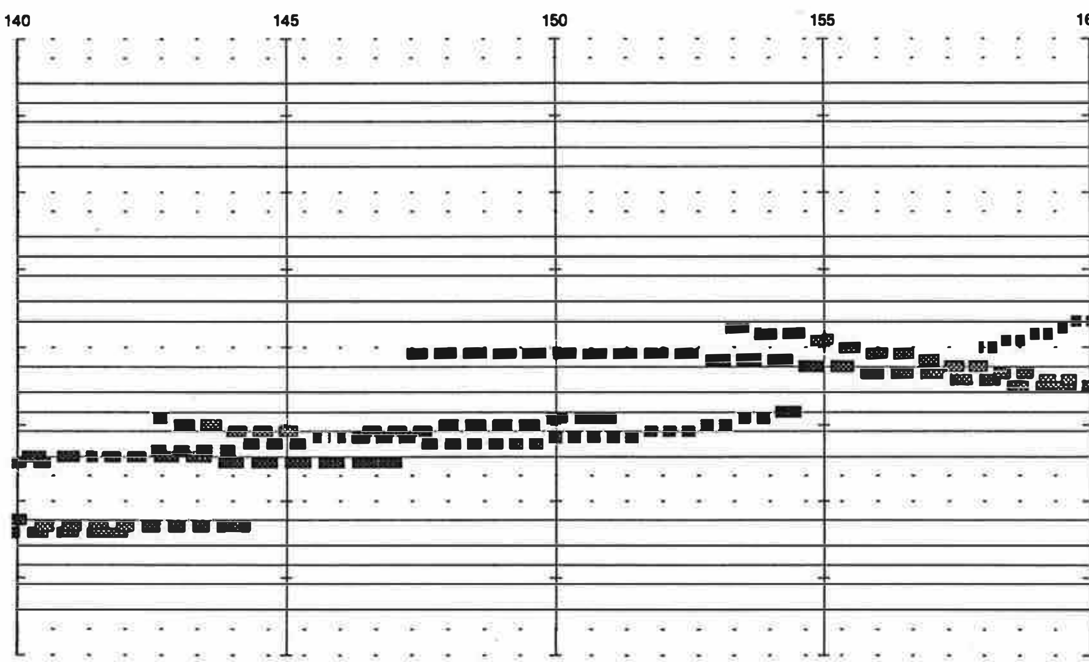
140
145
150
155
160

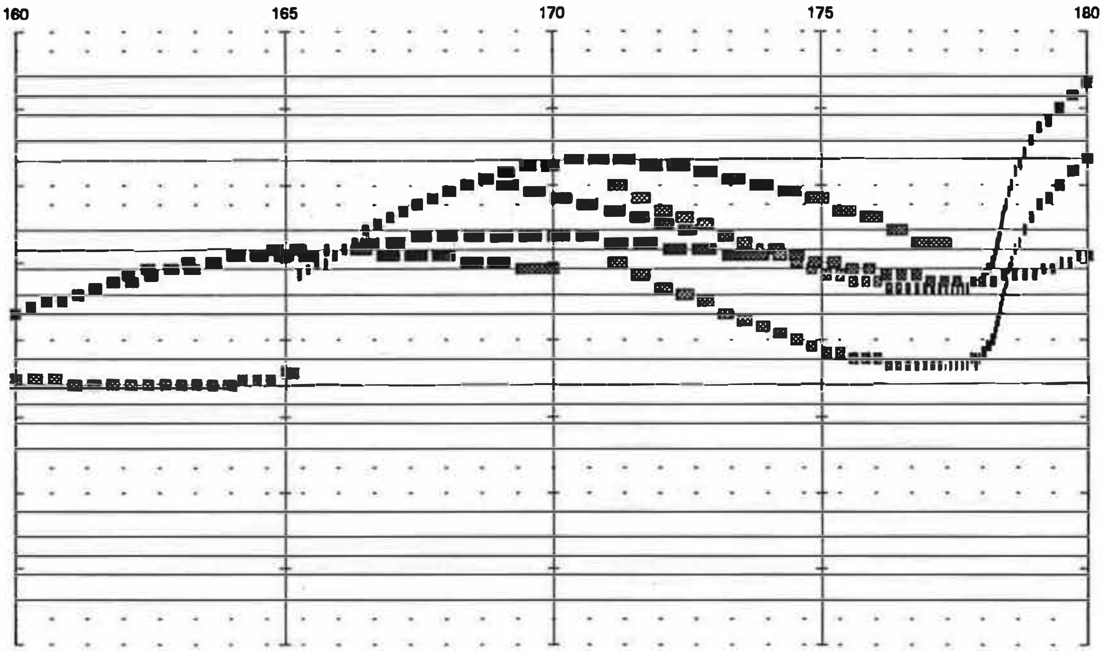

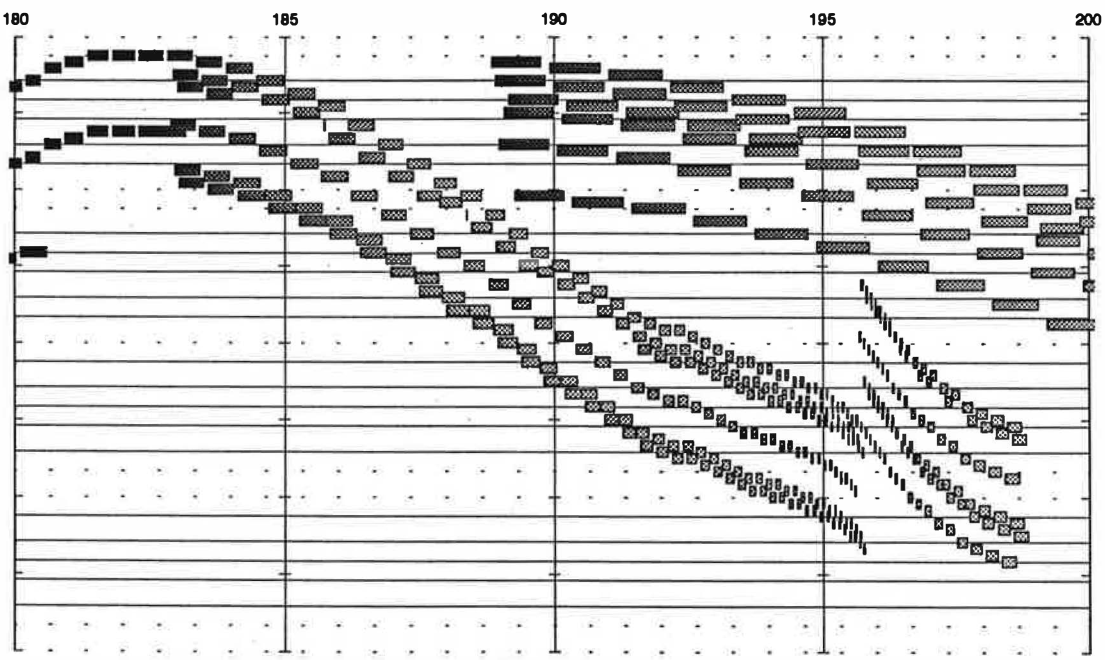

Canon IV A

Canon IV B

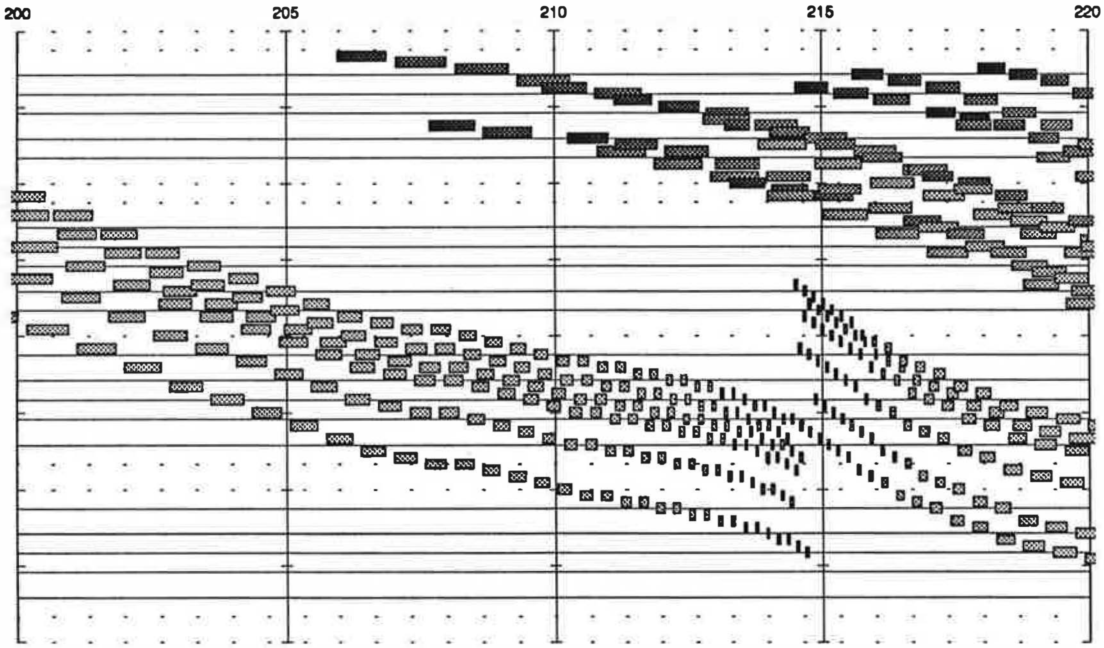

Canon V

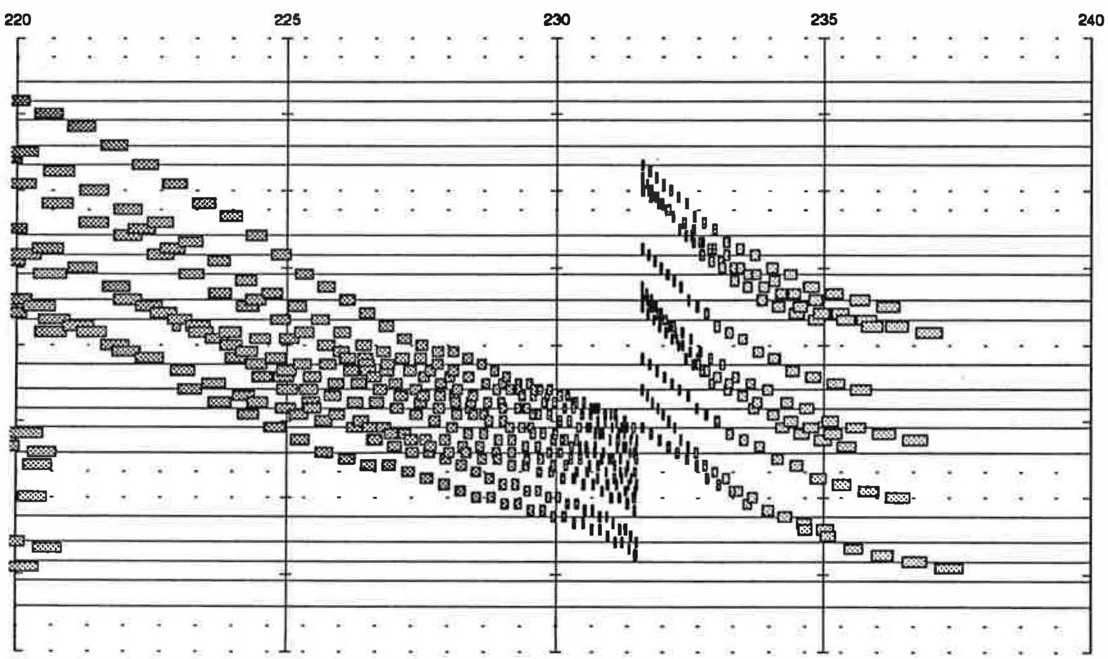

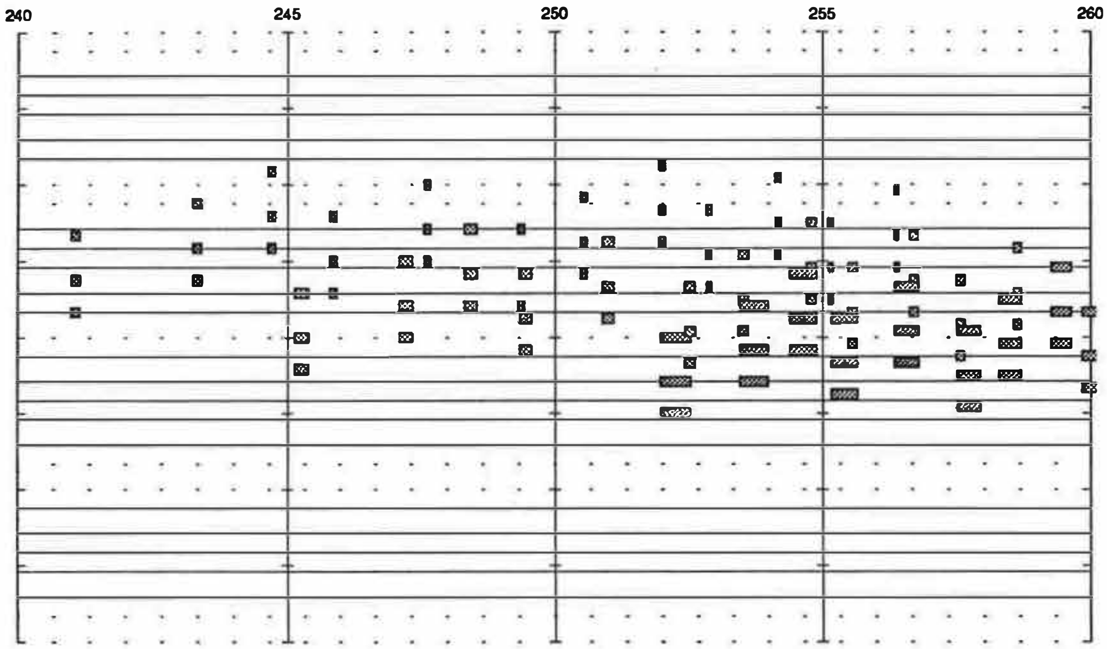

Canon VI

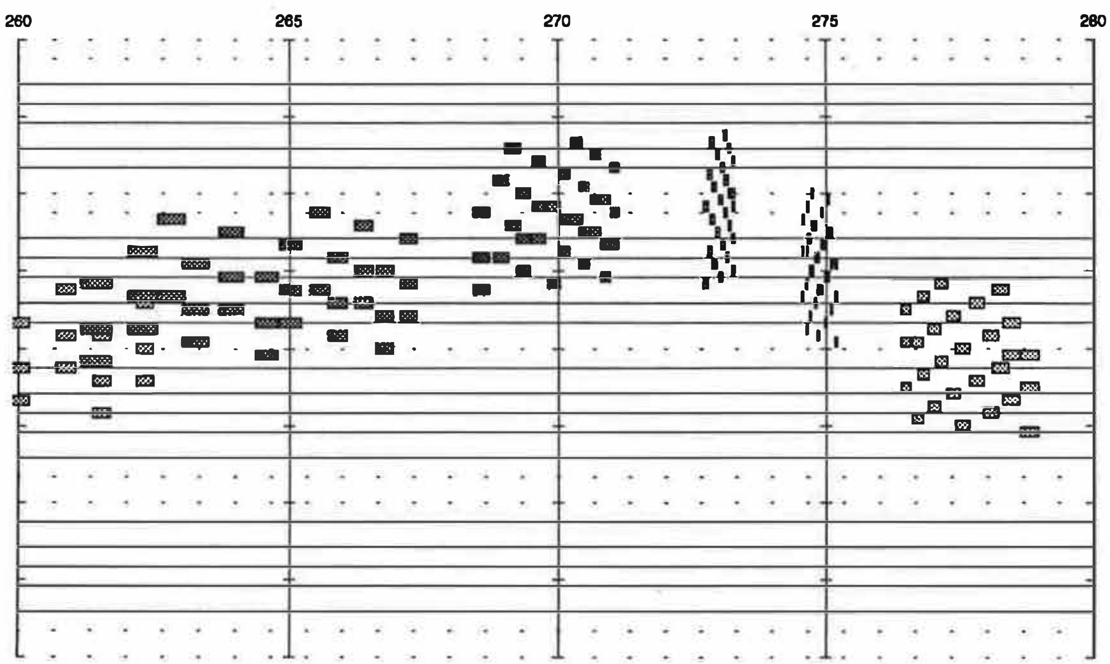

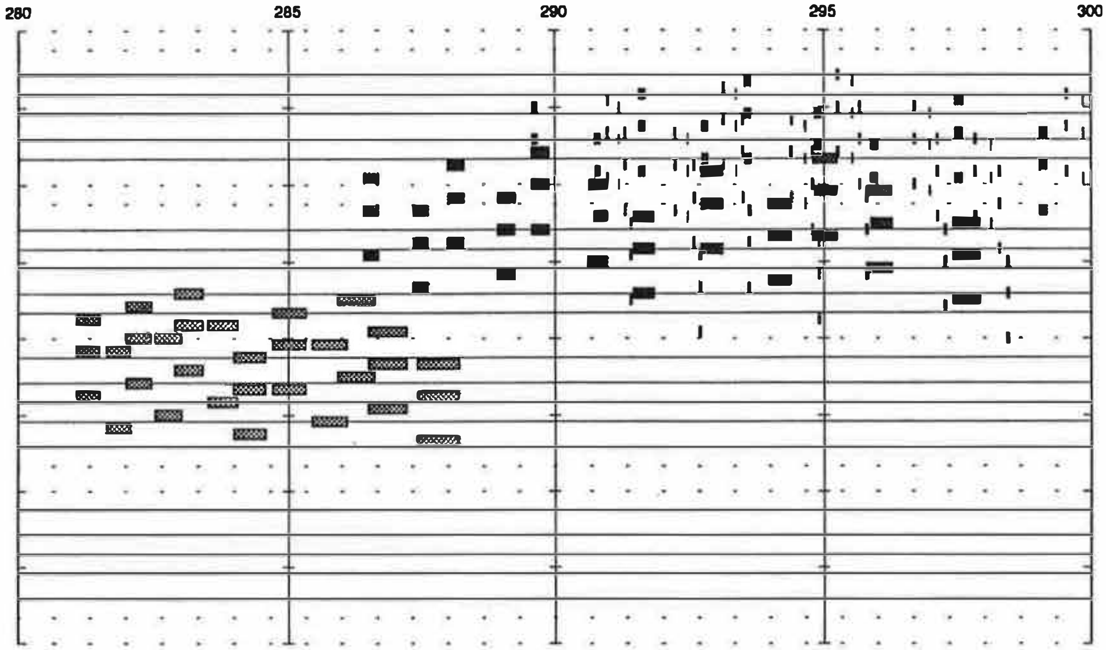

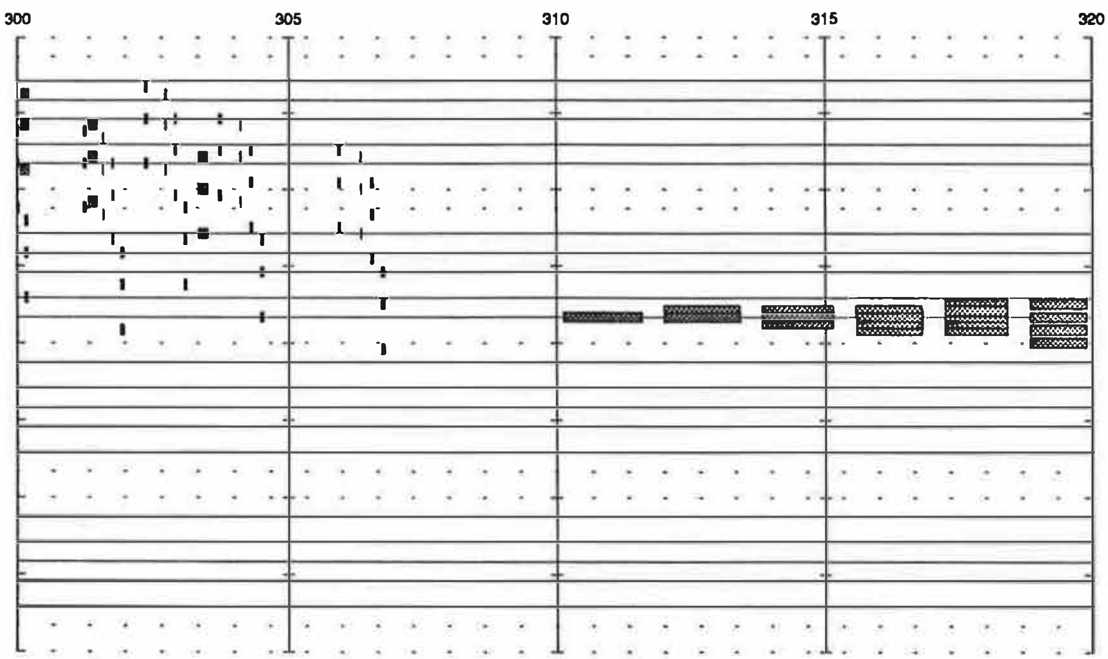

Canon VII

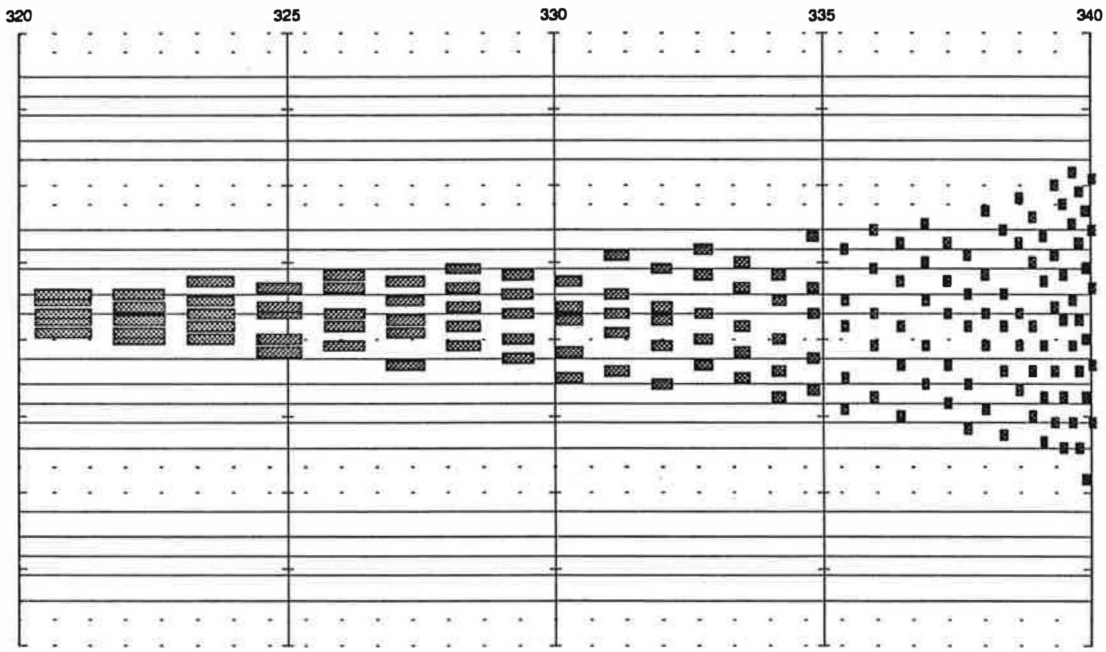
320
325
330
335
340

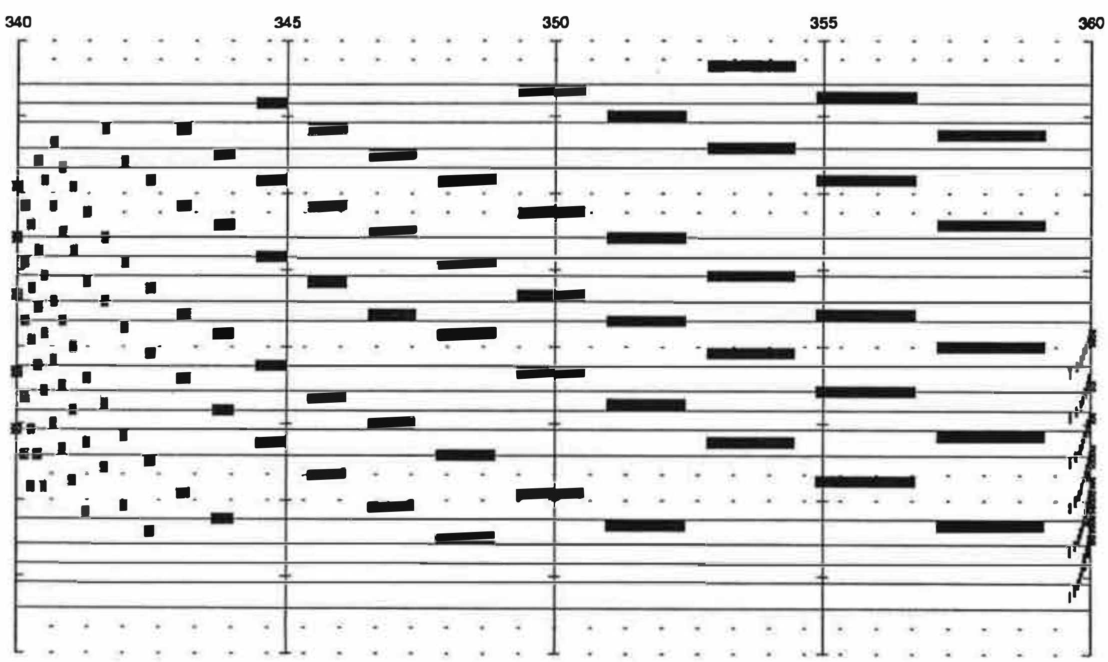
340
345
350
355
360

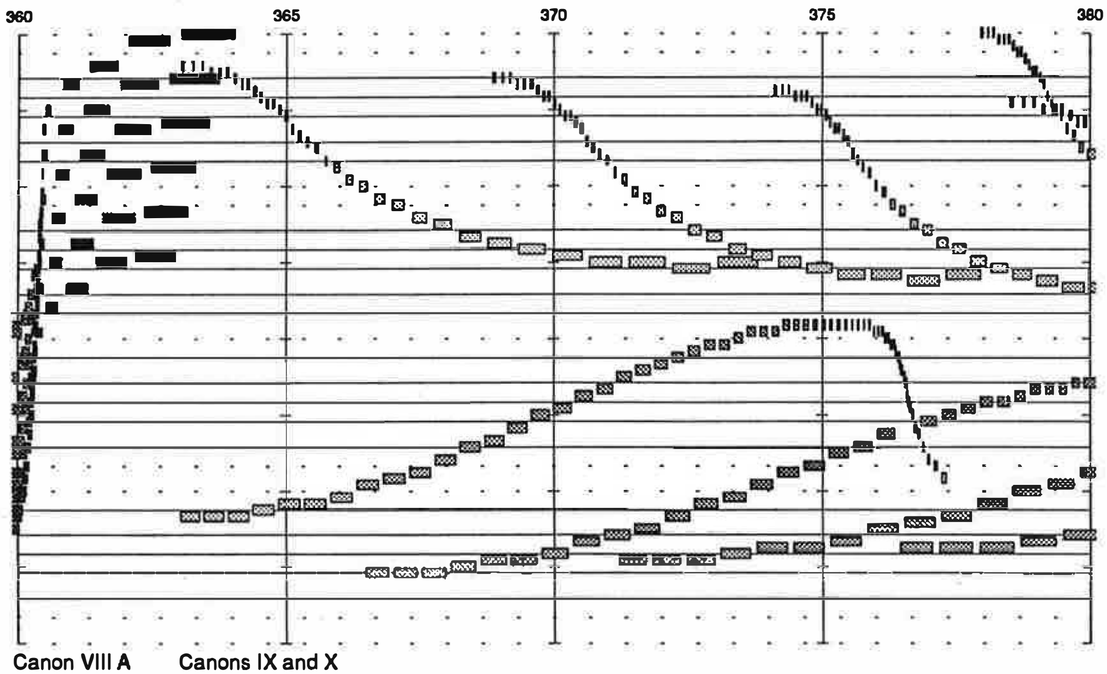
360
365
370
375
380
Canon VIII A
Canons IX and X

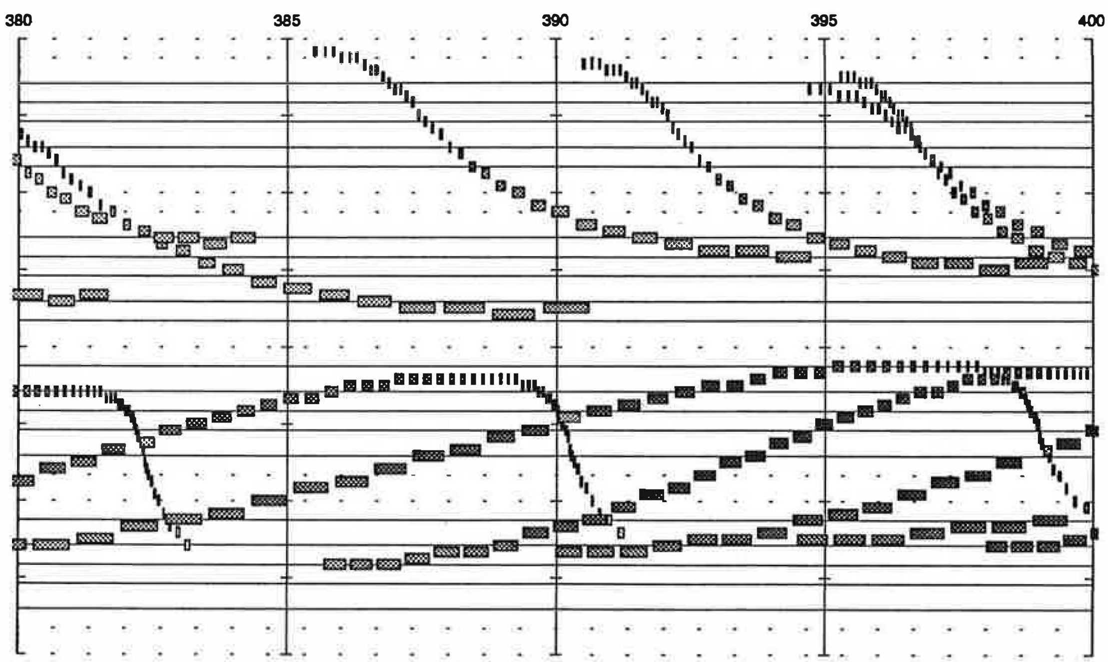
380
385
390
395
400

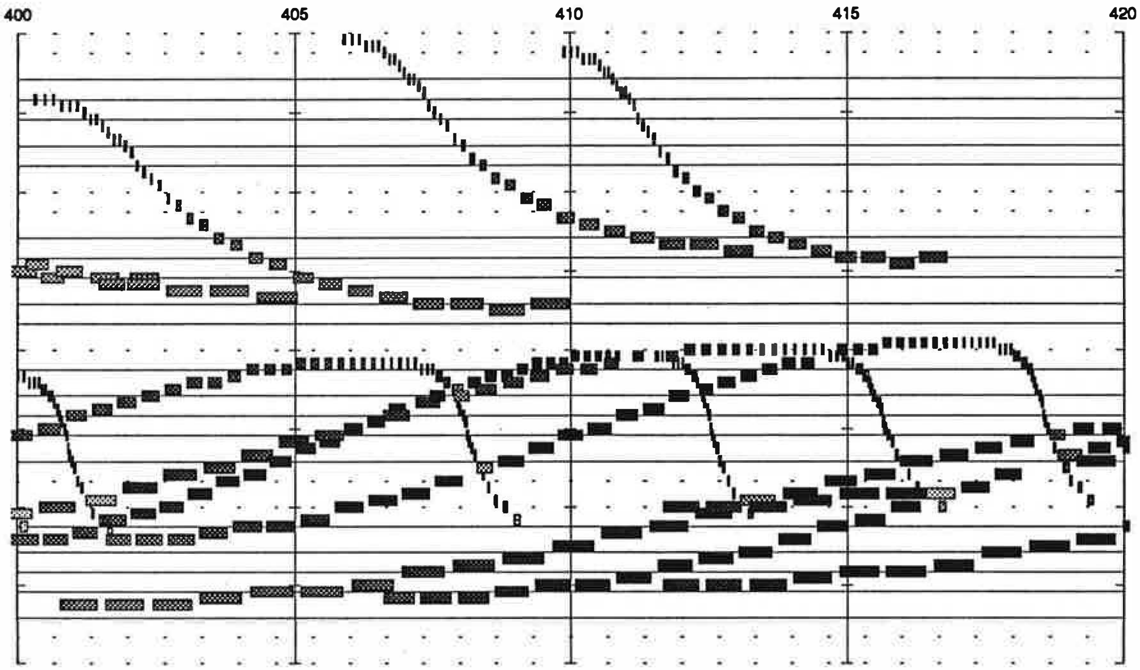

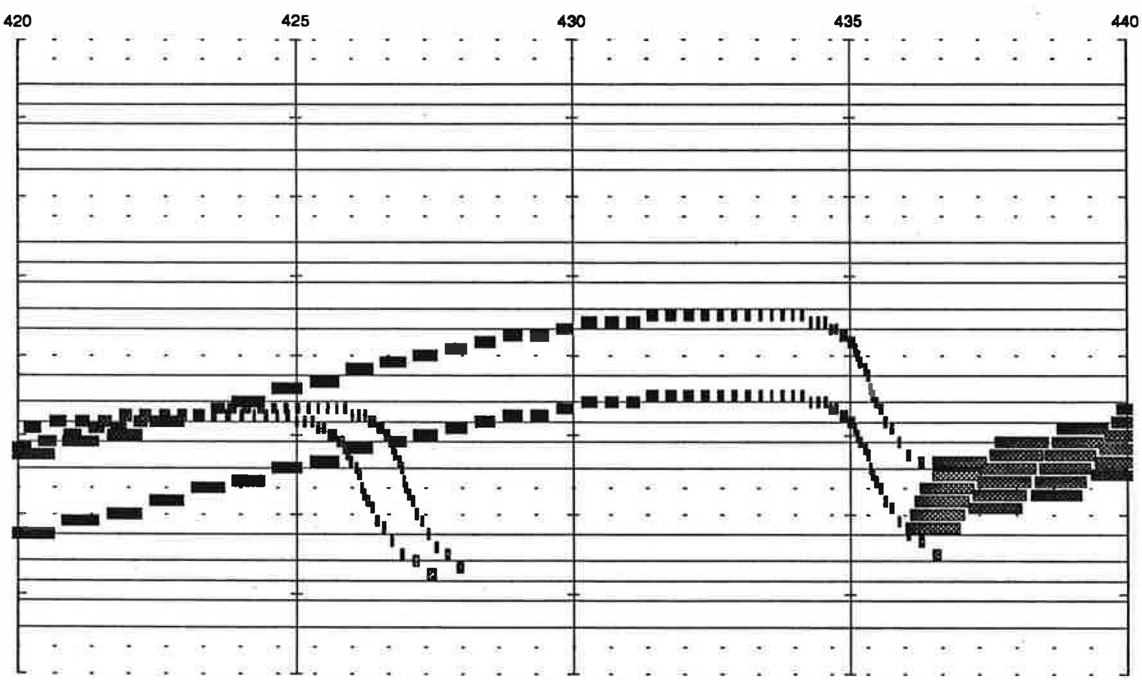

Canon XI A

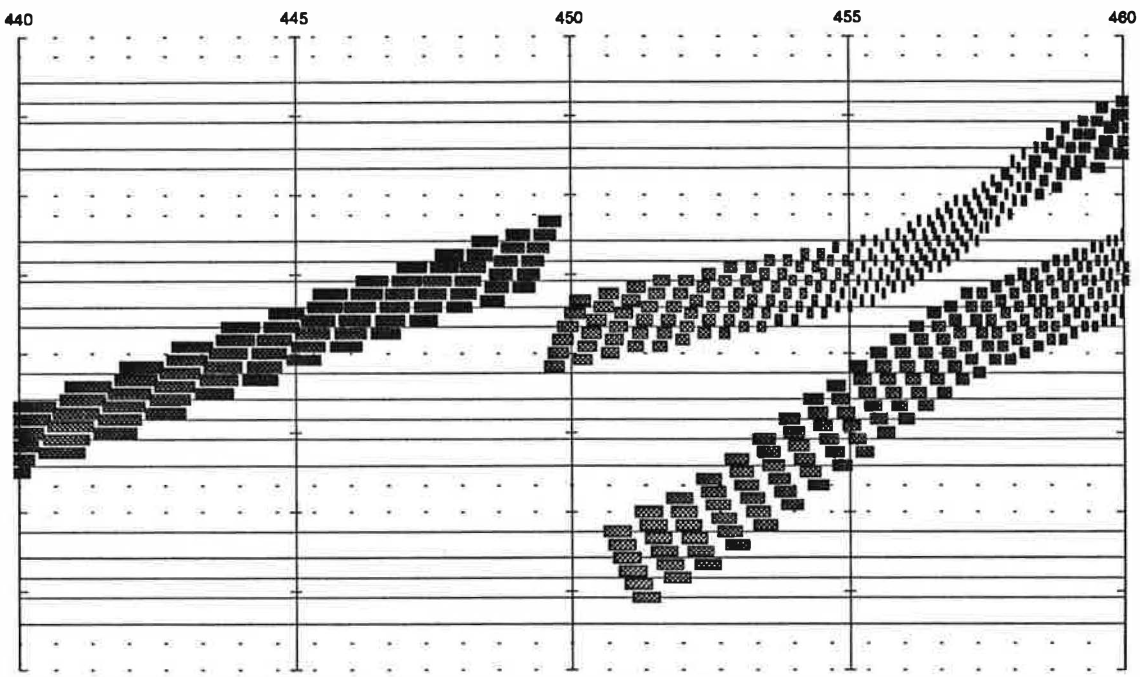

Canon XI B

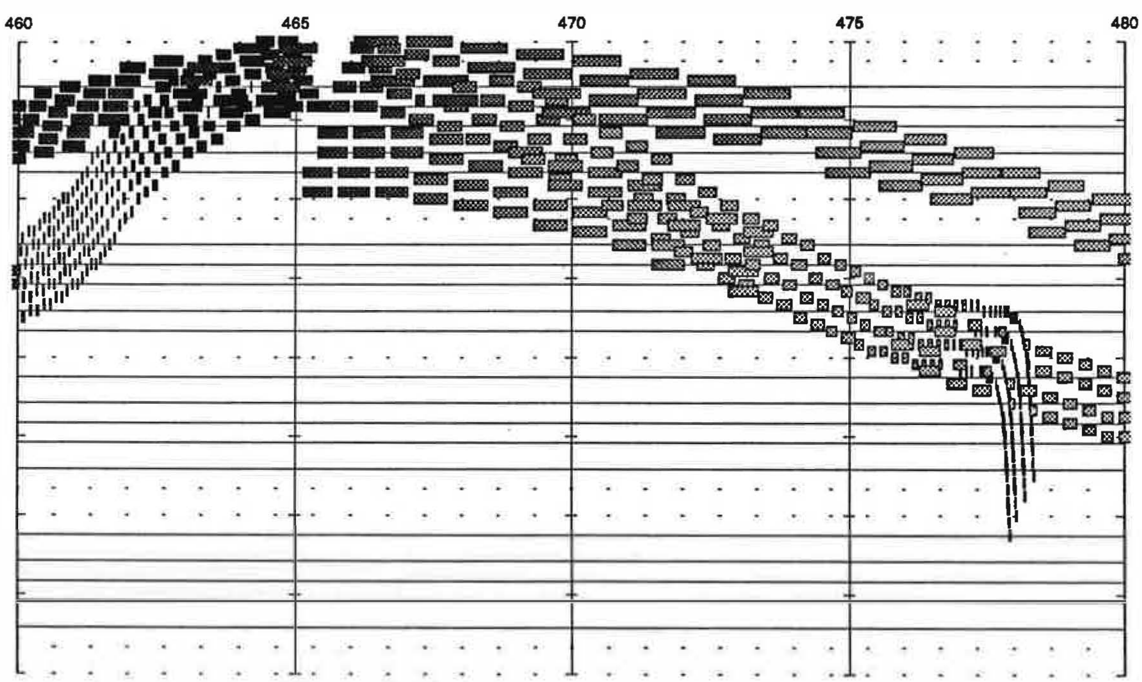

Canon XI C/D/E

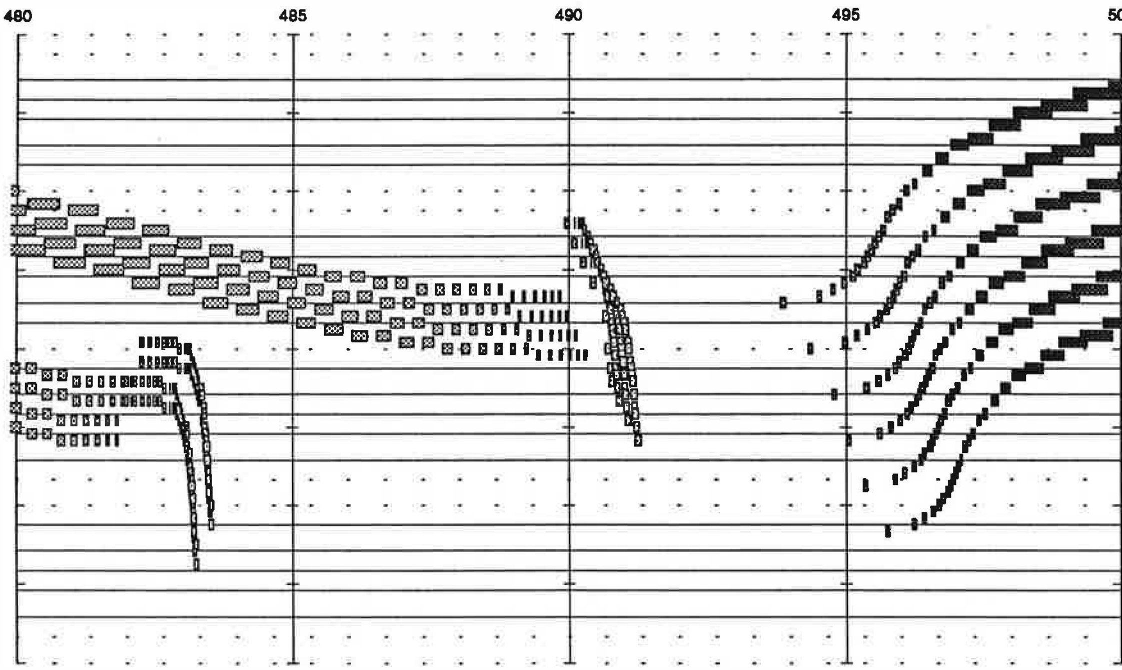

Canon VIII B

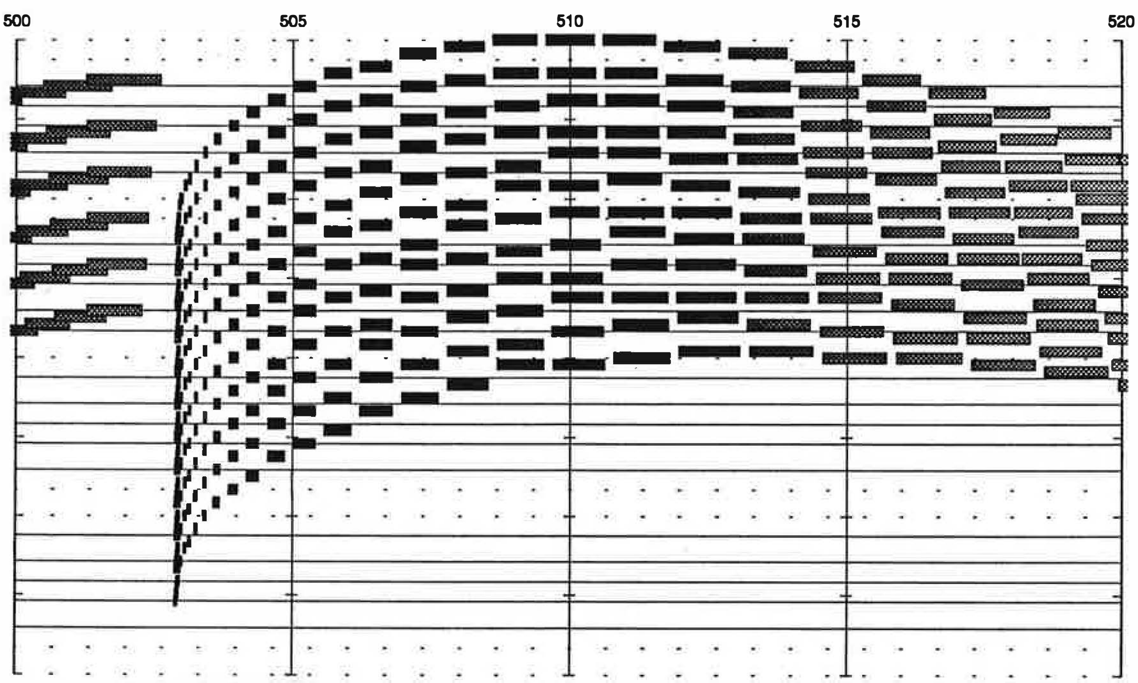

Canon XII

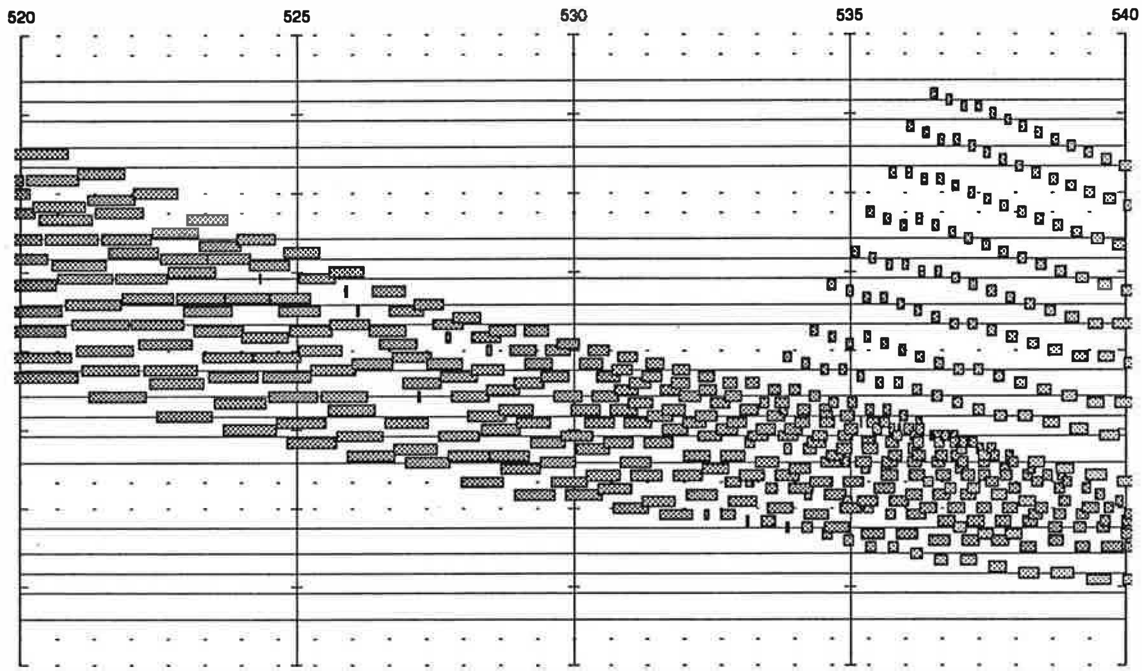
520
525
530
535
540

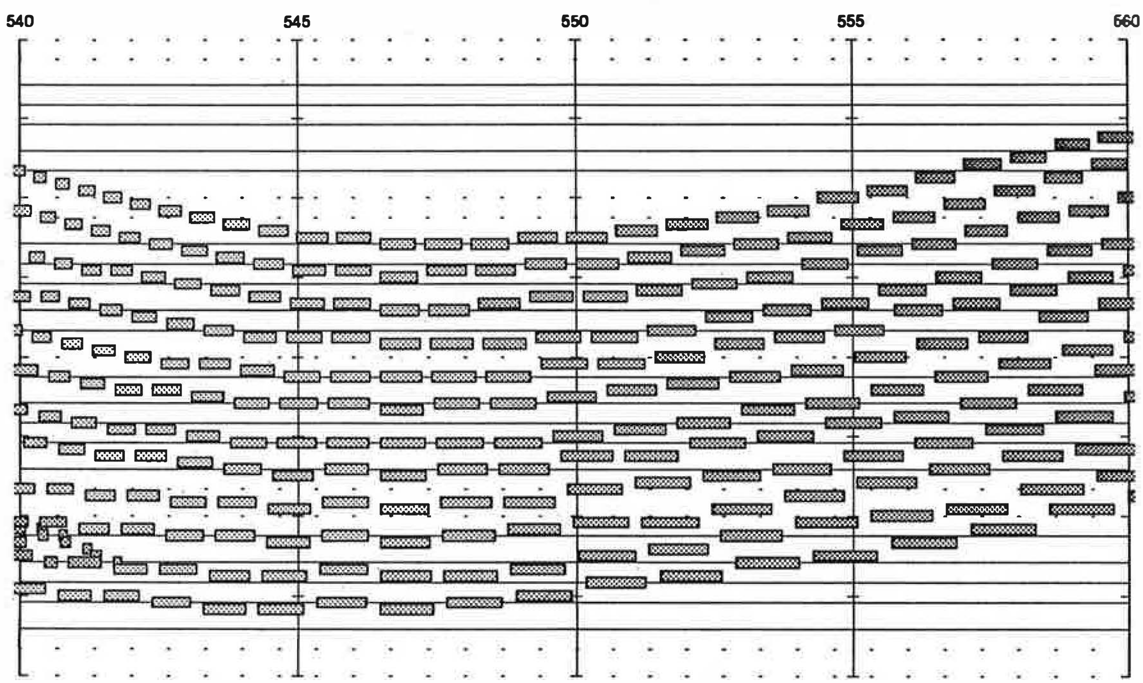
540
545
550
555
560

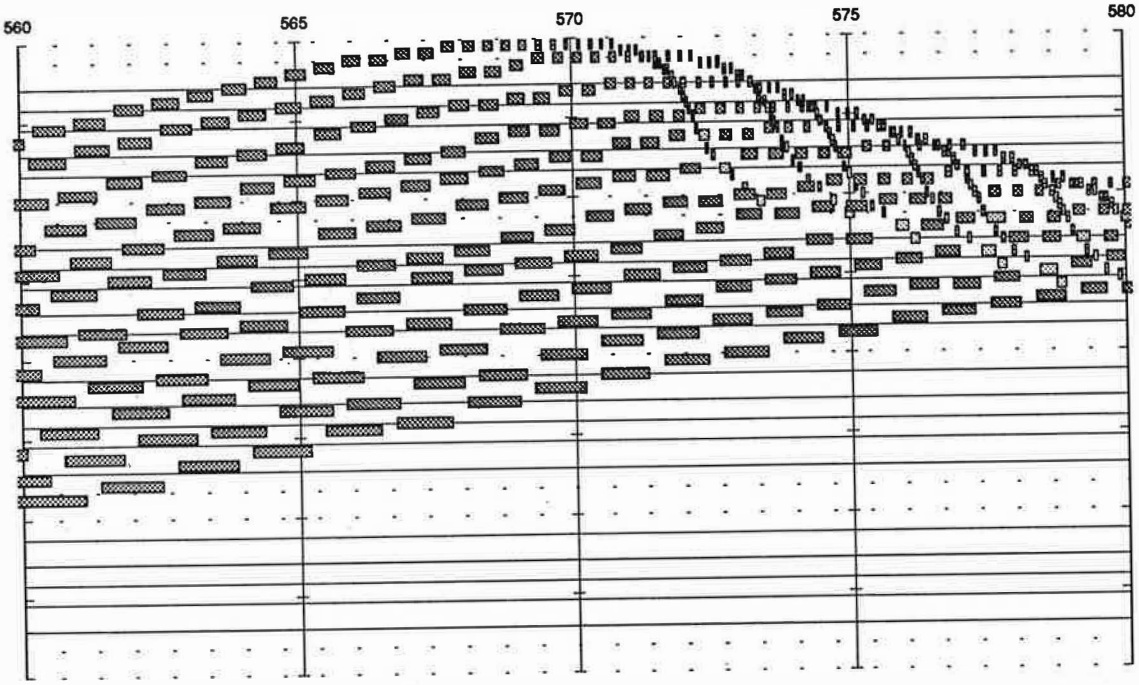

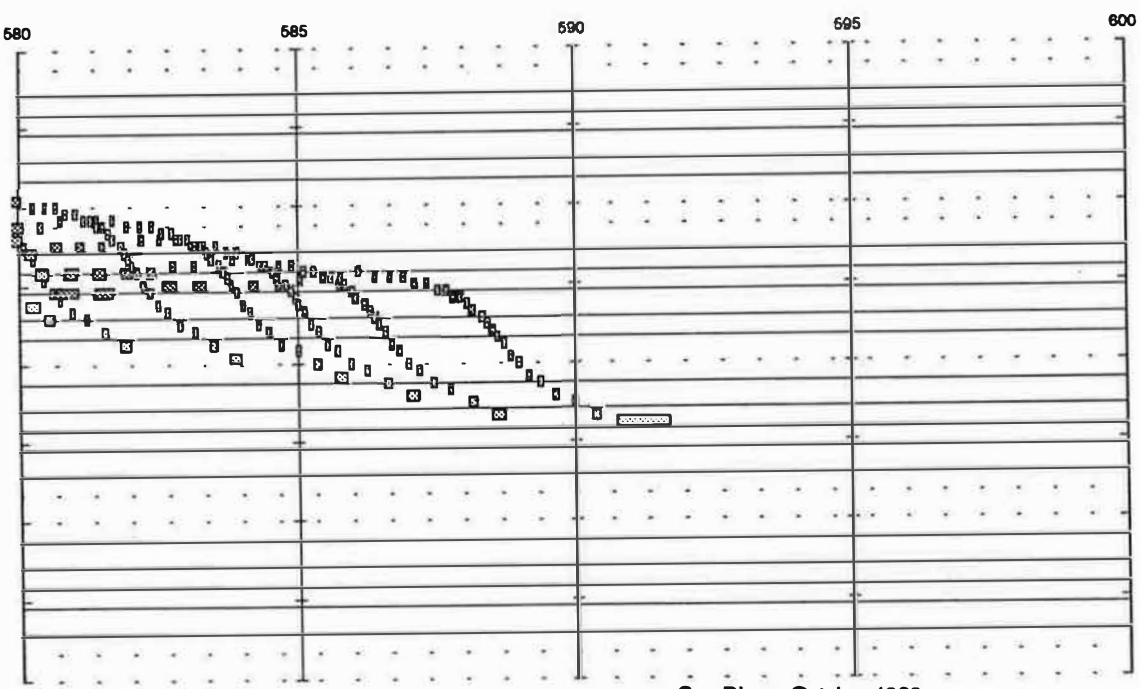

San Diego, October 1989

References

[1] Willi Apel. "Mathematics and music in the middle ages." In *Medieval Music*, chapter 14, Franz Steiner Verlag, Wiesbaden, 1986.

[2] Stephen Arnold and Graham Hair. "An introduction and a study: String Quartet No. 3." *Perspectives of New Music*, 14(2):155–186, 1976.

[3] Milton Babbitt. "Twelve-tone rhythmic structure and the electronic medium." *Perspectives of New Music*, 1(1):49–79, 1962.

[4] Gerald Balzano. "The group-theoretic description of 12-fold and microtonal pitch systems." *Computer Music Journal*, 4(4):66–84, 1980.

[5] Basil Barbanis. "An application of the third integral in the velocity space." *Zeitschrift für Astrophysik*, 56:56–67, 1962.

[6] James Barbour. *Tuning and Temperament: A Historical Survey.* Michigan State College Press, East Lansing, 1961.

[7] Jonathan W. Bernard. "The evolution of Elliott Carter's rhythmic practice." *Perspectives of New Music*, 26(2):164–203, 1988.

[8] Peter Beyls. "The musical universe of cellular automata." In *Proceedings of the 1989 International Computer Music Conference*, pages 34–41, Computer Music Society, San Francisco, 1989.

[9] Rick Bidlack. "Canonic structure in Conlon Nancarrow's *Study No. 37 for Player Piano*." Unpublished manuscript, University of California, San Diego. 1988.

[10] Pierre Boulez. *Orientations.* Harvard University Press, Cambridge, Massachusetts, 1985. Translated by Martin Cooper.

[11] Peter Bowcott. "Cellular automata as a means of high level compositional control of granular synthesis." In *Proceedings of the 1989 International Computer Music Conference*, Computer Music Society, San Francisco, 1989.

[12] John Cage. *Silence.* Wesleyan University Press, Middletown, Connecticut, 1961.

[13] Boris Chirikov. "A universal instability of many-dimensional oscillator systems." *Physics Reports (Review section of Physics Letters)*, 52(5):263–379, 1979.

[14] Douglas J. Collinge. "*MOXIE*: a language for computer music performance." In *Proceedings of the 1984 International Computer Music Conference*, pages 217–220, Computer Music Association, San Francisco, 1984.

[15] George Contopoulos. "A third integral of motion in a galaxy." *Zeitschrift für Astrophysik*, 49:273–291, 1960.

[16] A.S. Davydov. "High-temperature superconductivity in ceramic compounds and bisoliton model." In Pnevmatikos, Bountis, and Pnevmatikos, editors, *International Conference on Singular Behavior and Nonlinear Dynamics*, Volume 2, pages 327–341, World Scientific, Singapore, 1989.

[17] Bruno Degazio. "Musical aspects of fractal geometry." In *Proceedings of the 1986 International Computer Music Conference*, pages 435–442, Computer Music Society, San Francisco, 1986.

[18] Robert L. Devaney. *An Introduction to Chaotic Dynamical Systems.* Addison-Wesley, Redwood City, California, 1987.

[19] Charles Dodge. "PROFILE: a musical fractal." *Computer Music Journal*, 12(3):10–14, 1988.

[20] Friedhelm Döhl. *Weber's Beitrag zur Stilwende der Neuen Musik.* Berliner Musikwissenschaftliche Arbeiten, Musikverlag Emil Katzbicher, Munich, 1976.

[21] J.-P. Eckmann and David Ruelle. "Ergodic theory of chaos and strange attractors." *Reviews of Modern Physics*, 57(3):617–656, 1985.

[22] Doyne Farmer, James P. Crutchfield, Harold Froehling, Norman H. Packard, and Robert Shaw. "Power spectra and mixing properties of strange attractors." In Robert H. G. Helleman, editor, *Nonlinear Dynamics*, International Conference on Nonlinear Dynamics. Annals of the New York Academy of Sciences, Volume 357, pages 453–472, New York Academy of Sciences, New York, 1979.

[23] Joseph Ford. "The statistical mechanics of classical analytic dynamics." In E. G. D. Cohen, editor, *Fundamental Problems in Statistical Mechanics III*, pages 215–255, North-Holland Publishing Company, Amsterdam, 1975.

[24] Alan Forte. *The Structure of Atonal Music.* Yale University Press, New Haven, Connecticut, 1973.

[25] Harold Froehling, James P. Crutchfield, Doyne Farmer, Norman H. Packard, and Robert Shaw. "On determining the dimension of chaotic flows." *Physica*, 3D:601–617, 1981.

[26] James Gleick. *Chaos: Making a New Science.* Viking Press, New York, 1987.

[27] Ary L. Goldberger, David R. Rigney, and Bruce J. West. "Chaos and fractals in human physiology." *Scientific American*, 262(2):42–49, February 1990.

[28] Richard Franko Goldman. "Percy Grainger's *Free Music.*" *The Julliard Review*, 2(3):37, 1955.

[29] John Greene. "The calculation of KAM surfaces." In Robert H. G. Helleman, editor, *Nonlinear Dynamics*, International Conference on Nonlinear Dynamics. Annals of the New York Academy of Sciences, Volume 357, pages 80–89, New York Academy of Sciences, New York, 1980.

[30] F.G. Gustavson. "On constructing formal integrals of a Hamiltonian system near an equilibrium point." *The Astronomical Journal*, 71(8):670–686, 1966.

[31] Robert H. G. Helleman. "Self-generated chaotic behavior in nonlinear mechanics." In *Fundamental Problems in Statistical Mechanics V*, pages 165–233, North-Holland Publishing Company, Amsterdam, 1980.

[32] Michel Hénon. "A two-dimensional mapping with a strange attractor." *Communications in Mathematical Physics*, 50:69–77, 1976.

[33] Michel Hénon and Carl Heiles. "The applicability of the third integral of motion: some numerical experiments." *The Astronomical Journal*, 69(1):73–79, 1964.

[34] Roy Howat. *Debussy in Proportion.* Cambridge University Press, Cambridge, England, 1983.

[35] Rodney Waschka II and Alexandra Kurepa. "Using fractals in timbre construction: an exploratory study." In *Proceedings of the 1989 International Computer Music Conference*, pages 332–335, Computer Music Society, San Francisco, 1989.

[36] Helmut Kirchmeyer. "On the historical constitution of a rationalistic music." In *Die Reihe*, Volume 8, pages 11–24, Theodore Presser, Bryn Mawr, Pennsylvania, 1959.

[37] Joel L. Lebowitz and Oliver Penrose. "Modern ergodic theory." *Physics Today*, 26(2):23–29, 1973.

[38] A. J. Lichtenberg and M. A. Lieberman. *Regular and Stochastic Motion.* Applied mathematical sciences, Volume 38, Springer-Verlag, New York, 1983.

[39] Llewellyn S. Lloyd. *Intervals, Scales and Temperaments.* St. Martin's Press, New York, second edition, 1978.

[40] Edward N. Lorenz. Private conversation at the Institute for Nonlinear Science, University of California, San Diego, February 1990.

[41] Edward N. Lorenz. "Deterministic nonperiodic flow." *Journal of the Atmospheric Sciences*, 20:130–141, 1963.

[42] Gareth Loy. "Preface to the special issue on parallel distributed processing and neural networks." *Computer Music Journal*, 13(3):24–27, 1989.

[43] P. Luchini. "On a singularity encountered during the numerical study of a fluid-dynamics boundary-layer problem." In Pnevmatikos, Bountis, and Pnevmatikos, editors, *International Conference on Singular Behavior and Nonlinear Dynamics*, Volume 2, pages 581–600, World Scientific, Singapore, 1989.

[44] Benoit B. Mandelbrot. *The Fractal Geometry of Nature.* W.H. Freeman, New York, 1983.

[45] Robert M. May. "Nonlinear problems in ecology and resource management." In Iooss, Helleman, and Stora, editors, *Comportement chaotique des systèmes déterministes*, pages 513–564, North-Holland Publishing Co., Amsterdam, 1983.

[46] Robert M. May. "Simple mathematical models with very complicated dynamics." *Nature*, 261:459–467, June 10 1976.

[47] Leonard B. Meyer. *Music, the Arts, and Ideas.* University of Chicago Press, Chicago, 1967.

[48] Werner Meyer-Eppler. "Musical communication as a problem of information theory." In *Die Riehe*, Volume 8, pages 7–10, Theodore Presser, Bryn Mawr, Pennsylvania, 1968.

[49] *Musical Instrument Digital Interface Specification 1.0.* International MIDI Association, North Hollywood, California, 1983.

[50] Francis C. Moon. *Chaotic Vibrations: An Introduction for Applied Scientists and Engineers.* John Wiley and Sons, New York, 1987.

[51] J. Moser. "Is the solar system stable?" *The Mathematical Intelligencer*, 1:65–71, 1978.

[52] Michael Nyman. *Experimental Music: Cage and Beyond.* Schirmer, New York, 1974.

[53] Harry Partch. *Genesis of a Music.* Da Capo Press, New York, 1974.

[54] Heinz-Otto Peitgen and Peter H. Richter. *The Beauty of Fractals.* Springer-Verlag, Berlin, 1986.

[55] Heinz-Otto Peitgen and Dietmar Saupe, editors. *The Science of Fractal Images.* Springer-Verlag, New York, 1988.

[56] Leon Plantinga. "Philippe de Vitry's *Ars Nova*: a translation." *Journal of Music Theory*, 5:204–223, 1961.

[57] William H. Press, Brian P. Flannery, Saul A. Teukolsky, and William T. Vetterling. *Numerical Recipes in C: The Art of Scientific Computing.* Cambridge University Press, Cambridge, England, 1989.

[58] A. Rauh, R.F.S. Andrade, and Ch. F. Kougias. "Symmetry in the normal form of the Hénon-Heiles Hamiltonian." In Pnevmatikos, Bountis, and Pnevmatikos, editors, *International Conference on Singular Behavior and Nonlinear Dynamics*, Volume 2, pages 97–108, World Scientific, Singapore, 1989.

[59] Lee Ray. *An Application of Computer-Aided Composition within an Independent Musical Context.* Master's thesis, University of California at San Diego, 1986.

[60] Roger Reynolds. *A Searcher's Path: A Composer's Ways.* Institute for Studies in American Music, Brooklyn College of the City of New York, Brooklyn, 1987.

[61] Curtis Roads. "Grammars as representations of music." In Curtis Roads and John Strawn, editors, *Foundations of Computer Music*, M.I.T. Press, Cambridge, Massachusetts, 1988.

[62] David Ruelle. "Dynamical systems with turbulent behavior." In Dell'Antonio, Doplicher, and Jona-Lasinio, editors, *International Conference on the mathematical problems in theoretical physics.* Lecture Notes in Physics, Volume 80: Mathematical Problems in Theoretical Physics, pages 341–360, Springer-Verlag, Berlin, 1978.

[63] David Ruelle. "Strange attractors." *The Mathematical Intelligencer*, 2:126–137, 1980.

[64] Robert Shaw. "Strange attractors, chaotic behavior, and information flow." *Zeitschrift für Naturforschung*, 36a:80–112, 1981.

[65] Colin Sparrow. *The Lorenz Equations: Bifurcations, Chaos and Strange Attractors.* Applied Mathematical Sciences, Volume 41, Springer-Verlag, New York, 1982.

[66] Manfred Stahnke. *Struktur und Ästhetik bei Boulez.* Hamburger Beiträge zur Musikwissenschaft, 21, Verlag der Musikalienhandlung Karl Dieter Wagner, Hamburg, 1979.

[67] Karlheinz Stockhausen. "...how time passes..." In *Die Reihe*, Volume 3, pages 10–40, Theodore Presser, Bryn Mawr, Pennsylvania, 1959.

[68] James Tenney. "Conlon Nancarrow's Studies for Player Piano." In Peter Garland, editor, *Conlon Nancarrow: Selected Studies for Player Piano*, Soundings Press, Santa Fe, New Mexico, 1977.

[69] J.M.T. Thompson and H.B. Stewart. *Nonlinear Dynamics and Chaos.* John Wiley and Sons, Chichester, 1986.

[70] Leo Treitler. "Regarding meter and rhythm in the *Ars Antiqua.*" *Musical Quarterly*, 65(4):524–558, 1979.

[71] Yvain M. Treve. "Theory of chaotic motion with application to controlled fusion research." In Siebe Jorna, editor, *Topics in Nonlinear Dynamics: A Tribute to Sir Edward Bullard.* AIP Conference Proceedings, No. 46, pages 147–200, American Institute of Physics, New York, 1978.

[72] Eric Werner. "The mathematical foundation of Philippe de Vitry's *Ars Nova.*" *Journal of the American Musicological Society*, 9:128–132, 1956.

[73] Bruce West. "Fractal physiology; a paradigm for adaptive response." In Pnevmatikos, Bountis, and Pnevmatikos, editors, *International Conference on Singular Behavior and Nonlinear Dynamics*, Volume 2, pages 643–664, World Scientific, Singapore, 1989.

[74] W. Wunderlich, E. Stein, and K.-J. Bathe, editors. *Nonlinear Finite Element Analysis in Structural Mechanics.* Springer-Verlag, Berlin, 1981.

[75] Iannis Xenakis. *Formalized Music: Thought and Mathematics in Composition.* Indiana University Press, Bloomington, 1971.